Blends and Nanocomposites of Sulfonated Polystyrene and Polybenzimidazole

A Thesis Submitted for the degree of

DOCTOR OF PHILOSOPHY

By
Mousumi Hazarika

School of Chemistry
University of Hyderabad
Hyderabad-500 046
INDIA

December 2012

Dedicated

to

Maa and deuta

DECLARATION

I hereby declare that the matter embodied in the thesis entitled "***Blends and Nanocomposites of Sulfonated Polystyrene and Polybenzimidazole"*** is the result of investigations carried out by me in the School of Chemistry, University of Hyderabad, Hyderabad, India under the supervision of **Dr. Tushar Jana** and it has not been submitted elsewhere for the award of any degree or diploma or membership, etc.

In keeping with the general practice of reporting scientific investigations, due acknowledgements have been made wherever the work described is based on the findings of other investigators. Any omission or error that might have crept in is regretted.

December 2012 **Mousumi Hazarika**

UNIVERSITY OF HYDERABAD
Central University (P.O.), Hyderabad-500046, INDIA

Dr. Tushar Jana
Associate Professor
School of Chemistry

Tel: 91-40-23134808 (Office)
91-9440127016 (Mobile)
Fax: 91-40-23012460
E-mail: tjsc@uohyd.ernet.in
tjscuoh@gmail.com
Web: http://chemistry.uohyd.ernet.in/~tj/

CERTIFICATE

This is to certify that the work described in this thesis entitled "***Blends and Nanocomposites of Sulfonated Polystyrene and Polybenzimidazole***" has been carried out by Mrs. Mousumi Hazarika under my supervision and the same has not been submitted elsewhere for any degree.

Dean
School of Chemistry
University of Hyderabad
Hyderabad-500 046
India

Dr. Tushar Jana
(Thesis supervisor)

PREFACE

The present thesis entitled *"**Blends and Nanocomposites of Sulfonated Polystyrene and Polybenzimidazole**"* has been divided into seven chapters. ***Chapter 1*** provides a brief introduction on polymer blends, polymer nanocomposites. The properties, synthesis and application of sulfonated polystyrene, polybenzimidazoles poly(vinylidene fluoride-co-hexafluoro propylene), poly(vinyl-1,2,4-triazole), graphene, graphite and graphite oxide are discussed. The advanced application of phosphoric acid doped polybenzimidazole as an electrolyte membrane in high temperature fuel cell application has also discussed. ***Chapter 2*** describes the influence of sulfonation reaction time, temperature and the parent polystyrene particle size on the degree of sulfonation, ion exchange capacity, morphology and glass transition temperature of sulfonated polystyrene particles. ***Chapter 3*** deals with the formation of core (polystyrene)-shell (polybenzimidazole) nanoparticles from a new blend system consisting of an amorphous polymer polybenzimidazole and an ionomer sodium salt of sulfonated polystyrene (SPS-Na). ***Chapter 4*** describes synthesis of partially miscible polymer blends of polybenzimidazole with poly(vinylidene fluoride-co-hexafluoro propylene) for their use as polymer electrolyte membrane (PEM) in high temperature PEM fuel cell after being doped with phosphoric acid. ***Chapter 5*** also describes the application of polybenzimidazole and poly(1-vinyl-1,2,4-triazole) blends as polymer electrolyte membrane in high temperature PEM fuel cell. ***Chapter 6*** describes the synthesis of nanocomposite of sulfonated polystyrene with graphene. The influence of graphene concentration on properties of sulfonated polystyrene is investigated. ***Chapter 7*** summarizes the findings of the present investigations, presents a concluding remark and the future scope and upcoming challenges.

December, 2012 **Mousumi Hazarika**

Acknowledgement

It is my immense pleasure to express my sincere gratitude to my research supervisor Dr. Tushar Jana, for his constant cooperation, encouragement and kind guidance. He has been quite helpful to me in both academic and personal fronts. It has been great pleasure and fortune to work with him who introduced me to the field of polymer chemistry. His discipline working style and honesty for the research has paved a new path in my career. I am also indebted to him for the work freedom he has given me during the last five years.

I would like to thank the former and present Dean, School of Chemistry, for their constant inspiration and for allowing me to use the available facilities. I am extremely thankful individually to all the faculty members of the school for their kind help and cooperation at various stages of my stay in the campus.

I am grateful to UGC-CAS and CSIR, New Delhi, for providing fellowship support.

I would also like to express my sincere gratitude to Dr. S.M. Ahmed, Dr. Manjunath and Mr. Murthy of central Instrumental Laboratory (CIL), UoH for their help with SEM, DSC experiments. I sincerely acknowledge Dr. S. Srinath of School of Physics, UoH for helping me with FE-SEM experiments. I also sincerely thank Mr. Durgaprasad of Centre for Nanotechnology, UoH for allowing me to use the TEM facility.

I am deeply predicated to all my teachers starting from my school to the university for their wonderful teaching and education throughout my academics.

I wish to thank my friendly and cooperative lab mates Arindam da, Arunbabu, Murali, Sandip da, Sudhangshu, Malkappa, Shuvra, Raju, Niranjan and Narashima in my ph.d life. I am very grateful to my seniors Arindam da, Arun, Murali and Sandip da for their support and help during my Ph.D life. I acknowledge my juniors Sudhangshu, Malkappa, Shuvra, Raju and Narashima for maintaining the friendly and cooperative atmosphere in the lab.

I also thank all non-teaching staff for their timely help. I thank Mr. Sathyanarayana, Mr. Bhaskar Rao, Mr. Thurab Syed, Smt. Vijayalakshmi for their help in recording NMR spectra. I thank Mr. Shetty, Mr. Vijay Bhaskar, Mr. Dilip, Mr. Sai, Mr. Sharma, Mr. Jayaram, Mr. Desbandu, Mr. Durgesh, Mr. Shetty, Mr. Joseph for their cooperation.

I would also like to convey my sincere thanks to all my dadas Bipul da, Ranjit da, Sanjeev da, Pranjal da and Pankaj da for their help and support during my Ph.D life in Hyderabad. My pleasant association with some friends in UOH such as Tridip, Barnali, Abdul, Sapan, Jayshree, Supriya, Munmi, Swarnali ba, Stuty, Naba, Jahnu, Nita, Indu, Rava is unforgettable.

I would also like to thank few of my friends in School of Chemistry Tulika, Geetha, Somya, Sanghamitra, Sridevi, Pramiti, Sutanuka, Sjjna, Sudha, Hari, Gupta, Vignesh, Ganesh, Satishkumar, DK Sriivash, Bharat, Kishor, Satpal, Supratim, Chandrashekar.

I want to thanks my M.Sc. friends Mridusmita, Moushumi, Rupam, Harjyoti, Bapan, Prasenjit, Priyanka, Shyamalee, Dabajit, Rihana, Sujata, Dhruba.

I thank my elder sister "Majoni" for her help, guidance and support in every stage of my life. A special thanks to my elder brother "baba", brother in law, sister in law, my nieces and my family members for their love and affection.

I would like to thank Dr. Naba Kamal Nath, my husband, for all the chemistry discussions, teaching me how to generate ideas and most importantly standing beside me during my hard times with all his encouragement and love.

I would like to express my love and gratitude to my parents for their unconditional love and blessings. They made me what I am today and I owe everything to them. Dedicating this thesis to them is a minor recognition for their relentless support and love.

December 2012 **Mousumi Hazarika**

University of Hyderabad

Hyderabad-500 046

India

CONTENTS

Chapter 1

Introduction

1.1. Polymer blends

Polymer science has a major impact on our daily life. It is difficult to find an aspect of our lives that is not affected by polymers.[1] The necessitate for plastics (polymers) in daily life is increasing day by day. The success of plastics is due its wide range of properties which replace metals, glass, ceramics, paper, natural fibers, packaging, consumer products, piping, furniture, etc.[2]

Blends mean mixture of two or more components. But there is no precise definition for the word 'blends'. Blending is a natural way to widen the range of properties of the resultant new material which obtained upon mixing. From ancient time people are blending different materials to get a new material. For example color can also be blended. If red color is mixed with blue it gives purple. Similarly blue color is mixed with yellow it gives green color. Blending is there in many fields such as food, metals and polymers etc.

Polymer blends are class of materials analogous to metal alloys; in which two or more polymers are mixed together to create new material with enhanced physical properties. A schematic diagram is shown in Figure 1.1.

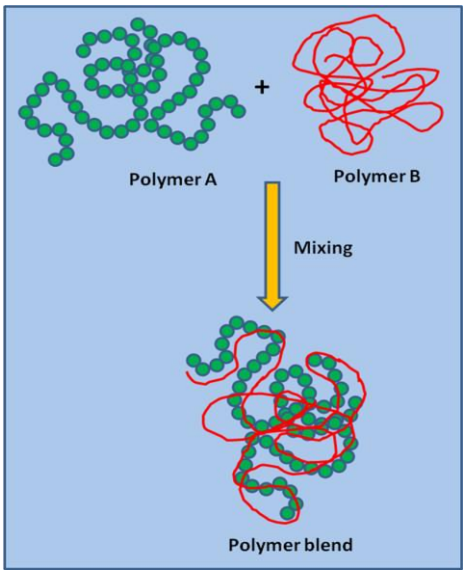

Figure 1.1: Schematic diagram showing the formation of polymer blend (Adapted from reference 3a)

Polymer blending is a convenient way for the development of new polymeric materials. It can combine the excellent properties of one or more polymers. This technique is simple, cheaper and less time-consuming than the development of new polymers.[3-5] Polymer blends have received significant attention in last past decades because the blending of polymers provides a powerful route for obtaining materials with improved property.[6] Blending also benefits the manufacturer by offering improved processability, product uniformity, quick formulation changes, plant flexibility and high productivity.

The science and technology of polymer blend was developed in eighteen century. In 1846 Alexander Parkes introduced the first blends of natural rubber (NR).[7] He mixed NR with gutta percha to obtain material suitable either for water proofing cloth or after vulcanization for production of molding. In 1910 J. W. Aylsworth invented a method which described material obtained by simultaneous vulcanization of natural rubber and condensation of phenol with formaldehyde, making it the first simultaneous interpenetrating polymer network (IPN) material.[8] F. E. Matthews first modified rubber by incorporating polystyrene. Expecting finer dispersion and better control he mixed rubber with styrene and polymerized styrene in presence of rubber. The production of rubber-polystyrene blends started from 1929. Polymer blends were also developed along with the emerging polymers. When nitrocellulose (NC) was invented, it was mixed with natural rubber (NR). Blends of NC with NR were patented in 1865 which is three years before the commercialization of NC. Polyvinylchloride (PVC) was commercialized in 1931 while its blends with nitrile rubber (NBR) were patented in 1936, two years after the NBR patent was issued. The modern era of polymer blending began in 1960, after Alan Hay synthesized polyphenyleneether (PPE) by oxidative polymerization of 2,4-xylenols. Its blends with styrenics (polymeric materials based on styrenes), *Noryl*^{TM} (blend of polyphenylene oxide and polystyrene), were commercialized in 1965.[9] The market for polymer blend based materials has increased continuously during the past two decades. Polymer blends segment of the plastics industry increases at about three times faster than the whole plastics industry and is expected to increase by 8-10% in the coming decade.[10a] The major markets are

automotive, electrical and electronic, packaging, building and household. Nowadays, the total market for polymer blends is estimated to be 2.2 million tonnes per year.[10b,10c]

1.1.1. Thermodynamical requirements

Usually polymers do not mix each other owing to their big molecular size and absence of favourable interaction since they determine the blend final properties. Miscibility and compatibility are essential issues in the development of polymer blends. Miscibility of polymer blend is governed by Gibb's free energy of mixing (ΔG_{mix}). Homogeneous miscibility in polymer blends requires a negative free energy of mixing, ($\Delta G_{mix}<0$).[9,11,12] The following condition should be fulfilled for complete miscibility of two polymers

$$\Delta G_{mix} = \Delta H_{mix} - T\Delta S_{mix} < 0 \qquad (1.1)$$

where ΔG_{mix}, ΔH_{mix} and ΔS_{mix} are the free energy, enthalpy and entropy of mixing, respectively. For miscibility to occur, ΔG_{mix} must be smaller than zero. This is a necessary requirement but not a sufficient requirement. For complete miscibility of binary mixtures of composition (ϕ) at fixed temperature T and pressure P, the following expression must also be satisfied:

$$\left(\frac{\partial^2 \Delta G_{mix}}{\partial \phi_i^2}\right)_{P,T} > 0 \qquad (1.2)$$

For polymers the value of $T\Delta S_{mix}$ is always positive because polymers itself remain in high entropy state and they hardly gain any entropy on mixing. ΔG_{mix} can only be negative if the heat of mixing, ΔH_{mix} is negative. The polymer will form miscible blends only if the entropy of mixing exceeds the enthalpy of mixing i.e.

$$\Delta H_{mix} < T\Delta S_{mix} \qquad (1.3)$$

So for miscibility the mixing must be exothermic, which requires specific interactions between the blend components.[10a,13] These specific interaction is polar and range in

strength from the relatively weak (dipole-induced) to relatively strong (hydrogen bonding).[14]

A schematic phase diagram of polymer mixer is shown in Figure 1.2. There are three regions of different degree of miscibility. (i) The single-phase miscible region between the two binodals (ii) the four fragmented metastable regions between binodals and spinodals and (iii) the two-phase separated regions of immiscibility, bordered by the spinodals. The diagram also shows two critical solution temperatures, the lower, LCST (at higher temperature), and the upper, UCST (at lower temperature).[15]

For mixtures of low molar mass components phase diagram with two critical points is a rule, whereas the polymer blends usually show either LCST or UCST. The binodals separate miscible and metastable region, the spinodals separate metastable and two-phase region.

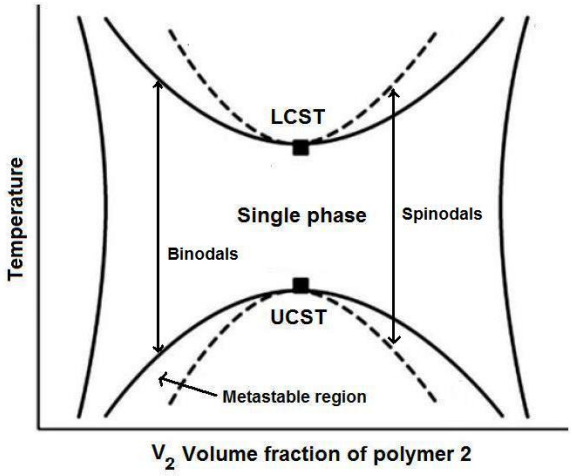

Figure 1.2: Phase diagram of polymer mixer with upper and lower critical solution temperature, UCST and LCST respectively.[15]

The thermodynamic conditions for phase separations are given by

Spinodal: $$\left(\frac{\partial^2 \Delta G_m}{\partial \phi_i^2}\right)_{P,T} = 0 \qquad (1.4)$$

Critical point: $$\left(\frac{\partial^2 \Delta G_m}{\partial \phi_i^2}\right)_{p,T} = \left(\frac{\partial^3 \Delta G_m}{\partial \phi^3}\right)_{P,T} = 0 \qquad (1.5)$$

When a single-phase system bears a change of composition, phase separation takes place and temperature or pressure that forces it to enter either the metastable or the spinodal region. When the system enters from single-phase region into the metastable region, the phase separation occurs by the mechanism which resembles crystallization (slow nucleation followed by growth of the phase separated domains).[16] When the system is forced to jump from a single-phase into the spinodal region of immiscibility, the phases separate spontaneously by a mechanism called spinodal decomposition.

The Flory-Huggins theory which originally developed for polymer solution can be extended to polymer-polymer miscibility by introducing restrictions such as no change of volume during mixing, the entropy of mixing is entirely given by the number of rearrangements during mixing and the enthalpy of mixing is caused by interactions of different segments after the dissolution of interactions of the same type of segments. For binary polymer mixer the entropy of mixing ΔS_{mix} can be expressed as

$$\Delta S_{mix} = -R\left[\frac{\phi_1}{r_1}\ln\phi_1 + \frac{\phi_2}{r_2}\ln\phi_2\right] \qquad (1.6)$$

where (ϕ_i) is the volume fraction of the component i and r_i is the number of polymer segments, R is the gas constant. From the equation it can be seen that the entropy of mixing decreases with increasing molar mass since r_i is proportional to the degree of polymerization and vanishes for infinite molar masses.

By assuming polymer-polymer mixer as solution the enthalpy of mixing ΔH_{mix} can be expressed as

$$\Delta H_{mix} = RT\chi\phi_1\phi_2 \qquad (1.7)$$

Where χ is the Flory-Huggins constant.

For binary systems the Flory-Huggins equation can be expressed in the following form[17,18]

$$\Delta G_{mix} = RT\left[\frac{\phi_1}{r_1}\ln\phi_1 + \frac{\phi_2}{r_2}\ln\phi_2 + \chi\phi_1\phi_1\right] \qquad (1.8)$$

Where χ is the Flory-Huggins binary interaction parameter. R is the gas constant and T is the absolute Temperature. For polymers having high molar mass the entropy contribution is very small and miscibility of the blend system depends on the value of enthalpy of mixing. Miscibility can only be achieved when χ is negative.

1.1.2. Morphology

After mixing polymer blend forms different phases (morphology). The complex interplay between viscosity of the phases, interfacial properties, blend composition and processing conditions results the shape, size and spatial distribution of the phases in blends. Phase structure of polymer blends is very important for their application. For example an immiscible blend of 1 and 2, when content of 2 is low it will form particles which will be dispersed in the matrix of 1 component. As the amount of 2 component increases the particles get bigger and bigger and it will look like the middle image in Figure 1.3. With further increase in the amount of 2, phase inversion will take place. At this stage component 2 will form the continuous matrix and component 1 will disperse on it.

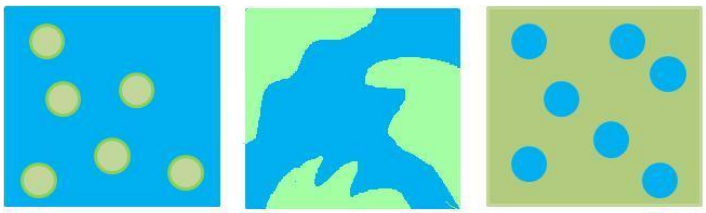

Figure 1.3: Schematic diagram showing different morphology development during blending. (Adapted from reference 19)

Utracki and Lyngaae-Jørgensen proposed a theory based on the assumption that the critical volume fractions relate to the percolation thresholds of droplets, and phase inversion appears at the composition at which the blend with dispersed component 1 and matrix 2 has the same viscosity as the blend with dispersed component 2 and matrix 1.[20] Polystyrene and polybutadiene are immiscible. When polystyrene is mixed with a small amount of polybutadiene, the polybutadiene will separate from the polystyrene

into little spherical blobs (Figure 1.4). The rubbery nature of these polybutadiene blobs improves the brittleness of polystyrene. This immiscible blend has more ability to bend instead of breaking than regular polystyrene. Immiscible blends of polystyrene and polybutadiene is commercially known as high-impact polystyrene, or in short HIPS. Another example is acrylonitrile-butadiene-styrene (ABS) terpolymers, which are basically styrene-acrylonitrile (SAN) block copolymers toughened with either polybutadiene or a polystyrene-polybutadiene copolymer. The combination of nylon-6 as the matrix with poly(ethy-lene terephthalate) as the minor component and the combination of nylon-6,6 with poly(hexamethylene isophthalamide) are use as fibres in car-tyre manufacture. In both cases the incorporation of the minor component raises the modulus and reduces the tendency to 'flat-spotting' of the tyres on standing.[21]

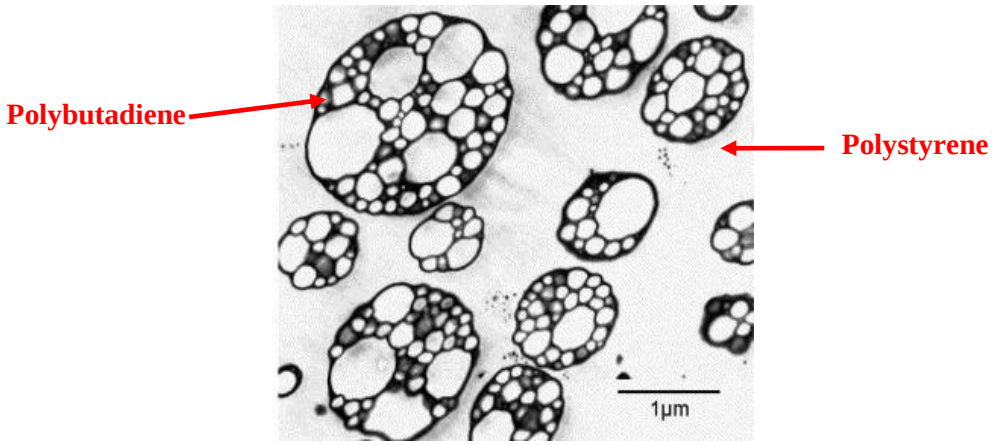

Figure 1.4: The phase morphology of HIPS (TEM image)[22]

1.1.3. Choices of polymer pairs

Generally more expensive polymer is combined with the less expensive polymer to provide adequate performance at a significant low price. Crystalline polymers have excellent chemical resistance, good mechanical properties, low viscosity whereas amorphous polymers provide good dimensional stability and excellent impact strength. So crystalline and amorphous polymers are blended to achieve a specific property range. This combination results in a polymeric material of good dimensional stability,

chemical resistance, mechanical properties and easy processing, High-density polyethylene (HDPE) is a highly crystalline polymer with a good combination of stiffness, strength and toughness suitable for most packaging applications. When it is blended with polyisobutylene the toughness, puncture resistance and environmental crack resistance has increased.[8]

Polymers are blended with elastomers. This combination gives the necessary stiffness, thermal resistance and strength. Blend of poly(vinyl chloride) (PVC) and butadiene-acrylonitrile (nitrile rubber, NBR) has been commercially available from 1940. The addition of butadiene-acrylonitrile elastomer to PVC yields permanently plasticized PVC resistant to plasticized migration and it is utilized for wire insulator, pollution control pond liner, fuel house covers etc.[23]

1.1.4. Classification of polymer blends

Polymer blends are either homogeneous or heterogeneous. In homogeneous blends the blend mixed homogeneously and the final properties of the blend are the average of both blend components. In heterogeneous blends, the blend components remain phase separated and the properties of all the blend components are present. Depending on the degree of mixing of the components, the polymer blends are divided into three categories: miscible blend, immiscible blend and partially miscible blend (Figure 1.5).[11]

Figure 1.5: Schematic diagram of miscible and immiscible blend formation.

In miscible blends the constituent polymers mix on a molecular level, to form a homogeneous material equivalent to a polymer-polymer solution. In this type of blend the final polymer exhibits properties somewhere in between the property of the

constituent polymers. The property of the blend depends on the fraction of each component.

In immiscible blends the constituent polymers do not mix, but remain in separate phases, leading to the formation of a dispersion of one of the polymers in a continuous matrix of the other. However, in an immiscible blend the property of the final polymer blend depends on the spatial arrangement of the phases (morphology), and the nature of the interface between them.

In partially miscible blend, a part of one component is dissolved in the other. This type of blend exhibits fine phase morphology and satisfactory properties.

1.1.5. Compatibilizers

Compatibilizers can be used to make immiscible blend stronger. Compatibilizer is anything that helps in bonding the two phases to bind each other more tightly. Mostly compatibilizers are block copolymer of the two component of the immiscible blend. Block copolymer tie the two phases of immiscible blend together and allow energy to be transferred from one phase to others.[9]

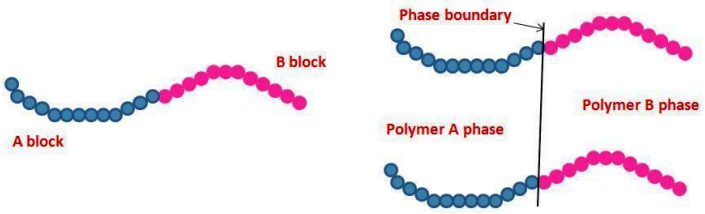

Figure 1.6: Schematic diagram showing compatibilization of an immiscible blend by a copolymer. (Adapted from Figure 19)

In immiscible blend the constituent polymers show a strong tendency for separation which leads to a coarse structure and low interfacial adhesion. In this case the final material shows poor mechanical properties. By controlling the structure formed by polymers in immiscible blend, the final property of the blend can be tuned.

Two methods are used for compatibilization of immiscible polymers:

(i) Incorporation of suitable block or graft copolymer: In this method block or graft copolymer are added along with the constituent polymers during blend synthesis. For example styrene-butadiene block copolymers and styrene-hydrogenated butadiene analogues are used for compatibilization of styrene polymers with polyolefins[24] or ethylene-propylene copolymers for compatibilization of various polyolefins.[25]

(ii) Reactive compatibilization: In this process the graft or block copolymers acting as compatibilizers are generated in situ during melt blending.[26] These copolymers are formed at the interfaces between suitably functionalized polymers and they link the immiscible phases by covalent or ionic bonds. This method avoids the transfer of compatibilizer to interface of the polymer blend.

1.1.6. Methods of preparation of blends

Generally Polymer blends are prepared by using following methods. These methods are described briefly here.

(i) ***Solution casting method:*** Solution blending is frequently used for the preparation of polymer blend on a laboratory scale. In this method the polymers are dissolved in a common solvent and vigorously stirred. Then film cast, coagulated, spay dried or freeze dried to collect the blend. The main advantages of this method are rapid mixing of the blend components and the unfavorable chemical reactions can be avoided. The disadvantage is that this method is expensive because of the use of solvent.[15] Also this method relies on the choice of the solvent and mostly depends upon the solubility of the two polymers in one common solvent. Therefore, this method cannot be applied for all kinds of polymer pairs.

(ii) ***Melt mixing method:*** In this method the polymers are heated above their glass transition temperature and they are mixed in their molten state in extruders or batch mixers. This method is an industrial method of preparation of blend polymer. The advantages of this method are well defined components and the same extruders or batch mixers can be used for a wide range of polymers. High energy consumption and

possible unfavorable chemical changes in the blend component are the main disadvantages of this method.

(iii) ***In situ blending:*** In this method in presence of one polymer the other component polymer is polymerized. Impact polystyrene and ABS are usually prepared by polymerizing styrene or styrene acrylonitrile in presence of a high molecular weight rubber.

1.1.7. Characterization of polymer blends

The miscibility of polymer blends can be confirmed by measuring the glass transition temperature (T_g). Calorimetric method is used for the characterization of polymer blends. Differential scanning calorimetry is typically employed for these studies. Miscible blend exhibits only one glass transition temperature (T_g) which is between the T_g's of both blend components and composition dependent.

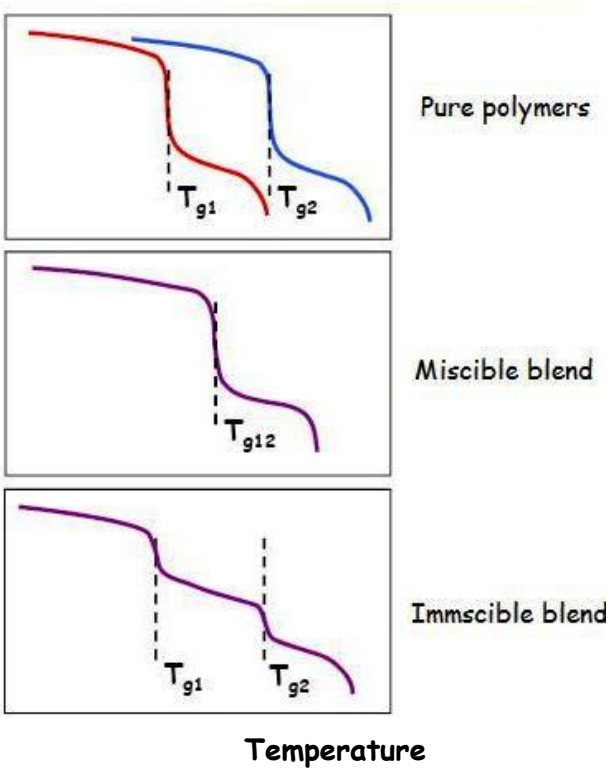

Figure 1.7: T_g of pure polymer, miscible and immiscible polymer blend.[27]

Immiscible blend shows more than one T_g because they possess more than one phase and each phase undergoes its glass transition at unique temperature corresponding to its composition.[28,29]

Partially miscible blend also exhibits two T_g's. In this type of blend the phase separated domains may contain some fraction of the component. Both blend phases (one being rich in polymer 1, the other phase being rich in polymer 2) are homogeneous. Both T_g's are shifted from the values for the pure blend component towards the T_g of the other blend component.[28] In other words T_g of this type blend are composition dependent. Figure 1.7 depicts the changes in T_g for various type of blend.

The miscibility of the polymer blend can be characterized by different techniques such as thermal analysis, dynamic mechanical analysis, inverse gas chromatography, electron microscopy, viscosimetry etc.[28]

For miscible blend the glass transition temperature as a function of weight fraction can be predicted by different equations. Fox's equation, Gordon-Taylor equations are used in the estimation of the miscibility of polymer blends.

The Fox's equation is given as follows

$$\frac{1}{T_g} = \frac{W_1}{T_{g1}} + \frac{W_2}{T_{g2}} \qquad (1.9)$$

The Gordon-Taylor equation can be used to evaluate the dependency of T_g on the blend composition.

$$T_g = \frac{W_1 T_{g1} + kW_2 T_{g2}}{W_1 + kW_2} \qquad (1.10)$$

where W is the weight fraction, T_g is the glass transition temperature of the blends, T_{g1} and T_{g2} are those of the pure components and k is an adjustable fitting parameter (Gordon-Taylor constant) that describes the strength of the intermolecular interaction between the components in miscible polymer blends: the lower the value of k the poorer is the interaction.[30]

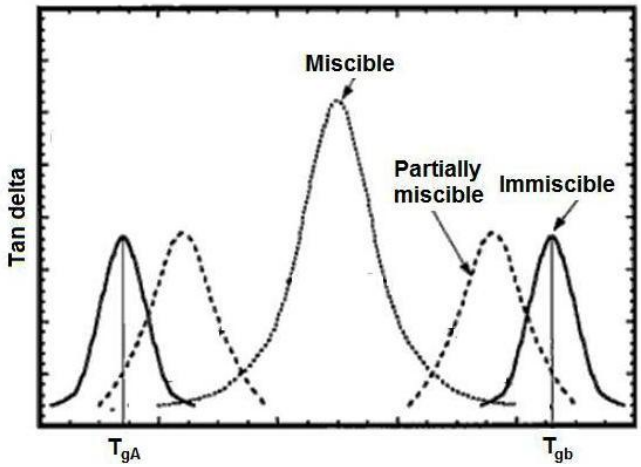

Figure 1.8: Generalized Tan δ behavior of polymer blends.[31]

Dynamic mechanical method (Figure 1.8) is also used to determine the miscibility of polymer blends. If the polymer blend is miscible then it will show a well defined single tan δ relaxation. The immiscible blend exhibits T_g of the component polymers. The immiscible blend possesses T_g's shifted inward due to incorporation of minor concentration of the other polymer constituent. This method is more sensitive than calorimetric method because it can observe low concentration of specific phases in polymer blend. In case of partially miscible blend the T_g's of both components shifted from the parent T_g and this shift is composition dependent.

1.1.8. Importance of blends

Polymer blending is an attractive route to produce new material with desired properties. But it has both advantages and disadvantages. Some of its advantages and disadvantages are listed below.

Advantages:

- The main advantage of polymer blending is that using this technique existing polymers can be combines into new material with commercializable properties which are not easily obtained with new polymeric structures.

- It offers the advantage of reduced research and development expense compared to the development of new monomer and polymers to yield a similar property profile.
- Blends can be formulated, optimized and commercialized generally at a much faster rate than new polymer.
- The toughness of brittle polymers can be improved and this eliminates the use of low molecular weight additives e.g. plasticizer in the flexible PVC formulations.

Disadvantages:

- Polymer blending is a trial and error method. Sometimes properties may not improve at all.
- Sometimes improvement of one property leads to deterioration of another property.
- Long term properties of polymer blends and environmental stress are strongly influenced by coreactivity between individual component polymers. The final effect on the lifetime of blends is difficult to predict on the basis of known behaviour of individual polymers.[32]

1.2. Polymer nanocomposites

Nanomaterials are recognized as unique because they show quantitatively new behavior when compared with their macroscopic counterparts.[33] Different nanofillers such as buckyballs, carbon nanotubes, clays, silica particles, graphene are used to prepare polymer nanocomposites.[35-38] In recent years polymer nanocomposites have attracted the interest of many scientists because of their unique properties and many applications. Polymer nanocomposites have attracted great attention worldwide academically and industrially due to the exhibition of superior properties such as increased strength and heat resistance, decreased gas permeability and flammability, and increased biodegradability of biodegradable polymers.[39-43] Small amount of nanocfillers can significantly improve the property and performance of the material compared to

pristine polymer due to following properties of nanofillers: (i) low percolation threshold (ii) particle-particle correlation (orientation and position) arising a low volume fraction (iii) large number of density of particles per particle volume (iv) extensive interfacial area (communication between matrix and filler) per volume of particles.

The final properties of nanocomposites are strongly dependent on the dimension and micro structure of the filler phase. Uniform dispersion of nanofillers can lead to large interfacial area between the constituents. In addition the distance between the nanoelements begins to approach molecular dimension at extremely low loadings of the nanofillers.[44] Depending on the nature of the nanofillers used and the method of preparation, significant differences in composite properties may be obtained.[45] Nanofillers can be divided into three categories depending on the number of dimensions of their nanometer size, i.e., one dimension, two dimensions, and three dimensions as shown as Figure 1.9.

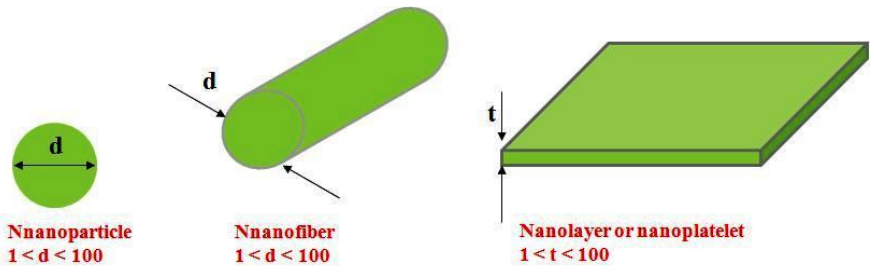

Figure 1.9: Schematic diagram showing different types of nanofillers.[34]

1.2.1. Polymer nanocomposites preparation and properties

In general there are three preparation methods including in situ polymerization, solution mixing and melt mixing. In situ polymerization[46] involves the dispersion of nano fillers in the monomer followed by polymerization. In solution mixing method[47,48] polymer is dissolved in a solvent and the nanofiller is dispersed in the same solution. In melt mixing method nano filler is mixed within the polymer matrix in molten stage. The

conventional methods such as extrusion and injection molding are used for dispersion of nano filler within the polymer matrix.

Nanofillers, also known as reinforcement agent, are added to the polymer matrix to improve the polymer properties so that it can fulfil the desired properties. The first and important aim of addition of nanofillers into the polymer is to improve the mechanical properties of the polymer.[49] The mechanism of the reinforcement is based on the higher resistance of rigid filler materials against straining due to their higher module. When a rigid filler is added to the soft polymer matrix, it will carry the major portion of applied load to the polymer matrix under stress conditions, if the interfacial interactions between filler and matrix is adequate.[50,51] Nanofillers improve the thermal stability of the polymer. This is because of the reason that nano filler act as insulation and mass transport barrier against the volatile compounds generated during the decomposition of polymer under thermal conditions.[52] Vyazovkin et al.[53] reported that the thermal stability of polystyrene/clay nanocomposite compared to pure polystyrene is 30-40°C higher degradation temperature compared to pure PS under nitrogen and air heating degradation conditions. Nanofillers also decrease the ignition property of the polymer. This is very important because polymers are especially use in domestic applications so there is need to reduce their potential for ignition in order to make them safer in applications. Polymers are widely used as anticorrosive coatings on metals to prevent the corrosion. Primarily polymeric coatings act as physical barrier against the diffusion of aggressive species to the metal surface. Addition of nanofillers such as layered silicates, effectively improves the anticorrosive barrier effect of polymer coatings by increasing the length of the diffusion pathways for aggressive species. Sandip et al. prepared polymer nanocomposites of poly (4,4'-diphenylether-5,5'-bibenzimidazole) (OPBI) with two structurally different organoclays, namely, montmorillonite (OMMT) and kaolinite (OKao).[36] The incorporation of nanoclays in OPBI results in an increase in mechanical, thermal and oxidative stabilities. Also the proton conductivity of all the nanocomposite membranes increases with increasing caly content in the polymer. In another study Sandip et al. incorporate OPBI with unmodified silica (UMS) and amine modified silica (AMS). They observe significant

improvement of mechanical, thermal and oxidative stability. The proton conductivity is also improve significantly compare to neat OPBI.[39]

1.3. Graphene

Among varities of nano filler graphene is the latest one. Graphene is the basic structural unit of carbon allotropes including graphite, carbon nanotubes and fullerenes (Figure 1.10). Graphene is a two-dimensional carbon sheet with one molecular thickness and sp^2-hybridized carbons covalently bonding in honeycomb structure. The term graphene was coined by Hanns-Peter Boehm[54,55] who described single-layer carbon foils in 1962. The carbon-carbon bond length in graphene is about 0.142 nm.[56] Graphene sheets stack to form graphite with an interplanar spacing of 0.335 nm. Graphene is the building block of graphite.[57] Graphene was first isolated in 2004 by physicists Andre Geim at the University of Manchester and the Institute for Microelectronics Technology, Chernogolovka, Russia by using adhesive tape.[55]

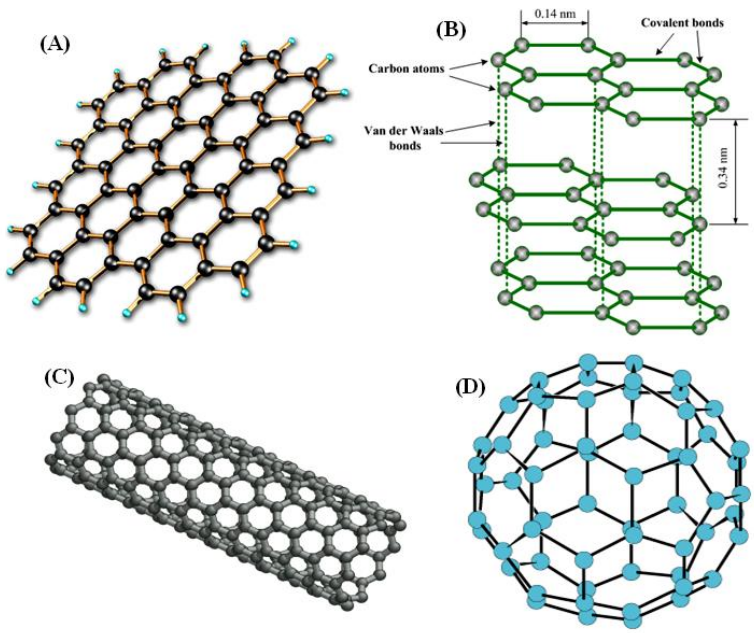

Figure 1.10: Allotropes of carbon, (A) graphene (B) graphite (C) carbon nanotube and (D) fullerene.[58]

Graphene has attracted tremendous attention in recent years because of its exceptional thermal, mechanical and electrical properties.[59,60] It has wide range of applications in various fields such as energy devices,[61,62] catalysts,[63,64] sensors,[65,66] conductive materials,[67,68] drug delivery[69,70] and polymer nanocomposites,[71,72] ultracapacitor[73] etc. The electrons in graphene obey a linear dispersion relation and behave as mass less relativistic particles.[74] Because of this property it results a number of very peculiar electronic properties such as the quantum hall effect,[75,76] ambipolar electric field effect,[77,78] good optical transparency[79,80] and transport via relativistic Dirac fermions[75,81] It also has high carrier nobilities (200000 cm^2/Vs). Since graphene consist of a single sheet of sp^2 carbon atoms, it can undergo a wide class of organic reactions. It can incorporate into polymers and inorganic systems to enhance mechanical strength, thermal and electrical conductivity.

1.3.1. Synthesis of Graphene

Recently, many studies have been reported on the synthesis of graphene. These include chemical vapor deposition,[82] micro-mechanical exfoliation of graphite,[83] epitaxial growth on silicon carbide[84] and chemical or thermal reduction of graphene oxide.[85] briefly these methods are as follows:

Chemical vapor deposition (CVD): CVD is a technique of thin solid film deposition on substrates from the vapor species through chemical reactions. There are many CVD variations. Thermal CVD is generally applied to graphene formation over transition metals such as copper, nickel iridium and ruthenium.[86]

Micro-mechanical exfoliation of graphite: This method involves peeling of the graphene from graphite using scotch tape.[77] After peeling the tape is dipped in acetone to release the graphene which is captured on a silicon wafer with a SiO_2 layer on top. This method is unfavorable for large scale synthesis.

Epitaxial growth on silicon carbide: In this method silicon carbide (SiC) is heated at high temperature (1100°C) to reduce it to graphene. In this process epitaxial graphene with dimensions dependent upon the size of the SiC substrate (wafer) is produced.

Chemical or thermal reduction of graphene oxide: This method is useful to prepare bulk quantity of graphene. Graphite oxide (GO) can be easily exfoliated by ultrasonication. Exfoliated graphite oxide is known as graphene oxide (G–O). So chemical reduction of G–O with reducing agents like hydrazine hydrate or hydrazine derivatives will convert the electrically insulating G–O layers to conducting graphene. However, the quality of graphene produced by graphite oxide reduction is lower compared to e.g. scotch-tape graphene due to incomplete removal of various functional groups by existing reduction methods. The reduction can be done by thermally also. This involves rapidly heating of heating of G–O in inert atmosphere to produce thermally reduced expanded graphene oxide which is a black powder of bulkdensity.[87-89] The main problem associated with this method is that when exfoliated G–O nanoplatelets are reduced, after reduction there is a probability of their irreversible coagulation which cannot be re-dispersed with prolonged ultrasonnication.[90,91] To overcome this problem reduction of G–O is carried out in presence of polymer/polymeric anions. This results in a stable polymer grafted dispersion of graphene.[92] Chemical reduction of G–O dispersions in presence of poly(sodium 4-styrenesulfonate)[93] or pyrene butyrate[94] results in stable aqueous suspension of coated graphene monolayers. Stankovich et al. prepared stable aqueous dispersions of polymer-coated graphitic nanoplatelets via an exfoliation of GO and followed by in-situ reduction of graphite oxide in the presence of poly(sodium 4-styrenesulfonate).[93] Hao et al prepared an aqueous dispersion of graphene from expanded graphite using 7,7,8,8-tetracyanoquinodimethane (TCNQ) anion as a stabilizer. With this route they prepared high quality water soluble and organic solvent soluble graphene sheets for a range of applications.[95] Wang et al. prepared graphene by annealing GO thin films at different temperatures and showed that the volume electrical conductivity of the reduced GO film obtained at 500°C was only 50 S/cm, while for those at 700 °C and 1100°C it could be 100 S/cm and 550 S/cm.[96]

In chapter 6 we have discussed the synthesis and characterization of sulfonated polystyrene (SPS)-graphene nanocomposites. The nanocomposites are prepared by reducing G–O in presence of SPS particles. We have seen that in absence of SPS

particles, after reduction the G–O layers are agglomerated and went back to layered structure.

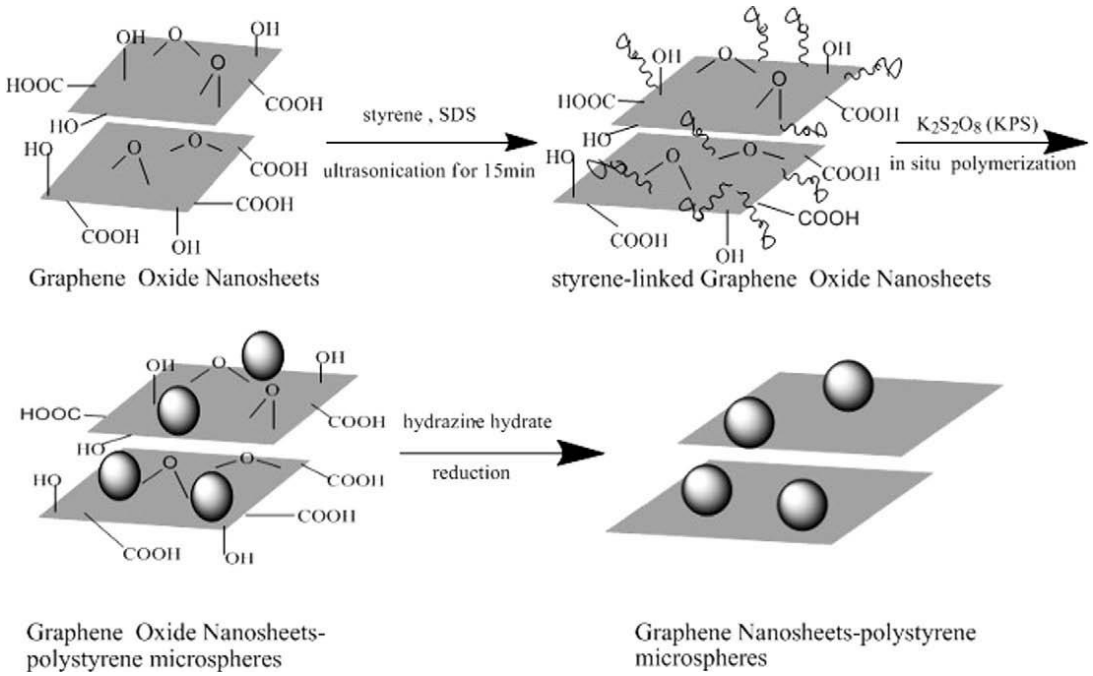

Figure 1.11: Schematic diagram showing formation of SPS-graphene nanocomposites.[97]

1.3.2. Polymer-Graphene nanocomposites

The development of a nano-level dispersion of graphene in a polymer matrix has opened a new and an interesting area of research in recent years. Polymer-graphene nanocomposites have attracted considerable attention due to their unique properties such as excellent mechanical, optical and electrical properties. The extent of improvement in properties is directly related to the degree of dispersion of graphene. There are many studies on polymer-graphene nanocomposites are reported which includes polystyrene-graphene, polyurethane-graphene, polyethylene-graphene, Poly(methyl methacrylate)-graphene etc.[97-99] Hu et al prepared graphene nanosheets- polystyrene (PS) nanocomposites via in situ polymerization and reduction of GO using hydrazine

hydrate.[97] They have shown that the nanocomposites have high thermal stability and high glass transition temperature than PS. The electrical conductivity of PS increases from 1.0×10^{-10} Scm^{-1} to 2.9×10^{-2} Scm^{-1} for nanocomposites containing 2 wt% graphene. In another study Zhou et al prepared poly (vinyl alcohol) (PVA)/graphene nanocomposites by reducing PVA/GO nanocomposite films in aqueous medium.[100] The observed a 40% increase in tensile strength and 70% improvement in elongation at break with 0.7 wt% of reduced GO. In another report Al-Mashat et al report the synthesis of a graphene-polyaniline (PANI) nanocomposite and its application in the development of a hydrogen (H_2) gas sensor. They observed that graphene-PANI nanocomposite-based device sensitivity is 16.57% toward 1% of H_2 gas, which is much larger than the sensitivities of sensors based on only graphene sheets and PANI nanofibers.[101]

There are various synthetic routes for the preparation of polymer-graphene nanocomposite. Many of these procedures are similar to those used (as discussed in section 1.3.1) for other polymer-nanocomposites.

1.4. Sulfonated Polystyrene (SPS)

The partially or lightly ionized polymers (known as ionomers) recently attracted great technological and scientific interest due to their unique properties such as hydrophilicity, and proton conductivity arise from the incorporation of ionic functional groups into hydrophobic polymers.[102] Sulfonated polystyrene (SPS) or polystyrene sulfonic acid (PSSA) is an ionomer based on polystyrene. Ionomers are normally defined as ion-containing polymers with a maximum ionic group content of about 15 mol % or less.[103,104] The ionomer possesses both covalent hydrocarbon polymeric chains and ionic salt species in the same molecule.[103] SPS is the most widely used ionomer in the literature (Figure 1.12). Ionomers are utilized in a wide range of applications such as adhesives, fuel cell membranes, catalysis, water purification systems, synthesis of magnetic particles, chromatography techniques and ion exchange resins.[103,105,106]

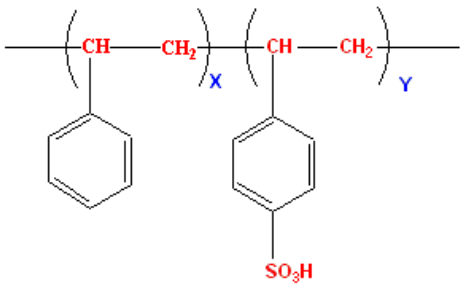

Figure 1.12: Chemical structure of sulfonated polystyrene

1.4.1. Synthesis of Sulfonated Polystyrene

In general, two routes were referred in the literature for the preparation of SPS and these are (i) direct emulsion copolymerization of styrene and sodium styrene sulfonated. (ii) Heterogeneous sulfonation i.e. sulfonation of preformed polystyrene (PS) using sulfonating agent.

In direct copolymerization method it is difficult to assure a random distribution of sulfonated groups.[107] But the advantage of this method over sulfonation of PS is that it avoids problems with solvents and the separation of the sulfonated product from the reaction mixture.[108-112] Another advantage of this process is that sulfonation proceeds without polymer degradation and cross linking.[113,114] Arunbabu et al. prepared a series of poly[styrene-*co*-(sodium styrene sulfonate)] copolymers containing various sodium styrene sulfonate (NaSS) loadings using emulsion polymerization technique. They have studied the effect of NaSS content in the reaction on copolymer kinetics.[110] In another study Yeole et al. prepared polystyrene sulfonated-sodium (PSS–Na) based macro-RAFT agent having thiocarbonyl thio end group in water medium. Using this hydrophilic PSS–Na based macro-RAFT agent they polymerized styrene by surfactant free emulsion polymerization.[111]

Sulfonation of preformed polystyrene has several advantages such as (i) sulfonation of the preformed polymer yields a random distribution of sulfonate groups along the polymer chain; (ii) a minimum of chain to chain heterogeneity is expected from this process; (iii) the reaction sulfonation proceeds without any significant

polymer degradation and (4) the characterization of SPS can be simplified by using polymers with narrow molar mass distributions.[115,116] PS can be sulfonated by different sulfonating agents, such as concentrated sulfuric acid, acetyl sulfate, and chlorosulfonic acid and SO_3 etc. The first studies on sulfonation of PS were published before World War II. PS was first sulfonated in a homogeneous phase by a method developed by Turbak[117] via reacting PS with trialkyl phosphate complex of sulfur trioxide as sulfonating agent in dichloroethane. Makowski et al.[118] also prepared lightly sulfonated polystyrene by using acetyl sulfate complexes as sulfonation reagent in a solution of dichloroethane.

The properties of SPS prepared by copolymerization differ considerably from SPS prepared by sulfonating preformed PS. In one report Weiss et al. compared the SPS ionomers prepared by copolymerization with ionomers of identical composition prepared by sulfonation of PS. Specific differences include the solubility behavior, the effect of sulfonate concentration on the T_g and the equilibrium hydration and sorption kinetics.[119] The difference in the sulfonate distribution is the reason for these property differences between the SPS prepared by copolymerization and SPS prepared by sulfonating preformed PS.

In chapter 2 we have discussed the effect of the influence of sulfonation reaction time, temperature and the parent polystyrene (PS) particle size on the degree of sulfonation (DS), ion exchange capacity (IEC), morphology and glass transition temperature (T_g) of sulfonated polystyrene (SPS) particles. SPS particles were prepared by sulfonating PS particles using sulfuric acid as sulfonating agent. [120]

1.4.2. Properties and application of sulfonated polystyrene

SPS has received considerable attention recently because of the scientifically interesting and potential technologically important properties arise from its ionomer characteristics. SPS has wide range of applications in numerous areas, e.g. drug delivery applications, catalysis, humidity sensors, as membranes for reverse osmosis, ion exchange materials and chromatography techniques etc.

Hydrated SPS exhibits high proton conductivity and has been used as a polymer electrolyte in proton exchange membrane fuel cells.[121,122] In the early 1960s Gemini space program were using sulfonated polystyrene-divinylbenzene copolymer membranes cells which were extremely expensive and had short lifetimes due to the oxidative degradation of the membrane. This is the first membrane which is used as PEM in fuel cell.[122] Ding et al. studied a model system where a sulfonated graft polymer composed of a PS backbone and a SPS side chain was synthesized via free-radical polymerization.[123,124] The copolymer with the longer graft chain exhibited higher proton conductivity. However, the commercial applicability of the fabricated grafted copolymers was limited, due to the poor stability of the styrene-based backbone and side chain.

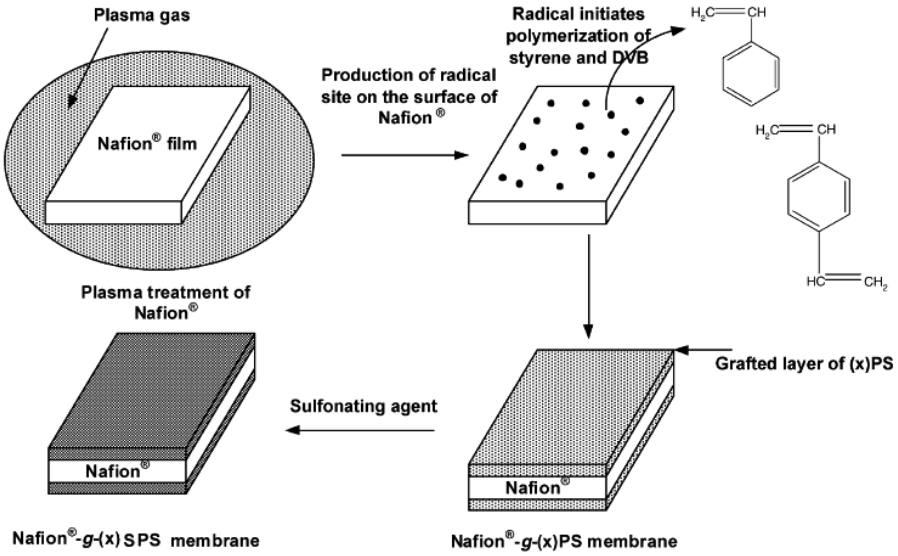

Figure 1.13: Schematic diagram showing preparation scheme of the Nafion-*g*-SPS membrane.[127]

Göktepe et al. developed novel proton conductors by doping SPS with 1H-1,2,4-triazole (Tri) and 1.12-diimidazol-2-yl-2,5,8,11-tetraoxadodecane (imi3). The maximum conductivity they could measure is 0.016 S cm^{-1} at 150°C.[125] Homogeneuosly SPS was prepared with various concentrations of sulfonic acid groups by N. Carretta and co

workers. They have found that membranes cast from some of these SPSs exhibited proton conductivity equal to that of Nafion membranes, which can be used in electrochemical devices. They also found that even at the highest degree of sulfonation, the methanol permeability of SPS is comparatively 70% lower than that of Nafion membranes. That is attractive particularly in relation to the methanol fuel cell technology.[126] In another study Nafion®-*graft*-SPS membranes (Figure 1.13) were prepared to reduce its methanol permeability in applications involving direct methanol fuel cells. The equilibrium water uptake, proton conductivity and methanol permeability were affected by both the extent of the grafting reaction and the cross-linking density. The SPS layers that were grafted reduced the methanol permeability of the membranes significantly.[127]

Many literatures of SPS blends as PEM for fuel cell are reported. Jung et al. prepared the blend of SPS with partially sulfonated poly(2,6-dimethyl-1,4-phenylene oxide) (sPPO) membranes for direct methanol fuel cell. The blend membranes exhibited relatively higher proton conductivity and methanol permeability than the neat polymers (SPS and sPPO).[128] SPS is also used as a template for synthesis of composite materials with hollow nano structures and core-shell structures (Figure 1.14). A general template synthesis approach towards composite hollow spheres using sulfonated polystyrene gel hollow spheres was proposed by Yang et al. Using this method many materials such as metal Pd nanoparticles, magnetite Fe_3O_4 nanocrystallites, conducting polyaniline, and inorganic titania and silica particles can be prepared. Hollow inorganic particles are obtained after the template (SPS) is calcined.[129-131] Zhang et al. prepared hollow polyaniline (PANI) and hollow polypyrrole (PPY) microspheres in the size of range 2.2–3.4 μm in diameter using SPS as template.[132] The template particles (SPS) were prepared by sulfonating PS microspheres. Aniline or pyrrole was oxidatively polymerized on the surface of SPS. SPS cores were removed from core-shell particles by dissolving it in dimethylfomamide.

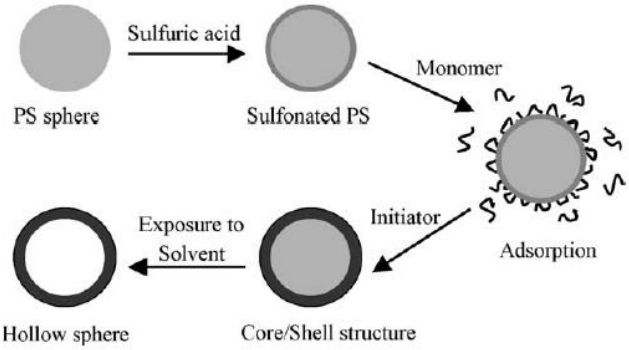

Figure 1.14: Schematic diagram for the fabrication of hollow spheres.[132]

1.5. Polybenzimidazoles (PBIs)

Polybenzimidazoles (PBIs) is an aromatic heterocyclic polymer. In order to fulfill the thermal stability requirement for heat-resistant plastic for high temperature and military applications aromatic heterocyclic polymers were introduced at the beginning of 1960s. Brinker and Rabinson invented the first aliphatic PBIs in 1959 3,3',4,4'-tetraaminobiphenyl and aliphatic diacids or derivatives. After two years in 1961 Vogel and Marvel at the University of Illinois with expectation that the polymers would have exceptional thermal and oxidative stability developed aromatic PBIs with impressive thermal properties for the U.S. Air Force.[133-136] Since then high performance PBIs received great attention in academic and industry. The fundamental research work on PBI in the early stage of development was carried out in Dupont and Hoechst Celanese Research Co by NASA and U.S. Air Force Materials Laboratory.[137,138] In 1967 NASA chooses PBI as a clothing for stronauts, fighter pilots and aerospace cabin accessories because of its superior thermal protective performance after a fire aboard an Apollo spacecraft killed three astronauts in 1967. Many aromatic variants of PBI have been prepared and investigated since their first synthesis in 1961. But poly[2,2'-(m-phenylene)-5,5'-bibenzimidazole] (Figure 1.15) is used in all commercial and most developmental applications. It was commercialized for the first time in the year 1983 by Celanese for the use in wide range of textile fibers.

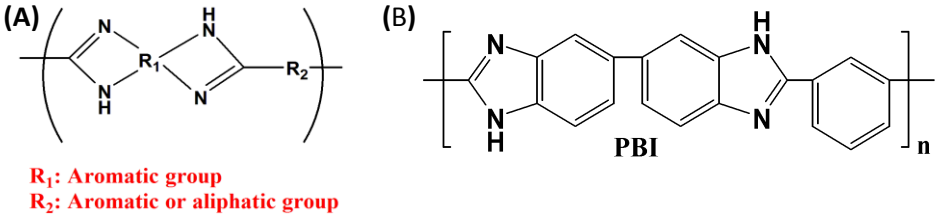

Figure 1.15: Chemical structure of (A) General PBI (B) poly[2,2'-(m-phenylene)-5,5'-bibenzimidazole]

Polybenzimidazoles are family of aromatic heterocyclic polymers with benzimidazole as a repeating unit. It has excellent thermal stability as well as flame retardation property, radiative stability, excellent mechanical, thermal stabilities, and strength retention over wide range of temperatures, toughness, chemical inertness and adhesion characteristics.[133,134] PBI is being used for various applications, in particular, for high temperature applications, fibre spinning, and reverse osmosis membranes, because of its excellent thermal-chemical tolerance and film forming capability. It is also to fabricate high-performance protective apparel such as firefighter turnout coats and suits, astronaut space suits, high temperature protective gloves, welders' apparel, race driver suits, braided packings, and aircraft wall fabrics. Recently, phosphoric acid (PA) doped PBI membrane was found to be the most promising material to use as polymer electrolyte in high-temperature proton exchange membrane fuel cell (PEMFC).

1.5.1. Properties of Polybenzimidazoles

The PBI powder is generally yellow to brown colour solid. It is an amorphous polymer with very high glass transition temperature (450°C).[133,136,139,140] Among different variants of PBI, poly [2,2'-(m-phenylene)-5,5'-bibenzimidazole] has received much attention academically and commercially. It is most commonly known as *m*-PBI. PBIs are soluble in aprotic solvents such as N,N-dimethyl sulfoxide, N,N-dimethyl formamide, N,N-dimethyl acetamide, N-methyl pyrrolidone and hexamethyl phosphoramide.[133,136,139,140] PBI is hygroscopic and it can absorbers 5-10% of its weight

moisture.[139,141] The thermal stability of PBI has been extensively studied by thermogravimetric analysis (TGA) and mass spectrometry (MS) of the purge gas from the TGA. Most of the aromatic polybenzimidazoles are thermally stable up to 600°C.[133] When it is kept several hours at 600°C in nitrogen only 5% weight loss is observed. At 100-120°C 5% wt loss is observed which is due to loosely bound water molecules associated for hygroscopic nature of the polymer.[139,141] PBI exhibits the highest compressive strength (390 MPa) known for any available unfilled thermoplastic or thermoset resin. In addition, the tensile strength of PBI (160 MPa) is higher than most unfilled thermoplastics. Flexural strength and modulus are also very high. PBI has the greatest surface hardness of any known molded thermoplastic.[142] PBI exhibits excellent chemical resistance to most organic chemical systems. Its mechanical properties or dimensional stability is not affected upon exposure to aerospace related environments such as kerosene, Skydrol hydraulic fluid, engine oils or methylene chloride.[142] PBI is highly stable to hydrolysis and are not attacked by hot strong sulfuric acid solutions or hot 25% potassium hydroxide solutions. The disadvantages of this polymer includes its high cost, difficult processing conditions (high temperature, high pressure, evolution of volatiles) and its unreprocessability.[143] PBI shows polyelectrolyte behaviour when doped with acids. Phosphoric acid doped PBI membrane is use as polymer electrolyte membrane in fuel cell.[144,145]

1.5.2. Application of polybenzimidazoles in fuel cell

Fuel cells are energy conversion devices, which convert the chemical energy stored in a fuel directly into electrical energy.[146-148] They have higher conversion efficiency and less emission compared to the traditional combustion engines. When pure hydrogen and oxygen are used as fuel and oxidant respectively, zero emission could be achieved as water is the only product in the reaction. Fuel Cells have attracted great attention as one of the most promising candidates for the power generators for both stationary and transportation applications. A fuel cell operates like a battery. Unlike a

battery which is an energy storage device, a fuel cell does not run down or require recharging.[149]

A fuel cell consists of a positive electrode (cathode), a negative electrode (anode), and an ion-conducting electrolyte.[147,148] The production of electricity by the fuel cells involves the oxidation of a fuel (e.g. H_2) and the reduction of an oxidant, which are fed, respectively, into the anode and cathode compartments. This process generates ion flow through the electrolyte and electron flow through the external circuit. Unlike a battery, a fuel cell can continue to provide power as long as the fuel and oxidant are available. The electrolyte acts as a physical barrier between hydrogen and oxygen to prevent directly mixing but conducts ionic charge between the electrodes and thereby completes the cell electric circuit.

Among varieties fuel cell polymer electrolyte membrane fuel cell (PEMFC) has attracted great research attention in recent years. The polymer electrolyte membrane (PEM) acts as a proton carrier from anode to cathode and completes the cell electrical circuit. It also provides a physical barrier from direct mixing of fuel (H_2) and oxygen gas. To show better performance in fuel cell the PEM should have some desires properties which are as follows: high proton conductivity, high mechanical, thermal and chemical stability, low gas permeability, good film-formation capacity, low cost, capable of fabrication into membrane electrod assembly (MEA), mechanical durability at high temperature (80-140°C).[150-152]

Perfluorinated polymer such as nafion and dow are widely used as PEM for low temperature fuel cell applications due to high proton conductivity and excellent chemical and thermal stability.[150] Their proton conductivity is depend on the presence of water. But the drawback of these polymers is that they cannot operate at high temperature (above 80°C).[153,154] They require complicated or expensive water management system for operating at 80°C or higher.[155] PA doped PBI membranes have many advantages in comparison with Nafion and these include: (i) high proton conductivity at temperatures up to 200^{o}C (ii) low gas permeability (iii) excellent oxidative and thermal stability (iv) good mechanical flexibility at elevated temperatures (v) nearly zero water drag coefficient and etc.

1.5.3. Polybenzimidazole blends

PBI possesses both proton donor (–NH–) and proton acceptor (–N=) hydrogen bonding which exhibit specific interactions with polar solvents[156-158] and with a variety of polymers upon blending.[159-162] A wide range of polymers with variety of polar functional groups such as carbonyl, sulfonyl in their backbone form miscible blend with PBI and the miscibility arises due to the specific hydrogen bonding interaction between the functional groups of these polymers. A large number of PBI blends with variety of polymers are reported in the literature. Example includes polyimides (PI),[163] polyamideimide (PAI),[164] poly(4-vinyl pyridine) (PVP),[165] high-modulus aramide (HMA),[166] sulfonated poly sulfone,[67] Nafion.[168] Wycisk et al prepared the blend of PBI with nafion.[168] They have studied the dependence of membrane proton conductivity and methanol permeability on the extent of proton substitution of nafion during blending and on the PBI content of the final membrane. Recently our group has reported the blend of PBI with poly(vinylidene fluoride) (PVDF) and their potential to use as a proton exchange membrane in PEMFC.[169] The PA doping level of the blend membrane is high compared to that of pure PBI because the hydrophobic PVDF which inhibits the water uptake capacity of the membranes and hence allows the acid to interact more efficiently with the PBI backbone which leads to the higher PA loading. In this thesis, we are reporting PBI blends with sulfonated polystyrene, PVDF-HFP and PVT.

1.6. Poly(vinylidene fluoride-co-hexafluoropropylene) (PVDF-HFP)

Poly(vinylidenefluoride-co-hexafluoropropylene) flouropolymer and the chemical structure is shown in Figure 1.16. PVDF-HFP is a copolymer of Poly(vinylidene fluoride) (PVDF) which attracted much attention as a potential membrane material. Fluoropolymers have various drawbacks. Because of high crystallinity fluoropolymers are less soluble in organic solvents and are not easily cured or cross-linked. That is why copolymers are generated so that the disadvantages of the homopolymers are removed without destroying the properties.[170]

PVDF-HFP possesses lower crystallinity and higher free volume compare to PVDF due to the incorporation of the amorphous group hexafluoropropylene (HFP).[171] The mechanical property is greater than the neat PVDF. It also exhibits certain dielectric properties but lower than PVDF. Addition of HFP group also increases the fluorine content and makes PVDF-HFP more hydrophobic than PVDF.[172]

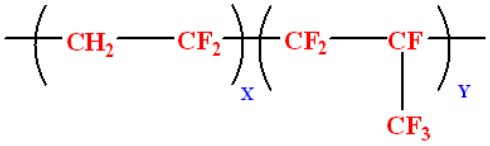

Figure 1.16: Chemical structure of PVDF-HFP

PVDF-HFP has also found various applications in different area because of its properties such as good film forming, high thermal and chemical stability. Cho et al. prepared Miscible PVDF-HFP/Nafion blend.[173] The hydrophobic nature of PVDF-HFP decreases the water uptake of the blend membranes resulting lower conductivity compare to Nafion. But methanol cross-over is reduced and an enhancement in cell performance is observed due to its improved compatibility with the electrodes. The PEMFC performances of PVDF-PSSA and PVDF-HFP-PSSA membranes have been reported by Saarinen et al.[174] PVDF-HFP has been shown to be a promising matrix for an electrolyte material in lithium ion batteries. It has high dielectric constant which facilitates a higher concentration of charge carriers. Though its crystallinity is lower than PVDF, it is sufficient to provide enough mechanical property to allow PVDF-HFP to act as a separator between the electrodes of battery. While the amorphous part of the polymer enhances the conductivity. PVDF-HFP copolymers can uptake more electrolyte solution than PVDF because of their lower degree of crystallinity.[171,175] Li et al prepared PVDF-HFP copolymer with narrow pore size distribution and low crystallinity.[176] The resulting polymer electrolyte shows a high ionic conductivity up to 1.76×10^{-3} Scm^{-1} at room temperature and exhibits low apparent activation energy of 10.35 kJ mol^{-1} for the transportation of ions. In another report Xu et al prepared porous PVDF-HFP membranes by solvent evaporation method using dibutyl phthalate (DBP),

polyvinylpyrrolidone (PVP- k30), polyethylene glycol 200 (PEG200) as additives. They investigated the influence of additives on morphology and structure, electrolyte uptake of porous membranes and lithium ionic conductivity of the activated membranes.[177] Other application of PVDF-HFP includes transducers for sensitive scientific instruments, electromechanical converters, actuators, ferroelectric memory devices and anticorrosive materials.[178]

Because of the presence of the fluorine atom it can form miscible blends with a variety of polymers. Many literatures related to PVDF-HFP blends are reported and these examples include PVDF-HFP/poly (vinyl acetate), PVDF-HFP/polystyrene, PVDF-HFP/ poly(vinyl pyrrolidone) etc.[179] Poly(ethyl methacrylate) (PEMA)/ PVDF-HFP blend polymeric gel films incorporated with lithium triflate salt is prepared by Arof et al. Polymer electrolyte sample with composition PEMA/PVDF-HFP [70:30]**:**$LiCF_3SO_3$**:**EC (65.8**:**28.2**:**6) has the highest conductivity of 1.05×10^{-4} S cm^{-1} at 298 K. The high conductivity is due to due to free ions dissociated from salt.[180] Xu et al. reported eport novel zinc ion conducting polymer electrolytes based on oligomeric polyether/PVDF-HFP blends with or without the incorporation of a small amount of organic carbonates. These blend electrolyte membranes exhibit very low volatility, high thermal stability, high ionic conductivity, wide electrochemical stability window, acceptable interfacial resistance with zinc, and the capability for reversible Zn plating/stripping. The ionic conductivity of these membranes is on the order of 10^{-4} S cm^{-1} at room temperature.[181]

1.7. Poly(1-vinyl-1,2,4-triazole) (PVT)

Poly(1-vinyl-1,2,4-triazole) (PVT PVTri; Figure 1.17) is a type of heteroaromatic polymer containing 1H-1,2,4-triazole. PVT is non-toxic, have a high hydrophilicity and high hydrolysis stability. PVT is biocompatible, thermally stable and easily soluble in polar solvents.[182] Because of these properties PVT are of particular interest and show promise for the food industry as well as for engineering and energetic materials.[183] PVT can synthesized by free radical polymerization of 1-vinyl-1,2,4-

triazole in polar solvents.[184] Monomers of PVT were first obtained by vinylation of 1,2,4-triazole with acetylene.[185]

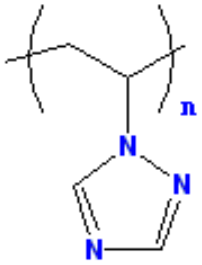

Figure 1.17: Chemical structure of PVT

PVT and its copolymers have found a wide range of applications in medicine and agriculture such as preparation of soft contact lenses, biosynthetic activation of connective tissue cells, clarification or stabilization of juices and wines.[186] PVT based salts are shown to be reliable binders in propellant and explosives as energetic polymers.[187] Abbas et al prepared water soluble PVT as novel dielectric layer for organic field effect transistors. PVT films showed considerably high breakdown voltage and low leakage current. They showed that PVT can be a very promising polymer dielectric for OFET devices, especially for ambipolar and light emitting OFETs. Its water solubility allows for a wide range of solution processed polymer based OFET devices.[187]

Recently acid doped PVT is a promising polymer for the design of proton-conducting membranes. In PVT three nitrogens are present in the ring. This may enhance long range proton diffusion which can be far better than imidazole based host polymer. 1H-1,2,4-triazole itself can conduct proton readily in anhydrous condition at higher temperature (> 100°C) via grothus mechanism as in imidazole. The proton conductivity of pure 1H-1,2,4-triazole is 1.5×10^{-4} S/cm (at 115°C) and ~1.2×10^{-3} S/cm (at the melting point).[188] The proton conduction for triazole-based systems is different from that for imidazole.[189] This is due to the presence of several proton-carrying isomers for triazoles. Therefore, triazoles can be doped into acidic host polymers and may improve the anhydrous conductivity of the materials in the dry

state.[190] Triazole and triazole derivatives act as proton transport facilitators in polymer electrolyte membrane fuel cells. This is investigated by Ghassemi and his coworkers. They demonstrated the proton affinity and its effect on the activation energy for proton transfer between molecules. They measured the proton conductivity from acid doped triazoles in both pellet form (powder triazole mixed with acid) and in composite forms wherein the acid group is contained in a polymer matrix. The important parameter in proton conductivity of triazole and triazole derivatives the hydrogen bonding networks.[191] Li et al. prepared 1H-1,2,4-triazole doped Sulfonated polysulfone (sPSU) and studied the effect of triazole ratio on proton conductivity of. They found that the conductivity increased both after doping with PA or by increasing the concentration of 1H-1,2,4-triazole. For a membrane with n= 8 (n is defined as the ratio of [1*H*-1,2,4-triazole] to [-SO_3H]), the conductivity reached 1.5×10^{-3} S/cm at 100°C and 5.0×10^{-3} S/cm at 140°C. The polymer sPSU has very low ion conductivity under anhydrous conditions, so they believed that the 1H-1,2,4-triazole is responsible for the observed ionic conductivity of sPSU-1H-1,2,4-triazole membranes.[188]

Phosphoric acid-doped PVT as water-free proton conducting polymer electrolytes is reported by Sevim et al.[192] They doped the polymer with phosphoric acid at various molar ratios x=1 and x=2. The proton conductivity of these materials increased with dopant concentration and the temperature. In the anhydrous state, the proton conductivity of PVT 1 H_3PO_4 is 5×10^{-3} S/cm at 150°C and the conductivity of PVT 2 H_3PO_4 was 4×10^{-3} S/cm at 140°C. Aslan et al. produced polymer electrolytes based on PVT doped with trifilic acid. They showed that the proton conductivity of these materials increased with trifilic acid concentration and temperature. They reported the maximum proton conductivity of 0.012 S/cm at 80°C for PVTriTA150 which is comparable to that of fully hydrated Nafion®.[193] The conductivity of Nafion−P(VTri)[1] blend membranes is 5.3×10^{-4} Scm^{-1} at 220°C, in anhydrous state. The conductivity of blend increased at least three orders of magnitude upon hydration at ambient temperature. Proton conducting polymer electrolytes based on poly(2-acrylamido-methyl-1-propanesulfonic acid) (PAMPS) and PVT were prepared and investigated by

Bozkurt et al. They fabricated the materials at several molar ratios to analyze the effect of vinyl triazole and AMPS contents on the proton conductivity of the samples. PVTriP(AMPS)$_2$ and PVTriP(AMPS)$_4$ showed proton conductivities of 0.30 and 0.06 S/cm at 100°C, respectively at 50% relative humidity.[194] In one another study blends of PVT and nafion is prepared. The blends are stable up to 300°C.[195]

1.8. AIMS of the Thesis

In this chapter we have discussed about the importance of blends and nanocomposites in the property improvement of polymers. We have also discussed the properties and applications of different polymers such as PBI, SPS, PVDF-HFP and PVT. Throughout the discussion we have seen that using blending and nanocomposite preparation techniques, the properties of polymers can be greatly improved. In chapter 2 we have discussed and investigated the influence of sulfonation reaction time, temperature and the parent polystyrene (PS) particle size on the degree of sulfonation (DS), ion exchange capacity (IEC), morphology and glass transition temperature (T_g) of sulfonated polystyrene (SPS) particles. Although a large amount of literature related to SPS preparation is there, unfortunately no study has been focused on the effect of PS particle size on the DS and other properties of SPS. In chapter 3, we have use these SPS particles and blended with Polybenzimidazole (PBI). Here we have slightly varied the method of synthesis of SPS particles and we have prepared sodium salt of SPS particles. Using the blending technique we have prepared core (polystyrene)-shell (polybenzimidazole) nanoparticles using sulfonated polystyrene as template. PBI is an ideal candidate as polyelectrolyte membrane (PEM) for high temperature fuel cell. When doped with acid PBI shows proton conductivity and the conductivity is directly proportional to the amount of doped acid. Large amount of efforts have been made to improve the properties of PBI so that the efficiency of this polymer as PEM can be increased. Keeping this in mind we have prepared blends of PBI in next two chapters. In Chapter 4 and Chapter 5 we have blended PBI with two different polymers (PVDF-HFP and PVT) to improve the proton conductivity of PBI. In chapter 6, we have prepared

SPS/graphene nanocomposites to generate single layer ~ 1nm thick graphene nanosheets and fabricate mechanically stable ion conducting SPS membrane. Therefore, the thesis mainly deals with polymer blending and polymer nanocomposites. The aims and objectives of each chapter of this thesis are elaborated at the introductory part of the individual chapters.

References

1. http://plc.cwru.edu/tutorial/enhanced/files/polymers/apps/apps.htm
2. Advances in Polymer blends and Alloys Technology Volume 1; Chapter 1, Kohudic, M. A. Technomic Publishing Co., USA, **1988**.
3. (a) http://homepage.ntu.edu.tw/~chingih/Polymer%20Blends.pdf. (b) Utracki, L**.** A. *Polymer Alloys and Blend; Thermodynamics and Rheology*, Hanser Gardner Publishers, Munich, **1989.**
4. Utracki, L. A. *Polym. Eng. Sci.* **1983**, *23*, 602.
5. Meijer, H. E. H.; Lemstra, P. J.; Elemans, P. H. M. *Makromol.Chem., Macromol. Symp.* **1988**, *16*, 113.
6. Miles, I. S.; Rostami, S., *Multicomponent Polymer Systems*, John Wiley and Sons, **2003**.
7. Sharma, K. R. *Polymer Thermodynamics: Blends, Copolymers and Reversible Polymerization*, CRC Press/Taylor and Francis, Baco Raton, **2012**.
8. Utracki, L**.** A. *Encyclopaedic Dictionary of Commercial Polymer Blends*, ChemTec Publishing, **1994**.
9. Utracki, L**.** A. Polymer *Blends Handbook, Volumes 1-2*, Springer-Verlag, **2002**.
10. (a) Koning, C.; Duin, M. V.; Pagnoulle, C.; Jerome, R. *Prog. Polym. Sri*. **1998**, *23*, 707. (b) Joss, J.; Jyotishkumar, P; George, S. M.; Thomas, S. *Recent Developments in Polymer Recycling*, **2011,** 187. (c) Engineering Resins, Polymer Alloys and Blends – Market Survey, 2008, (www.reportlinker.com).
11. He, Y.; Zhu, B.; Inoue, Y. *Prog. Polym. Sci.* **2004**, *29*, 1021.
12. Lu, X.; Weiss, R. A. *Macromolecules* **1992**, *25*, 3242**.**
13. Coleman, M. M.; Graf, J. F.; Painter, P. C. *Specific Interactions and the Miscibility of Polymer Blends: Practical Guides for Predicting & Designing Miscible Polymer Mixtures*, Technomic Publishing Company, Lancaster, PA, **1991**.
14. Coleman, M. M.; Painter, P. C. *Miscible polymer blend: Background and guide for calculation and design*, DEstech Publications, Pennsylvania, **2006**.

15. Yagci, Y.; Nuyken, O.; Graubner, V. *Encyclopedia of Polymer Science and Technology*, John Wiley & Sons, New York, **2005**.
16. Utracki, L. A. *"Thermodynamics of Polymer Blends" in "Polymer Blends Handbook", Vol. 1*, Kluwer Academic Publishers, Dordrecht, **2002**, p.123-201.
17. Merfeld, G. D.; Paul, D. R. *"Polymer-Polymer Interactions Based on Mean Field Approximations" in "Polymer Blends: Formulation", Vol. 1*, Wiley-Interscience Publication, New York, **2000**, p. 55-91.
18. Lohse, D. J.; Graesseley, W. W. *"Thermodynamics of Polyolefin Blends" in "Polymer Blends: Formulation", Vol.1*, Wiley-Interscience Publication, New York, **2000**, p. 219-237.
19. http://www.pslc.ws/macrog/iblend.htm.
20. Lyngaae-Jørgensen, J.; Utracki, L. A. *Makromol. Chem., Macromol. Symp.***1991**, *48/49*, 189.
21. Bower, D. I. *An Introduction to Polymer Physics* Cambridge University Press, **2002**.
22. Leibler, L. *Prog. Polym. Sci.* **2005**, *30*, 898.
23. Chanda, M.; Roy, S. K. *Commercial Polymer Blends and Alloy: Plastics Technology Handbook, Fourth Edition*, CRC Press, **2006**, pp A13-1–A13-4.
24. Fayt, R.; Jérôme, R.; Teyssié, P. *J. Polym. Sci. Polym. Phys*. **1982**, *20*, 2209.
25. Fayt, R.; Jérôme, R.; Teyssié, P. *Polym. Eng. Sci*.**1987**, *27*, 328.
26. (a) Baker, W. E.; Scott, C.; Hu, G. H. *Reactive Polymer Blending*, Carl Hanser-Verlag, Munich, **2001**. (b) Al Malaika, S. *Reactive Modifiers for Polymers*, Chapman & Hall, London, **1997**, pp. 84-159.
27. http://www.materialkemi.lth.se/courses/mat_func/mat_func_pdf/Patrics%20hand-out%203.pdf.
28. Cakar, F.; Sakar, D.; Cankurtaran, O.; Karaman, F. *Eur. Polym. J*. **2007**, *43*, 507.
29. Song, M.; Hammiche, A.; Pollock, H. M.; Hourston, D. J.; Reading, M.; *Polymer*, **1996**, *37*, 5661.
30. Ahn, T-K.; Kim, M.; Choe, S. *Macromolecules* **1997**, *30*, 3369.

31. Robeson, L. M. *Polymer Blends: A Comprehensive Review*, Hanser Fachbuchverlag, Macungie, PA, **2007**.
32. Pospíšil, J.; Horák, Z.; Kruliš, Z.; Nešpůrek, S.; Kuroda, S. *Polym. Degrade. Stab.* **1999**, *65*, 405
33. Bhattacharya, S. N.; Kamal, M. R.; Gupta, R. K. *Polymeric nanocomposites: Theory and practice*, Hanser Verlag, Cincinnati, **2008.**
34. Hussain, F.; Hojjati, M. *J. Comp. Mater.* **2006**, *40*, 1511.
35. Ajayan, P. M.; Stephen, O.; Colliex, C.; Trauth, D. *Science*, **1994**, *265*, 1212.
36. Ghosh, S.; Sannigrahi, A.; Maity, S.; Jana, T. *J. Phys. Chem. C* **2011**, *115*, 11474.
37. Vaia, R. A.; Krishnamoorti, R. *In Polymer Nanocomposites: Synthesis Characterization and Modeling*; American Chemical Society: Washington, DC, **2001**, 1.
38. Akcora, P.; Liu, H.; Kumar, S. K.; Moll, J.; Li, Y.; Benicewicz, B. C.; Schadler, L. S.; Acehan, D.; Panagiotopoulos, A. Z.; Pryamitsyn, V.; Ganesan, V.; Ilavsky, J.; Thiyagarajan, P.; Colby, R. H.; Douglas, J. F. *Nat. Mater*. **2009**, *8*, 354.
39. Ghosh, S.; Maity, S.; Jana, T. *J. Mater. Chem*. **2011**, *21*, 14897.
40. Burnside, S. D.; Giannelis, E. P. *Chem. Mater.* **1995**, *7*, 1597.
41. Gilman, J. W.; Jackson, C. L.; Morgan, A. B.; Harris, R., Jr.; Manias, E.; Giannelis, E. P.; Wuthenow, M.; Hilton, D.; Phillips, S. H. *Chem. Mater.* **2000**, *12*, 1866.
42. Xu, R.; Manias, E.; Snyder, A. J.; Runt, J. *Macromolecules* **2001**, *34*, 337.
43. Bharadwaj, R. K. *Macromolecules* **2001**, *34*, 1989.
44. Krishnamoorti, R.; Vaia, R. A. *Polymer Nanocomposites – Synthesis, Characterization and Modeling, ACS Symposium Series, Vol.* **2001**, *804*, ACS, Washington DC.
45. Park, C.; Park, O.; Lim, J.; Kim, H. *Polymer* **2001**, *42*, 7465.
46. Giannelis, E. P. *Adv. Mater*. **1996**, *8*, 29.

47. Ogata, N.; Jimenez, G.; Kawai, H.; Ogihara, T. *J. Polym. Sci. Part B: Polym. Phys.* **1997**, *35*, 389.
48. Lee, D. C.; Jang, L. W. *J. Appl. Polym. Sci.* **1998**, *68*, 1997.
49. Jiang, L.; Lam, Y.C.; Tam, K. C.; Chua, T. H.; Sim, G. W.; Ang, L. S. *Polymer*, **2005**, *46*, 243.
50. Tortora, M.; Vittoria, V.; Galli, G.; Ritrovati, S.; Chiellini, E. *Macromol. Mater. Eng.* **2002**, *287*, 243.
51. Gorrasi, G.; Tortora, M.; Vittoria, V.; Pollet, E.; Lepoittevin, B.; Alexandre, M.; Dubois, P. *Polymer*, **2003**, *44*, 2271
52. Zhu, J.; Uhl, F. M.; Morgan, A. B.; Wilkie, C. A. *Chem. Mater.* **2001,** *13*, 4649.
53. Vyazovkin, S.; Dranca, I.; Fan, X.; Advincula, R. *Macromol.Rapid Commun.* **2004**, *25*, 498
54. Boehm, H.-P.; Setton, R.; Stumpp, E.; *Pure & Appl. Chem.***1994**, *66*, 1893.
55. http://en.wikipedia.org/wiki/Graphene
56. Heyrovska, R. *"Atomic Structures of Graphene, Benzene and Methane with Bond Lengths as Sums of the Single, Double and Resonance Bond Radii of Carbon"*. http://arxiv.org/ftp/arxiv/papers/0804/0804.2488.pdf, **2008**.
57. Wallace, P. R. *Phys. Rev.* **1947**, *71*, 622.
58. (a) Kuilla, T.; Bhadra, S.; Yao, D.; Kim, N. H.; Bose, S.; Lee, J. H. *Prog. Polym. Sci*. **2010**, *35*, 1350. (b) *Fullerene: McGraw-Hill Science & Technology Encyclopedia*,http://www.answers.com/topic/fullerene(c)http://www.quirkyscience.com/graphene-isolation-characterization-application-and-production/.
59. Geim, A. K.; Novoselov, K. S. *Nat. Mater*. **2007**, *6*, 183.
60. Yavari, F.; Kritzinger, C.; Gaire, C.; Song, L.; Gullapalli, H.; Borca-Tasciuc, T.; Ajayan, P. M.; Koratkar, N. *Small* **2010**, *6*, 711.
61. Park, N.; Hong, S.; Kim, G.; Jhi, S. H. *J. Am. Chem. Soc*. **2007**, *129*, 8999.
62. Liang, M. H.; Zhi, L. J. *J. Mater. Chem*. **2009**, *19*, 5871.
63. Jafri, R. I.; Rajalakshmi, N.; Ramaprabhu, S. *J. Mater. Chem*. **2010**, *20*, 7114.
64. Pyun, J. *Angew. Chem., Int. Ed*. **2011**, *50*, 46.

65. Robinson, J. T.; Perkins, F. K.; Snow, E. S.; Wei, Z. Q.; Sheehan, P. E. *Nano Lett*. **2008**, *8*, 3137.
66. Keeley, G. P.; O'Neill, A.; McEvoy, N.; Peltekis, N.; Coleman, J. N.; Duesberg, G. S. *J. Mater. Chem.* **2010**, *20*, 7864.
67. Geng, J. X.; Liu, L. J.; Yang, S. B.; Youn, S. C.; Kim, D. W.; Lee, J. S.; Choi, J. K.; Jung, H. T. *J. Phys. Chem. C* **2010**, *114*, 14433.
68. Zhao, J. P.; Pei, S. F.; Ren, W. C.; Gao, L. B.; Cheng, H. M. *ACS Nano* **2010**, *4*, 5245.
69. Yang, X. Y.; Zhang, X. Y.; Ma, Y. F.; Huang, Y.; Wang, Y. S.; Chen, Y. S. *J. Mater. Chem.* **2009**, *19*, 2710.
70. Zhang, R. Y.; Hummelgard, M.; Lv, G.; Olin, H. *Carbon* **2011**, *49*, 1126.
71. Ramanathan, T.; Abdala, A. A.; Stankovich, S.; Dikin, D. A.; Herrera-Alonso, M.; Piner, R. D.; Adamson, D. H.; Schniepp, H. C.; Chen, X.; Ruoff, R. S.; Nguyen, S. T.; Aksay, I. A.; Prud'homme , R. K.; Brinson, L. C. *Nat. Nanotechnol*. **2008**, *3*, 327.
72. Verdejo, R.; Bernal, M. M.; Romasanta, L. J.; Lopez-Manchado, M. A. *J. Mater. Chem*. **2011**, *21*, 3301.
73. Yoo, E.; Kim, J.; Hosono, E. Zhou, H.; Kudo,T.; Honma, I. *Nano Lett.* **2008,** *8(8)*, 2277.
74. Loh, K. P.; Bao, Q.; Ang, P. K.; Yang, J. *J. Mater. Chem*. **2010**, *20*, 2277.
75. Gusynin, V. P.; Sharapov, S. G. *Phys. Rev. Lett.* **2005**, *95*, 146801.
76. Zhang, Y. B.; Tan, Y. W.; Stormer, H. L.; Kim, P. *Nature*, **2005**, *438*, 201.
77. Novoselov, K. S.; Geim, A. K.; Morozov, S. V.; Jiang, D.; Zhang, Y.; Dubonos, S. V.; Grigorieva, I. V.; Firsov, A. A. *Science*, **2004**, *306*, 666.
78. Latil, S.; Henrard, L. *Phys. Rev. Lett.* **2006**, *97*, 036803.
79. Nair, R. R.; Blake, P.; Grigorenko, A. N.; Novoselov, K. S.; Booth, T. J.; Stauber, T.; Peres, N. M. R.; Geim, A. K. *Science* **2008**, *320*, 1308.
80. Eda, G.; Fanchini, G.; Chhowalla, M. *Nat. Nanotechnol*. **2008**, *3*, 270.

81. Novoselov, K. S.; Jiang, Z.; Zhang, Y.; Morozov, S. V.; Stormer, H. L.; Zeitler, U.; Maan, J. C.; Boebinger, G. S.; Kim, P.; Geim, A. K. *Science* **2007**, *315*, 1379.
82. Guermoune, A.; Chari, T.; Popescu, F.; Sabri, S. S.; Guillemette, J.; Skulason, H. S.; Szkopek, T.; Siaj, M. *Carbon* **2011**, *49*, 4204.
83. Meyer, J. C.; Girit, C. O.; Crommie, M. F.; Zettl, A. *Nature* **2008**, *454*, 319.
84. Berger, C.; Song, Z.; Li, X.; Wu, X.; Brown, N. Naud, C.; Mayou, D.; Li, T.; Hass, J.; Marchenkov, A.; N.; Conrad, E. H.; First, P. N.; de Heer W. A. *Science* **2006**, *312*, 1191.
85. Stankovich, S.; Dikin, D. A.; Piner, R. D.; Kohlhaas, K. A.; Kleinhammes, A.; Jia, Y.; Wu, Y.; Nguyen, S. T.; Ruoff, R. S. *Carbon* **2007**, *45*, 1558.
86. Choi, W.; Lee, J.-W. *Graphene: Synthesis and Applications*, CRC Press, bocaraton, **2011**.
87. Steurer, P.; Wissert, R.; Thomann, R.; Mülhaupt, R. *Macromol. Rapid Commun*. **2009**, *30*,316.
88. Rafiee, M. A.; Rafiee, J.; Wang, Z.; Song, H.; Yu, Z.-Z.; Koratkar, N. *ACS Nano* **2009**, *3*, 3884.
89. Schniepp, H. C.; Li, J.-L.; McAllister, M. J.; Sai, H.; Herrera-Alonso, M.; Adamson, D. H.; Prud'homme, R. K.; Car, R.; Saville, D. A.; Aksay, I. A. **2006**, *110*, 8535.
90. Stankovich, S.; Piner, R. D.; Chen, X.; Wu, N.; Nguyen, S. T.; Ruoff , R. S. *J. Mater. Chem.* **2006**, *16*, 155.
91. Stankovich, S.; Dikin, D. A.; Dommett, G. H. B.; Kohlhaas, K. M.; Stach, Z. E. A.; Piner, R. D.; Nguyen, S. T.; Ruoff, R. S. *Nature let.* **2006**, *442*, 282.
92. Kuilla, T.; Bhadra, S.; Yaoa, D.; Kim, N. H. *Prog. Polym. Sci*. **2010**, *35*, 1350.
93. Stankovich, S.; Piner, R. D.; Chen, X.; Wu, N.; Nguyen, S. T.; Ruoff , R. S. *J. Mater. Chem.* **2006**, *16*, 155.
94. Xu, Y.; Bai, H.; Lu, G.; Li, C.; Shi, G. *J. Am. Chem. Soc.* **2008**, *130*, 5856.
95. Hao, R.; Qian, W.; Zhang, L.; Hou, Y. *Chem. Commun.* **2008**, 6576.
96. Wang, X.; Zhi, L.; Mullen, K. *Nano Lett*. **2008**, *8(1)*, 323.

97. Hu, H.; Wang, X.; Wang, J.; Wan, L.; Liu, F.; Zheng, H.; Chen, R.; Xu, C. *Chem. Phys. Lett*. **2010**, *484*, 247.
98. Kim, H.; Miura, Y.; Macosko, C. W. *Chem. Mater*. **2010**, *22*, 3441.
99. Wang, J.; Hu, H.; Wang, X.; Xu, C.; Zhang, M.; Shang, X.; *J. Appl. Polym. Sci.* **2011**, *122*, 1866.
100. Bao, C.; Guo, Y.; Song, L.; Hu, Y. *J. Mater. Chem.* **2011**, *21*, 13942.
101. Al-Mashat, L.; Shin, K.; Kalantar-zadeh, K.; Plessis, J. D.; Han, S. H.; Kojima, R. W.; Kaner, R. B.; Li, D.; Gou, X.; Ippolito, S. J.; Wlodarski, W. *J. Phys. Chem. C* **2010,** *114*, 16168.
102. Vorselaars, B.; Lyulin, A. V.; Michels, M. A. J. *Macromolecules* **2007,** *40*, 6401.
103. Eisenberg, A.; Kim, J. S. *Introduction to Ionomers* John Wiley & Sons, New York, **1998.**
104. Eisenberg, A. *Adv.Polym.Sci*.**1967**, *5*, 59.
105. (a) Elabd, Y. A.; Napadensky, E.; Sloan, J. M.; Crawford, D. M.; Walker, C. W. *J. Membr. Sci.* **2003,** *217*, 227. (b) Djinovic, V. M.; Antic, V. V.; Djonlagic, J.; Govedarica, M. N.; *React. Funct. Polym. 2*000, *44, 2*99.
106. (a) Yarusso, D. J.; Cooper, S. L. *Macromolecules*, **1983**, *16*, 1871. (b) Malini, K. A.; Anantharaman, M. R.; Sindhu, S.; Chinnasamy, C. N.; Ponpandian, N.; Narayanasamy, A.; et al, *J. Mater. Sci.* **2001**, *36***,** 821. (c) Boardman, N. K. *J. Chromatogr. A* **1959**, *2***,** 398.
107. Longworth, R. *The structure and properties of ionomers: In development in ionic polymer* Applied Science Publishers, London and New York, **1983**.
108. Kucera, F.; Jancar, J. *Chem. Papers* **1996**, *50(4)*, 227.
109. Baigl, D.; Seery, T. A. P.; Williams, C. E. *Macromolecules* **2002**, *35*, 2318.
110. Arunbabu, D.; Sanga, Z.; Seenimeera, K. M.; Jana, T. *Polym Int*. **2008**, *58*, 88.
111. Yeole, N.; Hundiwale, D.; Jana, T. *J. Colloid Interface Sci.* **2011**, *354*, 506.
112. Tran, Y.; Auroy, P. *J. Am. Chem. Soc.* **2001**, *123*, 3644.
113. Orler, E. B.; Dorie, J. Z.; Robert, B. M. *Macromolecule*. **1993**, *26*, 5157.
114. Lundberg, R**.** D.; Makowski, H. S. *Polym. Prepr.* **1978,** *19*, 287.

115. Turner, S. R.; Weiss, R**.** A.; Lundberg, R. D. *J. Polym. Sci.: Polym. Chem. Ed.* **1985**, *23*, 535.
116. Kucera, F.; Jancar, J. *Polym. Eng. Sci*. **1998**, *38*, 783.
117. Turbak, A. F. *Ind. Eng. Chem., Prod. Res. Dev.* **1962**, *1*, 275.
118. Makowski, H. S.; Lundberg, R. D.; Singhal, G. H.; *US pat.*3, 870, 841, **1975.**
119. Weiss, R. A.; Lundberg, R. D.; Turner, S. R. *J. Polym. Sci. Polym. Chem. Ed*. **1985**, *23*, 549.
120. Hazarika, M.; Malkappa, K.; Jana, T. *Polym. Int.* **2012**, 61, 1425.
121. Serpico, J. M.; Ehrenberg, S. G.; Fontanella, J. J.; Jiao, X.; Perahia, D.; McGrady, K. A.; Sanders, E. H.; Kellogg, G. E.; Wnek, G. E. *Macromolecules* **2002**, *35*, 5916.
122. Hickner, M. A.; Ghassemi, H.; Kim, Y. S.; Einsla, B. R.; McGrath, J. E. *Chem. Rev*. **2004**, *104*, 4587.
123. Ding, J.; Chuy, C.; Holdcroft, S. *Adv. Funct. Mater*. **2002**, *12*, 389.
124. Park, C. H.; Lee, C. H.; Guiver, M. D.; Lee, Y. M. *Prog. Polym. Sci*. **2011**, *36*, 1443.
125. Göktepe, F.; Bozkurt, A.; Günday, Ş. T. *Polym. Int.* **2008**, *57*, 133.
126. Carrettaa, N.; Tricoli, V.; Picchioni, F. *J. Memb. Sci*. **2000**, *166*, 189.
127. Bae, B.; Ha, H. Y.; Kim, D. *J. Memb. Sci*. **2006**, *276*, 51.
128. Jung, B.; Kim, B.; Yang, J. M. *J. Memb. Sci*. **2004**, *245*, 61.
129. Ding, S.-J.; Zhang, C.-L. Yang, M.; Qu, X.-Z.; Lu, Y.-F.; Yang, Z.-Z. *Polymer* **2006**, *47*, 8360.
130. Deng, H.; Li, X.; Peng, Q.; Wang, X.; Chen, J.; Li, Y. *Angew. Chem. Int. Ed.* **2005**, *44*, 2782.
131. Yang, M.; Ma, J.; Zhang, C.; Yang, Z.; Lu, Y.; *Angew. Chem. Int. Ed*. **2005**, *44*, 6727.
132. Yang, Y.; Chu, Y.; Yang, F.; Zhang, Y.; *Mater. Chem. Phys*. **2005**, *92*, 164.
133. Vogel, H.; Marvel, C. S. *J. Polym. Sci.* **1961**, *50*, 511.
134. Vogel, H.; Marvel, C. S. *J. Polym. Sci Part A* **1963**, *1*, 1531.
135. Plummer, L.; Marvel, C. S. *J. Polym. Sci Part A* **1964**, *2*, 2559.

136. Marvel, C. S.; Ariz, T.; Vogel, H. A. *U. S. Patent* 3 174 947, **1965**.
137. Lee, H.; Stoffey, D.; Neville, K. *New Linear Polymers; Chapter 9*, McGraw-Hill, New York, **1967**.
138. Choe, E. W., Choe, D. D. *Polymeric Materials Encyclopedia*; CRC Press: New York, **1996,** pp 5619-5638.
139. Neuse, E. W. *Adv. Polym. Sci.* **1982**, *47*, 1.
140. Iwakura,Y.; Uno, K.; Imai, Y. *J. Polym. Sci*. **1964**, *A2*, 2605.
141. Kulkarni, M.; Potrekar,R.; Kulkarni,R. A.; Vernekar, S. P. *J. Polym. Sci., Part A: Polym. Chem. **2008**, 46, 5776.*
142. Béland, S. *High Performance Thermoplastic Resins and Their Composites*, William Andrew, New Jersey, **1990.**
143. Powers, E. J.; Serad. G. A. *"History and Development of Polybenzimidoles" Symposium on the History of High Performance Polymer*s, American ChemicalSociety, New York, **1986**.
144. Savinell, R.; Yeager, E.; Tryk, D.; Landau, U.; Wainright, J.; Weng, D.; Lux, K.; Litt, M.; Rogers, C. *J. Electrochem. Soc.* **1994**, *141*, L46.
145. Xiao, L.; Zhang, H.; Jana, T.; Scanlon, E.; Chen, R.; Choe, E.-W.; Ramanathan, L. S.; Yu, S.; Benicewicz, B. C. *Fuel Cells* **2005**, *5*, 287.
146. Yeager, E. *Science* **1961**, *134*, 1178.
147. Fuel Cell Handbook, 6 th. Edition, EG & G Technical Services, Inc. U.S. Department of Energy, November **2002**.
148. Blomen, L. J. M. J. *Fuel Cell Systems*; Plenum Press, New York, **1993**.
149. Winter, M.; Brodd, R. J. *Chem. Rev.* **2004**, *104*, 4245.
150. Li, Q.; He, R.; Jensen, J. Q.; Bjerrum, N. J.; *Chem. Mater*. **2003**, *15*, 4896.
151. Sukumar, P. R.; *Ph.D. Thesis, Max-Planck-Institute for Polymer Science*, Mainz, **2006**.
152. Einsla, B. R. Ph.D.Thesis, Virginia Polytechnic, Blackburg, Virginia, **2005**.
153. Mehta, V.; Cooper, J. S. *J. Power. Sources*. **2003**, *114*, 32.
154. Shao, Y.; Yin, G.; Wang, Z.; Gao,Y. *Journal of Power Sources* **2007**,*167*, 235.
155. Scherer, G. G. *Fuel Cells II*, Springer, **2010.**

156. Sannigrahi, A.; Arunbabu, D.; Sankar, R. M.; Jana, T. *Macromolecules* **2007**, *40*, 2844.
157. Kojima, T. *J. Polym. Sci., Polym. Phys. Educ*. **1980**, *18*, 1685.
158. Sannigrahi, A.; Arunbabu, D.; Jana, T. *Macromol. Rapid Commun.* **2006**, *27*, 1962.
159. Hazarika, M.; Arufnbabu, D.; Jana, T. *J. Colloid Interface Sci.* **2010**, *351*, 374.
160. Deimede, V.; Voyiatzis, G. A.; Kallitsis, J. K.; Qingfeng, L.; Bjerrum, N. J. *Macromolecules* 2000, *33*, 7609.
161. Musto, P.; Karasz, F. E.; MacKnight, W. J. *Macromolecules* **1991**, *24*, 4762.
162. Wang, Y.; Goh, S. H.; Chung, T.-S. *Polymer* **2007**, *48*, 2901.
163. Jaffe, M.; Chen, Paul.; Choe, E-W.; Chang, T. S.; Makhija, S. *Adv. Polym. Sci.* **1994**, *117*, 297.
164. Jaffe, M.; Chen, Paul.; Choe, E-W.; Chang, T. S.; Makhija, S. *Adv. Polym. Sci.* **1994**, *117*, 297.
165. Makhija, S.; Pearce, E. M.; Kwei, T. K.; Liu, F. *Polym. Eng. Sci*. **1990**, *30*, 798.
166. Chang, T. S.; Herold, F. K.; *Polym. Eng. Sci.* **1991**, *31*, 1950.
167. Chang, T. S. *Polymer Reviews.* **1997**, *37*, 277.
168. Wycisk, R.; Chisholm, J.; Lee, J.; Lin, J.; Pintauro, P. N. *J. Power. Sources* **2006**, *163*, 9.
169. Arunbabu, D.; Sannigrahi, A.; Jana, T. *J. Phys. Chem. B* **2008,** *112*, 5305.
170. Ameduri, B. *Chem. Rev.* **2009**, *109*, 6632.
171. Gozdz, A. S.; Schmutz, C. N.; Tarascon, J.-M. *US Patent 5*, 296, 318, **1994**.
172. Shi, L.; Wang, R.; Cao, Y.; Liang, D. T.; Tay, J. H. *J. Memb. Sci.* **2008**, *315*, 195.
173. Cho, K.-Y.; Jung, H.-Y.; Sung, K. A.; Kim, W.-K.; Sung, S.-J.; Park, J.-K.; Choi, J.-H.; Sung, Y.-E. *J. Power Source* **2006**, *159*, 524.
174. Saarinen, V.; Himanen, O.; Kallio, T.; Sundholm, G.; Kontturi, K. *J. Power Source* **2007**, *163*, 768.
175. Tarascon, J.-M.; Gozdz, A. S.; Schmutz, C.; Shokoohi, F.; Warren, P. C. *Solid State Ionics* **1996**, *86-88*, 49.

176. Li, G.; Zhang, P.; Zhang, H.; Yang, L.; Wu, Y. *Electrochem. Commun*. **2008**, *10*, 1883.
177. Cao, J.-H.; Zhu, B.-K.; Xu Y.-Y. *J. Memb. Sci*. **2006**, *281*, 446.
178. He, X.; Yao K.; Gan B. K. *Sens. Actuators A* **2007**, *139*, 158. (a) Zhou, X.; Zhao, X.; Suo, Z.; Zou, C.; Runt, J.; Liu, S.; Zhang, S.; Zhang, Q. M. *Appl. Phys. Lett*. **2009**, *94*, 162901. (b) Ling, Q.-D.; Liaw, D.-J.; Zhu, C.; Chan, D. S.-H.; Kang, E.-T.; Neoh, K.-G. *Prog. Polym. Sci.* **2008**, *33*, 917.
179. (a) Ulaganathan, M.; Rajendran, S. *Ionics* **2010**, *16*, 515. (b) Huang, H.; Wunder, S. L. *J. Electrochem. Soc*. **2001**, *148*, A279. (c) Wang, Z.; Tang, Z. *Mater. Chem. Phy*. **2003**, *82*, 16.
180. Sim, L. N.; Majid, S. R.; Arof, A. K. *Solid State Ionics* **2012**, *209–210*, 15.
181. Ye, H.; Xu, J. J. *J. Power Sources* **2007**, *165*, 500.
182. Fink, J. K.; Andrew, W. *High Performance Polymers Volume1 of Industrial Polymers Technology and Applications Plastics Design Library***,** Norwich, NY, **2008.**
183. (a) Kizhnyaev, V. N.; Pokatilov, F. A.; Vereshchagin, L. I. *Polym. Sci., Ser. C* **2008**, *50*, 1. (translation from *Vysokomol. Soedin., Ser. C* **2008**, *50*, 1296-1321) (b) Audouin, F.; Birot, M.; Pasquinet, É.; Besnard, O. Palmas, P.; Poullain, D.; Deleuze, H. *Macromolecules* **2011**, *44*, 4879.
184. Tatarova, L. A.; Ermakova, T. G.; Berlin, A. A.; Razvodovskii, E. F.; Lopyrev, V. A.; Kedrina, N. F.; Enikolopyan, N. S. *Vysokomol. Soedin, Ser. A* 1982, 24, 2205.
185. Makhno, L. P.; Ermakova, T. G.; Dommina, E. S.; Tatarova, L. A.; Skvortsov, G. G.; Lopyrev, V. A. *USSR Inventor's Certificate*, No.464584, Byull. Izobret. No. 11, **1975**.
186. Abbas, M.; Cakmak, G.; Tekin, N.; Kara, A.; Guney, H. Y.; Arici, E.; Sariciftci, N. S. *Org. Electron*. **2011**, *12*, 497.
187. Xue, H.; Gao, H. X.; Shreeve, J. M.; *J. Polym. Sci. Polym. Chem*. **2008**, *46*, 2414.
188. Li, S.; Zhou, Z.; Zhang, Y.; Liu, M.; Li, W. *Chem. Mater*. **2005**, *17***,** 5884.

189. Zhou, Z.; Liu, R.; Wang, J.; Li, S.; Liu, M.; Brédas, J. L. *J. Phys. Chem. A* **2006,** *110*, 2322.
190. (a) Çelik, S. Ü.; Akbey, Ü.; Bozkurt, A. *Macromol. Chem. Phys*.**2008**, *209*, 593. (b) Günday, S. T.; Bozkurt, A.; Meyer, W. H.; Wegner,G. *J. PolymSci Part B: PolymPhys* **2006**, *44*, 3315. (c) Ozden, S.; Celik, S. U.; Bozkurt, A. *J. Polym. Sci. Polym. Chem.* **2010**, *48*, 4974
191. Subbaraman, R.; Ghassemi, H.; Zawodzinski Jr. T. *Solid State Ionics* **2009,** *180*, 1143.
192. Çelik, S. Ü.; Aslan, A.; Bozkurt, A. *Solid State Ionics* **2008**, *179*, 683.
193. Aslan, A.; Çelik, S. Ü.; Şen, Ü.; Haser, R.; Bozkurt, A. *Electrochim. Acta* **2009**, *54*, 2957.
194. Aslan, A.; Bozkurt, A.; *Polym. Bull*. **2011**, *66*, 1099.
195. Sen, U.; Bozkurt, A.; Ata, A. *J. Power Sources* **2010**, *195*, 7720.

Chapter 2

Particle-size-dependent properties of sulfonated polystyrene nanoparticles

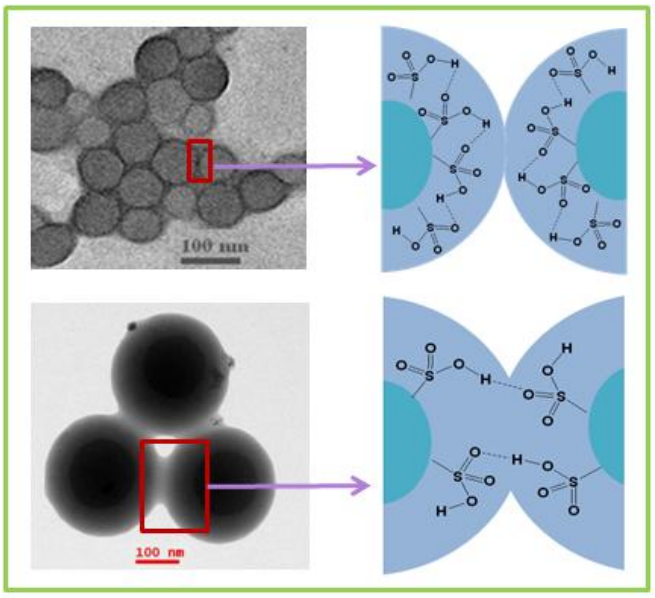

Degree of sulfonation (DS) of polystyrene (PS) particles depends not only on reaction time and temperature but also on the size of the parent polystyrene particle. Smaller size PS particles, longer reaction time (~2hrs) and 40°C temperature are found to be the best reaction conditions to achieve the higher DS.

Hazarika, M.; Malkappa, K.; Jana, T. *Polym. Int*. **2012**, *61*, 1425-1432

2.1. Introduction

The chemical modification of preformed polymers can be done by functionalizing the polymer backbone. This is a well studied avenue to obtain materials with desirable chemical and physical properties. More appropriately, this approach can be easily used to tune the polymer properties, e.g. hydrophobic or hydrophilic character, solubility, miscibility, changing the soft or rigid nature, polymer solution or melt viscosity, crystallinity, glass transition temperature etc.[1] One such approach which is well recognized in the literature is the sulfonation of rigid hydrophobic polystyrene (PS) to prepare soft hydrophilic sulfonated polystyrene (SPS, Figure 1.12).

In recent years, a large number of studies on SPS have been undertaken because of its wide range of applications in numerous areas, e.g. drug delivery applications,[2] catalysis,[3] humidity sensors,[4] as membranes for reverse osmosis[5] and chromatography techniques[6,7] etc. Hydrated SPS exhibits high proton conductivity and has been used as a polymer electrolyte in proton exchange membrane fuel cells.[8,9] SPS is also used as a template for synthesis of composite materials with hollow nano structures and core–shell structures.[10–12] The sulfonate groups of SPS readily interact with other functional groups of a variety of polymers, resulting in a large number of miscible blends of SPS with other polymers.[13–15] He *et al*. have demonstrated that SPS latex particles can be used very efficiently to make varieties of structure by self-assembly of the SPS latex at the emulsion–droplet interface.[16,17]

Sulfonation reactions of PS are often carried out by a sulfonation process either homogeneously or heterogeneously.[18–22] In homogeneous conditions, reagents like sulfuric acid, sulfur trioxide and its complexes, e.g. acyl sulfates and chlorosulfonic acid, are used to sulfonate PS.[18] Turbak[19] prepared sulfonated poly(vinyl toluene) and PS in a homogeneous phase by using trialkyl phosphate complex of sulfur trioxide as sulfonating agent. Lightly sulfonated PS was prepared by the reaction of a dichloroethane solution of PS with acetyl sulfate at ambient temperature for 1 h.[20,22] The preparation of SPS in a heterogeneous phase as in the copolymerization of styrene and sodium styrene sulfonate has advantages for industrial application over the

homogeneous process because it avoids problems with solvents and the separation of the sulfonated product from the reaction mixture. [21–25] Another advantage is that sulfonation proceeds without polymer degradation and crosslinking.[26,27]

In this chapter we have prepared SPS using concentrated sulfuric acid as sulfonating agent.[28–30] We used PS particles of various sizes obtained by emulsion polymerization and immersed them in concentrated sulfuric acid for different times and temperatures. The advantage of this sulfonating agent is that we can readily vary the degree of sulfonation (DS) by varying the reaction time and temperature. Despite the large amount of literature related to SPS preparation, no study has been focused on the effect of PS particle size on the DS and other properties of SPS. Hence, a detailed study is required to establish the method for the preparation of SPS with desirable DS for different particle sizes of PS. In the present work we focused on controlling the DS by varying parameters such as temperature and time of the reaction, and made an effort to understand the effect of PS particle size on the DS. We have developed a series of recipes to obtain SPS with various DSs of different PS particle sizes. Finally, we have characterized the resulting SPS by using Fourier transform infrared (FTIR) spectroscopy, NMR, transmission electron microscopy (TEM), thermogravimetric and differential thermal analyses (TG-DTA) and differential scanning calorimetry (DSC) and by measuring the ion exchange capacity (IEC) of the SPS particles.

2.2. Experimental Section

2.2.1. Materials

Styrene (Sisco, Mumbai, India) monomer was purified by the methods[31–33] discussed earlier. Sodium dodecyl sulfate (Merck, Mumbai, India), sodium bicarbonate (Sisco, India) and ammonium persulfate (Merck) as the surfactant, buffer and initiator, respectively, were used as received from the suppliers. Dowex mixed bed ion-exchange resin (Sigma Aldrich), sulfuric acid (Merck) and deuterated dimethyl sulfoxide (DMSO-d_6, Sigma Aldrich) were used as received. Milli Q water was used for all the experiments.

2.2.2. Synthesis and purification of PS particles

Synthesis of PS particles was carried out using method as described earlier[31–33] by us. Briefly the method was as follows. Spherical PS colloidal particles were synthesized by the emulsion polymerization technique in a four-neck mercury-sealed round-bottomed flask fitted with a reflux condenser, a Teflon stirrer attached to a high-torque overhead mechanical stirrer and nitrogen and reagent inlets. The temperature was maintained by placing the reaction vessel in a controlled temperature oil bath. The reaction vessel was charged with 75 mL of Milli Q water containing 0.1 g (0.001 mol) of sodium bicarbonate. The water solution was deoxygenated by bubbling nitrogen for 40 min. After thorough deoxygenation, the required amount [0.2 g (0.69 mmol), 0.0288 g (0.1 mmol), 0.0144 g (0.05 mmol)] of sodium dodecyl sulfate dissolved in 10 mL of water was added depending the desired particle size, and the temperature was increased to 50°C. Freshly deoxygenated styrene (33 g, 0.32 mol) was injected slowly at a constant rate of 4 mL min^{-1}. The temperature was increased to 70°C and the stirring speed to 350 rpm. After equilibration for 30 min, 0.4 g (17.54 mmol) of ammonium persulfate dissolved in 10 mL of water was injected into the reaction mixture. The reaction was refluxed for 3-4 hours. A nitrogen blanket and the stirring rate of 350 rpm were maintained during refluxing. A milky white colloidal solution was obtained upon completion of the reaction. It was then allowed to cool and filtered through glass wool. The filtered solution was dialyzed using cellulose ester dialysis membrane (MWCO, 100000) for 10 days by changing the water with fresh Milli Q water twice every day. After this colloidal juice was taken out and dried in a petri dish in a hot-air oven at 100°C.

2.2.3. Sulfonation of PS particles

PS (1 g, 5.43 mmol) was placed in a round-bottomed flask and 10 mL of H_2SO_4 was added to the flask. The reaction mixture was kept at a fixed temperature of 20°C, 30°C, 40°C, 50°C, 60°C or 70°C. The reaction mixture was stirred at the fixed temperature for a long time varying from 30 to 360 min. The precipitate was filtered and

washed with large quantities of water until the filtrate was neutral. Finally, the product was washed with ethanol. Then it was placed in a petri dish and dried in an oven at room temperature under vacuum for 24 h. We varied the time (30-360 min) and temperature (20-70°C) independently keeping all other parameters constant to obtain the various DSs. We also used different PS particle sizes for carrying out the sulfonation by varying the reaction time and temperature as mentioned above. We used three different particle sizes: 70, 160 and 260 nm. The detailed recipes of time and temperature variation for the sulfonation of PS are presented in Tables 2.1-2.4.

Table 2.1: Sulfonation recipe for different reaction time. In all the cases 1g polystyrene were taken. The particle size of polystyrene is 70 nm.

Sample ID	*Temperature (^{0}C)*	*Time (minutes)*	*Degree of sulfonation (%)*
MH 258	40	15	23
DC-18	40	30	42.80
DC-19	40	60	65.68
DC-110	40	90	64.30
DC-111	40	120	85.20
DC-112	40	180	62.20
DC113	40	240	68.2

Table 2.2: Sulfonation recipe for different reaction temperature. In all the cases 1g polystyrene of 70 nm particle size were taken.

Sample ID	*Time (minutes)*	*Temperature (^{0}C)*	*Degree of sulfonation (%)*
DC-118	120	20	38.9
DC-111	120	40	85.2
DC-119	120	50	63.7
SR-139	120	70	53.13
SR-141	120	100	38.46

Table 2.3: Sulfonation recipe for different reaction time. In all the cases 1g polystyrene of 160 nm particle size were taken.

Sample ID	*Temperature (^0C)*	*Time (minutes)*	*Degree of sulfonation (%)*
AK-143	40	30	28
AK-180	40	60	32.6
AK-181	40	90	45
AK-148	40	120	40
AK-182	40	180	51.6
AK-183	40	240	32.6
MH 246	60	180	72

Table 2.4: Sulfonation recipe for different reaction time. In all the cases 1g polystyrene of 260 nm particle size were taken

Sample ID	*Temperature (^0C)*	*Time (minutes)*	*Degree of sulfonation (%)*
MH-237	40	30	22.1
MH-238	40	60	24.9
MH-240	40	90	24.9
MH-243	40	120	32.6
MH-242	40	180	39
MH-239	40	240	36.6
MH 247	60	240	68

2.2.4. Characterization techniques

FTIR spectra of the samples were recorded on a Nicolet 5700 FTIR spectrometer at a resolution of 0.5 cm^{-1} with an average of 32 scans. ^1H NMR measurements were performed by using a Bruker 400 MHz NMR spectrometer to determine the DS of the SPS. The samples were prepared in DMSO-d_6. TG-DTA was carried out with a TG-DTA instrument (Netzsch STA 409PC) from room temperature to 800°C with a scanning rate of 10°C min^{-1} in the presence of a nitrogen gas flow. A differential scanning calorimeter (Pyris Diamond DSC, Perkin-Elmer) was used to study the glass transitions (T_g) of the samples. Samples were annealed at 250°C for 30 min, cooled to

50°C at a cooling rate of 200°C min^{-1}, and subsequently (after 30 min equilibration at 50°C) scanned from 50°C to 250°C at a heating rate of 10°Cmin^{-1}. A transmission electron microscope (FEI Tecnai model no. 2083) operating at 120 kV was used to image and study the morphology of the samples. The TEM samples were prepared by drop casting samples dispersed in water onto the carbon coated copper (200 mesh) grid. The IEC of the SPS particles was measured by a titration method. SPS particles (0.05 g) were treated with 10 mL of 20% NaCl solution and stirred for 24 h to allow the H^+ ions to exchange with the Na^+ ions. The H^+ released as a result of ion exchange was titrated with 0.01 mol L^{-1} NaOH solution using phenolphthalein as indicator. The IEC was calculated using the following equation:

$$\text{IEC (meq/g)} = \frac{\text{Consumed NaOH (mL)} \times \text{molarity of NaOH}}{\text{Weight of polymer}} \qquad (2.1)$$

2. 3. Results and Discussion

2.3.1. Spectral (FTIR, ^{1}H NMR) characterization

The FTIR spectrum of a representative SPS is shown in Figure 2.1. Similar spectra were obtained for all the samples studied here. The spectrum displays all the expected important IR frequencies of SPS as reported by several authors in the literature.[23,24,34,35] The broad peak at 3463 cm^{-1} results from O–H stretching vibrations due to both residual water in the sample and the SO_3H group of the SPS backbone. The peaks in the range 2800–3100 cm^{-1} represent various vibration bands of PS. The peak around 1033 cm^{-1} represents the symmetric stretching vibration of the SO_3^- group and the relatively broad peak around 1179 cm^{-1} represents the asymmetric vibration of the SO_3^- group. The sharp peak around 700 cm^{-1} is the out-of-plane bending vibration of the styrene ring. The peak around 756 cm^{-1} is characteristic of the out-of plane bending vibration of C–H groups in the mono-substituted benzene ring. These peaks are visible in all the samples indicating that sulfonation has successfully occurred in all the cases.

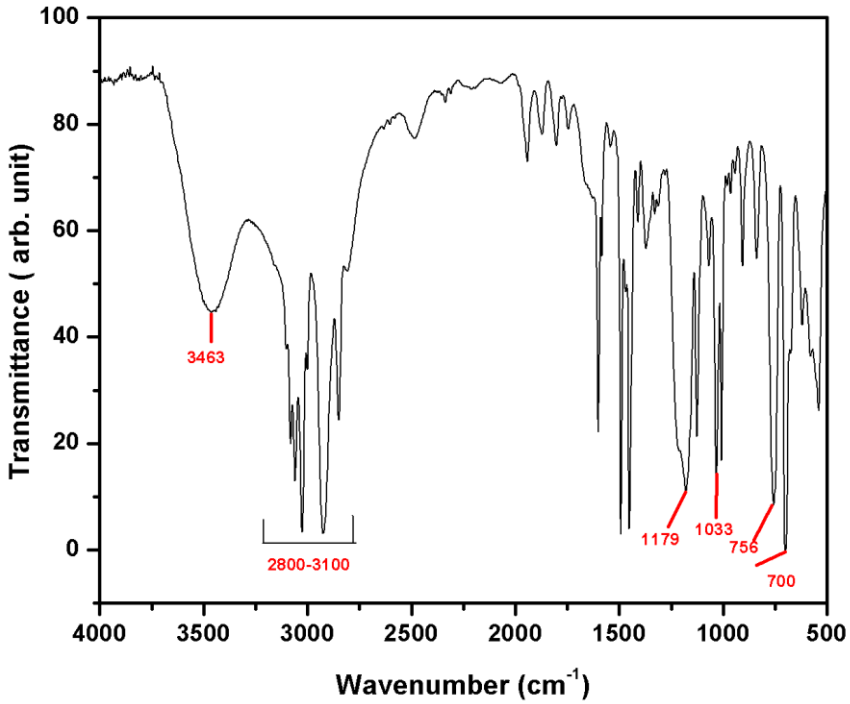

Figure 2.1: Representative FT-IR spectrum of sulfonated polystyrene.

A typical ^{1}H NMR spectrum of partially sulfonated PS recorded in DMSO-d_6 is shown in Figure 2.2. The broad band around δ = 0.8-2 ppm corresponds to the three aliphatic protons of the polymer backbone, a sharp peak at δ = 2.49 ppm corresponds to the residual protons from the imperfect deuteration of the solvent DMSO, and a second sharp peak at δ = 3.35 ppm is attributed to water. There are three broader peaks labeled A (δ = 6.5 ppm), B (δ = 7.1 ppm) and C (δ = 7.35 ppm) with roughly Gaussian shapes in the aromatic region of the spectrum. The assignments of the A, B and C peaks are shown in the inset of Figure 2.2 with the chemical structure of SPS. Peak A corresponds to the two ortho protons on the pendant aromatic ring. Peak B corresponds to meta and para protons on unsulfonated aromatic rings. Peak C is observed due to meta protons on the sulfonated aromatic rings.[22–24]

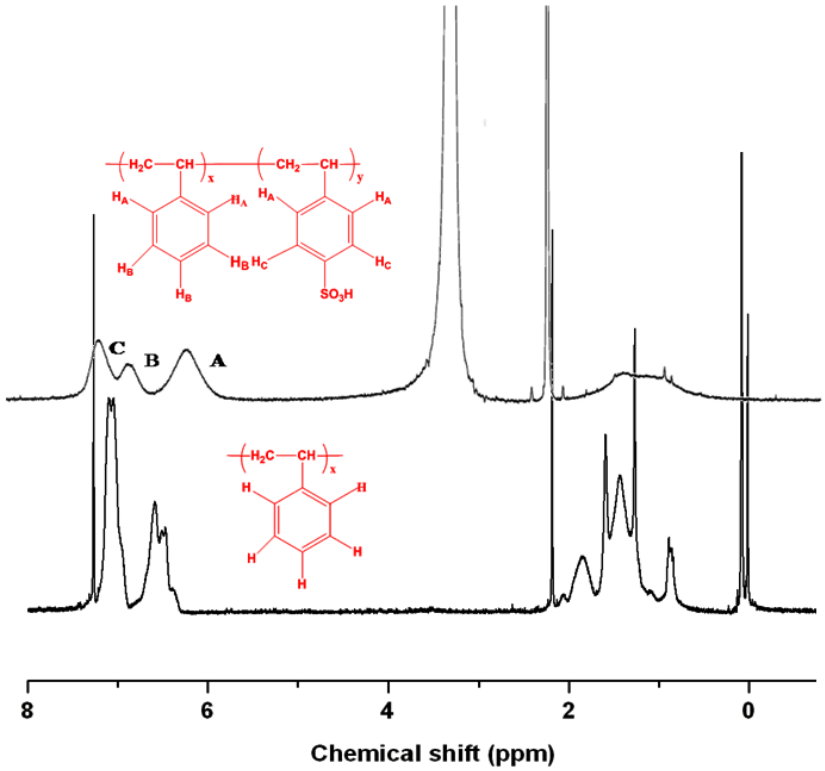

Figure 2.2: Typical ^{1}H NMR spectrum of sulfonated polystyrene (SPS). Polystyrene (PS) spectrum is included for comparison. SPS spectrum was recorded in DMSO-d_6 and $CDCl_3$ was used as NMR solvent in case of PS.

2.3.2. Degree of sulfonation

The accurate evaluation of the DS on the PS backbone is very important for understanding the properties of the resulting SPS. The DS is expressed as the percentage of sulfonated monomers in a PS chain, e.g. DS = 50% means that for each PS repeat unit there will be one sulfonated PS repeat unit on average. Earlier, it was demonstrated that the ^{1}H NMR spectrum of SPS can be used very precisely to determine the DS and it has several advantages over conventional elemental analysis. Peaks B and C of the ^{1}H NMR spectrum of SPS are used to estimate the sulfonation level as per the method adapted from references 22 and 23. If β is the ratio of peak C to B ($\beta = I_C/I_B$), then the sulfonation level (DS) is determined as

$$\text{Degree of Sulfonation} = \frac{100 \times 3\beta}{3\beta + 2} \qquad (2.2)$$

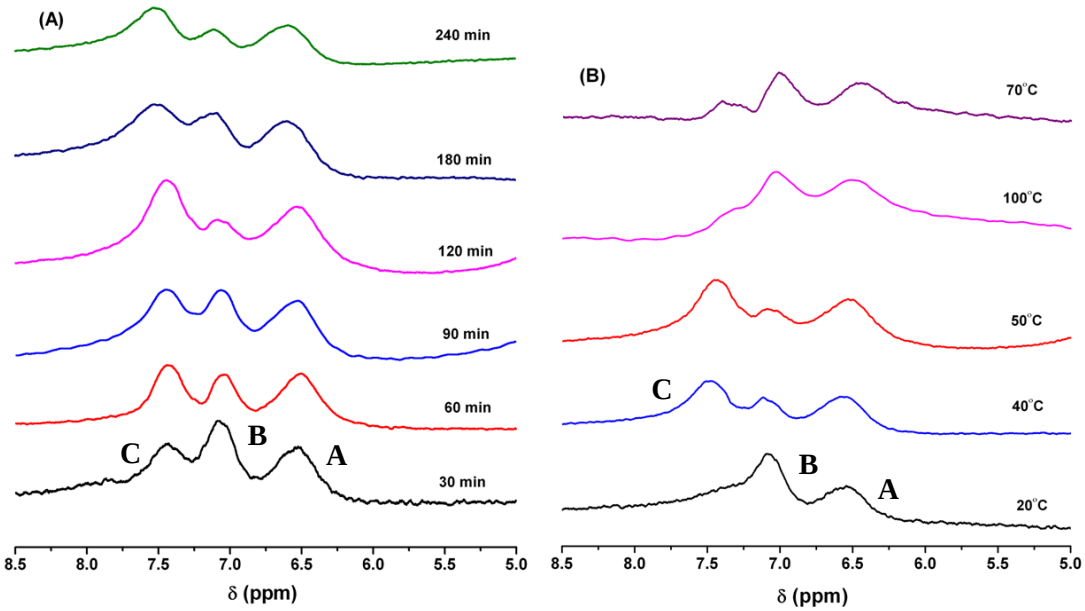

Figure 2.3: ^{1}H NMR spectra of SPS for (A) different reaction times at 40°C and (B) 120 min at different temperatures. The particle size of the PS used was 70 nm.

The aromatic region of the ^{1}H NMR spectra of SPSs obtained by varying the sulfonation reaction times and temperatures are shown in Figure 2.3.The particle size of the PS from which these SPSs are obtained is 70 nm. The ^{1}H NMR spectra of other SPSs obtained from bigger PS particles (160 and 260 nm) by altering the reaction time and temperature are shown in Figures 2.4. The DSs of all the samples were calculated using Eqn. (2.1) and are tabulated in Tables 2.1-2.4. It is evident from the DS values shown in the tables that DS varies with reaction time, temperature and, most surprisingly, with PS particle size. In fact, a careful analysis reveals that for similar sulfonation reaction time and temperature the DS decreases significantly with increasing PS size; e.g. at 40°C if the sulfonation reaction is carried out for 90 min then the DS values for 70, 160 and 260 nm particles are 64.3%, 45% and 24.9%, respectively.

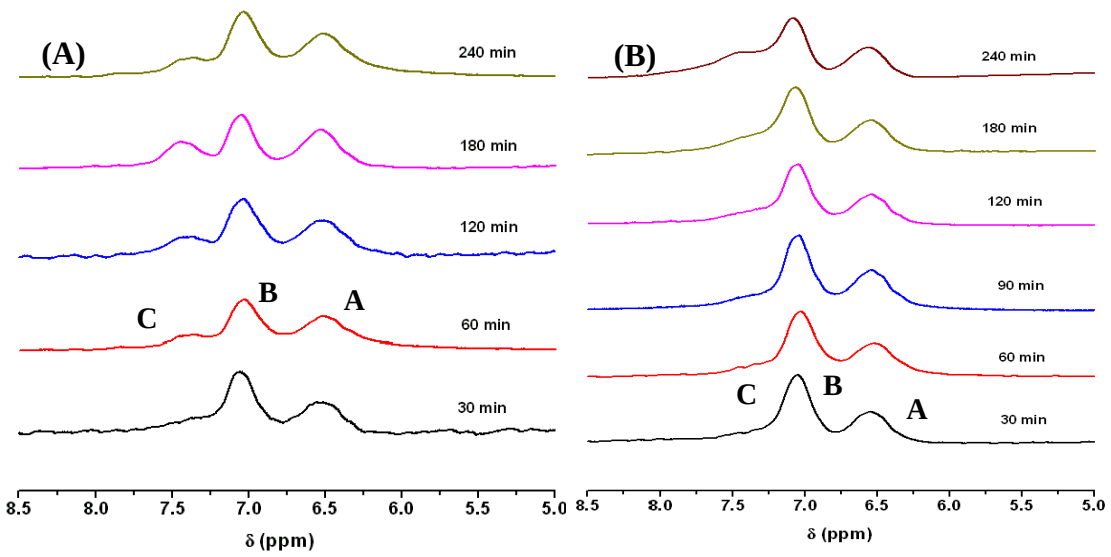

Figure 2.4: ^{1}H NMR spectra of (A) 160 nm (B) 260 nm sulfonated polystyrene particles for different reaction time at 40°C.

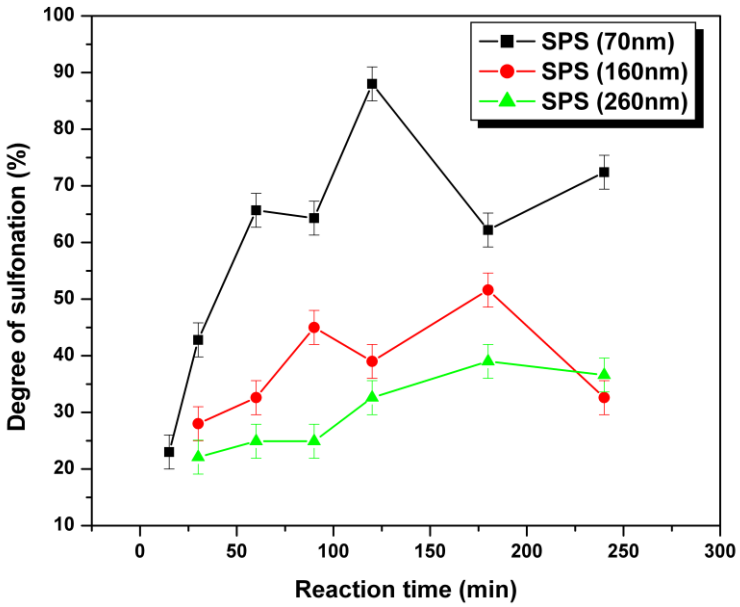

Figure 2.5: Variation of DS with reaction time for PS of different particle sizes. The sulfonation reaction temperature is 40°C for all cases.

To understand and get a better clarity of this observation of PS particle size dependence on DS, we plotted the DS data against time for all the PS particles (Figure 2.5). It is observed that for the three different sizes of PS particles, with

increasing reaction time the DS increases (Figure 2.5) and reaches a maximum at about 2-3 h (depending on the PS size: for 70 nm it is 2 h and for other two it is 3 h); after that the DS decreases. The decrease in sulfonation for longer reaction times may be due to a desulfonation process.[18]

Hence from Figure 2.5 it is proved that the DS of SPS particle is highly dependent upon the particle size of PS particles. Two important observations can be made from the figure: (1) a higher DS can be achieved readily for smaller particle size by carrying out the sulfonation for longer time, but bigger particles do not yield higher DSs even for longer reaction time, and (2) the dependence of DS with time is significantly higher for smaller particles and this dependence decreases with increasing particle size. For example the maximum DS achieved in the case of 70 nm particles is 88%; however, for 160 nm it is 51% and for 260 nm the maximum DS obtained is 39%. Despite our repeated attempts, we could not achieve higher DSs for larger sized particles. It is well known in the literature that sulfonation takes place in the PS particle surface. The probable reason behind these observations; achieving a higher DS and the marked dependence of DS with time for smaller sized particles, is the larger surface area per volume for smaller particles compared with bigger particles. A greater number of sulfonic acid groups ($-SO_3H$) can be accommodated readily in the larger surface area compared with the smaller surface area since the $-SO_3H$ groups experience less repulsion between themselves in the case of the former. Therefore, a higher DS can be achieved readily with relatively shorter reaction time in the case of smaller particles compared with bigger particles.

Figure 2.6 reveals that the reaction temperature also affects the sulfonation reaction when the reaction time is kept constant. For a reaction time of 120 min the DS is only ~38% when the reaction temperature is 20°C. However, when the reaction temperature is 40°C for 120 min time then the DS is 85%, but it again decreases when we further increase the temperature (Figure 2.6). Hence from the above results (Figure 2.5 and 2.6) we can conclude that the highest DS is achieved when the reaction time is 2 h, the temperature is 40°C and the particle size is small. However, it must be noted that

the reaction recipes developed in this work can easily tune the DS of PS as per requirements by simply altering the reaction temperature, time and most importantly the particle size independently.

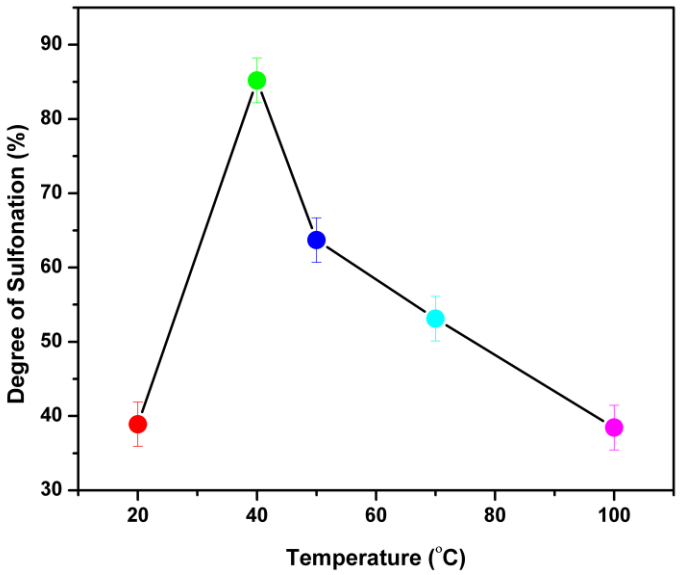

Figure 2.6: Dependence of DS on temperature. The particle size of the PS is 70 nm. The reaction time is kept constant at 120 min for all cases.

2.3.3. Ion exchange capacity

Knowledge of the IEC gives a direct measure of the amount of $-SO_3H$ groups present on the particle surface the H^+ of which can easily be exchanged with cations. A higher IEC value indicates the presence of a larger number of $-SO_3H$ groups which are free from any kind of interactions and hence their H^+ can be readily exchanged with cations. It has been mentioned in the literature that a higher IEC is attributed to the greater incorporation of $-SO_3H$ groups (higher DS) in the particle surface.[36,37] None of the earlier studies looked at the effect of particle size on the relationship between IEC and DS. We found in our study that the particle size significantly influences the proportionalities of IEC and DS. Figure 2.7 presents the plot of IEC versus DS for two different particle sizes.

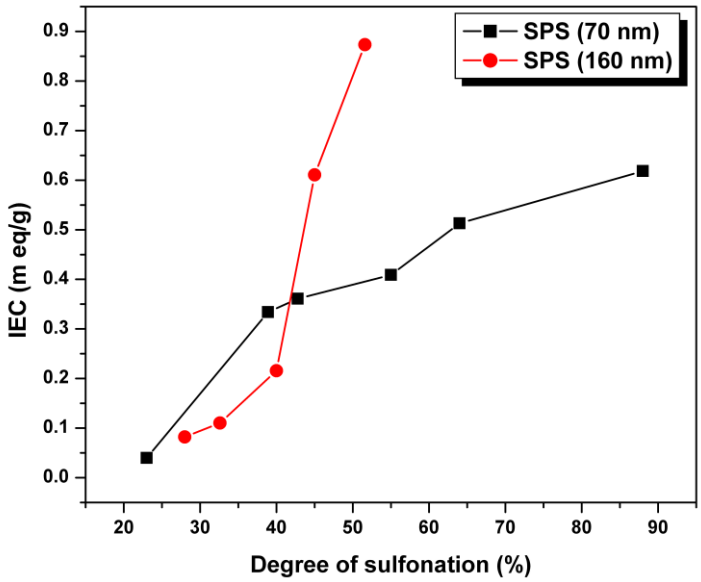

Figure 2.7: Dependence of the IEC of SPS particles on their DS.

From the figure it is observed that the rate of increase of IEC with DS is higher for larger particles than for smaller particles. A maximum IEC value of 0.8734 meq g^{-1} is obtained for 51% SPS in the case of larger particles whereas the maximum IEC value is 0.513 meqg^{-1} when the DS is 88% for smaller particles. This observation clearly demonstrates that a higher DS value alone does not ensure a higher IEC value; the size of the particles plays a major role in the exchange capacity of $-SO_3H$ groups. This conclusion is attributed to the fact that perhaps in the case of smaller particles the $–SO_3H$ groups are not as free as in the case of bigger particles which prevents them from exchanging with cations readily and yields a low IEC compared with bigger particles even though the DS is similar. A lesser degree of freeness of $–SO_3H$ groups in the case of smaller particles compared with bigger particles may be due to higher crowding of $-SO_3H$ groups in the former owing to the smaller size. Because of their crowding, the $-SO_3H$ groups start interacting with each other in an intraparticle manner and hence fewer $-SO_3H$ groups are available to undergo exchange with cations, resulting in a smaller IEC value. However, for larger particles this intraparticle interaction between $-SO_3H$ groups is not possible owing to the larger size and hence less crowding. Therefore more $-SO_3H$ groups are available for exchange yielding a

higher IEC. A schematic model for intra and inter particle interaction for smaller and bigger particles, respectively is shown in Figure 2.8. The morphological features of particles as shown here is discussed in the next section (2.3.3)

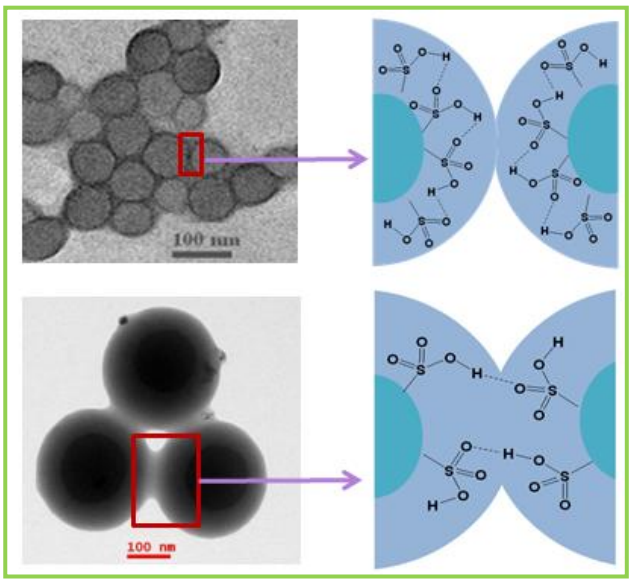

Figure 2.8: Intra and inter particle interactions for smaller and bigger particles, respectively.

We carried out FTIR experiments to prove the interaction between the $-SO_3H$ groups in the case of smaller particle size. Figure 2.9 represents the IR spectra of SPS with different particle sizes and comparable DSs. The S=O asymmetric stretching at 1180 cm^{-1} shift towards lower frequency and becomes very broad with decreasing particle size. It is almost invisible in the case of 70 nm particles but a peak at 1127 cm^{-1} appears gradually and becomes intense. This 1127 cm^{-1} band corresponds to the stretching vibration of the benzene ring substituted with free SO_3^- as an anion.[38,39] The appearance of the 1127 cm^{-1} peak and disappearance of the 1180 cm^{-1} peak are attributed to the $-SO_3H$ groups at the particle surface interacting strongly with each other within the same particle. Therefore the S=O frequency (1180 cm^{-1}) moves towards lower wave number[15] and the presence of free SO_3^- is observed for 70 nm particles. Hence, it can be concluded that intraparticle interaction for smaller sizes plays a major role in the dependence of IEC on DS.

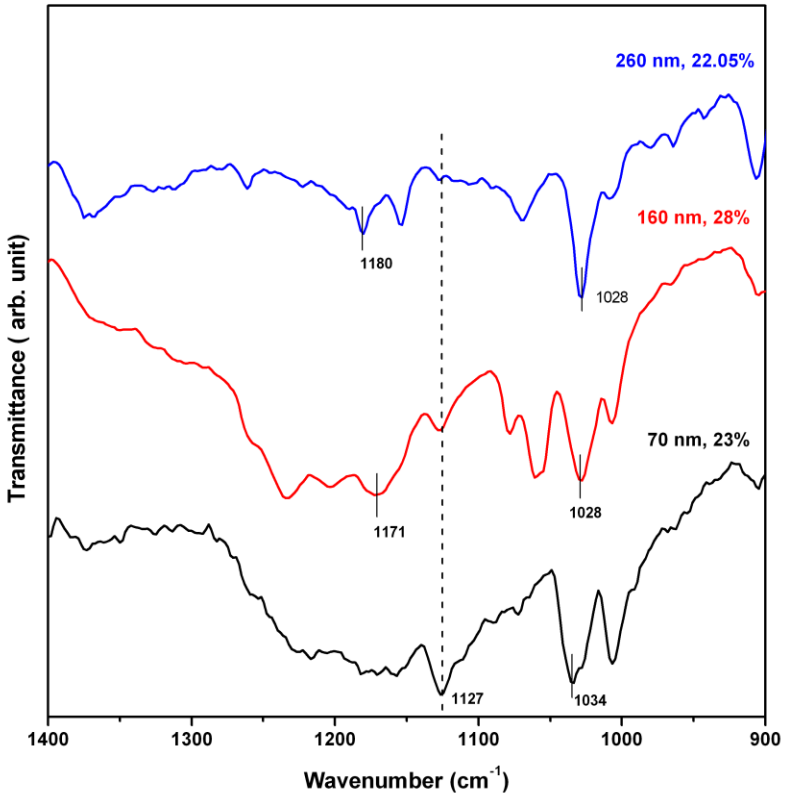

Figure 2.9: FTIR spectra of SPS of different particle sizes with almost similar DSs. Particle sizes and DSs are indicated in the figure.

The above discussion clearly highlights the fact that in the case of smaller particles intraparticle interactions between $–SO_3H$ groups dominate and that interparticle interaction between $–SO_3H$ groups of different particles are predominant for larger particles. If this argument is valid, we can expect that larger particles with a higher DS should yield a physically crosslinked material owing to their stronger interparticle interactions whereas smaller particles with a higher DS should not yield a crosslinked structure but instead should produce dispersed colloidal particles. To verify this expectation, we tried to prepare SPS particles with higher DSs from different sized PS. As can be seen in Figure 2.5, a longer sulfonation reaction time at 40°C readily yields a higher DS (>60%) for 70 nm particles; however, despite repeated attempts we could not obtain a higher DS for larger particles for a reaction temperature of 40°C.

However, sulfonation carried out at 60°C for longer reaction times (180-240 min) with larger particles resulted in a higher DS (>60%). In the case of 160 nm we obtained 72% DS and for 260 nm we obtained 68% DS if the reaction was carried out at 60°C for 180-240 min (Tables 2.3 and 2.4). To our surprise these two samples obtained from larger particles were in the form of a sticky, gummy and jelly mass (Figure 2.10) which was not dispersible in water, as seen in the figure. However, when 70 nm particles were subjected to similar reaction conditions we did not see this; instead we obtained particles with a higher DS (>60%) which are easily dispersible in water. These observations suggest a viscoelastic or gel type nature of the samples indicating the presence of physical crosslinking in the materials. The crosslinking happens because the larger particles with a high DS have a very strong interparticle interaction which results in a crosslinked structure yielding the gel material. On the other hand smaller particles do not have an interparticle interaction; hence they do not result in gel material.

Figure 2.10: Photograph of sulfonated polystyrene (260 nm, 68% DS) showing sticky, gummy and jelly nature.

2.3.4. Morphological studies

The PS colloidal particles used for this work were synthesized using emulsion polymerization. We used three (70, 160 and 260 nm) different sizes of PS particles

prepared by varying the emulsifier concentration during the reaction. As expected from emulsion polymerization, we obtained spherical highly monodisperse PS particles. Representative TEM micrographs of PS particles are shown in Figure 2.11. The particles shown here are highly monodisperse and spherical in shape and in particular their surface is very smooth. The morphology of SPS was studied thoroughly using TEM. Representative TEM images of SPS with different DSs of all three particle sizes are shown in Figure 2.12.

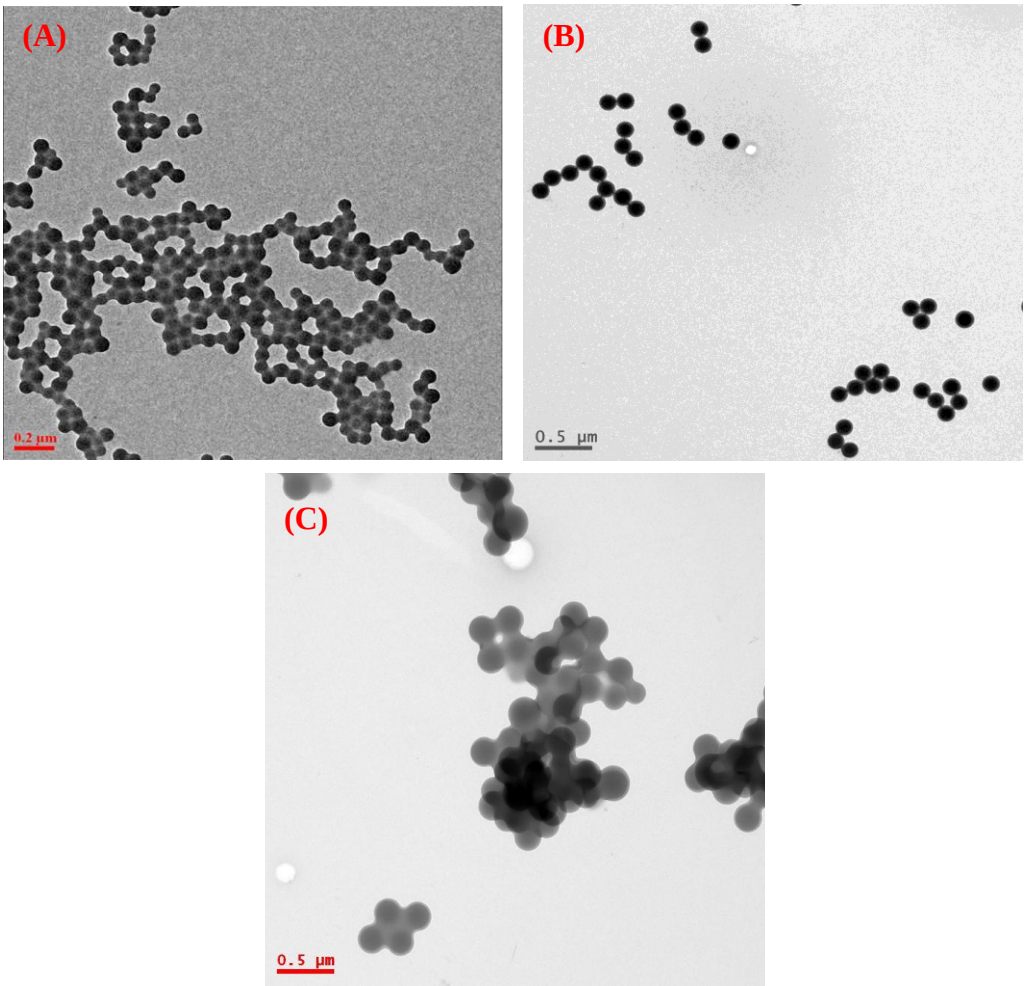

Figure 2.11: TEM images of polystyrene particles of different sizes. (A) 70 nm, (B) 160 nm, (C) 260 nm. The SDS concentrations used in the reaction are 13.8 mM, 1mM and 0.1 mM, respectively.

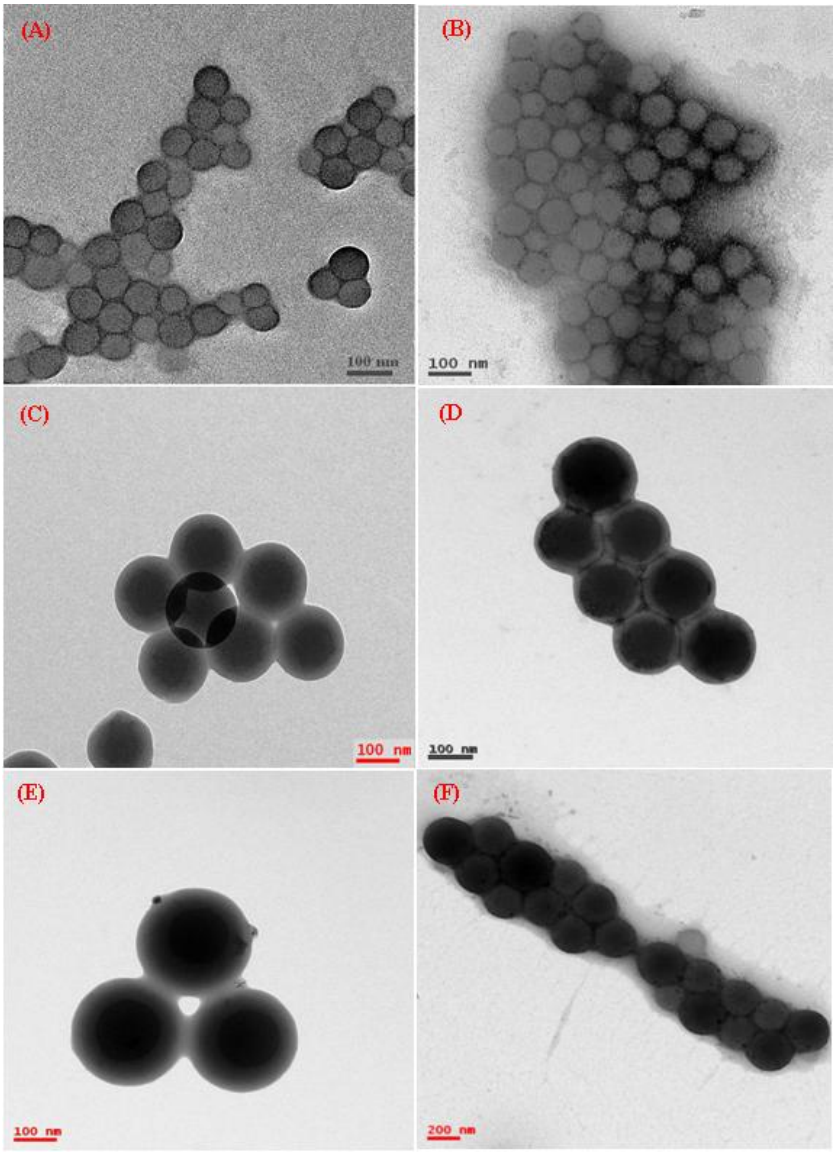

Figure 2.11: TEM images of SPS: (A) 70 nm, 64% DS; (B) 70 nm, 88% DS; (C) 160 nm, 28% DS; (D) 160 nm, 51.6% DS; (E) 260 nm, 26% DS; (F) 260 nm, 68% DS.

All the SPS particles shown here are spherical in shape and almost monodisperse. The particle sizes are similar to those of the PS particles from which they were made. Hence we can conclude that the particle size did not alter much after sulfonation. The size of the particles does not change because the sulfonation reaction occurs inwardly from the PS particle surface.[12,40,41] However, differences between the

particle morphology before (Figure 2.11) and after (Figure 2.12) sulfonation are observed. All the SPS particles show core-shell morphology, whereas PS particles do not have such morphology. All the SPS particles are surrounded by a shell with a core inside the particle. Earlier, several authors observed this and it has been concluded in the literature that the shell is due to the sulfonation of PS and consists of sulfonate groups.[21,42] The sulfonation process occurred synchronously through the whole PS particle surface, ensuring that the sulfonation thickness is uniform. The hydrophilicity of the PS particle surface increases as sulfonation occurs and hence the SPS particles are readily dispersed in water. It must also be noted that the SPS particle surfaces are rough in nature compared with the PS particle surfaces which are smooth. A careful analysis of Figure 2.12 reveals that the thickness of the core and shell vary with DS and particle size. We have measured these data and tabulate in Table 2.5. These data clearly demonstrate the following: (i) the shell thickness decreases with increasing DS; (ii) shells are thicker for larger particles than smaller particles even though their DSs are similar; (iii) the ratio of core to shell thickness is much higher for the smallest particles compared with larger particles. Earlier reports suggest that the shell thickness increases with increasing DS;[30,43] however, our observation as stated above contradicts the reported observation. Unfortunately, no concrete explanation has been suggested in the literature for this observation. We believe the predominant intraparticle interaction between $-SO_3H$ groups for smaller particles and the predominant interparticle interactions in the case of larger particles are the reasons behind our observations (Figure 2.8). As the DS increases, more and more $-SO_3H$ groups are available in the particle surface which undergoes strong interactions between them and the shell thickness decreases. It can be observed in Figure 2.12 that in the case of larger particles the particles are interconnected with each other, whereas in the case of smaller particles this interconnection is not observed. This is because of the interaction between particles in the case of larger particles, which results in gel type material when the DS is high.

Table 2.5: Core and shell thicknesses of sulfonated polystyrene (SPS) particles of different sizes.

Degree of sulfonation (%)	*Core size*	*Shell size*	*Core size/Shell size*
SPS (70 nm)			
23	55	7.3	3.76
35	60	6.25	4.8
42.8	58	5.8	5
55	60	6.8	4.4
64	60	5.5	5.4
72.4	59	4.3	6.8
88	62.5	4.86	6.3
SPS (160 nm)			
28	100	30	1.66
45	106	27	1.96
51.6	110	22	2.5
SPS (260 nm)			
22	170	45	1.88
39	145	60	1.21
68	240	24	5

2.3.5. Thermal studies

First, we verified the thermal stability of all the samples using TGA analysis (Figure 2.13). All the samples show stability up to 300°C. We carried out DSC experiments from 30 to 200°C to measure T_g since within this temperature range no degradation takes place. The DSC thermograms of PS and SPS of different particle sizes are shown in Figure 2.14 and 2.15. The T_g values were plotted against DS for two different size particles and are shown in Figure 2.16. The T_g of SPS particles increases with increasing DS of the samples in both cases. This is because of the lower flexibility of SPS due to $–SO_3H$ groups. The segmental mobility of the polymer chains is restricted with increasing DS in the backbone owing to the ionic interaction. In all cases we obtained only one T_g indicating that sulfonation happened in a random manner in the backbone resulting in a random copolymer of PS and SPS. This observation is in agreement with previous reports.[23,24,44]

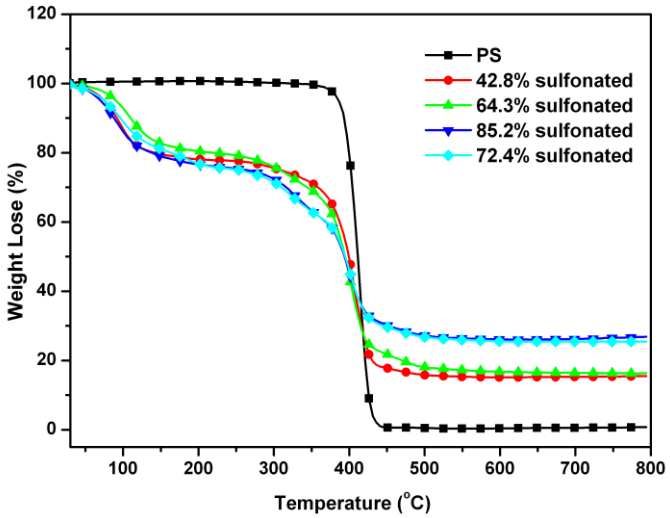

Figure 2.13: TGA thermograms of polystyrene and sulfonated polystyrene for various degree of sulfonation.

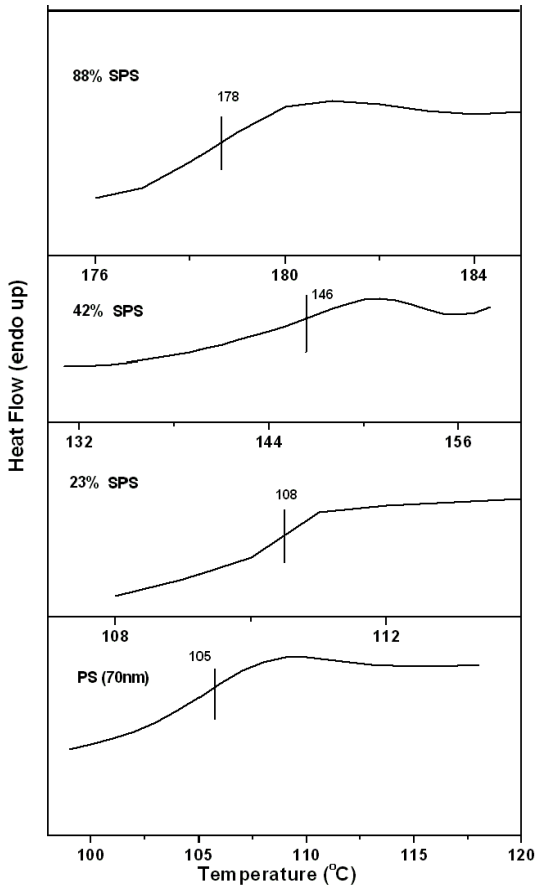

Figure 2.14: DSC thermograms of polystyrene and different sulfonated polystyrene. The particle size is 70 nm.

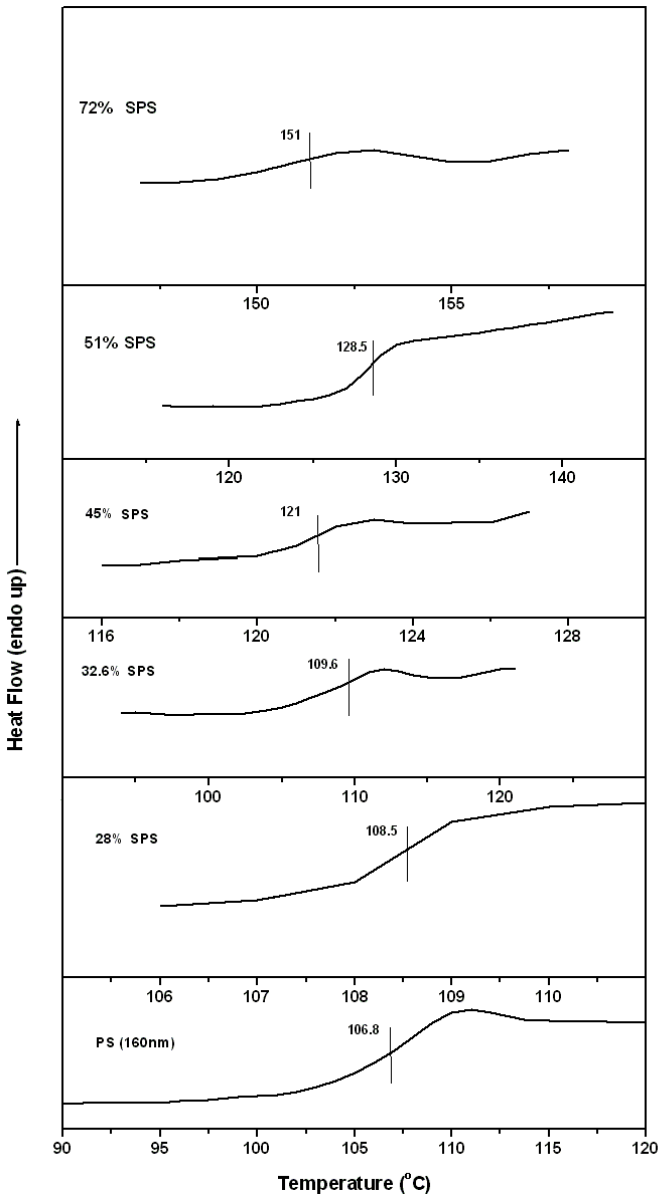

Figure 2.15: DSC thermograms of polystyrene and different sulfonated polystyrene. The particle size is 160 nm.

However, it must be noticed from Figure 2.16 that the increase in T_g of SPS above neat PS is always higher in the case of smaller particles than bigger particles and it is more pronounced for particles with a higher DS. For example the T_g of 55% sulfonated (DS) 70 nm particles is 154°C whereas the T_g of almost similarly sulfonated

(51% DS) 160 nm particles is only 128°C. Although the DS is similar in these two cases the T_g of the smaller particles is ~ 26°C higher than that of the larger particles. This observation once again reconfirms our statement about the presence of strong intraparticle interactions between $–SO_3H$ groups in the case of small sized particles. Since the interaction within the particle is more for smaller particles, the segmental mobility of the PS chains is much more restricted in this case compare to bigger particles, where interparticle interaction is more predominant. Hence the above discussion clearly indicates that particle size plays an important role for the variation of T_g with DS.

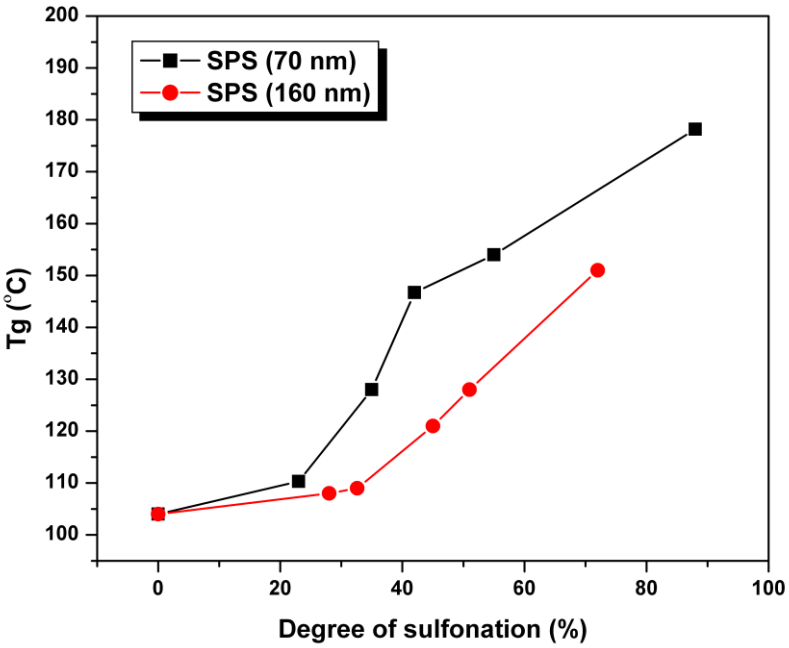

Figure 2.16: T_g *versus* DS of SPS for different particle sizes.

2.4. Conclusion

We prepared a series of SPS particles with various DSs. FTIR, ^{1}HNMR, IEC measurements, TEM, TGA and DSC were used to characterize the SPS particles. It was found that the DS of PS particles, calculated using NMR data, depends not only on reaction time and temperature but also on the size of the parent PS particles. Smaller PS particles, a longer reaction time (~ 2 h) and 40°C temperature are found to be the best

reaction conditions to achieve the higher DS. It was demonstrated that the proportionality of IEC to DS is substantially influenced by the PS particle size: a higher IEC value is obtained for larger particles compared with smaller particles even though their DSs are similar; this is due to the strong interaction between the $–SO_3H$ groups within the particle for smaller particles. SPS particles exhibit core-shell morphology and a thicker shell is obtained for low DS and larger particle size. The T_g of PS increases after sulfonation and increases with increasing DS. Also, the T_g values are influenced by particle size, reinforcing our claim that the particle size of the parent PS plays an important role in the properties of SPS.

2.5. References

1. Schulz, D. N.; Patil, A. O. *Functional Polymers: An Overview*, ACS Symposium Series. American Chemical Society, Washington, DC, Ch. 1, pp. 1–14, **1998**.
2. Wen Hand Park, K.*Oral Controlled Release Formulation Design and Drug Delivery: Theory to Practice.* Wiley, Hoboken, NJ, pp. 7–9, **2010**.
3. Aoki, S.; Otsu, T.; Imoto, M. *Makromol. Chem.* **1966**, *99*, 133.
4. Rubinger, C. P. L.; Martins, C. R.; De Paoli, M. A.; Rubinger, R. M. *Sens. Actuators, B.* **2007**, *123***,** 42.
5. Shah, T. N.; Goodwin, J. C.; Ritchie, S. M. C. *J. Membr. Sci.* **2005**, *251*, 81.
6. Reid, K. R.; Kennedy, L. J.; Crick, E. W.; Conte, E. D. *J. Chromatogr. A.* **2002**, *975*, 135.
7. Cottet, H.; Gareil, P. *J. Chromatogr. A.* **1997**, *772*, 369.
8. Serpico, J. M.; Ehrenberg, S. G.; Fontanella, J. J.; Jiao, X.; Perahia, D.; McGrady, K. A.; Sanders, E. H.; Kellogg, G. E.; Wnek, G. E. *Macromolecules* **2002**, *35*, 5916.
9. Hickner, M. A.; Ghassemi, H.; Kim, Y. S.; Einsla, B. R.; McGrath, J. E. *Chem. Rev.* **2004**, *104*, 4587.
10. Lee, J. M.; Lee, D. G.; Lee, S. J.; Kim, J. H.; Cheong, I. W. *Macromolecules* **2009**, *42*, 4511.
11. Deng, Z.; Chen, M.; Gu, G.; Wu, L. *J. Phys. Chem B.* **2008**, *112*, 16.
12. Yang, Z.; Niu, Z.; Lu, Y.; Hu, Z.; Han, C. C. *Angew. Chem. Int. Ed.* **2003**, *42*, 1943.
13. Lu, X.; Weiss, R. A. *Macromolecules* **1991**, *24*, 4381.
14. Sahu, A. K. ; Selvarani, G. ; Bhat, S. D. ; Pitchumani, S. ; Sridhar, P. ; Shukla, A. K. ; Narayanan, N. ; Banerjee, A. ; Chandrakumar, N. *J. Membrane Sci.* **2008**, *319*, 298.
15. Hazarika, M.; Arunbabu, D.; Jana, T. *J. Colloid Interface Sci.* **2010**, *351*, 374.
16. He, X. D.; Ge, X. W.; Liu, H. R.; Wang, M. Z.; Zhang, Z. C.; *Chem. Mater.* 2005, *17*, 5891.

17. He, X. D.; Ge, X. W.; Wang, M. Z.; Zhang, Z. C. *Polymer* **2005**, *46*, 7598.
18. Kucera, F. ; Jancar, J. *Polym. Eng. Sci.* **1998**. *38*, 783.
19. Turbak, A. F. *Ind Eng. Chem, Prod- Res. Dev.* **1962**, *1*, 275.
20. Makowski, H. S.; Lundberg, R. D.; Singhal, G. H. Flexible polymeric compositions comprising a normally plastic polymer sulfonated to about 0.2 to about 10 mole % sulfonated. US Patent 3870841, **1975**, *870*, 841**.**
21. Weiss, R. A.; Lundberg, R. D.; Turner, S. R. *J. Polym Sci Polym Chem Ed.* **1985**, *23*, 549.
22. Baigl, D.; Seery, T. A. P.; Williams, C. E. *Macromolecules* **2002**, *35*, 2318.
23. Arunbabu, D.; Sanga, Z.; Seenimeera, K. M.; Jana, T. *Polym Int*. **2008**, *58*, 88.
24. Yeole, N.; Hundiwale, D.; Jana, T. *J. Colloid Interface Sci.* **2011**, *354*, 506.
25. Tran, Y.; Auroy, P. *J. Am. Chem. Soc.* **2001**, *123*, 3644.
26. Orler, E. B.; Dorie, J. Z.; Robert, B. M. *Macromolecule*. **1993**, *26*, 5157.
27. Lundberg, R**.** D.; Makowski, H. S. *Polym. Prepr*. **1978,** *19*, 287.
28. Yang, M.; Ma, J.; Zhang, C.; Yang, Z.; Lu, Y. *Angew. Chem. Int. Ed.* **2005**, *44*, 6727.
29. Niu, Z.; Yang, Z.; Hu, Z.; Lu Y.; Han, C. C. *Adv. Funct. Mater*. **2003**, *13*, 949.
30. Wang, X.; Tang, S.; Liu, J.; He, Z.; An, L.; Zhang, C.; Hao, J.; Feng, W. *J. Nanopart Res.* ***2009****, 11*, 923.
31. Arunbabu, D.; Sannigrahi, A.; Jana, T. *J. Appl. Polym. Sci*. **2008**, *108*, 2718.
32. Arunbabu, D.; Hazarika, M.; Naik, S.; Jana, T. *Bull. Mate. Sci*. **2009**, *32*, 633.
33. Arunbabu, D.; Jana, T. *J. Colloid Interface Sci.* **2011**, *361*, 534.
34. Yang, J. C; Jablonsky, M. J.; Mays, J. W. *Polymer* **2002**, *43*, 5125.
35. Lee, J. H.; Kang, S. J.; Lee, Y.; Nam, J. D.; *Polym. Bull*. 2010, 64, 717.
36. Bhuttoa, A. A. Veselyb, D., Gabrys, B. J. *Polymer* **2003**, *44*, 6627.
37. Brijmohan, S. B.; Swier, S.; Weiss, R. A.; Shaw, M. T. *Ind. Eng. Chem. Res.* **2005**, *44*, 8039.
38. Castagna, A. M.; Wang, W.; Winey, K. I.; Runt, J. *Macromolecules*, **2010**, *43*, 10498.
39. Zhou, N. C.; Burghardt, W. R.; Winey, K. I. *Macromolecules*, **2007**, *40*, 6401.

40. Ziwei, D.; Min, C.; Guangxin, G.; Limin, W. *J. Phys. Chem. B* **2008**, *112*, 16.
41. Yang, Z. Z.; Li, D.; Rong, J. H.; Yan, W. D.; Niu, Z. W. *Macromol. Mater. Eng.* **2002**, *287*, 627.
42. Yang, Y.; Chu, Y.; Zhang, Y.; Yang, F.; Liu, J. *J. Solid State Chem.* **2006**, *179*, 470.
43. Wang, X.; Tang, S.; Zhou, C.; Liu, J.; Feng, W. *Synth. Met.* **2009**, *159*, 1865.
44. Su, Z.; Li, X.; Hsu, S. L. *Macromolecules* **1994**, *27*, 287.

Chapter 3

Formation of core (polystyrene)–shell (polybenzimidazole) nanoparticles using sulfonated polystyrene as template

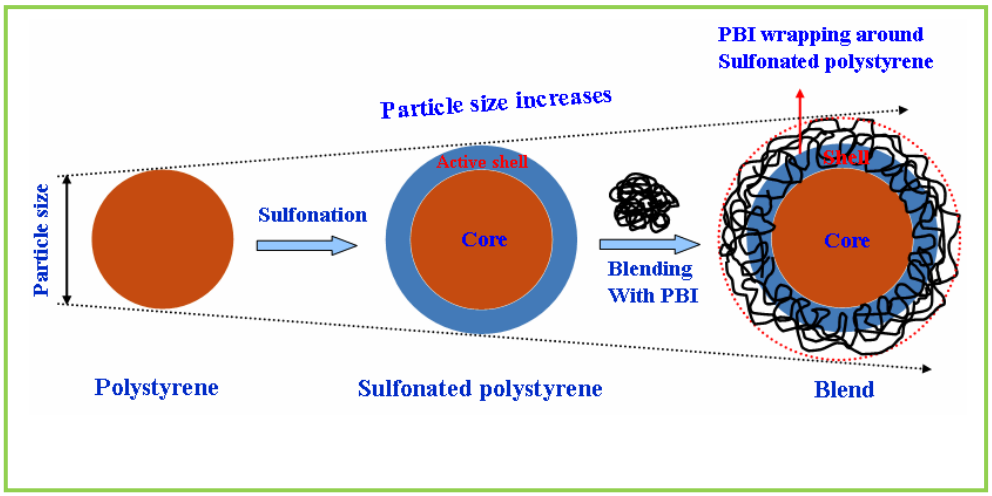

The disruption of polybenzimidazole chains self-association owing to the interaction between the functional groups upon blending with sulfonated polystyrene particles is the driving force for the formation of core-shell nanoparticles.

Hazarika, M.; Arunbabu, D.; Jana, T. *J. Colloid Interface Sci.* **2010**, *351*, 374-383.

3.1. Introduction

In the past several decades, polymer blending technique has been utilized extensively to develop new materials with superior and desirable physical properties by combining advantages of the individual components of two or more polymers.[1-3] Unfortunately, very often polymer pairs of interest do not mix each other due to the relatively small contribution of the entropy of mixing and the unfavorable (positive) enthalpy of mixing of most high molecular weight polymers.[3,4] The lack of specific interactions between the polymers is held responsible for not satisfying the thermodynamical constraint for the miscibility. As an outcome of this, many polymer pairs form immiscible blend and yield multiphase materials. The most suitable approach to resolve this problem is to induce the specific exothermic interactions between the polymer pairs and in consequence they become miscible. This approach demands the appropriate modification of the individual component(s) by suitable functionalization of the polymer backbone.[5-7]

The partially or lightly ionized polymers, known as ionomers, are exciting materials because of their unique physical properties. The ionomer possesses both covalent hydrocarbon polymeric chains and ionic salt species in the same molecule.[8] The ionic part of the ionomer can induce the specific interactions to facilitate the miscibility of wide range of polymers which are otherwise immiscible through various types of interactions such as acid- base, hydrogen bonding, ion-dipole, dipole-dipole, transition metal complexation, etc.[5-7,9-20] The most widely used ionomer in the literature is sulfonated polystyrene (SPS). A large number of miscible blend systems have been developed with variety of polymers by utilizing the specific interactions arising from the ionomeric behavior of SPS. Among these blend systems, SPS-polyamide.[6,7] SPS-poly (ε-caprolactam),[17] SPS-polyurethane,[19] SPS-poly (vinyl alcohol),[20] etc. have studied extensively. There are few more ionomers such as sulfonated polyester,[4,21] sulfonated polysulfone,[12,13] sulfonated polyphenylsulfone,[13] sulfonated poly (arylene ether ketone)[22,23] have also been used to develop the miscible blends with variety of polymers. In all the above examples, the driving forces for the formation of miscible

blend are the specific interactions between the ionic groups of ionomers and functional groups of other polymers. It has also been demonstrated that the strength of interactions and thereby the phase behavior of the resulting blends can be controlled by varying the degree of ionizations of ionomer and the type of counter ion of the ionic part of the ionomer[5,12]

In addition to its extensive utility as ionomer, sulfonated polystyrene (SPS) also has find numerous applications in the areas of catalysis, water purification, chromatography techniques, etc.[24-27] Hydrated SPS exhibits proton conductivity and it has been used as proton conducting component in proton exchange membrane (PEM) fuel cells.[16,28-30] The proton conductivity, water uptake and methanol permeability have improved significantly when SPS is blended with poly (2,6-dimethyl-1,4-phenylene oxide), etc.[14] SPS particles (micro or nano spheres) have been extensively used as template for the synthesis of composite materials with hollow nanostructures and core-shell morphology.[31-35]. Hollow micro spheres of inorganic oxides like cerium oxide, titanium oxide, zinc oxide, etc. were prepared using SPS as template.[32-35] These core-shell materials are applicable to various fields such as coating, electronics, catalysis, separations and diagnostics.

Polybenzimidazole (PBI; Scheme 3.1) is an amorphous polymer. It has very high glass transition temperature and shows good proton conductivity after doping with phosphoric acid (PA). PBI has been used widely as a non flammable fiber for high temperature applications owing to its exceptional thermal, oxidative stability and fire retarding capacity.[36,37] Phosphoric acid doped PBI is being used in high temperature direct methanol fuel cell as well as H_2/O_2 fuel cells because of its very high thermo chemical stability and low gas permeability.[38-41] PBI possesses both proton donor (–NH–) and proton acceptor (–N=) hydrogen bonding sites, which exhibit specific interactions with polar solvents[42-45] and upon blending with a variety of polymers.[12,46-50] A wide range of polymers with variety of polar functional groups such as carbonyl, sulfonyl in their backbone form miscible blend with PBI and the miscibility arises due to the specific hydrogen bonding interaction between the functional groups of these polymers. A large number of PBI blends with variety of polymers are reported in the

literature. Example includes polyimide, polyamide, poly (ether imides), polysulfone, etc.[12,46,47,51,52,56,58] Recently, our group has demonstrated that the hydrophobic contribution of PVDF component in the blends of PBI and PVDF helps to reduce the water uptake capacity of the PBI in the blend which allows the PBI chain to absorb higher quantities of PA than pure PBI.[48]

The above discussion about PBI and SPS clearly indicates that both these polymers have few interesting and important properties; however they have few disadvantages too. Hence, we hypothesize that blends of these two polymers may generate new materials with better properties and possibly eliminate the individual disadvantages of these two components in the blends. We expect to improve the properties like solubility, flexibility and processability upon blending. The resulting materials produce from the blending of spherical SPS particles with PBI may have core-shell type morphology in which core is the SPS and shell is the PBI. It is possible to prepare the hollow PBI micro/nano spheres by dissolving the SPS core from the core-shell structure. Hollow PBI particles may find applications in the PEM fuel cell since a large quantity of PA can be filled inside the hollow space. As per our knowledge there is no report in the literature on PBI/SPS blend. Sulfonated polystyrene has sulfonate (SO_3^-) group with S=O bonds. On the other hand PBI possesses both donor and acceptor hydrogen bonding site, which can participate specific interaction with other functional groups. So we expect that PBI may form blend with SPS by interacting with SO_3^- groups. In the present work, sodium salt of sulfonated polystyrene (SPS-Na; Scheme 3.1) with different degrees of sulfonation was prepared by sulfonation of polystyrene particles. Furthermore, blends of these SPS-Na particles with PBI were prepared. The structural analysis of blend membranes and the effect of interaction between the two polymers are studied as a function of the sulfonation degrees and the blend composition. The blends have been characterized using FT-IR and differential scanning calorimeter (DSC). The particle size and morphology of SPS-Na and the blend were also studied using transmission electron microscopy (TEM).

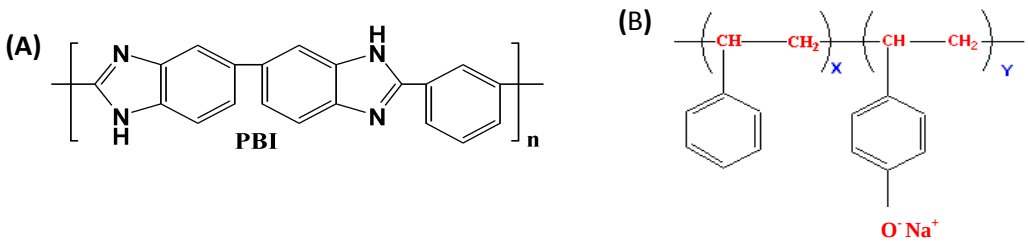

Scheme 3.1: Structure of (A) PBI and (B) SPS-Na.

3.2. Experimental Section

3.2.1. Materials

Poly [2,2′-(m-phenylene)-5,5′-benzimidazole] (PBI) was obtained by polymerizing 3,3′,4,4′-tetraaminobiphenyl (TAB) and isophthalic acid in poly phosphoric acid medium (115%) in the laboratory using our standard method described earlier and reaction scheme is shown in section 4.1 of Chapter 4.[37,42] Styrene (Sisco, India), sodium dodecyl sulfate (SDS, Merck), sodium bicarbonate (Sisco, India), and ammonium per sulfate (APS, Merck) as the monomer, surfactant, buffer, and initiator, respectively, were used as received from the suppliers. Dowex mixed bed ion-exchange resin (Sigma-Aldrich), acetic anhydride (Fisher Scientific), Sulfuric acid (Merck), 1,2-dichloroethane (Loba Chemie), dimethylsulfoxide (Merck), deuterated dimethyl sulfoxide (DMSO-*d6*) were used as received. Milli Q water was used for all the experiments. This water was obtained from the Millipore water purification system (Elix 10).

3.2.2. Synthesis and purification of polystyrene particles

Spherical polystyrene colloidal particles were synthesized by emulsion polymerization technique[53] as described in section 2.2.2 of Chapter 2. The emulsifier concentration was chosen for this chapter work is in such a way so that the resulted PS particle size is 50 nm.

3.2.3. Sulfonation of polystyrene particles

The sulfonation of polystyrene particles was carried out according to the method described by Baigl et al.[54] Briefly the procedure is as follows: 1 g of polystyrene particle was taken into a three-neck round bottom glass flask. The middle neck was fitted with water-cooled condenser; nitrogen gas was introduced through the right-hand neck. 15 mL of 1,2-dichloroethane (DCE) was added to the reaction flask and it was then stirred for 1 h under a nitrogen atmosphere at 50°C. The sulfonation reagent was prepared by mixing acetic anhydride (AA) and sulfuric acid (H_2SO_4) in 60 mL of DCE in ice cooled condition. The quantity of AA and H_2SO_4 in DCE were varied depending upon the target sulfonation degree. The molar ratio of H_2SO_4 and AA was kept constant at 1.8. Then this sulfonation reagent was slowly added in the reaction mixture. Then the reaction was continued at 50°C for 2 h. The reaction was quenched by placing the hot reaction vessel in cold water bath at 10°C. Then the organic solvents were evaporated in a rotary evaporator. The resulting sulfonated polymer product had the appearance of chewing gum. This material was dissolved in 100 mL of Milli Q water. If the polymer was not soluble in water then dimethyl sulfoxide (DMSO) was used instead of water. The sulfonated polystyrene was converted into sodium salt of sulfonated polystyrene (SPS-Na) by slowly adding NaOH until the solution pH reached to 10. Then the solution was loaded into dialysis membrane bag (Himedia, MWCO: 30,000) and dialyzed in Milli Q water to remove the ions (NaOH in excess, sulfates, acetates) for one week by changing the water twice in a day. After one weak polymer solution was taken out from the dialysis bag and the dialyzed solution was freeze dried and the free flowing sodium salt of sulfonated polystyrene (SPS-Na) particles were collected.

3.2.4. Blend preparation

Blends were prepared by mixing two polymers (PBI and SPS-Na) in DMSO. The concentration of the polymer solution in DMSO was kept 0.5% (w/v). The required amount of the two polymers were taken in the measured quantity of DMSO and was mixing was continued for 24 h by stirring with the help of magnetic stirrer in a close

glass vessel at room temperature. The homogeneous blend solutions were filtered through a 0.5 μm PTFE membrane and then poured into a clean glass petri dish at 80°C to cast the blend films. Transparent homogeneous thin films were obtained and dried in a vacuum oven at 100°C for 3 days to evaporate the trace amount of solvent completely.

3.2.5. Characterization techniques

Fourier transforms infrared (FT-IR) spectra of the thin blend films were recorded on Nicolet 5700 FT-IR spectrometer at resolution of 0.5 cm^{-1} with an average of 32 scans. A differential scanning calorimeter (Pyris Diamond DSC, Perkin-Elmer) was used to study the glass transitions (T_g) of the blend samples. Blend samples were annealed at 450°C for 30 min, cooled to 100°C at a cooling rate of 200°C/min, and subsequently (after 30 min equilibration at 100°C) scanned from 100°C to 450°C at a heating rate of 10°C/min. The lower PBI or higher SPS-Na content samples were annealed at 300°C instead of 450°C which was maintained for other samples. The reproducibility of DSC results was checked by repeating the experiment at least thrice. DSC was calibrated using In and Zn as calibration material prior to scan the blend samples. A transmission electron microscope (TEM, FEI Tecnai Model No. 2083) operating at 120 kV was used to image and study the morphology of the samples. The TEM samples were prepared by drop casting samples dispersion in the carbon coated copper (200 mesh) grid. To determine the sulfonation degree of sodium salt of sulfonated polystyrene, ^{1}H NMR measurements were performed by using a Bruker 400 MHz NMR spectrometer. The samples were prepared in deuterated dimethyl sulfoxide (DMSO-d_6). The degree of sulfonation is measured using the method described earlier in Chapter 2.[54,55]

3. 3. Results and Discussion

3.3.1. FT-IR study

The blending of polybenzimidazole (PBI) and sodium salt of sulfonated polystyrene (SPS-Na) in various compositions is studied thoroughly using FT-IR

spectroscopy. The interactions in PBI blends with wide range of polymers have been extensively examined by FT-IR spectroscopic technique in the literature by several authors.[12,46-48,56] Most of the crucial informations of PBI are based on the N–H stretching region of the imidazole moiety of the PBI polymer. The spectrum of PBI shows a series of N–H stretching bands in the 3600-3000 cm^{-1} region and, moreover, SPS-Na does not have any distinct vibrational frequency in this region (Figure 3.1). Hence, any possible changes in this frequency range due to the interaction between imidazole moieties of PBI with SPS-Na can be easily identified and analyzed.

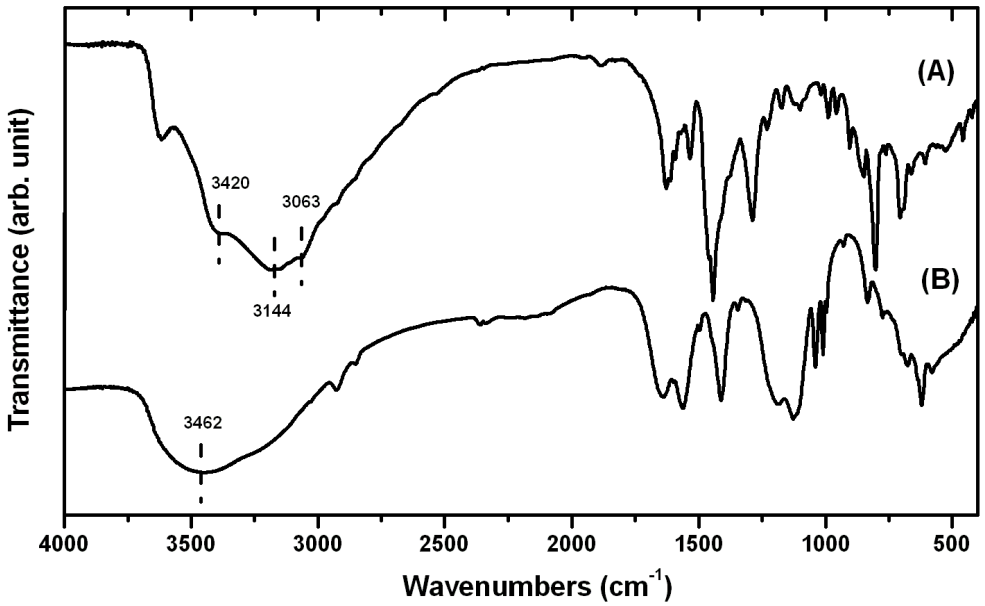

Figure 3.1: FT-IR spectra recorded from the thin films (30µm) of (A) Poly [2, 2'-(*m*-phenylene)-5, 5' benzimidazole] (PBI) and (B) sodium salt of sulfonated polystyrene (SPS-Na); The degree of sulfonation is 75%.

IR spectrum of PBI has been separated into three distinguishable contributions of different signature stretchings as shown in Figure 3.2. These are as follows: (i) a relatively sharp peak at 3420 cm^{-1} due to isolated, non hydrogen-bonded free N–H groups, (ii) a very broad asymmetric peak centered at around 3144 cm^{-1} owing to the self associated, hydrogen-bonded N–H groups, and (iii) a third low intensity peak at 3063 cm^{-1} due to the stretching modes of the aromatic C–H groups.[48,56] The broad peak

at around 3462 cm^{-1} in SPS-Na is due to the O–H stretching vibration of residual water and the sulfonate groups.[54]

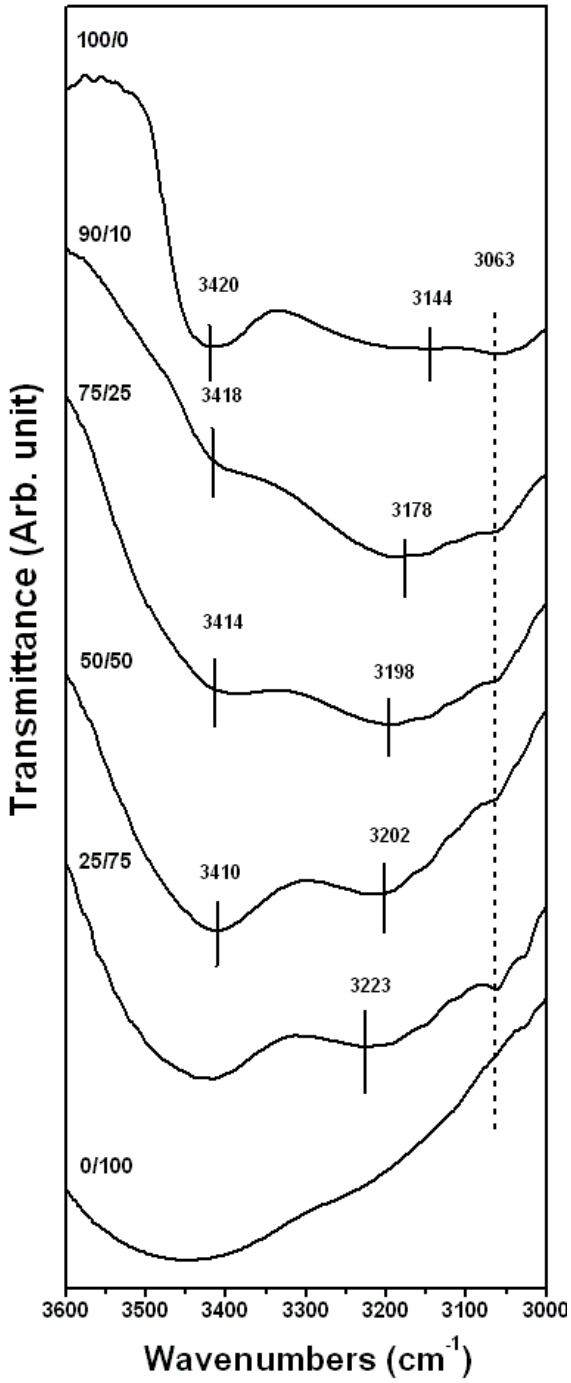

Figure 3.2: FT-IR spectra of the PBI/SPS-Na (75% sulfonated) blend film samples at their indicated blend compositions. The thicknesses of the films are 30 μm.

The FT-IR spectra of PBI and representative blends of PBI with SPS-Na (75% sulfonated) in the 3600–3000 cm^{-1} region are presented in Figure 3.2. It can be seen from Figure 3.2 that the free non hydrogen-bonded N–H stretching band at 3420 cm^{-1} displays a substantial broadening and shifts to lower frequencies with increasing SPS-Na content in the blends. In the 50/50 blends, this peak shifts to 3410 cm^{-1}. After 50/50 blend composition, it becomes difficult to assign the free N–H peak position due to the mixing of broad SPS-Na peak around 3462 cm^{-1}. However, the peak at 3063 cm^{-1} which is due to C–H aromatic stretching does not change its position. Hence the shifting of the free N–H band position upon blending indicates the formation of hydrogen bonding interaction between the N–H group of the PBI and the functional groups of the SPS-Na. Similar kinds of interactions of the free N–H group of PBI with many other functional groups of wide variety of polymers are reported in the literature.[12,46,48,57] It has also been demonstrated that this interaction of PBI with other blend component is stoichiometric in nature.[48,57] However, in the present case it is not possible to predict the stoichiometric nature of the interactions due to the overlapping of broad SPS-Na peak with free N–H peak after 50/50 blends (Figure 3.2). In the later section, we will discuss about which functional group of SPS-Na takes part in the interaction. Another important observation from Figure 3.2 needs to be looked at very carefully. Figure 3.2 show that with increasing SPS-Na content in the blends, the intensity of the self associated hydrogen-bonded broad N–H band centered at 3144 cm^{-1} diminishes, and a new broad band at higher frequency appears. This new broad band shifts gradually towards higher frequency with increasing SPS-Na content in the blend. We could analyze this peak up to 25/75 composition and in this case this peak comes at 3223 cm^{-1}. Hence, a maximum 79 cm^{-1} (3144-3223 cm^{-1}) shift is observed (Figure 3.3). Previously, shifting of this self associated peak is reported and explained as owing to the weakening of self associated N–H–N hydrogen bonding of the PBI chains.[12,48]

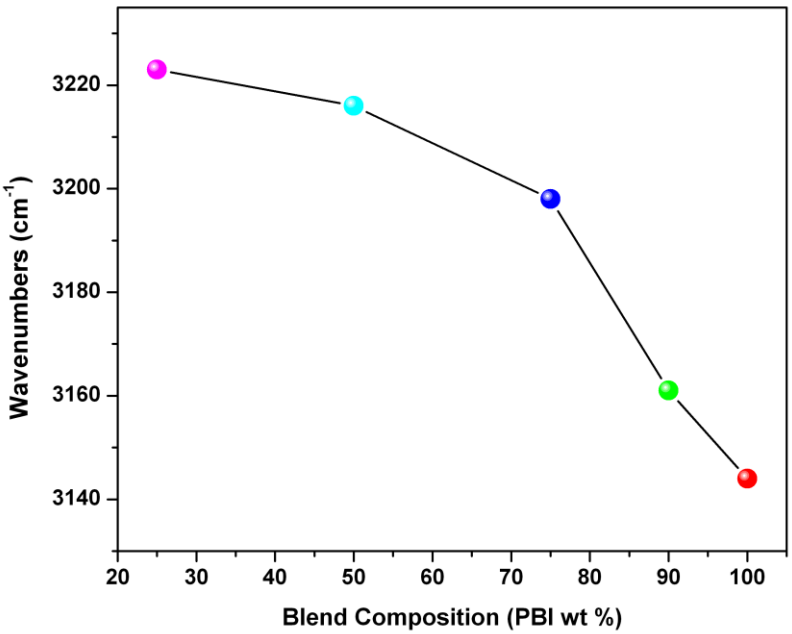

Figure 3.3: Variation of the self associated N–H stretching frequencies of PBI as a function of blends composition. The SPS-Na used here is 75% sulfonated.

However, in all the previous reports the extent of shift are very less; in most of the cases it is only 30-40 cm^{-1}. This huge shift (79 cm^{-1}) in the present case is quite interesting and attributing a greater degree of disruption of the self association of the PBI chains. A significantly smaller (~10 cm^{-1}, 3420-3410 cm^{-1}) shift of the free N–H stretching band of PBI and undoubtedly a larger (79 cm^{-1}) displacement of self associated N–H band of PBI compare to all other reported blends of the PBI in the literature suggesting that in the present blend system the functional group of SPS-Na is interacting with the self associated N–H group of PBI more strongly than the free N–H group of PBI. This kind of observation is not obtained previously for the PBI blends. The stronger interaction of self associated N–H peak of PBI with other functional group of the second polymer can results the complete diminish of the PBI self association. It is also known that the PBI chains self association partially contributes the inherent strong rigidity of PBI chains. Therefore, we can expect that upon blending with SPS-Na, PBI chains will lose its rigidity and become flexible owing to the considerable disruption of

PBI self association due to blending. In the later section, we will be discussing the decrease of glass transition temperature (T_g) of the PBI upon blending, which is a reflection of the significant loss of the PBI chains rigidity. The driving force for this change in rigidity of PBI is indeed the blending of the two polymers. However, the question remains why the self associated N–H group of PBI interacts with SPS-Na stronger than the free N–H of PBI? Our answer to this puzzling question is as follows: SPS-Na is a spherical particle (as seen in the microscope images presented in the later section) with sulfonate groups on the surface of the particle. Upon blending the N–H of PBI interacts with the sulfonate groups of SPS-Na. Since the sulfonate groups are randomly distributed on the spherical particle surface[33,34] hence for a successful interaction between N–H of PBI and $–SO_3^-$ Na^+ of SPS-Na; the PBI chains need to be wrapped around the SPS-Na sphere. Therefore, blending demands wrapping of PBI chains on top of SPS-Na particles. However, this wrapping in not possible unless the PBI chain is flexible enough. Therefore to achieve the flexibility of PBI chain so that it can wrap SPS-Na particle and successful blending is possible, the significant elimination of N–H self association of PBI chain is required. As a result of this above requirement we observed a stronger interaction of self associated N–H with SPS-Na. The above discussion hints that the final blends should have particle morphology with core and shell structure, where core is made up of SPS-Na and shell constitutes PBI. In the later section, we have studied morphology using transmission electron microscopic technique and the result matches with the above justification.

In the previous section, we have demonstrated that N–H functionality of PBI interacts with the SPS-Na. Since in SPS-Na the only functional group is $–SO_3^-$ Na^+, hence it is expected that N–H of PBI interacting with S=O of SPS-Na. Therefore, noticeable changes in S=O stretching band is expected in the blend samples. In case of SPS-Na the band at 1182 cm^{-1} and 1041 cm^{-1} are attributed to the asymmetric and symmetric stretching vibrations of S=O group, respectively. The infrared band located at 834 cm^{-1} is assigned to C–H out-of-plane vibration in para substituted benzene ring of SPS-Na.[55] Figure 3.4A shows that the 1182 cm^{-1} peak of pure SPS-Na (0/100) shifts to 1175 cm^{-1} and similarly 1041 cm^{-1} peak of SPS-Na (0/100) moves to 1022 cm^{-1} for the

90/10 sample. These are because of the interaction of S=O bond with the N–H group of PBI. These observations indicate the weakening of the S=O bond upon blending. The peak position at 834 cm^{-1} of SPS-Na (0/100) shifted to higher frequency (850 cm^{-1}) in the 90/10 blend (Figure 3.4B). This is due to the interaction between two polymer compounds. Because of this interaction the free movement of C–H vibration is perturbed and hence the frequency moves to the higher side.[55] Therefore, all the above IR studies prove the successful interaction between the N–H of PBI and S=O of SPS-Na, which result in the blending of these two polymer components.

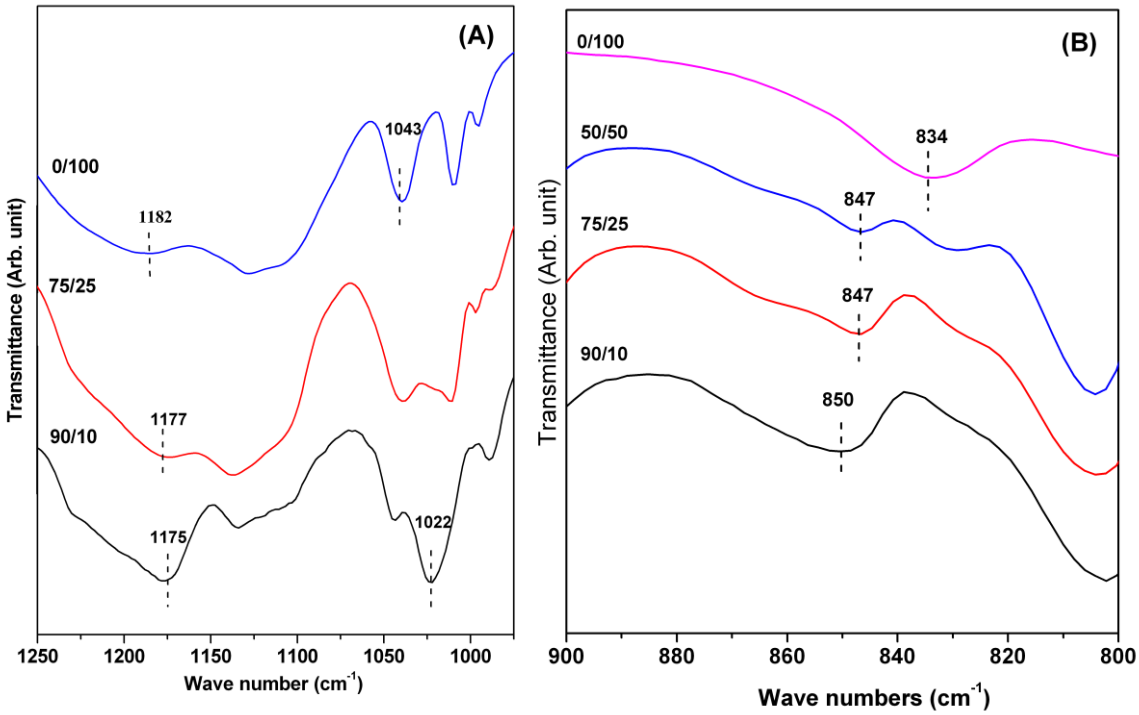

Figure 3.4: FT-IR spectra of the PBI/SPS-Na (75% sulfonated) blend film samples (thickness 30 μm) at their indicated blend compositions.

3.3.2. Thermal study

The blend samples of PBI and SPS-Na (75% sulfonated) are obtained as thin (30 μm) films by slowly evaporating the solvent. These thin films are homogeneous and transparent (Figure 3.5), indicating the blending of the two polymer components. In the

previous section, the detail FT-IR studies of these blend films proved the presence of specific interaction between the functional groups of the two polymers.

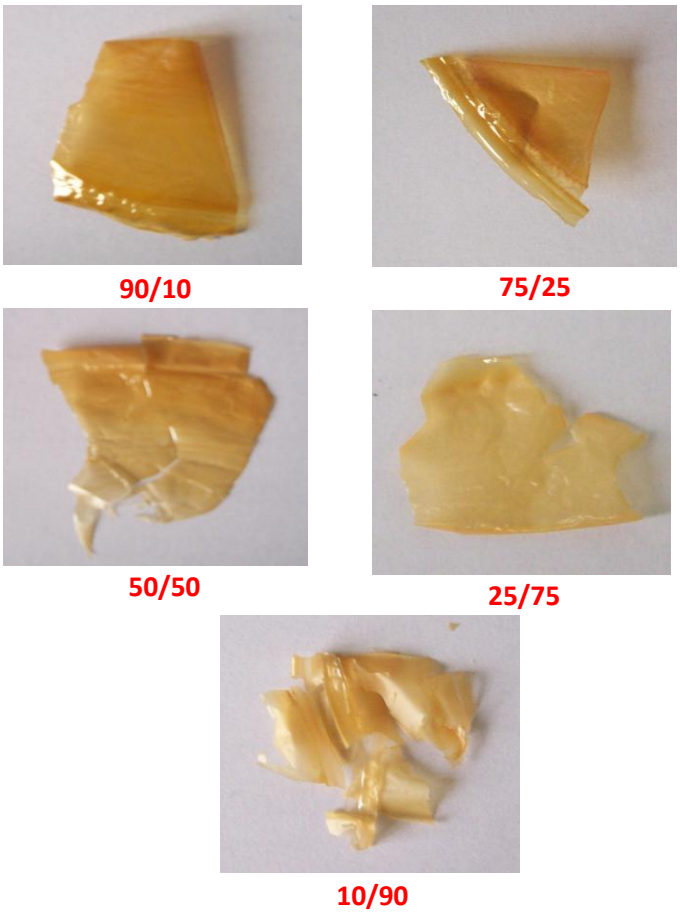

Figure 3.5: Photographs of PBI/SPS-Na (75% sulfonated) blend samples.

Differential scanning calorimetric (DSC) studies are carried out for these blends to prove the miscibility behavior and study the specific interaction between the polymer components. The samples were annealed for 30 min inside the DSC. The higher PBI content samples (up to 50/50 blend compositions) are annealed at 450°C and the lower PBI content samples are kept at 300°C. Thermo gravimetric analysis (TGA) shown in Figure 3.6 clearly demonstrate that the blend samples are stable at the annealing temperatures mentioned above except the initial weight loss due to the absorbed moisture. The moisture absorption takes place because of the hygroscopic nature of both the PBI and SPS-Na.[37,55]

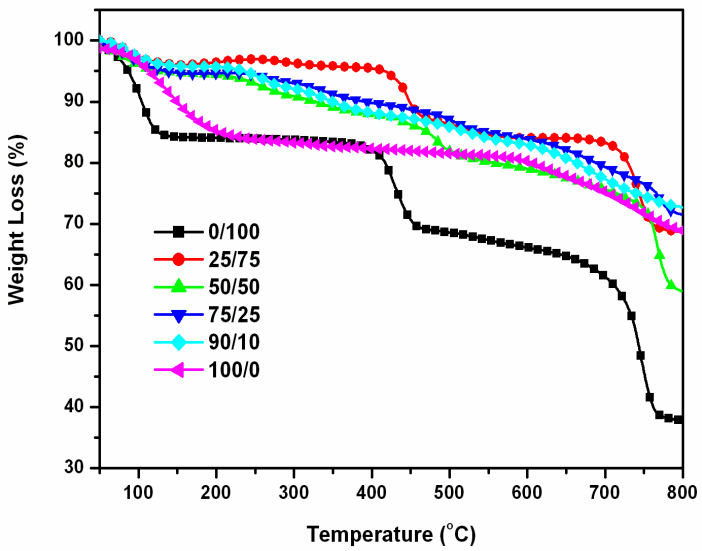

Figure 3.6: TGA plots of PBI/SPS-Na_{75} blends at their indicated compositions.

The glass transition temperatures (T_g) obtained from the DSC experiments are 398°C and 169°C for PBI and SPS-Na (75% sulfonated), respectively (Figure 3.7). The measured T_g values of these polymers are matching with the reported values for these polymers in the literature.[37,48,55] All the blend samples studied here exhibit two distinct T_g values. Representative DSC thermograms of 25/75 (PBI/SPS-Na_{75}) is shown in Figure 3.7 along with the neat PBI and neat SPS-Na_{75}.

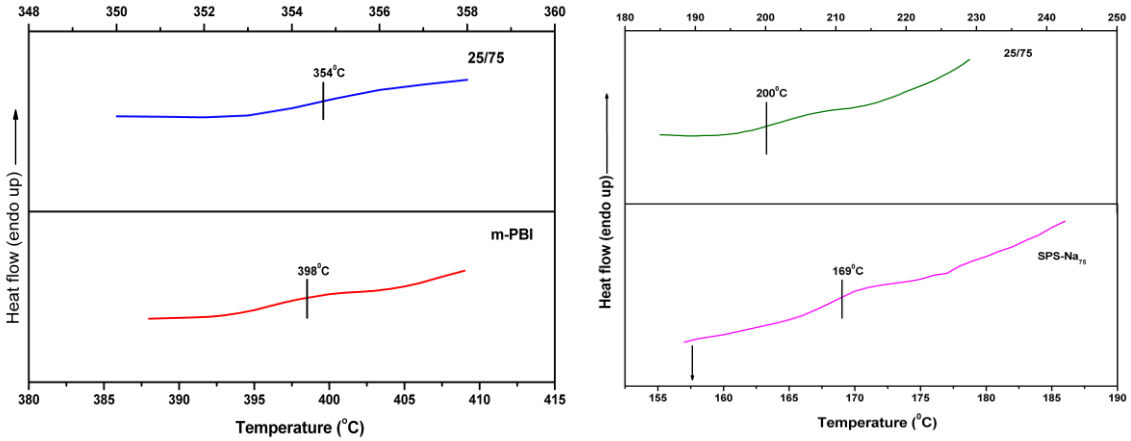

Figure 3.7: DSC thermograms of neat PBI, neat SPS-Na (75% sulfonated) and 25/75 (PBI/SPS-Na_{75}) blend. The horizontal lines and the corresponding values in the thermograms are the T_g of the samples. The blend shows two T_g's.

DSC thermograms for all other blend compositions of the PBI/SPS-Na_{75} blends are presented in Figure 3.8. In all the blends two T_g's are observed and they do not vary with the blends composition. Among these two T_g's in case of blend samples, the lower temperature T_g which comes at ~200°C is close to the neat SPS-Na75 and the higher temperature Tg which observes at ~350°C is close to the neat PBI. Hence, the lower T_g (~200°C) is the contribution component of SPS-Na_{75} and higher T_g (~350°C) is due to PBI component in the blend. Figure 3.7 and 3.8 exhibit that in all the blend samples of PBI/SPS-Na_{75} blend system two T_g's are present and they are independent of the blend compositions. A better depiction of this observation can be realized from Figure 3.9, where the T_g's of the blend samples are plotted against composition of PBI/SPS-Na_{75} blend. The solid line in Figure 3.9 is the line drawn by connecting expected T_g's of the blends according to the linearity rule (Fox equation) of miscible blend system. The presence of two T_g's (each of them somewhat close to the neat component T_g) and invariant with the blend compositions for blend systems are reported in the literature by several authors.[58] Sauer et al. reported similar kind of glass transition behaviors for poly(aryl ether ketone)/thermoplastic polyimide blend system.[59]

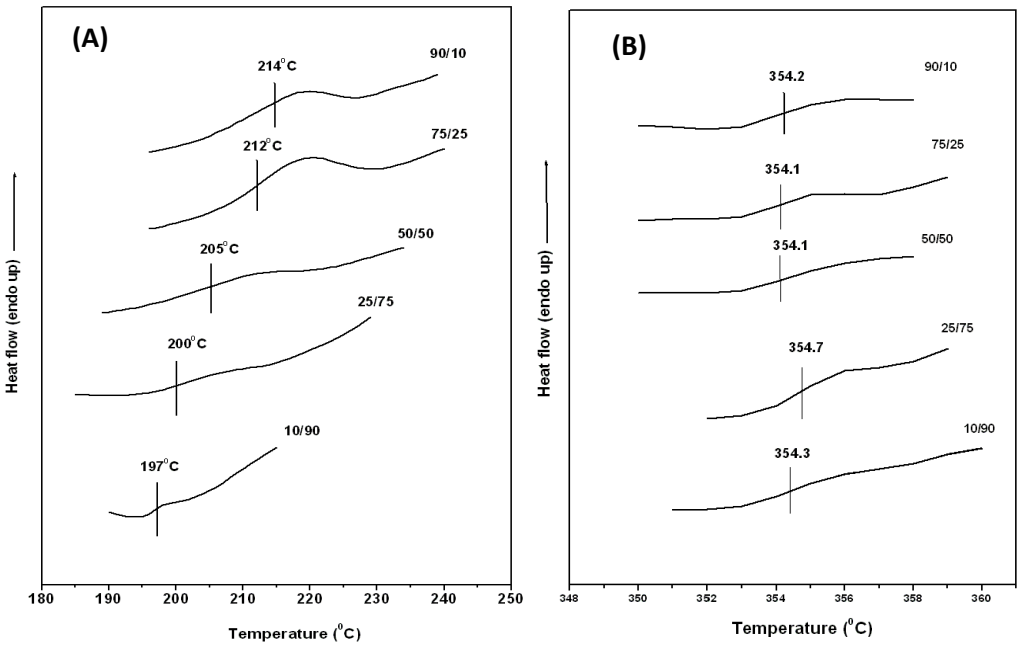

Figure 3.8: DSC thermograms of PBI/SPS-Na_{75} blends at their indicated compositions. Lower T_g is shown in (A) and higher T_g is shown in (B)

A single T_g will indeed be obtained if a system is miscible but also a single T_g does not ensure the miscibility since many immiscible systems with finely dispersed phase also show single T_g. The chemical nature of the blend system, its morphology and especially the domain size of heterogeneity (d_d) in the polymer blend dictate the phase behavior, miscibility and as well as the T_g of the blend.[58] Earlier, the presence of double T_g's in the blend has been reported for the blend in which the domain size of heterogeneity (d_d) is >15-20 nm.[58] One of the components (SPS-Na) in the present blend system is in the form of spherical particles with size ~70 nm (see in the next section), hence it is expected that the domain size of heterogeneity (d_d) in this blend system is bigger than 20 nm and hence double T_g for this blend system is obvious. However, it should be noticed that in the blends the lower T_g (~200°C) is increased by ~30°C from the neat SPS-Na (169°C) and the higher Tg (~350°C) is lowered by ~48°C from the neat PBI (398°C).

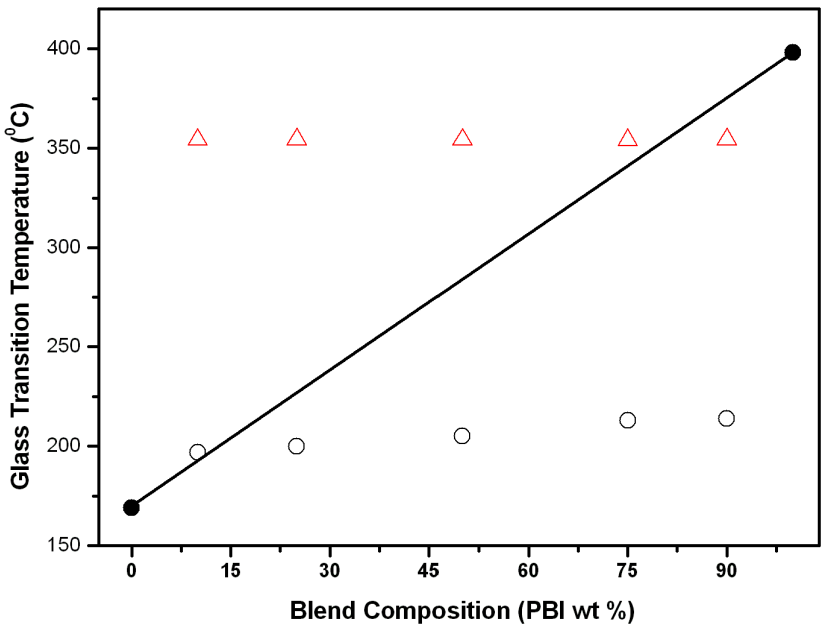

Figure 3.9: The glass transition temperatures dependence on the blends composition. The solid line is drawn by connecting the expected T_g values of the blends according to the Fox linearity rule. Each blend has two T_g's. The lower one is shown by ○ and higher one shown by Δ. The solid circles represent the T_g's of the neat polymers.

These changes in T_g are due to the specific interactions between the two polymer components which we have observed in IR studies. The changes in T_g indeed prove that the presence of interaction between PBI and SPS-Na components which results the partial miscibility upon blending.. The presence of two Tg's is an indication of two phases. We have carried out the DSC experiments of all the blend samples with scanning rates of 10, 30, 50, and 100°C/min to see the effect of scan rate (dT/dt) on the T_g values and data are tabulated in Table 3.1. We always obtained two Tg's for the all the blend samples irrespective of the scanning rate. This attributes the presence of two phases. However, these two phases are not the pure components phases since the T_g's obtained for the blend samples are not the T_g's of the neat polymer components. Hence these phases are the partially miscible phases of the two pure components. Figure 3.9 shows that the T_g of PBI in the blend samples (90/10) decreases by ~48°C and then its remains invariant with the blend composition. The decrease of PBI T_g is due to the decrease of PBI segmental motion owing to the blending. After 90/10 (PBI/SPS-Na) blend composition T_g of blends remains unchanged with the increase in SPS-Na (Figure 3.9) content. One can draw a conclusion that a small amount of SPS-Na is enough to disturb the rigidity by disrupting the self associated N–H interaction of PBI chains and even if we increase SPS-Na in the composition it is not changing the rigidity further and hence does not change the T_g (Figure 3.9). Earlier our IR study also proves the greater extent of disruption of self association. Similarly, the T_g of SPS-Na moves to higher side in the 10/90 blend composition and then remains constant (Figure 3.9). This once again reinforcing the fact that a small quantity of PBI is sufficient to cover the SPS-Na particle. The above observations allow us to conclude to the fact that PBI chains come closer to SPS-Na particle and sit over these particles making shell of PBI chains around spherical SPS-Na core. Similar conclusion we have arrived from our IR studies also. Therefore, upon blending of SPS-Na particle with rigid PBI; a core-shell structure is formed in which the core is SPS-Na and shell is PBI. All the IR and DSC results reveal the above conclusion. To prove our core-shell structure formation, we have studied the

morphological features of the blend samples using transmission electron microscope (TEM). We have obtained core-shell structure from the microscopic studies which are discussed in the next section.

Table 3.1: Glass transition temperatures of the blend samples (PBI/SPS-Na_{75} obtained from the DSC heating experiments with scanning rates of 10, 30, 50 and 100^0C/min.

PBI/ SPS-Na_{75}	10°C/min		30°C/min		50°C/min		100°C/min	
	Lower T_g	Higher T_g	Lower T_g	Higher T_g	Lower T_g	Higher T_g	Lower T_g	Higher T_g
90/10	214	354	201	373	212	353	212	375
75/25	212	354	212	371	210	354	215	354
50/50	205	354	209	365	210	364	207	353
25/75	200	354	202	379	212	367	205	343
10/90	197	354	221	371	215	376	221	347

3.3.3. Morphological study

Both IR and DSC studies discussed in the previous sections demonstrated the presence of specific interactions between the two components which results this partially miscible phase separated blends. In addition, both these studies revealed that perhaps the morphology of the blends might have played the major role to dictate the nature and extent of phase separation of these two polymer components. Also, IR and as well as DSC studies attributed a core-shell particle type morphology of the blend samples where SPS-Na constitutes the core and the shell is made up of PBI. Therefore it becomes mandatory for us to study the morphology to validate the conclusion drawn from the IR and DSC results. The morphology of polystyrene, SPS-Na_{75} and blends were studied by using transmission electron microscope (TEM). The TEM images of polystyrene (PS), SPS-Na_{75} and the representative blend of PBI/SPS-Na_{75} (10/90) are shown in the Figure 3.10.

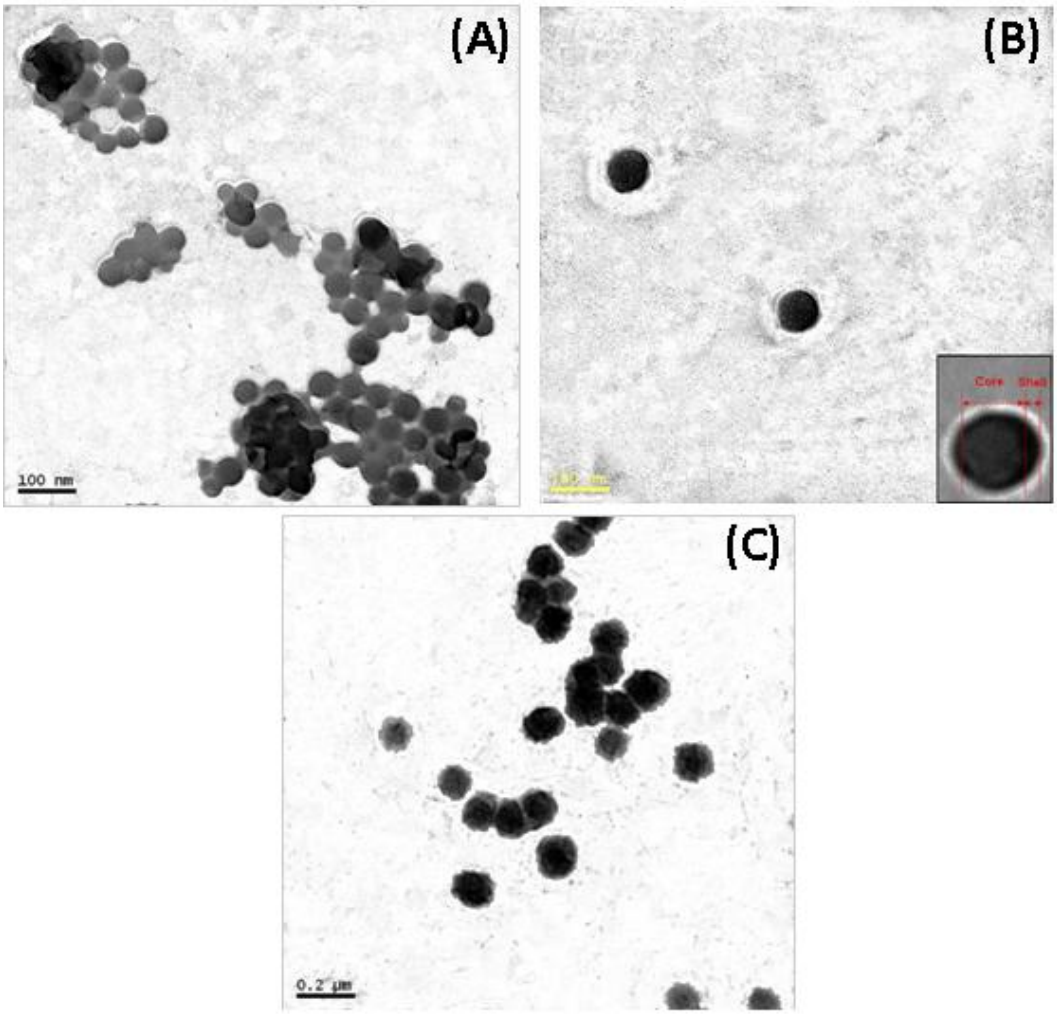

Figure 3.10: Transmission electron microscope images of: (A) polystyrene, (B) SPS-Na_{75}, and (C) 10/90 blends of PBI/SPS-Na_{75}. The average particle sizes are 50, 70, and 120 nm, respectively. Inset of B: one particle is digitally zoomed to show the core-shell structure.

The average particle diameters measured from the TEM images are as follows: PS = 50 nm, SPS-Na_{75} = 70 nm and 10/90 blend =120 nm. Therefore from Figure 3.10 and particle size values, it is clear that the particle size increases upon sulfonation of PS and it further enhances upon blending with PBI although the spherical nature of the particle remains unaltered. This observation clearly attributes that the sulfonation takes place on the surface of the polystyrene particles and increases the particle size. SPS-Na

self-assembles into particle type morphology upon dispersion into the solvents owing to the hydrophobic interaction of un-sulfonated PS moiety. Hence the size of the particles depends on the degree of sulfonation. Here the degree of sulfonation is quite high (75%) and therefore the size enhances from 50 to 70 nm after sulfonation of PS. Further upon blending with PBI, the sulfonate groups of SPS-Na which are present in the surface of the particle interacts with the PBI through the specific interactions (as proved by IR and DSC studies) and forces the PBI chains to wrap over the particle surface since the sulfonate groups are randomly distributed on the particle surface. Due to this wrapping the particle size further increases upon blending. The wrapping of the PBI chains would not have possible unless a strong interaction between PBI and SPS-Na present which forces the rigid PBI chains to become flexible to some extent. In IR studies, we have observed that a greater degree of disruption of self association of the PBI chains, which allows the PBI chains to become flexible enough to wrap over the SPS-Na particle. The flexibility adaptation of PBI chains is also manifested in their sudden decrease of T_g upon blending as observed from the DSC study.

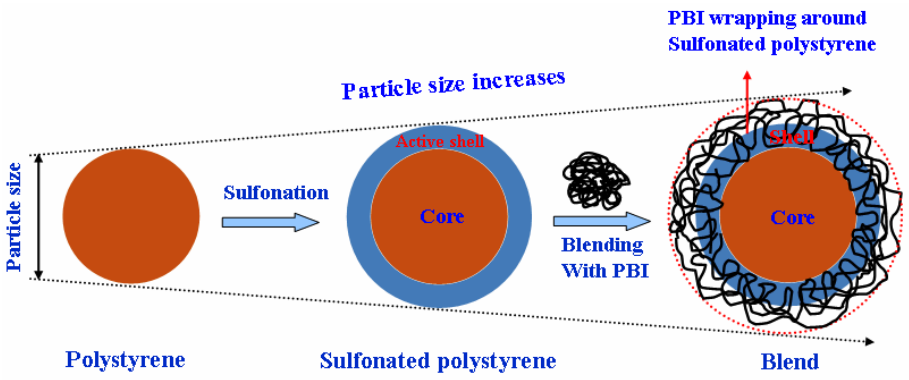

Figure 3.11: Schematic representation of core–shell type morphology formation upon blending of PBI with SPS-Na particles.

A schematic presentation of the above observation is presented in Figure 3.11. The sulfonation of polystyrene (PS) particle creates a reactive sulfonate ($-SO_3^- Na^+$) shell on the surface of the PS core by increasing the particle size. This reactive sulfonate shell interacts strongly with the PBI molecule, disrupts the N–H self association, and

forces them to wrap over the active shell surface yielding a thicker shell of PBI by increasing the particle size. A careful look on the TEM morphological feature presented in Figure 3.10 clearly demonstrates the core-shell structure formation. The spherical PS particles have 50 nm diameter and smooth surface (Figure 3.10A). An increase in both surface roughness and diameter is observed for SPS-Na (Figure 3.10B) and blend sample (Figure 3.10C). In case of SPS-Na a dark black ring (shell) is visible with light black core (Inset of Figure 3.10B) and the size of the particle is 70 nm. Again upon blending the particle diameter has increased to ~120 nm and no core-shell morphology is visible. However the roughness of the surface of the blend particle has increased significantly compared to SPS-Na (Figure 3.10C). This indicates that the active $-SO_3^- Na^+$ layer is now completely covered by the PBI molecules and producing a shell of PBI and core of PS to form the core-shell structure. In conclusion it is very much clear that core-shell nanostructure is formed due to the blending of PBI and SPS-Na.

3.3.4. Effect of sulfonation degrees

All the results discussed in the earlier sections of this chapter are obtained from the blending of PBI with sodium salt of 75% (degree of sulfonation) sulfonated polystyrene (SPS-Na_{75}). The results very clearly suggest that the blending and the core-shell structure formation of the blend materials are manifestation of the specific interaction between N–H group of PBI and the sulfonate functionality of SPS-Na. Hence, it is expected that the amount of sulfonate groups (degree of sulfonation) on the surface of the spherical SPS-Na particle may influences the compatibility of the blending of these two polymeric components and the morphology of the end product (blend) materials. Therefore, a systematic study of this blending process by varying the degree of sulfonation of SPS-Na is absolutely necessary to understand the effect of amount of sulfonated groups. We have prepared a series of SPS-Na particles using the sulfonation process discussed in the experimental section and produced wide range (20-90%) of sulfonated samples. The degree of sulfonation is measured by using ^{1}H NMR spectroscopy and all the relevant ^{1}H NMR spectra are presented in Figure 3.12. Only the

relevant parts of the spectra which are required for the degree of sulfonation calculation are shown in Figure 3.12.

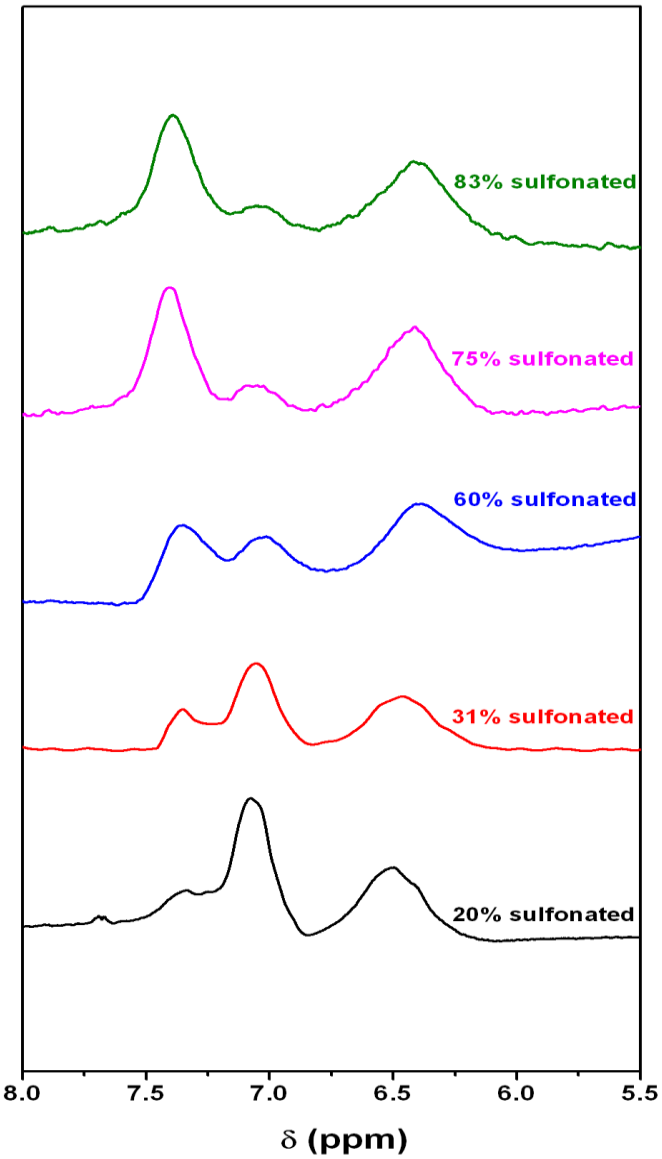

Figure 3.12: The ^{1}H NMR spectra of SPS-Na recorded using DMSO-d_6 as NMR solvent.

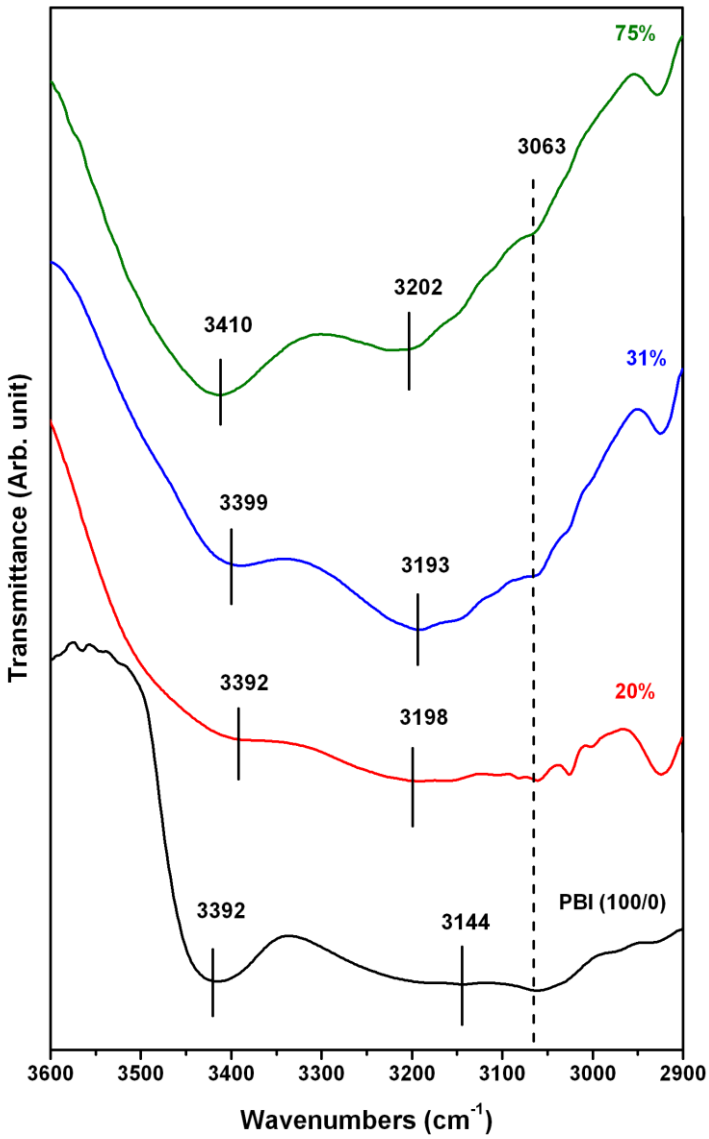

Figure 3.13: FT-IR spectra of 50/50 (PBI/SPS-Na) blends with regard to the degree of sulfonation of SPS-Na component. The neat PBI spectrum is also presented for comparison.

The N–H stretching region FT-IR spectra of PBI/SPS-Na (50/50) blends with regard to the degree of sulfonation of SPS-Na component are presented in Figure 3.13. The pure PBI (100/0) spectrum is also shown in Figure 3.13 for comparison. The

displacement of free N–H peak (3420 cm^{-1} for pure PBI) towards lower wavenumber and shift of self associated peak (3144 cm^{-1} for pure PBI) towards longer wavenumber are visible from Figure 3.13. More importantly, it is worthwhile to note from Figure 3.13 that the extent of peak shift and the nature of peak broadening depend upon the degree of sulfonation. The peak shifting and broadening of the free N–H peak decreases with increasing degree of sulfonation. On the other hand, the extent of self associated N–H peak shift increases with increasing sulfonation degree. Also it must be noted that this self associated peak becomes sharper for the sample with higher degree of sulfonation. A much better clear scenario of these above observation emerges in Figure 3.14, where we have plotted the shift of the peak position free N–H in Figure 3.14A, and self associated N–H in Figure 3.14B as a function of blend compositions with regard to the degree of sulfonation. Figure 3.14A clearly suggests that the extent of free N–H peak shift is bigger for the blend samples made from SPS-Na with lower degree of sulfonation. In contrary, the self associated N–H peak shifted to a greater extent for the blends prepared from SPS-Na with higher degree of sulfonation. In summary, our results from the previous sections, Figure 3.13 and 3.14 suggesting the fact that the disruption of N–H self association of PBI becomes very successful when PBI is blended with highly sulfonated SPS-Na. However, the specific interaction between free N–H of PBI and SPS-Na becomes stronger when PBI is blended with lightly sulfonated SPS-Na. Earlier sections (FT-IR and morphology studies) we have demonstrated that successful disruption of self associated N–H of PBI leads to core-shell morphology (Figure 3.10 and 3.11) of the blends in which PS core is wrapped by the PBI shell. This core-shell morphology formation is the driving force for the blending of these polymer pair. Therefore the above results and discussion reveal that the extent of blending between these two polymeric components increases with increasing degree of sulfonation of SPS-Na. Figure 3.11 schematically explained the wrapping of PBI on the SPS-Na particle, which yields the miscible blend. The lightly sulfonated SPS-Na does not have enough attraction to break the self association of PBI chains as evident from the FT-IR studies (Figure 3.14) and hence PBI cannot wrap over SPS-Na particle to produce miscible blend.

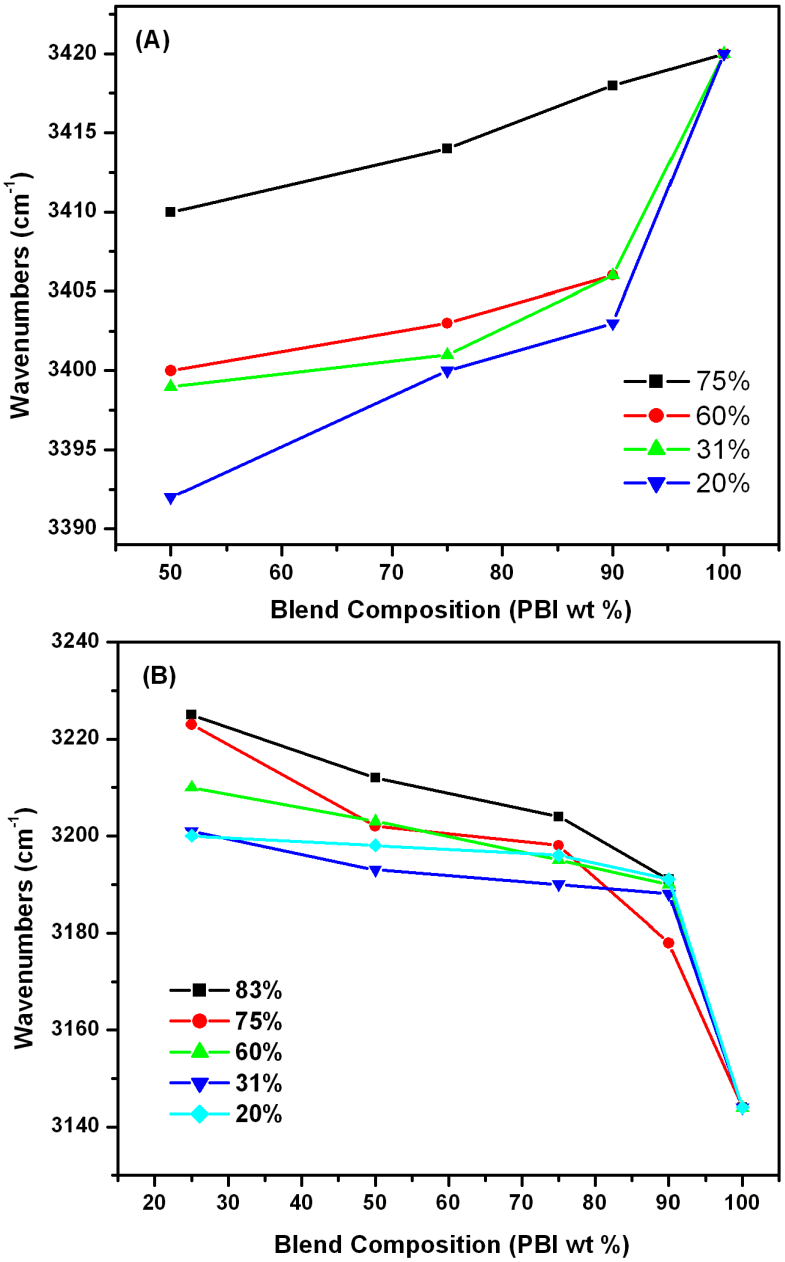

Figure 3.14: Displacement of PBI peak positions (stretching frequencies) as obtained from the FT-IR studies as a function of blends composition: (A) free N–H peak of PBI and (B) self associated N–H peak of PBI. The degree of sulfonation of the SPS-Na indicated in the figure.

A better understanding of this will be followed in the next section where we have studied DSC thoroughly. The T_g of all the blend samples prepared by using a series of SPS-Na with wide range (20-83%) of sulfonation degree are measured by DSC and presented in Table 3.2. The T_g of pure SPS-Na increases with increasing degree of sulfonation (all the representative thermograms are presented in Figure 3.15).

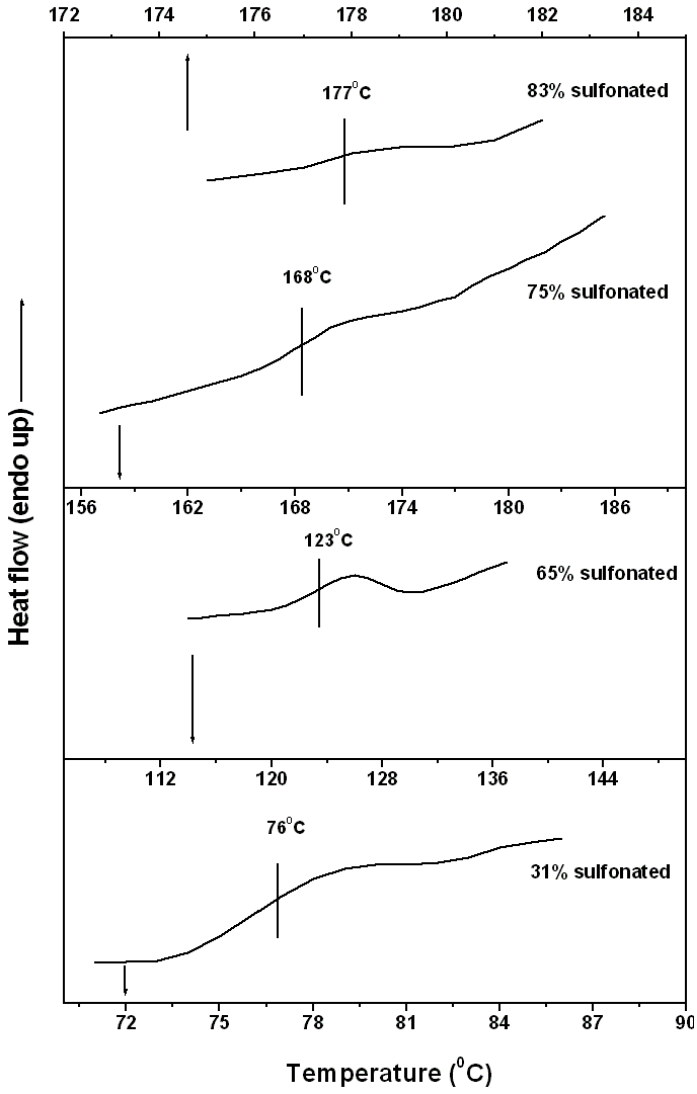

Figure 3.15: DSC thermograms of SPS-Na at their indicated degree of sulfonation. The T_g is show by the marking on the thermograms.

Table 3.2: The glass transition temperature (T_g) obtained from the DSC studies for all the blend samples. These samples are prepared by blending PBI and SPS-Na with wide range of sulfonation degree.

PBI/ SPS-Na	Degree of sulfonation									
	83%		75%		60%		31%		20%	
	Lower Tg	Higher Tg	Lower Tg	Higher Tg	Lower Tg	Higher Tg	Lower Tg	Higher Tg	Lower Tg	Higher Tg
100/0 (PBI)	397.98									
90/10	264.52	354.2	214.45	354.36	135.91	355.07	76.47	397.63	76.33	397.82
75/25	263.78	354.03	212.82	354.05	132.04	354.37	76.30	397.65	76.32	397.88
50/50	264.44	354.36	205.15	354.21	132.54	354.54	76.49	397.56	76.5	397.79
25/75	264.61	354.35	200.47	354.37	132.20	354.62	76.15	397.56	76.49	397.87
10/90	264.26	354.35	197	354.24	131.88	354.70	76.48	397.55	76.49	397.86
0/100 (SPS-Na)	177.18		168.81		123.53		75.42		76.34	

The increase of T_g with degree of sulfonation is expected because of the lowering of the flexibility owing to sulfonate groups.[55] In all the blend samples two T_g's are observed (Table 3.2). The two T_g's of the highly sulfonated (namely 83%, 75%, and 60%) blend samples are not identical with their respective neat polymer components (SPS-Na and PBI) as shown in the Table 3.2. For example the T_g's of 50/50 blend of 83% SPS-Na sulfonated polystyrene ($SPS\text{-}Na_{83}$) are ~354°C and ~264°C, which are not the T_g of their respective components (PBI = 397.98°C, $SPS\text{-}Na_{83}$ = 177.18°C). However, the two T_g's obtained for the lightly sulfonated (31% and 20%) blend samples are exactly identical with their neat components (Table3.2). This result clearly indicates that for the lightly sulfonated samples the interaction between the components are not strong enough to influence each other flexibility and hence the T_g's do not alter. In lower sulfonation blends perhaps the interactions are not sufficient enough for the PBI

chains to wrap over the SPS-Na particle and to produce core-shell structure. As a result they do not produce blends with core-shell structure. Hence our IR, DSC and TEM studies agree well each other.

The above results clearly demonstrated that to produce blends with core-shell structure, higher degree of sulfonation of SPS-Na is required. A careful look into the Table 3.2 data is also strengthening our above conclusion. The net change in the T_g of SPS-Na upon blending increases significantly for highly sulfonated blend systems compared to lightly sulfonated blends. A bar diagram presented in Figure 3.16 shows that upon blending the increase of T_g of SPS-Na is much bigger for the highly sulfonated blend system than the lightly sulfonated system. In fact T_g is unaltered for lower sulfonation degree. Figure 3.16 clearly shows that the change in T_g of SPS-Na from neat to 10/90 blend sample increases with increasing degree of sulfonation. Hence the above results attribute that the higher degree of sulfonation is absolutely necessary to prepare the blends of PBI and SPS-Na with core-shell type structure.

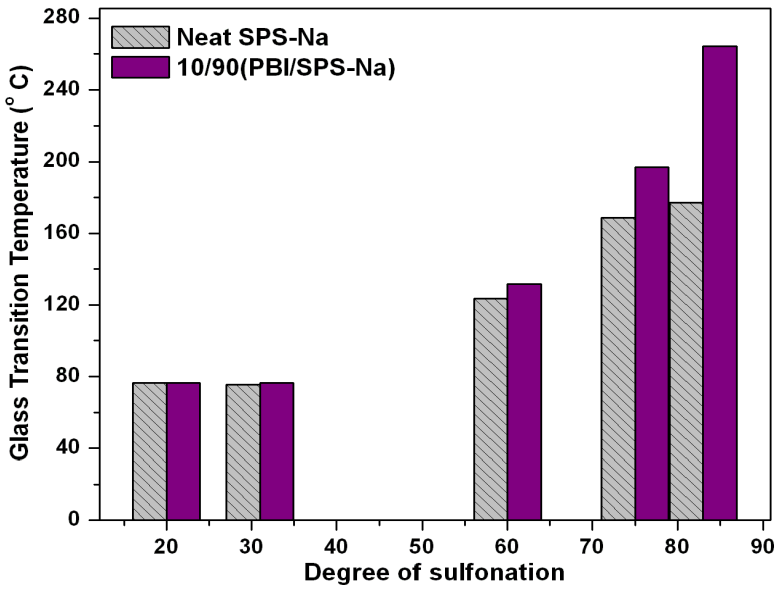

Figure 3.16: Bar diagram to represent the change in T_g of SPS-Na from neat SPS-Na to 10/90 (PBI/SPS-Na) blend as a function of the degree of sulfonation of SPS-Na component.

3. 4. Conclusions

New blend system of PBI with ionomeric sodium salt of sulfonated polystyrene (SPS-Na) spherical particles of various composition and sulfonation degrees have been prepared using the solution casting method. The spectroscopic, thermodynamical and morphological properties of these blends are studied using FT-IR, DSC, and TEM. The successful disruption of N–H self association of PBI and the presence of specific hydrogen bonding interaction between free N–H of PBI and the sulfonate groups of SPS-Na are the driving forces for the formation of partially miscible two phases blends of PBI with SPS-Na particles. DSC studies of the blends exhibit two glass transition temperatures (T_g), the higher one corresponds to PBI component and the lower one is due to SPS-Na, since the domain size of the heterogeneity (d_d) is greater than 20 nm owing to the fact that the one of the component (SPS-Na) is 90 nm in size. A large displacement of self association N–H stretching and composition independent T_g of the blends reveal the wrapping of PBI chains on the SPS-Na spheres and formation of core-shell type morphology. TEM study provides a direct proof of core-shell morphology of the blends in which SPS-Na stays as core and PBI constitutes the shell. The higher degree of sulfonation of SPS-Na is required to form the blends with core-shell morphology.

3. 5. References

1. Paul, D. R.; Bucknall, C. B. *Polymer Blends: Formulation and Performance*: Wiley: New York, 2000.
2. Han, C. D. *Multiphase Flow in Polymer Processing;* Academic Press: New York, 1981.
3. Utracki, L. A. *Polymer Alloys and Blends*; Hanser: Munich, 1989.
4. Ng, C. W. A.; MacKnight, W. J. *Macromolecules* **1996**, *29*, 2412.
5. Ng, C. W. A.; Bellinger, M. A.; MacKnight, W. J. *Macromolecules* **1994**, *27*, 6942
6. Lu, X.; Weiss, R. A. *Macromolecules*, **1991**, *24*, 4381.
7. Gao, Z.; Molnar, A.; Morin, F. G.; Eisenberg, A. *Macromolecules* **1992**, *25*, 6460.
8. Eisenberg, A. and Kim, J. S. *Introduction to Ionomers*; New York: Wiley, **1998**.
9. Zhou, A. L.; Eisenberg, A. *J. Polym. Sci, Polym. Lett. Edu.* **1983,** *21*, 223.
10. Hara, M.; Eisenberg, A. *Macromolecules* **1984,** *17*, 1335
11. Clark, J. N.; Higgins, J. S.; Peiffer, D. G. *Polym. Sci. Eng.* **1992**, *32*, 49.
12. Deimede, V.; Voyiatzis, G. A.; Kallitsis, J. K.; Qingfeng, L.; Bjerrum, N. J. *Macromolecules*, **2000**, *33*, 7609.
13. Sun, H. ; Venkatasubramanian, N.; Houtz, M. D.; Mark, J. E.; Tan, S.C. Arnold, F. E.; Lee, C. Y. C. *Colloid Polym. Sci*. **2004**, *282*, 502.
14. Kim, B.; Jung, B.; *Macromol. Rapid Commun*. **2004**, *25*, 1263.
15. Schönberger, F.; Hein, M.; Kerres, J. *Solid State Ionics* **2007**, *178*, 547.
16. Göktepe, F.; Bozkurt, A.; Gunday, S. T. *Polym. Int.* **2008**, *57*, 133.
17. Ghebremeskel, Y.; Weiss, R. A. *J. Polym. Sci.; Part B: Polym. Phys.* **2008**, *46*, 1602.
18. Molnar, A.; Eisenberg, A. *Macromolecules* **1992**, *25*, 5774.
19. Tannerbaum, R.; Rutkowska, M.; Eisenberg, A. *J. Polym. Sci., Polym. Phys.* **1987**, *25*, 663.

20. Sahu, A. K.; Selvarani, G.; Bhat, S. D.; Pitchumani, S.; Sridhar, P.; Shukla, A. K.; Narayanan, N.; Banerjee, A.; Chandrakumar, N. *J. Membrane Sci.* **2008**, *319*, 298.
21. Ng, C. W. A.; MacKnight, W. J. *Macromolecules* **1996**, *29*, 2421.
22. Xing, P. X.; Robertson, G. P.; Guiver, M. D.; Mikhailenko, S. D.; Kaliaguine, S. *Macromolecules* **2004**, *37*, 7960.
23. Shang, X.; Li, X, Xiao, M.; Meng, Y. *Polymer* **2006**, *47*, 3807.
24. Koyama, K.; Otsu, T. *J. Macromol. Sci. Chem.* **1974**, *A8*, 1295.
25. Hanai, T.; Walton, H. F. *Anal. Chem.* **1977**, *49*, 764.
26. Kim, J. H.; El-Aasser, M. S.; Klein, A.; Vanderhoff, J. W. *J. Appl. Polym. Sci.* **1988**, *35*, 2117.
27. Matyjaszewski, K.; Pintauer, T.; Gaynor, S. *Macromolecules* **2000**, *33*, 1476.
28. Smitha, B.; Sridhar, S.; Khan, A. A. *J. Membrane Sci.* ***2005,*** *259*, 10.
29. Serpico, J. M.; Ehrenberg, S. G.; Fontanella, J. J.; Jiao, X.; Perahia, D.; McGrady, K. A.; Sanders, E. H.; Kellogg, G. E.; Wnek, G. E. *Macromolecules* **2002**, *35*, 5916.
30. Hickner, M. A.; Ghassemi, H.; Kim, Y. S.; Einsla, B. R.; McGrath, J. E. *Chem. Rev.* **2004**, *104*, 4587.
31. Lee, J. M.; Lee, D. G.; Lee, S. J.; Kim, J. H.; Cheong, I. W. *Macromolecules* **2009**, *42*, 4511.
32. Yamaguchi, I.; Watanabe, M.; Shinagawa, T.; Chigane, M.; Inaba, M.; Tasaka, A.; Izaki, M. *ACS Appl. Mater. & Interf.* **2009** *1*, 1070.
33. Deng, Z.; Chen, M.; Gu, G.; Wu, L. *J. Phys. Chem. B* **2008**, *112*, 16.
34. Xu, H.; Wei, W.; Zhang, C.; Ding, S.; Qu, X.; Liu, J.; Yunfeng; Yang, Z. *Chem. Asian. J.* **2007**, *2*, 828.
35. Yang, Z.; Niu, Z.; Lu, Y.; Hu, Z.; Han, C. C. *Angew. Chem. Int. Edu.* **2003**, *42*, 1943.
36. Choe, E. W.; Cho, D. D. In *Polymeric Materials Encyclopedia*; Salamone, J. C. Ed.; CRC Press, New York, **1996**.

37. Sannigrahi, A.; Arunbabu, D.; Sankar, R. M.; Jana, T. *J. Phys. Chem. B* **2007**, *111*, 12124.
38. Xiao, L.; Zhang, H.; Jana, T.; Scanlon, E.; Chen, R.; Choe, E.-W. ; Ramanathan, L. S.; Yu, S.; Benicewicz, B. C. *Fuel Cells* **2005**, *5*, 287.
39. Savinell, R.; Yeager, E.; Tryk, D.; Landau, U.; Wainright, J.; Weng, D.; Lux, K.; Litt, M.; Rogers, C. *J. Electrochem. Soc.* **1994**, *141*, L46.
40. Samms, S. R.; Wsmus, S.; Savinell, R. F. *J. Electrochem. Soc.* **1996,** *143*, 1225.
41. Li,Q.; Jensen, J. O.; Savinell, R. F.; Bjerrum, N. J. *Prog. Polym. Sci.* **2009**, *34*, 449.
42. Sannigrahi, A.; Arunbabu, D.; Sankar, R. M.; Jana, T. *Macromolecules* **2007**, *40*, 2844.
43. Shogbon, C, B.; Brousseau, J.-L.; Zhang, H.; Benicewicz, B. C.; Akpalu, Y. *Macromolecules* **2006,** *39*, 9409.
44. Sannigrahi, A.; Arunbabu, D.; Jana, T. *Macromol. Rapid Commun.* **2006**, *27*, 1962.
45. Kojima, T. *J. Polym. Sci.: Polym. Phys. Ed.* **1980**, *18*, 1685.
46. Musto, P.; Karasz, F. E.; MacKnight, W. J. *Macromolecules* **1991,** *24*, 4762.
47. Wang, Y.; Goh, S. H.; Chung, T-S. *Poymer* **2007**, *48*, 2901.
48. Arunbabu, D.; Sannigrahi, A.; Jana, T. *J. Phys. Chem. B* **2008,** *112*, 5305.
49. Wycisk, R.; Chisholm, J.; Lee, J.; Lin, J.; Pintauro, P. N. *J. Power Sources* **2006**, *163*, 9.
50. Daletou, M. K.; Gourdoupi, N.; Kallitsis, J. K. *J. Memebrane Sci.* **2005**, *252*, 115.
51. Guerra, G.; Choe, S.; Williams, D. J.; Karasz, F. E.; MacKnight, W. J. *Macromolecules* **1988**, *21*, 231.
52. Liang, K.; Banhegyi, G.; Karasz, F. E.; MacKnight, W. J.; *J. Polym. Sci., Part B: Polym. Phy.* **1991**, *29*, 649.
53. Arunbabu, D. ; Sannigrahi, A. ; Jana, T. *J. Appl. Polym. Sci.* **2008**, *108*, 2718.
54. Baigl, D.; Seery, T. A. P.; Williams, C. E. *Macromolecules* **2002,** *35*, 2318.
55. Arunbabu, D.; Sanga, Z.; Seenimeera, K. M.; Jana T. *Polym. Int.* **2009**, *58*, 88.

56. Musto, P.; Karasz, F. E.; MacKnight, W. J. *Polymer* **1993,** *34*, 2934.
57. Ahn, T-K.; Kim, M.; Choe, S. *Macromolecules* **1997**, *30*, 3369.
58. Utracki, L. A. Ed., *Polymer Blends Handbook*; Kluwer: The Netherlands, **2002**, Vol 1, Pages 135-137.
59. Sauer, B. B.; Hsiao, B. S.; Faron, K. L. *Polymer* **1996**, *37*, 445.

Chapter 4

Partially miscible blend of polybenzimidazole and poly(vinylidene fluoride-co-hexafluoro propylene)

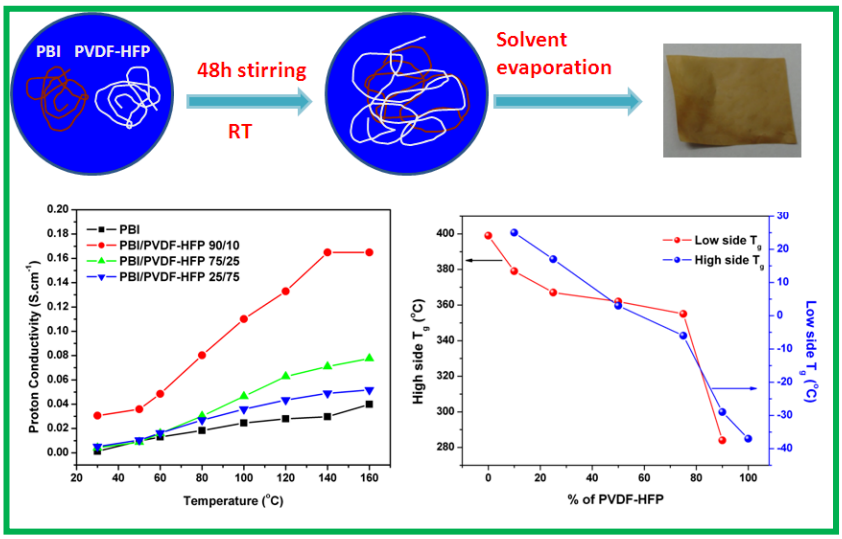

Partially miscible polymer blend of polybenzimidazole (PBI) with poly(vinylidene fluoride-co-hexafluoro propylene) (PVDF-HFP) were prepared for their use as polymer electrolyte membrane (PEM) in high temperature. The blending significantly enhanced the proton conductivity and oxidative stability.

Hazarika, M.; Jana, T. Communicated to *Euro. Polym. J.*

4.1. Introduction

Over the last decade research on proton exchange membrane fuel cells (PEMFC) operating at high temperature has been an area of active interest.[1-3] Proton exchange membrane (PEM) must have mechanical, chemical, and thermal stability and good proton conductivity.[4] Perfluorinated polymers are widely used as PEMs for low temperature fuel cell applications due to high proton conductivity and excellent chemical stability.[5-7] But these membranes have several drawbacks e.g. cannot operate at high temperature because proton conductivity is dependent on the presence of water, high ethanol cross over and high price.[3,8-10] Therefore, various alternative PEMs have been studied for high temperature operation.[4,11]

Phosphoric acid (PA) doped polybenzimidazole (PBI; Scheme 4.1) are recently explored widely as PEM in high temperature PEM-FC because of its very high thermo chemical stability and low gas permeability.[12-14] The proton conductivity of PBI increases with increasing PA doping level of the membrane. But the mechanical strength of the PBI decreases with increasing level of doping. To achieve a superior quality of PA doped PBI membrane, the acid doping level has to increase without destroying the other properties of the polymer. Varieties of approaches are reported in the literature to obtain high PA-doped PBI membranes such as synthesis of PBI derivatives[15] PBI nanocomposites[16,17] and PBI blends etc.[18] PEM via blending requires optimal combination of properties of more than one polymer so that a tough membrane with adequate proton conductivity can be achieved.

Polymer blending is a versatile and economic method to generate novel material with enhanced physical and chemical properties.[19] Polymer blending is designed to yield materials with optimized properties such as chemical, structural, mechanical, morphological etc. The main advantages of blend-based polymer electrolytes are simplicity of preparation and easy control of physical properties by changing the composition of blended polymers composition. Polymer blends may be miscible, partially miscible and immiscible. Miscible blends have properties somewhere between those of the neat polymers and therefore very useful materials since they exhibit

properties of both the polymers. Partially miscible blends are also of great interests because they also offered improved properties compared to the neat polymers. For example polystyrene (PS) is commonly blended with rubber to improve its impact properties. The resulting high impact PS (HIPS) blend is composed of two immiscible phases. Ning et al prepared and studied mechanical and electrical properties of partially miscible blends of poly (lactic acid) and poly (propylene carbonate) filled with carbon black.[20]

PBI has both proton donor (−NH−) and proton acceptor (−N=) hydrogen bonding sites. Because of the availability of the hydrogen bonding sites in the polymer backbone, it exhibits specific interactions with polar solvents[21,22] and forms miscible blend[23,24] with variety of polymers. The main aim of PBI blending is to improve the properties, performance and reduce the price specifications through combinations of low cost or high-performance materials. A large number of blends based on PBI with variety of polymers are reported in the literature. Example includes PBI/nafion,[25] PBI/poly(4-vinyl pyridine),[26] PBI/polyimide,[27] PBI/poly(ether imides),[28] PBI/polysulfone,[24] PBI/poly(arylene ether sulfones),[29] PBI/sulfonated polystyrene[30] etc. Recently from our group we have reported PBI/poly(vinylidene fluoride) (PVDF) blends and studied their potential for the use as a proton exchange membrane in PEMFC.[18] We observed the enhancement of the PA doping level of the blend membrane compared to that of pure PBI because the hydrophobic PVDF inhibits the water uptake capacity of the membranes and hence allows the acid to interact more efficiently with the PBI backbone which leads to the higher PA loading.

Poly(vinylidene fluoride-co-hexafluoro propylene) (PVDF-HFP; Scheme 4.1) has found much attention recently as a promising membrane material because of its desirable properties such as high hydrophobicity, favorable ionic conductivity, excellent chemical and thermal resistances and availability in different crystalline forms.[31-34] Because of the presence of more fluorine groups, PVDF-HFP is more hydrophobic than PVDF. Many literatures related to PVDF-HFP blends are reported and these examples include PVDF-HFP/poly(vinylacetate),[35] PVDF-HFP/polystyrene,[36] PVDF-HFP/poly(vinyl pyrrolidone)[37] etc.

Here we are reporting partially miscible blends of PBI with PVDF-HFP. Since later component is more hydrophobic than PVDF, therefore, it can further decrease the water uptake of PBI thereby increase its acid loading level. The miscibility of the blend membranes are studied by FT-IR and SS-NMR. Their thermal stability, water uptake, and swelling ratio are measured. Also, the temperature dependent proton conduction behavior of these membranes and oxidative stability are studied.

4.2. Experimental Section

4.2.1. Materials

Poly [2, 2'-(*m*-phenylene)-5, 5'-benzimidazole] (PBI, Scheme 4.1) was obtained by polymerizing 3, 3', 4, 4'-tetraaminobiphenyl (TAB) and isophthalic acid in polyphosphoric acid medium (115%) in laboratory using our standard method described earlier.[22,38] The inherent viscosity of synthesized PBI is 2.2 dL/g, when measured from 0.2 g/dL H_2SO_4 solution. Poly(vinylidene fluoride-co-hexafluoro propylene) (PVDF-HFP) was purchased from Sigma Aldrich having a weight average molecular weight ($\bar{M}_w$) of 400,000. The PVDF-HFP was recrystallized from dilute solution of polymer in acetophenone (0.5 wt%), repeatedly washed with methanol, and dried in vacuum at 80°C for 3 days. Dimethylacetamide (DMAc; HPLC grade) and 85% phosphoric acid (PA) were obtained from Merck (India) and used as received. Sulfuric acid (Merck) and deuterated dimethyl sulfoxide (DMSO-d_6) were used as received.

4.2.2. Blend preparation

Blends were prepared by mixing two polymers (PBI and PVDF-HFP) in DMAc. The concentration of the polymers in DMAc solution was kept 1% (w/v). The required amount of the two polymers were taken in the measured quantity of DMAc, dissolved in DMAc and mixing was continued for 2 days by stirring with the help of magnetic stirrer in a close glass vessel at room temperature. The homogeneous blend solutions were filtered through a 0.2 µm PTFE membrane and then poured into a clean glass petri dish. The solvent was evaporated at 50°C to cast the blend films.

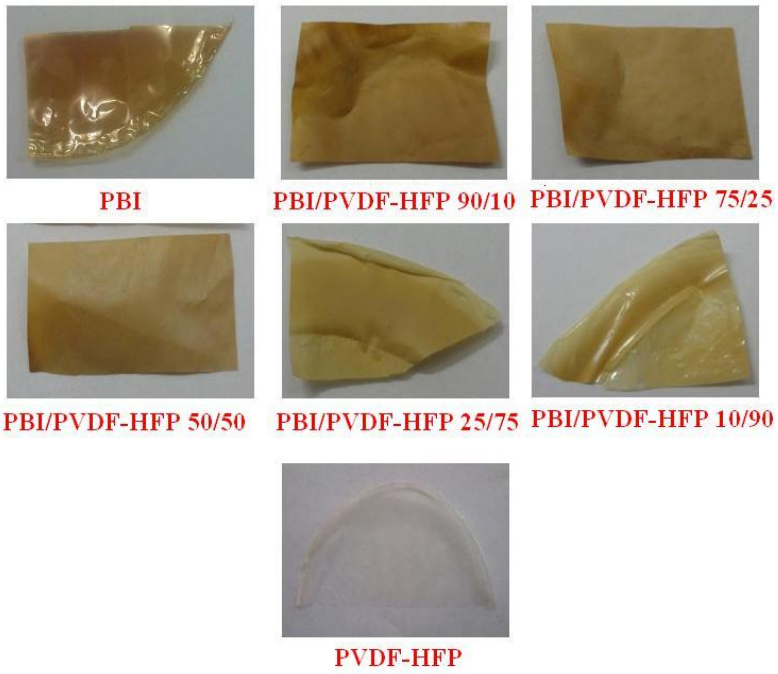

Figure 4.1: Photographs of PBI/PVDF-HFP blend membranes

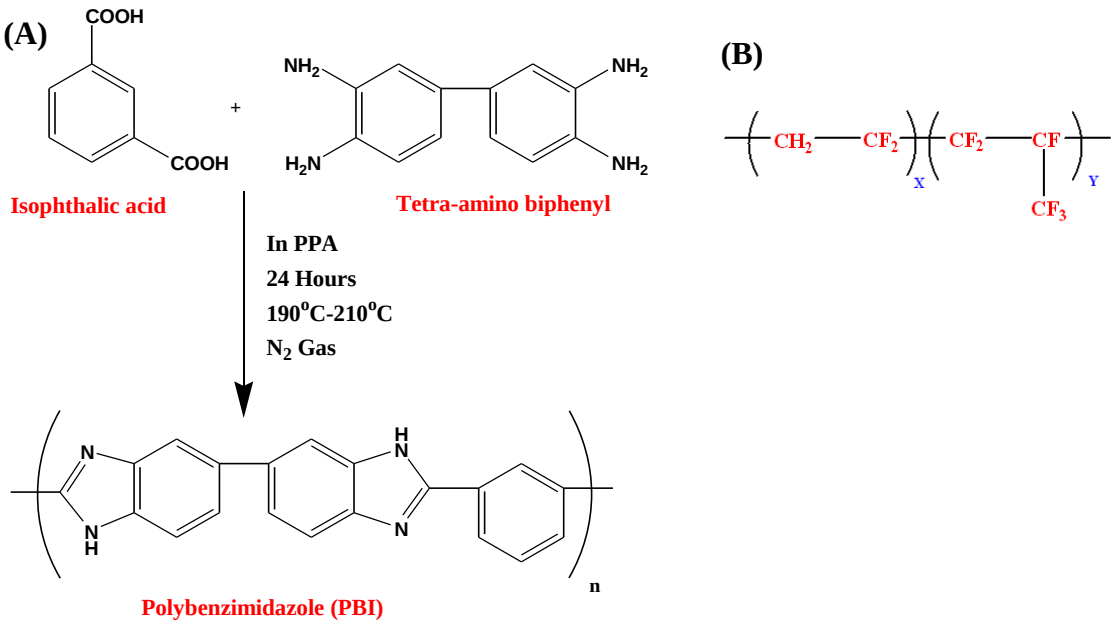

Scheme 4.1: (A) Synthesis of Poly [2, 2'-(*m*-phenylene)-5, 5'-benzimidazole] (m-PBI), (B) Chemical structure of Poly(vinylidene fluoride-co-hexafluoro propylene) (PVDF-HFP)

Transparent homogeneous thin films (Figure 4.1) were obtained and dried in a vacuum oven at 100°C for 3 days to evaporate the trace amount of solvent completely. The thicknesses of all the blend films were ~60 μm. The blend compositions were widely varied from 10/90 (PBI/PVDF-HFP) to 90/10. In addition, we have prepared neat PBI and neat PVDF-HFP films by following exactly equivalent method like any other blend compositions.

4.3. Characterization techniques

4.3.1. FT-IR and SS-NMR Spectroscopy

Fourier transforms infrared (FT-IR) spectra of the thin blend films were recorded on a Nicolet 5700 FT-IR spectrometer at resolution of 0.5 cm^{-1} with an average of 32 scans. ^{13}C CPMAS measurements were performed by using a Bruker 400 MHz NMR spectrometer.

4.3.2. Thermal Study

Thermogravimetric and differential thermal analysis (TG-DTA) were carried out on a (Netzsch STA 409PC) TG-DTA instrument from 50-800°C with a scanning rate of 10°C/ min in presence of nitrogen flow. A differential scanning calorimeter (Pyris Diamond DSC, Perkin-Elmer) was used to study the glass transitions (T_g) of the blend samples. All the blend samples display two composition dependent T_gs, one is higher temperature range (>250°C) and other one is in lower temperature range (<50°C). To determine these T_gs we have carried out two separate DSC experiments as follow: (a) for higher side T_g, samples were kept in isothermal condition at 400°C for 20 minutes and then fast cooled (200°C/min) to 50°C. Then after 30 minute equilibration at 50°C samples were scanned from 50°C to 400°C with scanning rate 10°C/min, (b) for lower side T_g, samples were hold in isothermal condition at 200°C for 20 minute and then fast cooled (200°C/min) to -60°C. Then after 30 minutes equilibration at -60°C samples were scanned from -60°C to 200°C with scanning rate 5°C/min. The crystalline melting temperature (T_m) of PVDF-HFP in the blend samples were determined from the first

DSC experiments from which we determined the higher side T_g. The crystallization temperature (T_c) of PVDF-HFP in the blend samples were also obtained from the cooling scan of the first DSC experiments from 400°C to 50°C with scan rate 5°C/min. The reproducibility of DSC results was checked by repeating the experiments. DSC was calibrated using In and Zn as calibration materials prior to scan of the blend samples.

4.3.3. X-ray Diffraction

The wide angle X-ray diffraction (WAXD) patterns of the samples were collected from an X-ray generator (Model PW 1729, Philips, Holland) with Cu Kα radiation (λ = 1.5418 Å) source at voltage 40 kV and 30 mA current in the 2θ range 5-45°.

4.3.4. Oxidative Stability

The stability of all the blend membranes to oxidation were investigated by immersing the membranes into Fenton's reagent (3% H_2O_2 aqueous solution containing 4 ppm Ammonium iron (II) sulfate, or Mohr's Salt) at 70°C. The oxidative stability was measured for time variation up to 120 hours. The membranes were taken out at certain time intervals, dried in vacuum oven at 80°C overnight, and weights were recorded. The oxidative stabilities of all the membranes were calculated as a weight remained after taking out the membranes from the Fenton's reagent.

4.3.5. H_3PO_4 (PA) Doping, Water Uptake, and Swelling Ratio

The PA doping level was calculated as the number of PA mols present per PBI repeat unit. The dried blend membranes were dipped into phosphoric acid (85%) for 3 days and then titrated against NaOH using an Autotitrator (Metrohm 702). The PA doping level measurements of the membranes were carried out in triplicate independently with different pieces of membranes to check the reproducibility of the results, and the average values are presented. Water uptakes of the membranes were obtained by immersing the dry membranes in water for 3 days. The weights of the

membrane were measured before and after dipping in water. The weights of wet membranes were measured after wiping the surface water. Water uptake values of the membranes were calculated as

$$\text{Water Uptake} = \frac{W_w - W_d}{W_d} \times 100\% \qquad (4.1)$$

where W_w and W_d are the weights of the wet and dry membranes, respectively. The % in thickness increase and swelling ratio of the membranes upon dipping in PA were measured. The thickness and length of the membranes were measured before dipping in PA. After 3 days, membranes were taken out from the PA bath and quickly wiped to remove the surface PA. Then again thickness and length of the PA loaded membranes were measured. The swelling ratio of the membranes were calculated

$$\text{Swelling Ratio} = \frac{L_w - L_d}{L_d} \times 100\% \qquad (4.2)$$

where L_w and L_d are the lengths of the wet and dry membranes, respectively.

4.3.6. Conductivity study

Proton conductivities of the blend samples were measured with a four-point probe technique. The impedance of the membranes was measured with an impedance analyzer by using a Zahner Impedance Spectrometer (ZENNIUM PP211) over a frequency range from 1 Hz to 100 Hz. The acid loaded membrane was cut into a rectangular shape and mounted onto the in house built conductivity cell. The conductivity of the membranes was measured from 30°C to 160°C and the data presented here is the 2nd heating scan data. After 1st heating scan, the cell is cooled down and again the conductivity was measured from 30°C to 160°C. The conductivities of the samples were obtained from the direct-current potential difference between the two inner electrodes. The conductivity was calculated with the following equation:

$$\sigma = \frac{D}{RBL} \qquad (4.3)$$

where, σ is the proton conductivity (S/cm), D is the distance between the electrodes, and B and L are the thickness and width of the blend samples, respectively. In all cases R was obtained from Nyquist plots.

4.3.7. Stress-Strain Study

The stress-strain relationship of the PA doped blend membranes were measured utilizing a Universal Testing Machine (Autograph Model AGS 10, ANG, Shimadzu) with 0.3(N) load cell. Dumb-bell specimens were cut following the ASTM standard D653 (Type V specimens). Tensile properties of all films were measured in an air atmosphere at room temperature with a cross head speed of 1 mm min^{-1}.

4. 4. Results and Discussion

4.4.1. FT-IR study

Often, FT-IR spectroscopy is used to study the interaction between the two polymers in the blends. The interactions can either shift or diminish intensities of either both the polymers and at least one polymer characteristic frequencies.

The spectrum of PBI shows a series of N-H stretching bands in the 3600-3000 cm^{-1} region and moreover PVDF-HFP does not have any distinguishable vibrational frequency in this region (Figure 4.2). The relatively sharp peak at 3408 cm^{-1} is the characteristic peak of non-hydrogen bonded free N-H groups, the broad peak at 3144 cm^{-1} is due to the self-associated hydrogen bonded N-H groups and the low intensity peak at 3063 cm^{-1} is due to the stretching modes of the aromatic C-H groups. Almost in all the blend systems of PBI studied earlier,[18,24,28,30] these N–H peaks displayed the peak shifting and broadening. We expect similar shifting in these blend system, owing to the probable interactions between the N–H of PBI and C–F of PVDF-HFP.

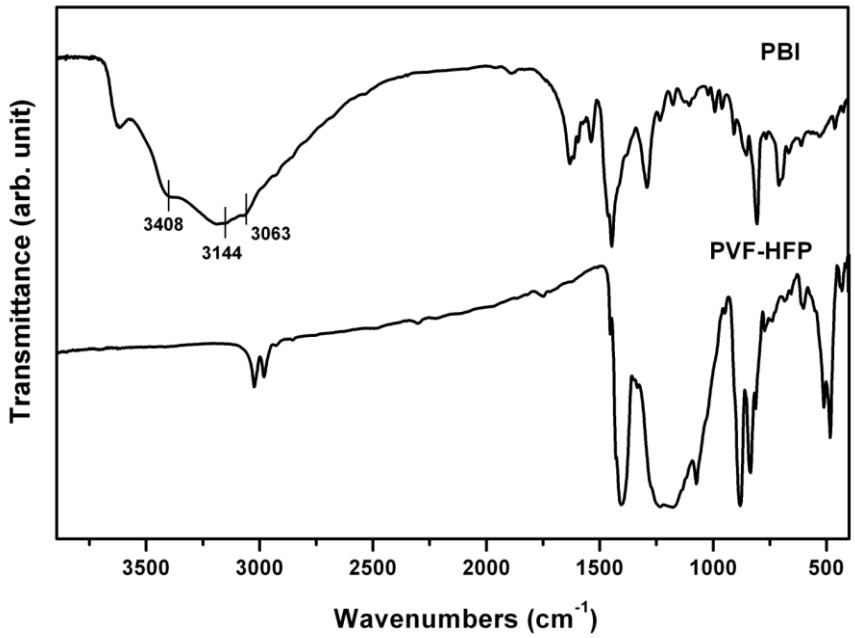

Figure 4.2: FT-IR spectra recorded from the thin films (60µm) of (A) Poly [2, 2'-(*m*-phenylene)-5, 5' benzimidazole] (PBI) and (B) Poly (vinylidene fluoride-co-hexafluoropropylene); PVDF-HFP.

The FT-IR spectra (3600-2900 cm^{-1} region) of PBI and representative blends of PBI with PVDF-HFP are presented in the Figure 4.3. From the Figure it can be seen that the free non hydrogen bonded N-H stretching band at 3408 cm^{-1} shift to lower frequency with increasing PVDF-HFP content in the blends. In the 10/90 blends, this peak shifts to 3385 cm^{-1}. Also the peak broadening is observed with increasing PVDF-HFP content in the blend. However, the C–H aromatic stretching peak at 3063 cm^{-1} does not change its position. So the frequency shift of the free N–H band position upon blending indicates the interaction between the two components of the blend. From Figure 4.3 it can also be observed that the self-associated hydrogen bonded N–H peak at 3144 cm^{-1} shows significant broadening and the peak is shifted to higher frequency with increasing PVDF-HFP content in the blend. For the 25/75 composition this peak shifted to 3166 cm^{-1}. Hence, a maximum 22 cm^{-1} shift is observed. This shifting suggested weakening of the self-associated N–H–N hydrogen bonding of the PBI chains. These

spectral changes arise because of the interaction between the two components in the blend and attributing the presence of interaction in the blends.

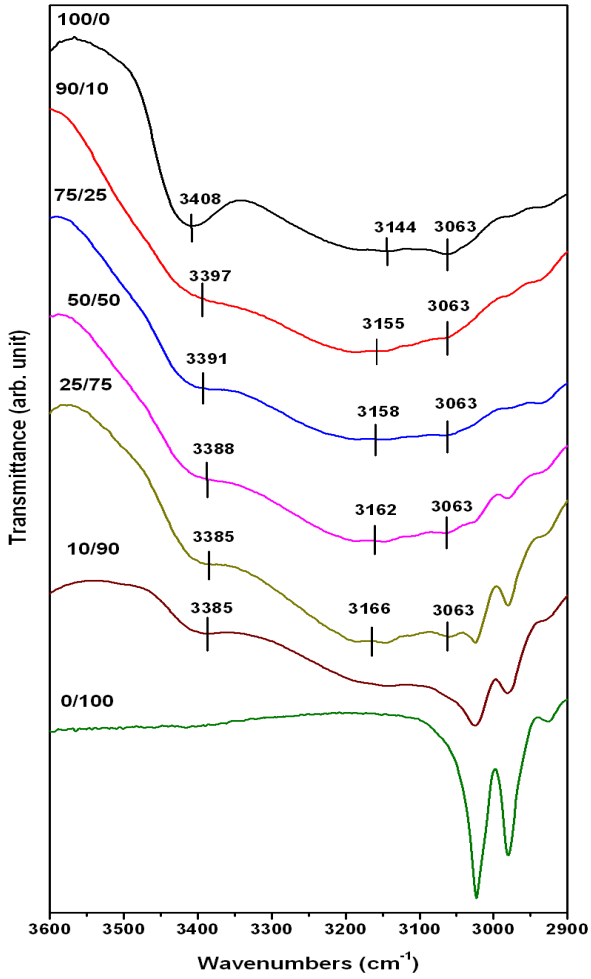

Figure 4.3: FT-IR spectra (3600-2900 cm^{-1}) of the PBI/PVDF-HFP blend film samples at their indicated blend compositions.

It is clear from the above observation that there is some interaction between the NH functionalities of PBI and one of the functional groups of PVDF-HFP in the blend system. We need to understand which functional group of PVDF-HFP is interacting with N–H of PBI. Hence it is expected that there will be some changes in the vibrational frequencies of the PVDF-HFP component in the blends. But it is difficult to

distinguish PVDF-HFP frequencies in the blend system, because of overlapping of the PBI peaks.

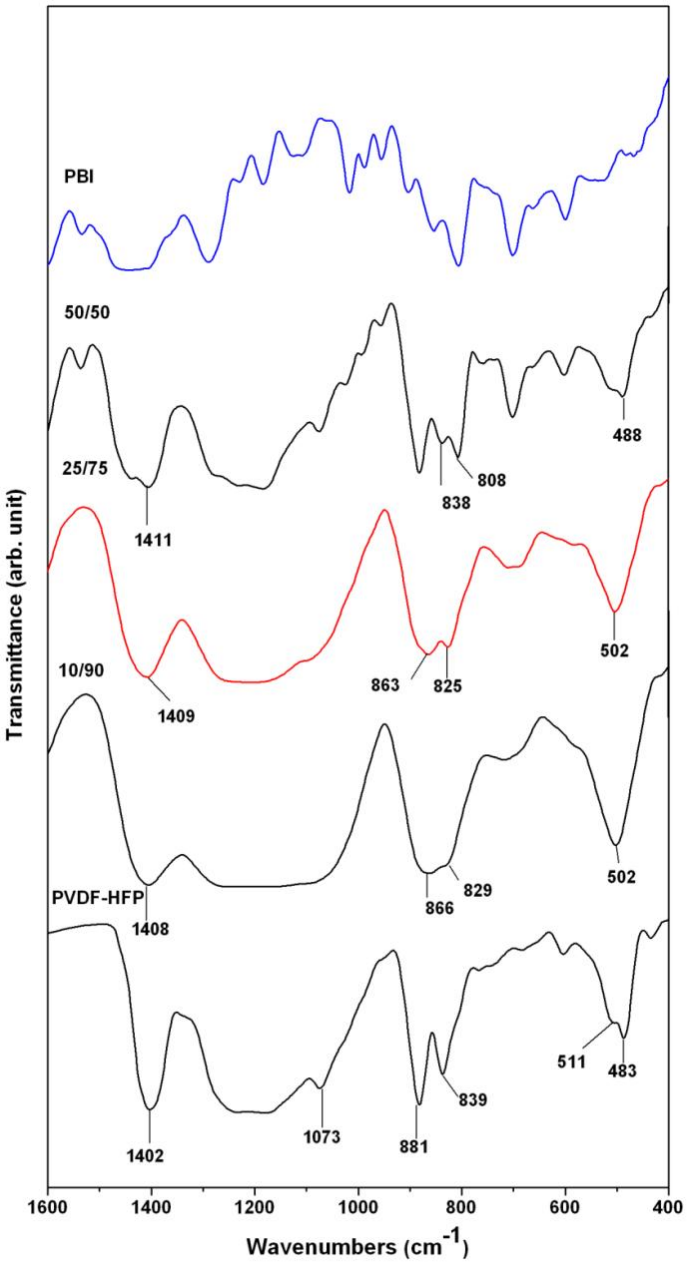

Figure 4.4: FT-IR spectra (1600-400 cm^{-1}) of the PBI/PVDF-HFP blend film samples at their indicated blend compositions.

The spectrum of PVDF-HFP contains several characteristic peaks in the range 400-1600 cm^{-1} (Figure 4.4) which are distinguishable from the PBI peaks.[39,40] These frequencies are listed in Table 4.1. It is observed that with addition of PBI in the blend mixture, the FTIR spectra undergo significant changes. The intensity of the peak at 1402 cm^{-1} decreases and shifted to higher frequency upon blending. This shifting can be attributed to the enhancement of the C–C bond strength because of the interactions between the two polymers. The peaks at 511 cm^{-1}, 483 cm^{-1} of neat PVDF-HFP which are $–CF_2$ group vibrations disappear and a new peak at 502 cm^{-1} is observed in case of blend samples. This change may be due to the hydrogen bonding interaction between the imidazole rings of PBI and C–F groups of PVDF-HFP. Also the peak at 881 cm^{-1} and 839 cm^{-1} shifted to lower wavenumber with increasing of PBI content in the blend mixture and the intensity of the peak at 1073 cm^{-1} is diminished. From the above observations the interactions between the two polymers in the blend system can be concluded.

Table 4.1: FT-IR stretching frequencies of PVDF-HFP and PBI/PVDF-HFP blends.

		PBI/PVDF-HFP blend (Peak position (cm^{-1}))		
Stretching frequencies	PVDF-HFP	10/90	25/75	50/50
CF_2 bending and wagging	483	502	502	488
Deformation vibration of CF_2	511	502	502	488
CH_2 rocking vibration	839	829	825	808
CH_2 wagging vibration of vinylidene band	881	866	863	838
C-F symmetric stretching	1073	1073	1073	-
Deformation vibration of CH_2	1402	1408	1409	1411

4.4.2. Solid State ^{13}C CPMAS study

Solid state NMR is an important tool for the characterization of polymer blends. The mixing of polymer chains causes changes in the structure of the polymers which can be measured by monitoring the NMR spectra. Hydrogen bonding is a strong

interaction that can affect the chemical shifts of the carbons on the donor and acceptor groups. So we expect chemical shift changes to occur upon blending. The solid state NMR spectra of PBI, PVDF-HFP and blend samples are shown in the Figure 4.5.

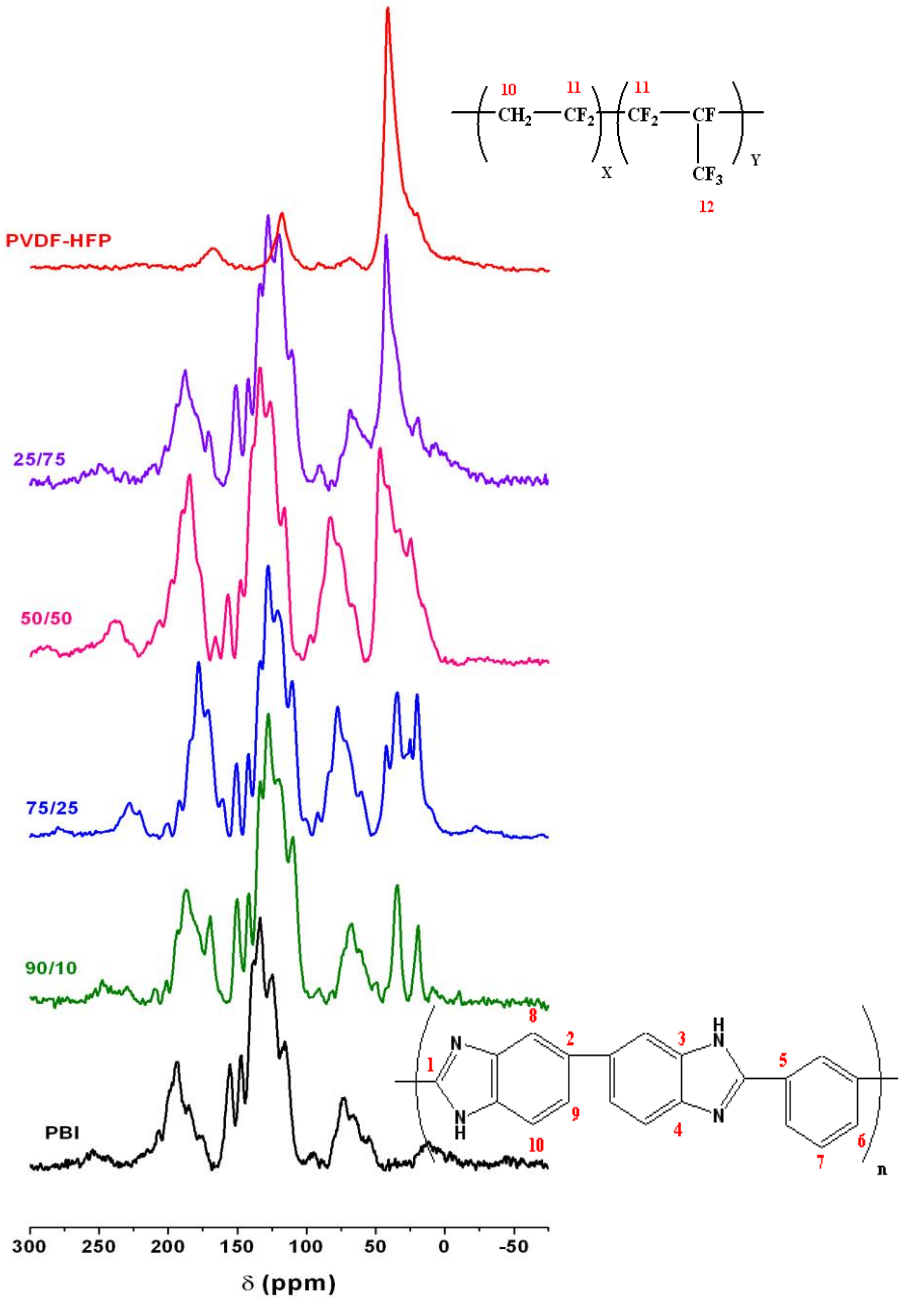

Figure 4.5: ^{13}C CPNMR spectra of PBI, PVDF-HFP and blend samples along with the chemical shift assignments for the neat samples.

The chemical shift assignments of neat polymers and blend samples are shown in Figure 4.5 tabulated in the Table 4.2. The spectrum of PBI consists of several lines. The peak at 155 is due to the carbons of imidazole rings attached to phenylene rings, peak at 146 ppm is due to the carbons connecting benzimidazole rings in the benzimidazole system and the peak at 133 ppm is due to the aromatic carbons bound to the nitrogen atoms. The remaining peaks at 124 and 115 are due to the protonated carbons of PBI with a contribution from the nonprotonated carbon of the phenylene ring to the line centred at 124 ppm.[41]

Table 4.2: ^{13}C chemical shifts of PBI and blend samples in the solid state.

Carbon	PBI (100/0)	90/10	75/25	50/50	25/75	PVDF-HFP (0/100)	Carbon
						164	12
1	155.15	150.26	150.54	156.77	150.77		
2	146.97	141.80	141.75	147.85	147.55		
3,4	133.42	133.51	133.43	133.86	127.36		
5,6,7	124.55	127.84	127.71	126.66	120.47		
						118.5	11
8,9	115.61	110.34	110.27	116.17	-		
		35,19	43,33,25,18	45,24	42.4	41.6	10

From the Table 4.2 and Figure 4.5, it can be observed the peaks at 155, 146 and 115 have been shifted to higher field and the peak at 125 shifted to lower field in case of blend samples. The spectrum of PVDF-HFP consists of three lines. The peak at 41.6 ppm can be assigned to the methylene carbons in PVDF-HFP. The small peak around 164 ppm is assigned to the carbon atom attached to the $–CF_3$ group of PVDF-HFP and the peak at 118.5 ppm is due to the carbon atom of CF_2[42] From the Figure 3 and table 4.2 it can be observed that the peak at 41.6 is shifting to lower field and slowly splitted into two or multiple peaks. For PBI/PVDF 50/50 the peak splitted and appears at 45, 24 and for 90/10 the peak becomes two peaks at 35 and 19. These observations clearly attributes that because of the interactions between the polymers through their respective functional groups, the methylene carbon display significant shifting. So there is a significant chemical shift difference between neat polymers and blend samples. These

changes in chemical shift provide strong evidence for the interaction between the blend components.

4.4.3. Thermal stabilities

The thermal stabilities of PBI, PVDF-HFP and blend samples are measured by TGA. The TGA thermograms of all the blend samples including the neat polymers are shown in Figure 4.6. The TGA thermograms confirms that all the samples are stable up to 400°C and the thermal stability of the blend membranes are decreasing with the increasing PVDF-HFP content. This is obvious because the thermal stability of PVDF-HFP is lower than PBI, so with increasing PVDF-HFP content in the blend the stability decreases. However, it must be noted that the onset of weight loss decreases as the PBI content in the blend increases. This attributes that the hydrophobic character of the material decreases as we increase the PBI content in the blend and this is due to the hydrophilic nature of PBI. In other words it can be said that the blend samples are more hydrophobic than the neat PBI.

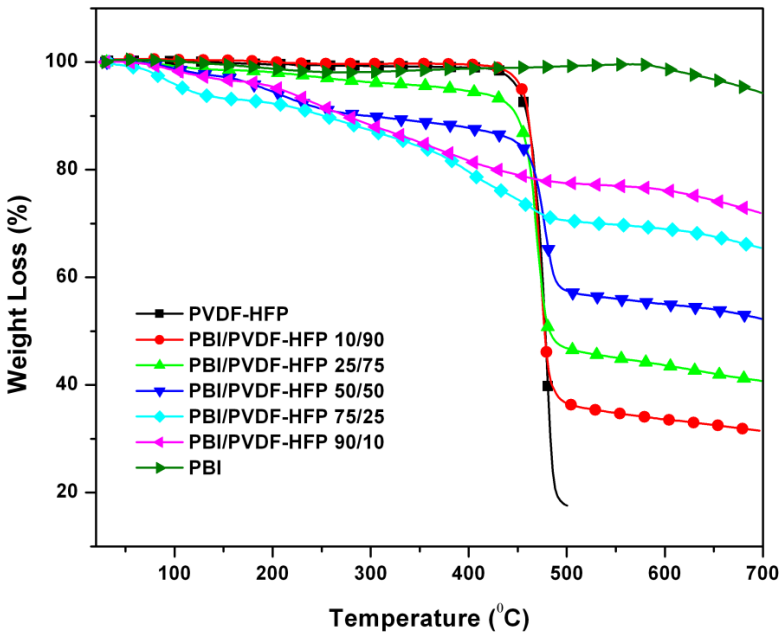

Figure 4.6: TGA curves of PBI, PVDF-HFP and blend samples

4.4.4. Miscibility studies of blends

The spectroscopic studies (FT-IR, SS-NMR) described in the previous section unarguably indicated the presence of interactions between the functional groups of two polymers of current blend system. These interactions are the driving forces for the miscibility of the polymers.

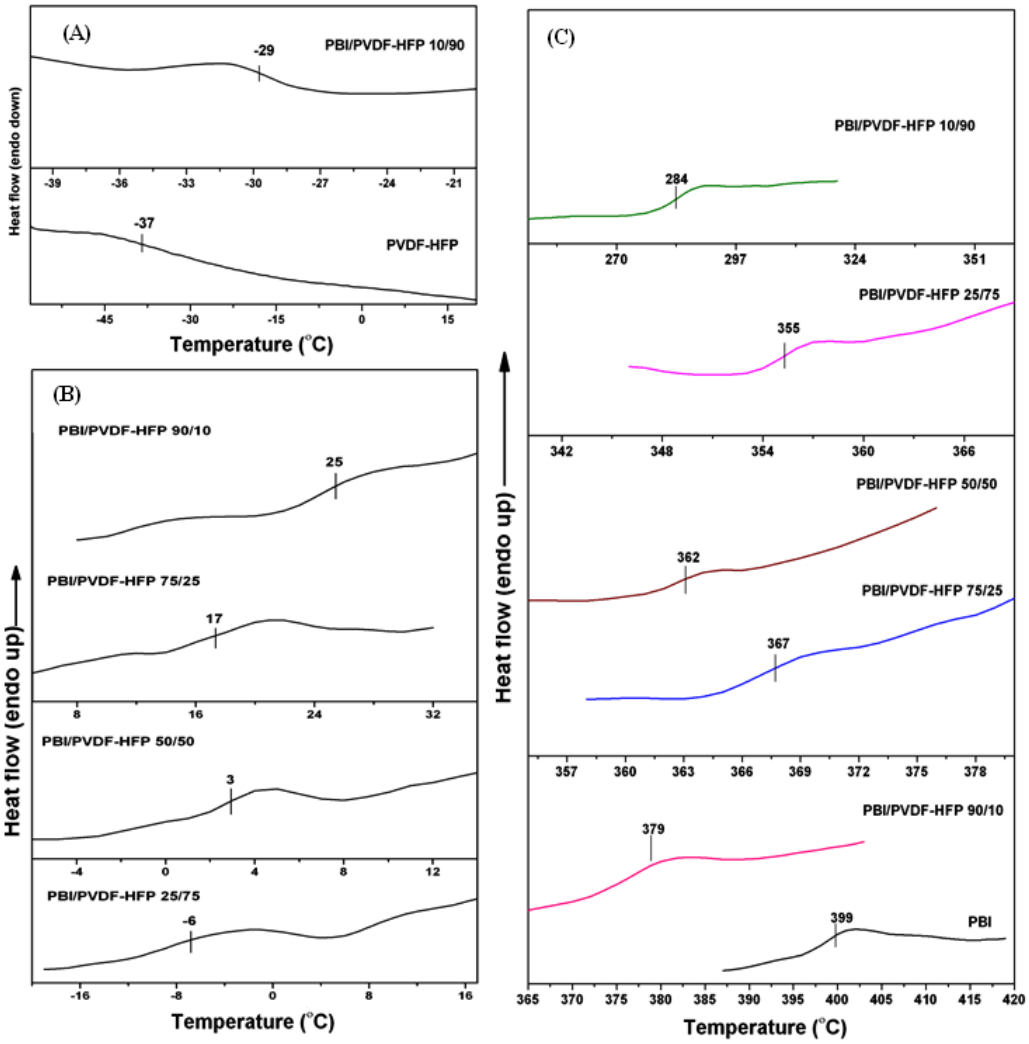

Figure 4.7: DSC thermograms of neat PBI, PVDF-HFP and blends. (A) Lower temperature T_g of PVDF-HFP and 10/90 (B) Lower temperature T_g of other blend composition as indicated (C) higher temperature range T_g. The horizontal lines and the corresponding values in the thermograms are the T_g's of the samples.

The miscibility between the two components of binary polymer blends such as the current system can be classified as either completely miscible blends or partially miscible blends. The nature and extend (strength) of interactions between the components detect the types of miscibility. It is generally believed that stronger interaction results completely miscible blend and weaker interactions produces partially miscible blend. Miscible blends exhibit single composition dependent glass transition (T_g) temperature whereas partially miscible blends display two composition dependent T_g's.[43]

We have used DSC to study the miscibility behavior of the current blend system and DSC thermograms are shown in Figure 4.8. The glass transition temperatures (T_g) of PBI obtained from DSC study is 399°C and PVDF-HFP shows a crystalline melting temperature (T_m) at 139°C and a crystallization temperature (T_c) at 109°C. These are agreement in with the literature data.[33] All the blend samples exhibit two T_g's, one is in higher temperature range below neat PBI T_g and another one is in lower temperature range above the neat PVDF-HFP T_g, and both the T_g's are composition dependent (Figure 4.8).

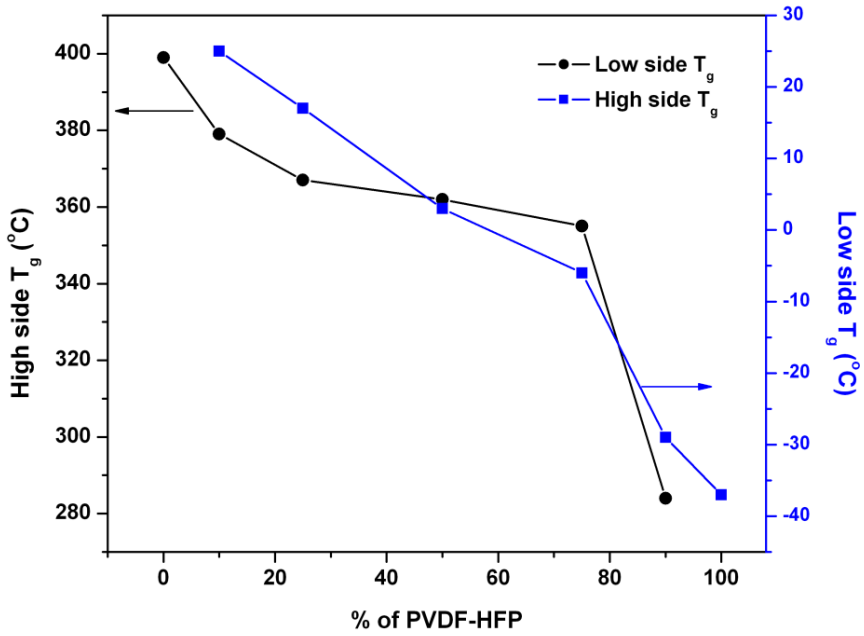

Figure 4.8: Glass transitions (T_g) vs. PVDF-HFP weight %.

As PVDF-HFP weight % increases in the blends the higher temperature T_g decrease and lower temperature T_g increases. These composition dependencies in T_g's are due to the specific interactions between the two polymer components upon blending which helps to form partially miscible blend. As a result of such specific interactions, the PVDF-HFP chains force the PBI chains to begin their segmental motions at lower temperature and vice-versa, and hence the T_g's alter. The effect of this specific interaction can be better understood by analyzing the melting and cooling thermograms as shown in Figure 4.9.

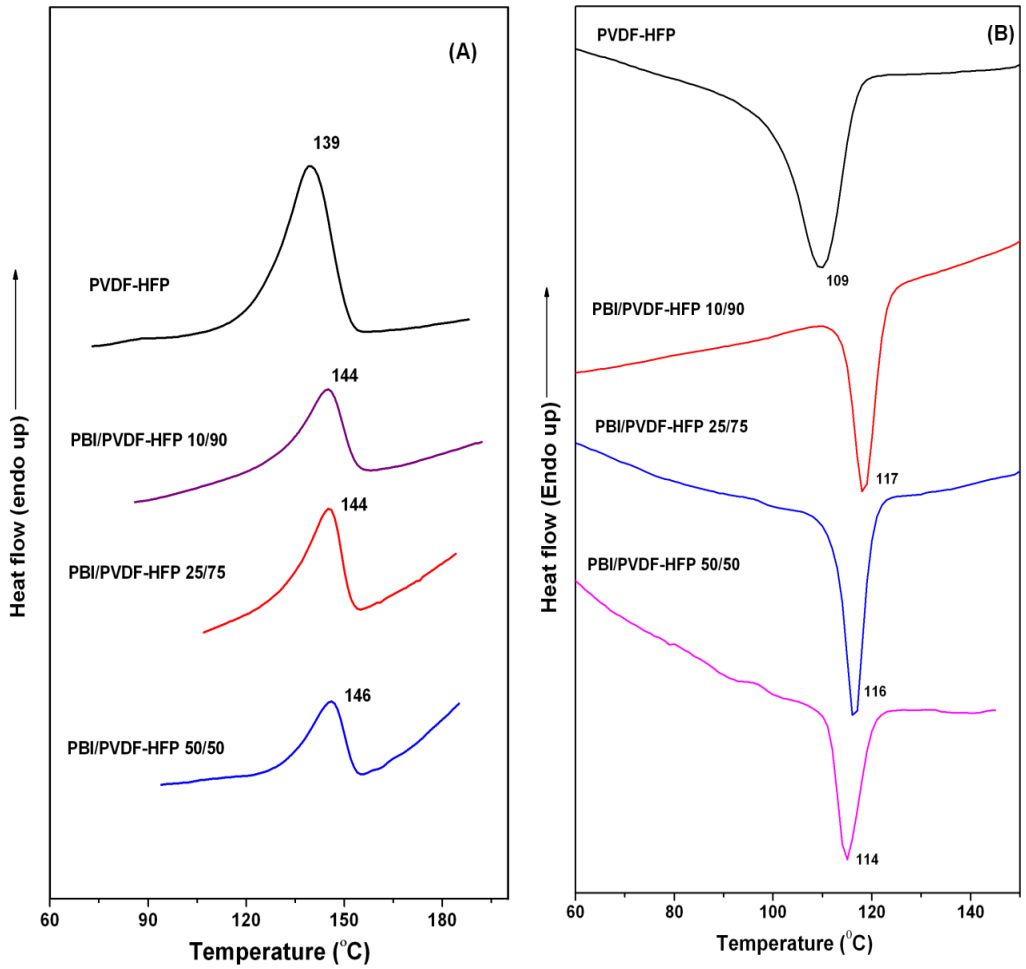

Figure 4.9: The (A) melting temperature (T_m) and (B) crystallization temperature (T_c) of the PBI/PVDF-HFP blends at their indicated blend compositions.

The 90/10 and 75/25 blend (PBI/PVDF-HFP) compositions do not show any melting endotherm (T_m) and crystallization exotherm (T_c). The blends containing greater than 25% PVDF-HFP show both melting endotherm and crystallization exotherm, this is because perhaps below this concentration of PVDF-HFP the crystalline nature of the polymer is completely suppressed by the PBI chains due to interaction. From Figure 4.9 it is observed that the both T_c and T_m of the blends are greater than that of neat PVDF-HFP. Polymer blends containing a crystalline component, the variation in values of T_c and T_m is usually attributed to the interactions between the components. The higher T_m and T_c indicate that the PBI chains are interfering in the crystallization of PVDF-HFP chains resulting the higher T_m and T_c. A better picture of this phenomenon is emerged when we calculate the crystallinity index of PVDF-HFP. The crystallinity index (χ_c) of the blend samples are calculated using the following equation

$$\chi_c = \frac{\Delta H_f}{\Delta H_f^\circ} \qquad (4.4)$$

where ΔH_f° = 104.6 J/g is the heat of fusion of 100% crystalline PVDF,[44] and ΔH_f is the heat of fusion of the samples obtained from the DSC. The heat of fusion of the samples and calculated crystallinity index are tabulated in Table 4.3.

Table 4.3: Thermodynamical data obtained from the DSC studies of PBI/PVDF-HFP blends

PBI/PVDF-HFP	ΔH_f (J/g_{blend})	ΔH_f (J/$g_{PVDF-HFP}$)	χ_c (PVDF-HFP) (%)
50/50	2.95	5.9	5.64
25/75	9.77	13.03	12.46
10/90	18.41	20.46	19.56
0/100	44.61	44.61	42.64

From the table it is observed that the crystallinity indexes of the blend samples are lower than the neat PVDF-HFP and decreases with increasing PBI content in the blend. The increase of T_m and T_c and decrease of χ_c values with increasing PBI content in the blend indicating the presence of interaction between PBI and PVDF-HFP. The crystallization of PVDF-HFP is completely suppressed when the PBI content in the

PBI/PVDF-HFP blends reaches 75% PBI. That is why we did not obtain the melting endotherm and crystallization exotherm for 90/10 and 75/25 blends compositions. This observation indicates the presence of interaction between the two polymers which is the driving force for the formation of partially miscible blends of these two polymers.

4.4.5. X-ray diffraction study

The XRD patterns of PBI/PVDF-HFP blend samples and the neat polymers are shown in Figure 4.10. The peaks at 17.5°, 18.5°, 20.2° and 30° correspond to the (1 0 0), (0 2 0), (1 1 0) and (0 2 1) reflections of crystalline PVDF-HFP.[45,46]

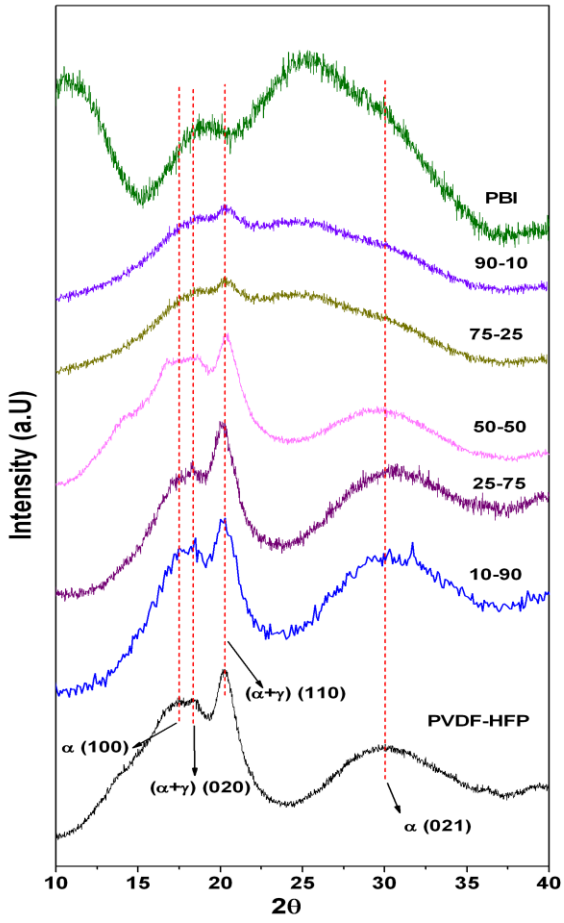

Figure 4.10: XRD patterns of PVDF-HFP, PBI and blend samples (PBI/PVDF-HFP) at their indicated composition.

The XRD pattern of PBI/PVDF-HFP blend membranes also exhibits the same peaks but of lower relative intensity and the intensities of the crystalline peaks of PVDF-HFP decreases and broadens with increase of PBI content in the blends (Figure 4.10). So the crystallinity of the PVDF-HFP in the blend has been considerably decreased upon the addition of PBI. This is because addition of PBI reduces the long range order of PVDF-HFP. For 90/10 and 75/25 compositions the peaks are almost disappeared. This is in accordance with the DSC data because for these two samples we did not observe the melting and crystallization peaks and for other blends χ_c value decreases significantly as seen in Table 4.3. This decrease in crystallinity in the blend membranes indicates the presence of interaction between the two polymers. This X-ray result once again proves that the PBI/PVDF-HFP blend system is a partially miscible blend.

4.4.6. H_3PO_4 (PA) doped blend membrane

The proton conducting character of the PBI based membrane is very important properties to be studied for the use as PEM in fuel cell. PBI membrane doped with H_3PO_4 (PA) exhibits high proton conductivity at temperatures up to 200°C. The proton conductivity increases with the increasing phosphoric acid (PA) content in the membrane. The PA doping level of the membrane is expressed as number of PA moles per PBI repeat unit. The PA doping level of the all blend membranes including neat polymer are shown in Table 4.4.

Table 4.4: PA doping level of the PBI/PVDF-HFP blend membranes. In case of blend membranes the doping levels are calculated based on the weight fraction of PBI in the samples.

PBI/PVDF-HFP	Mole of PA/PBI repeat unit	Water uptake (%)	Thickness increased (%) in PA	Swelling ratio (%) in PA
100/0	7.27	12.59	96.3	43.5
90/10	9.32	0	50	15.93
75/25	7.54	0	66.7	7.89
50/50	5.61	0	25	1.69
25/75	5.27	0	37.6	0
10/90	2.32	0	40	0
0/100	0.101*	0	0	0

** This value corresponds to PA content per PVDF-HFP*

From the Table 4.4, we observed that the acid loading increases initially, remain almost similar up to 75/25 composition and then decreases slowly beyond 75/25 composition in comparison with neat PBI. Since PVDF-HFP does not hold PA readily, as seen from the very low value of PA loading (0.101, Table 4.4), hence it is expected that with increasing PVDF-HFP content PA loading will decrease. Despite of the above fact, we see an increase in PA loading in case of 90/10 and 75/25. For 90/10 sample the acid loading is more compared to neat PBI membrane. This is due to the increase in the hydrophobic nature of the blend membranes. Since PVDF-HFP is a hydrophobic polymer, the blend membranes are more hydrophobic than PBI membrane. We have seen earlier also in our previous blend system of PBI/PVDF blend that with increasing hydrophobic character of the membrane, more PA loading takes place due to the better accessibility of imidazole groups to the PA molecules. We believe similar reason for this increase of PA loading when PVDF-HFP content is low. But when PVDF-HFP composition more than 25% the acid loading decreases. This may be due to the fact that PVDF-HFP increases the hydrophobicity of the blend membranes up to such an extent that the membranes are not allowing the aqueous PA molecule to interact with imidazole group and as a result membrane are not able to hold much PA. For the high PVDF-HFP content blends (> 50%) the PA doping level is less than PBI since PVDF-HFP cannot hold PA.

From Table 4.4, it is observed that all the blend membranes do not absorb water at all because of the hydrophobic nature of PVDF-HFP. This is in agreement with our observation of PA loading and TGA studies. The thickness of the resulting PA doped PBI membrane is an important issue which needs to be controlled for the better cell performance in an operating fuel cell. Often too thick membranes found to be not suitable for the membrane electrode assembly (MEA) fabrication. Unfortunately, it has been observed that PBI membrane increases thickness quite significantly after PA loading, especially when PA loading is more. Table 4.4 data clearly shows that increase in thickness is much smaller in blend membranes then the neat PBI despite the fact that the PA loading of blends high or comparable with PBI. The same trend is observed in swelling ratio also, when the membranes are dipped in PA.

4.4.7. Proton conductivity

The proton conductivity of the membrane is the most essential properties to be studied for the potential application in fuel cell. The proton conductivities of all the blend membranes are measured in the temperature range of 30°C to 160°C. All the membranes were soaked in PA solution for 3 days for acid doping before the measurement.

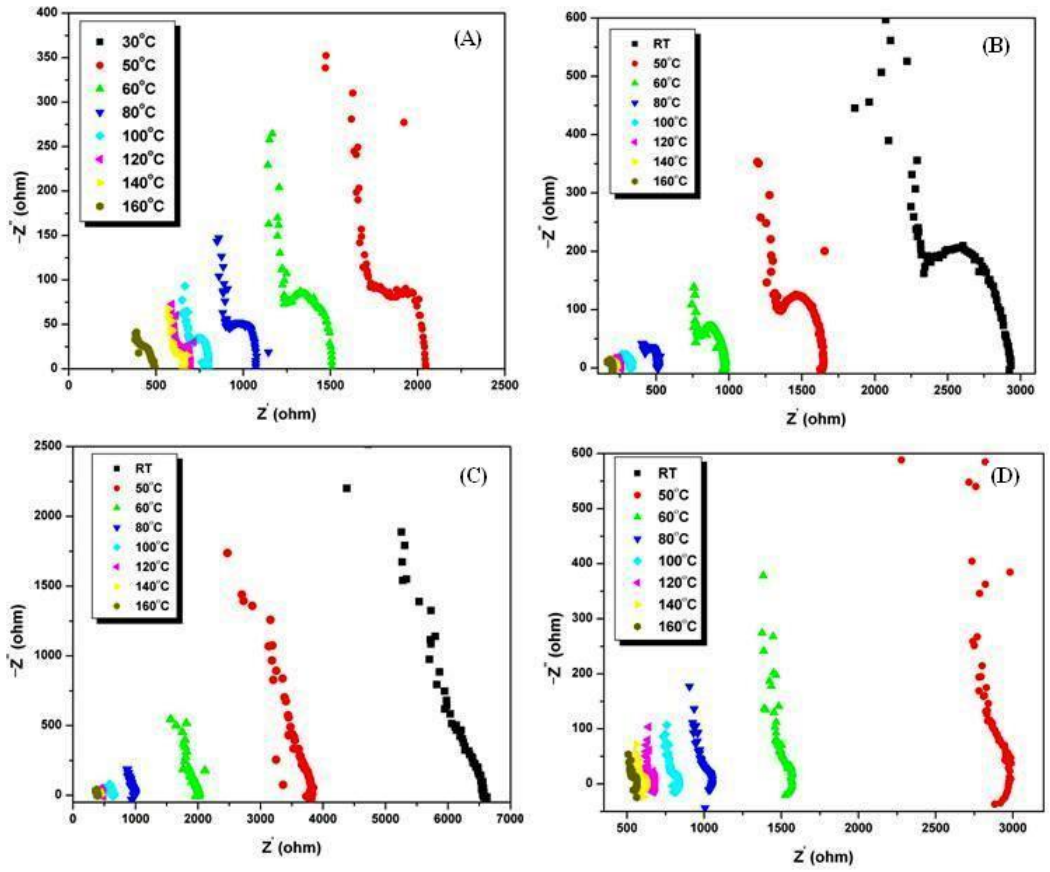

Figure 4.11: Nyquist plots of (A) PBI and PBI/PVDF-HFP blends (B) 90/10, (C) 75/25, (D) 50/50.

The PA loaded PBI membrane fixed in the home made four probe conductivity cell and impedance was measured by varying the temperature from 30°C to 160°C. This 1st heating data is not reliable since the water is present in the membrane. Hence after 1st heating scan, we cooled the cell and again measure the impedance by varying

temperature from 30°C to 160°C. The conductivity data presented here is the 2nd heating data and the conductivity was measured without any humidification. Therefore conductivity values are in the 0% relative humidity condition. The proton conductivities of the representative membranes obtained from the Nyquist plots (Figure 4.11) are plotted against temperature and shown in Figure 4.12. As expected in all the cases the proton conductivity increases with increasing temperature. The proton conductivity of the blend samples is higher than neat PBI.

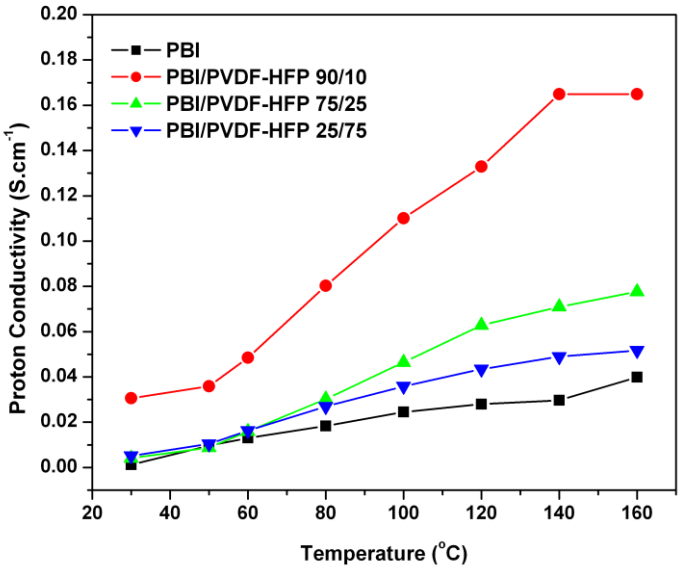

Figure 4.12: Proton conductivity against temperature for PBI/PVDF-HFP blend membranes

The proton conductivity of PBI at 160°C is 3.9×10^{-2} S/cm. For 90/10 blend the proton conductivity at 160°C is 1.64×10^{-1} S/cm, which is higher compare to neat PBI. The 75/25 blend which has comparable acid loading with PBI also shows higher conductivity than PBI. 25/75 whose acid loading is lower than the PBI is also display higher conductivity than PBI. Higher proton conductivity of the blend membranes than the neat PBI is due to the PVDF-HFP component in the blend membranes. Because of the large electronegativity of fluorine present in PVDF-HFP component, the fluorine moiety activates nearby H^+ of the N–H bond of the imidazole ring. This makes an

additional contribution for the proton transport in the membranes, resulting higher proton conductivity of the blend membranes than neat PBI.[47]

The dependency of proton conductivity on temperature obeys Arrhenius equation as follows

$$\ln(\sigma T) = \ln \sigma_{\circ} - \frac{E_a}{RT} \qquad (4.5)$$

Where σ is the protonic conductivity of the membrane (S cm^{-1}), $\sigma_{\circ}$ is the pre-exponential factor (S K^{-1} cm^{-1}), Ea is the proton conducting activation energy (kJ mol^{-1}), R is the ideal gas constant (J mol^{-1} K^{-1}) and T is the temperature (K). Arrhenius plots of temperature dependent conductivity are shown in Figure 4.13. The activation energy (E_a) is obtained from the slope of the linear fit of equation (4.5) and is shown in Figure 4.13. The data fits well with the equation, suggesting that the proton conduction is mainly governed by the Grotthuss mechanism. The E_a of the blend membranes are comparable with PBI. The E_a values obtained here are in agreement with already reported data.

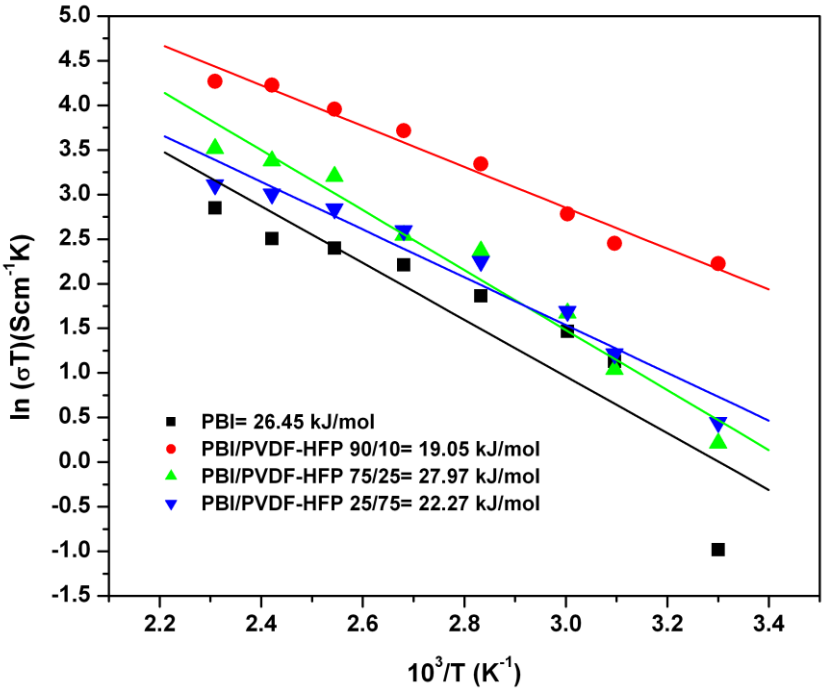

Figure 4.13: Arrhenius plots for the proton conduction of the blend samples.

4.4.8. Oxidative stability

Since in real operating fuel cell conditions, PEMs are exposed to oxidative environment, hence the membrane stability towards the oxidative environment is an essentially parameter to be checked for its suitability as PEM. All the blend membranes including the neat polymer membranes were tested in oxidizing condition, in the Fenton's reagent (3% H_2O_2 containing 4 ppm $FeSO_4$) at 70°C to check their durability in this environment. The data are presented in Figure 4.14 as a plot of remaining weight VS time and the total time duration followed here is 120°C hours. Blend samples exhibit significant improvement in the oxidative stability compared to neat PBI since neat PVDF-HFP does not show any weight loss in the oxidative environment. Figure 4.14 data clearly shows that the stability increases with increasing content of PVDF-HFP in the blend.

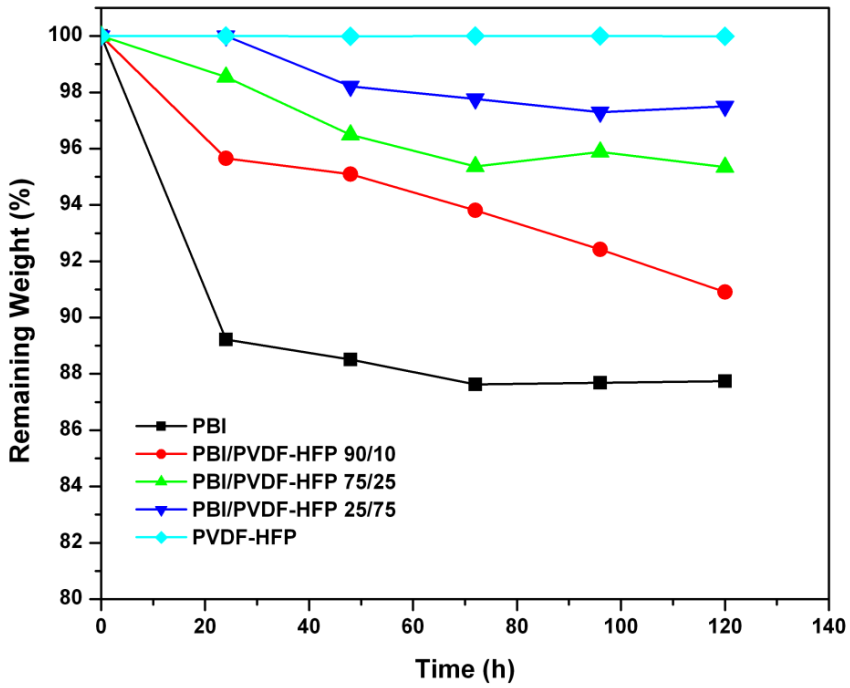

Figure 4.14: Oxidative stability of PBI/PVDF-HFP blend membranes at their indicated composition.

4.4.9. Mechanical Stability

The mechanical and dimensional stabilities of the acid doped membranes are important criterions for the construction of efficient membrane electrode assembly (MEA). It has been reported in the literature that the mechanically and dimensionally weak membranes loose the continuity during the fabrication of MEA since the fabrication process involves the pressing of PEM in between two electrode layers under high pressure. MEA with discontinuous PEM cannot be used in fuel cell and hence mechanically strong membrane is very much desirable. We have observed that all our PA doped blend membranes are dimensionally stable and Table 4.5 lists the tensile data of the few representative acid doped blend membranes. Our results clearly indicate the better mechanical stability of the blend membranes compared to the neat PBI.

Table 4.5: Mechanical strength data of PA doped blend membranes obtained from stress-strain experiment.

PBI/PVDF-HFP	Tensile strength (MPa)	Elongation at break (%)
100/0	3.27	21
90/10	5.25	34
50/50	6.85	40

4.5. Conclusion

Partially miscible blends of PBI with PVDF-HFP at various compositions have been prepared. The presence of hydrogen bonding interactions between the functional groups of two polymers is found to be the driving force for their partial miscibility. A thorough DSC study shows the presence of two compositions dependent T_g's indicating that the two components are partial miscible. The blending of PBI with PVDF-HFP affected the crystallinity as observed from XRD and DSC studies. The PA doping level of PBI in the blend membranes are not significantly increases because of the high hydrophobic nature of PVDF-HFP. Only for 90/10 blend composition the PA doping

level is higher than PBI. Although the PA doping level is not increasing much, the blend membranes are showing higher proton conductivity than PBI because of the presence of strong electronegative F atom. The oxidative stability of blend membranes is higher than neat PBI.

4. 5. References

1. Peckham, T. J.; Schmeisser, J.; Rodgersab, M.; Holdcroft, S. *J. Mater. Chem.* **2007**, *17*, 3255.
2. *Fuel Cell Handbook*, 6th ed.; EG & G Technical Services, Inc.: U.S. Department of Energy, Washington, DC, November **2002**.
3. Rikukawa, M.; Sanui, K. *Prog. Polym. Sci.* **2000**, *25*, 1463.
4. Hickner, M. A.; Ghassemi, H.; Kim, Y. S.; Einsla, B. R.; McGrath, J. E. *Chem Rev.* **2004**, *104*, 4587.
5. Mauritz, K. A.; Moore, R. B. *Chem Rev.* **2004**, *104*, 4535.
6. Li, Q.; He, R.; Jensen, J. O.; Bjerrum, N. J. *Chem. Mater.* **2003,** *15*, 4896.
7. Sahu, A. K.; Selvarani, G.; Bhat, S. D.; Pitchumani, S.; Sridhar, P.; Shukla, A. K.; Narayanan, N.; Banerjee, A.; Chandrakumar, N. *J. Membr. Sci.* **2008**, *319*, 298.
8. Chuang, S. W.; Hsu, S. L. C. *J. Polym. Sci., Part A: Polym. Chem.* **2006**, *44*, 4508.
9. Mehta, V.; Cooper, J. S. *J. Power Sources*, **2003**, *114*, 32.
10. Shao, Y.; Yin, G.; Wang, Z.; Gao, Y. *J. Power Sources*, **2007**, *167*, 235.
11. Higashihara, T.; Matsumoto, K.; Ueda, M. *Polymer*, **2009**, *50*, 5341.
12. Savinell, R.; Yeager, E.; Tryk, D.; Landau, U.; Wainright, J.; Weng, D.; Lux, K.; Litt, M.; Rogers, C. *J. Electrochem. Soc.* **1994**, *141*, L46.
13. Xiao, L.; Zhang, H.; Jana, T. Scanlon, E.; Chen, R.; Choe, E. W. Ramanathan, L. S.; Yu, S.; Benicewicz, B. C. *Fuel cells*, **2005**, *5*, 287.
14. Xiao, L.; Zhang, H.; Scanlon, E.; Ramanathan, L. S.; Choe, E. W.; Rogers, D.; Apple, T.; Benicewicz, B. C. *Chem. Mater.* **2005,** *17*, 5328.
15. Kumbharkar, S. C.; Islam, Md. Nazrul.; Potrekar, R. A.; Kharul, U. K. *Polymer* **2009**, *50*, 1403.
16. Ghosh, S.; Sannigrahi, A.; Maity, S.; Jana, T. *J. Phys. Chem. C* **2011**, *115*, 11474.
17. Ghosh, S.; Sannigrahi, A.; Maity, S.; Jana, T. J. *J. Mater. Chem.* **2011**, *21*, 14897.

18. Arunbabu, D.; Sannigrahi, A.; Jana, T. *J. Phys. Chem. B* **2008,** *112*, 5305.
19. Krutphun, P.; Supaphol, P. *Eur. Polym. J.* **2005**, *41*, 1561.
20. Ning, W.; Xingxiang, Z.; Jiugao, Y.; Jianming, F. *Polym. Int.* **2008**, *57*, 1027.
21. Shogbon, C. B.; Brousseau, J. L.; Zhang, H.; Benicewicz, B. C.; Akpalu, Y. *Macromolecules* **2006**, 39, 9409.
22. (a) Sannigrahi, A.; Arunbabu, D.; Sankar, R. M.; Jana, T. *Macromolecules* **2007**, *40*, 2844. (b) Ghosh, S.; Sannigrahi, A.; Maity, S.; Jana, T. *J. Phys. Chem. B* **2010,** *114*, 3122.
23. Musto, P.; Karasz, F. E.; MacKnight, W. J. *Macromolecules* **1991**, *24*, 4762.
24. (a) Deimede, V.; Voyiatzis, G. A.; Kallitsis, J. K.; Qingfeng, L.; Bjerrum, N. J. *Macromolecules* **2000**, *33*, 7609.
    (b) Aili, D.; Hansen, M. K.; Pan, C.; Li, Christensen, E.; Jensen, J. O.; Bjerrum, N. J. *Int. J. Hyd. Eng.* 2011, *36*, 6985.
25. Wycisk, R.; Chisholm, J.; Lee, J.; Lin, J.; Pintauro, P. N. *J. Power Sources* **2006**, *163*, 9.
26. Makhija, S.; Pearce, E. M.; Kwei, T. K.; Liu, F. *Polym. Eng. Sci.* **1990,** *30*, 13.
27. Jaffe, M.; Chen, P.; Choe, E-W.; Chang, T.S.; Makhija, S. *Adv. Polym. Sci*. **1994**, *117*, 297.
28. Musto, P.; Karasz, F. E.; MacKnight, W. J. *Macromolecules* **1991**, *24*, 4762.
29. Schönberger, F.; Hein, M.; Kerres, J. *Solid State Ionics* **2007**, *178*. 547.
30. Hazarika, M.; Arunbabu, D.; Jana, T. *J. Colloid Interface Sci.* **2010**, *351*, 374.
31. Kumara, G. G.; Shin, J.; Nho, Y. C. Hwang, I. Se.; Fei, G.; Kim, A. R.; Nahm, K. S. *J. Membr. Sci.* **2010,** *350*, 92.
32. Kima, K. M.; Kob, J. M.; Park, N. G. *Solid State Ionics* **2003**, *161*, 121.
33. Tiwari, V. K.; Kulriya, P. K.; Avasthi, D. K.; Maiti, P. **2009**, *113*, 11632.
34. Shia, L.; Wang R.; Cao Y.; Liang D. T.; Tay J. H. *J. Membr. Sci.* **2008**, *315*, 195.
35. Ulaganathan, M.; Rajendran, S. *Ionics* **2010**, *16*, 515.
36. Huang, H.; Wunder, S. L. *J. Electrochem. Soc.* **2001**, *148*, A279.
37. Wang, Z.; Tang, Z. *Mater. Chem. Phy.* **2003**, *82*, 16.

38. Sannigrahi, A.; Arunbabu, D.; Sankar, R.M.; T. Jana, *J. Phys. Chem. B* **2007**, *111*, 12124.
39. Missan, H. P. S.; Chu, P. P.; S. Sekhon, S. *J. Power Sources* **2006**, *158*, 1472.
40. Tian, X.; Jiang, X. *J. Hazard. Mater*. **2008,** *153*, 128.
41. Grobelny, J.; Rice, D. M.; Karasz, F. E.; MacKnight, W. J. *Macromolecules* **1990**, *23*, 2139.
42. Saikia, D.; Wu, H.-Y.; Pan, Y.-C.; Lin, C.-P.; Huang, K.-P.; Chen, K.-N.; Fey, G. T. K.; Kao, H.-M. *J. Power Sources* **2011**, *196*, 2826.
43. (a) Cakar, F.; Sakar, D.; Cankurtaran, O.; Karaman, F. *Eur. Polym. J.* **2007**, *43*, 507. (b) Qiu, Z.; Ikehara, T.; Nishi, T. *Polymer*, **2003**, *44*, 2503.
44. Nakagawa, K.; Ishida, Y. *J. Polym. Sci. Polym. Phys.* **1973**, *11*, 2153.
45. Kim, K. M.; Kim, J.-C.; Ryu, K. S. *Macromol. Chem. Phys.* **2007**, *208*, 887.
46. Stephan, A. M.; Nahm, K. S.; Kulandainathan, M. A.; Ravi, G.; Wilson, J. *Eur. Polym. J.* **2006**, *42*, 1728.
47. Pu, H.; Wang, L.; Pan, H.; Wan, D. *J. Polym. Sci: Part A: Polym. Chem.* **2010**, *48*, 2115.

Chapter 5

Proton exchange membrane developed from novel blends of polybenzimidazole and poly (vinyl-1,2,4-triazole)

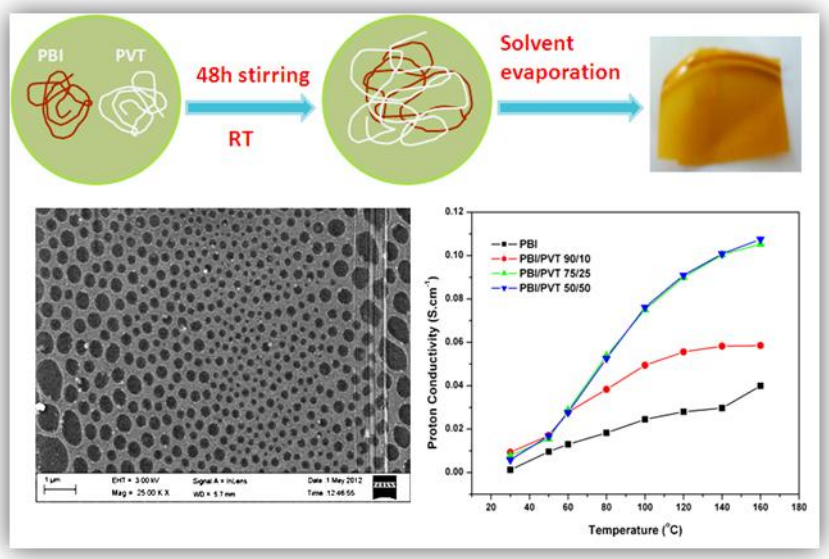

Novel polymer blend membranes of PBI and poly(1-vinyl-1,2,4-triazole) (PVT) were prepared using solution blending method. The proton conductivity of the blend membranes have improved significantly compared to neat PBI because of the presence of triazole moiety which acts as a proton facilitator in the conduction process.

Hazarika, M.; Jana, T. *ACS Appl. Mater. Interfaces*, **2012,** *4*, 5256-5265.

5.1. Introduction

Proton exchange membrane fuel cells (PEMFCs) have received significant attention as promising candidates for clean and efficient energy conversion devices.[1–3] The conventional perfluorinated polymer-based proton exchange membrane (PEM) can operate only at low temperature; above 120°C, this PEM displays negligible proton conductivity. Therefore, the last couple of years, an enormous amount of effort has been exerted to develop high-temperature PEMs that can conduct protons readily up to 180°C.[4–12] Fuel cells consisting of this type of PEM offers many advantages, including simpler water management, higher CO tolerance, and faster electrode kinetics.[8–14] Heteroaromatic polymers containing groups such as imidazole, pyrazole, and triazole exhibit high conductivity in the anhydrous state at higher temperature and they are found to be suitable for fabricating high-temperature PEMs.[15–19] The basic nitrogen sites of these heterocyclic polymers act as strong proton acceptors, with respect to strong acid groups, and thus facilitate the proton conduction when doped with acid at higher temperature.[20,21]

Triazole and its derivatives have been studied extensively for use in high-temperature PEMs because of their excellent proton conduction behavior.[22–29] 1H-1,2,4-triazole, a heterocyclic molecule, can conduct protons readily under anhydrous conditions at higher temperature (>100°C) via the Grotthuss mechanism as in imidazole. The reported proton conductivity of pure 1H-1,2,4-triazole is 1.5×10^{-4} S/cm (at 115°C) and $\sim 1.2 \times 10^{-3}$ S/cm (at the melting point).[22] Three N atoms in the triazole ring increase the long-range proton transport via structure diffusion, which is the driving force for the proton conduction. In several reports, 1H-1,2,4-triazole has been used as a dopant in an acidic polymer or to modify a polymer backbone with triazole units.[22,30–32] The disadvantage of using triazole as a dopant is that it may form a liquid phase in the polymer matrix, because of its low melting point, which results in diffusion from the polymer matrix into the electrodes and, at high humidity, because of its solubility, triazole may go out of the membrane.[26]

Poly(1-vinyl-1,2,4-triazole) (PVT, Scheme 5.1) is an promising polymer where the triazole ring is attached to the polymer backbone and, hence, can be used as an PEM in high temperature fuel cells after doping with appropriate dopants. Bozkurt et al.[33–35] has pioneered the PVT-doped membranes for their use as PEMs. They doped the polymer with a variety of acids at various molar ratios and showed that proton conductivity increases with dopant concentration and temperature. The mechanism of proton conductivity in the membranes was found to be the Grotthuss mechanism. The proton conductivity increased as the amount of dopant concentration, as well as the temperature, increased. But the main drawback of this polymer is that it does not form films that are very strong mechanically and, hence, its use may be limited.

Polymer blending is an easy and economical method to produce new polymeric materials, because, by mixing two or more polymers with different physical properties, a material with enhanced physical and chemical properties can be generated. Therefore, the blending of PVT with another polymer, which can provide mechanical strength without destroying the other properties (such as proton conducting character), can be useful for the development of free-standing mechanically strong films with high thermal stability and high proton conductivity. The reported Nafion/PVT blend[36] membranes were homogeneous and thermally stable at least up to 300°C and have displayed a conductivity that increased by three orders of magnitude upon hydration. But this blend membrane cannot be used for high-temperature proton exchange membranes (HT-PEMs). Hence, the search for another polymer that can be blended with PVT is still ongoing for the development of HT-PEM.

Phosphoric acid (PA)-doped polybenzimidazole (PBI, Scheme 5.1) has received much attention over the past few years and, to date, it is the best-known alternative of Nafion for high-temperature operations. PA-doped PBI exhibits high proton conductivity at temperatures up to 200°C and very high mechanical stability. It has some other advantages also, such as low gas permeability, excellent oxidative and thermal stability, and an almost-zero water drag coefficient. The proton conductivity of PA-doped PBI membranes is dependent on the doping level. PBI possesses both proton donor (–NH–) and proton acceptor (–N=) hydrogen bonding sites. Because of the

availability of the hydrogen bonding sites in the polymer backbone, it can form miscible blends[37,38] with a variety of polymers. So the blend of PVT with PBI would be interesting, because combining the two polymers may result in a material where the properties of both polymers will combine and, as a result, the material may show high proton conductivity with high thermal and mechanical stability. We have demonstrated, in a series of articles, that PBI forms miscible and partially miscible blends with a variety of polymers, such as poly-(vinylidene fluoride), sulfonated polystyrene (chapter 3), and poly(vinylidene fluoride-co-hexafluoropropene) (Chapter 4).[39,40] In all of these cases, we have observed that, upon blending, the PBI properties (especially proton conduction behavior) have improved significantly. Therefore, we expect to see better conduction properties in the current blend also.

In the present work, PVT, which has also acceptor sites in the side chain, was synthesized by free radical polymerization and blended with PBI. The miscibility, thermal stability, and proton conductivity of the blend membranes are studied using a variety of spectroscopic, thermal, and electrical techniques, respectively. Morphology of blend membranes was probed by microscopic techniques to understand the micro structural influences on the properties.

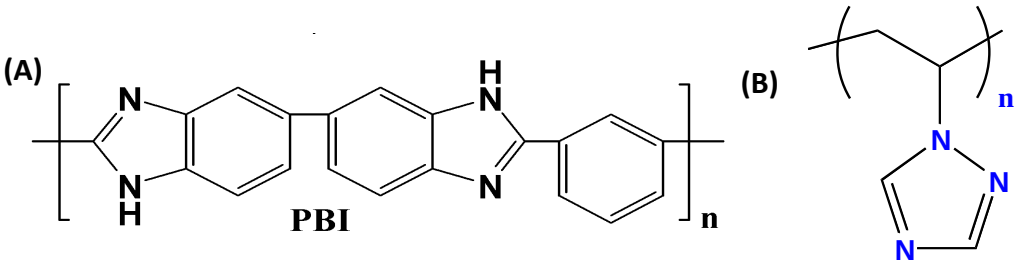

Scheme 5.1: Structure of (A) Poly[2, 2'-(*m*-phenylene)-5, 5'-benzimidazole] (PBI) and (B) Poly(1-Vinyl-1,2,4-triazole) (PVT)

5.2. Experimental Section

5.2.1. Materials

Poly [2,2′-(m-phenylene)-5,5′-benzimidazole] (PBI) was obtained by polymerizing 3,3′,4,4′-tetraaminobiphenyl (TAB) and isophthalic acid in a polyphosphoric acid medium (115%) in the laboratory, using the standard method that we described earlier.[41,42] The measured inherent viscosity (IV) from H_2SO_4 solution is 1.04 dL/g and the calculated viscosity-average molecular weight is 70,000. The concentration of the polymer solution in H_2SO_4 was 0.2 g/dL for the viscosity measurements. The viscosity-average molecular weights of the PBI samples were obtained using the Mark-Houwink equation, where $K = 5.2 \times 10^{-5}$ dL/g and a = 0.92 for H_2SO_4 (98%) solvent at 30°C. The intrinsic viscosity ([η]) values of the synthesized PBIs were obtained using the Kuwahra single-point method. 1-Vinyl-1,2,4-triazole (>97%) was purchased from Sigma-Aldrich. Azobisisobutyronitrile (AIBN) is recrystallized from tetrahydrofuran (THF). Dimethylacetamide (DMAc; HPLC grade), dimethyl formamide (DMF; HPLC grade), phosphoric acid PA (85%), and deuterated dimethyl sulfoxide (DMSO-d_6) were obtained from Merck (India) and used as-received.

5.2.2. Synthesis of poly (1-vinyl-1,2,4-triazole)

Poly(1-vinyl-1,2,4-triazole) (PVT) was synthesized via a free-radical polymerization method, using AIBN (5 mol %) as an initiator.[43] The monomer weight concentration is 10%, with respect to DMF as solvent. The reaction mixture was heated at 60°C under a N_2 environment for 24 h. After polymerization, the solution was poured into a large excess of ether. The resulting precipitate was washed in ether and dried in a vacuum oven at 60°C for 1 day. The IV value of the polymer measured from DMSO solution is 2.69 dL/g, and the calculated viscosity-average molecular weight using the Mark-Houwink equation is 12,000. The PVT polymer was confirmed using ^{13}C CPMAS NMR (SS-NMR) and FT-IR spectroscopy (Figures 5.1 and 5.2). The NMR spectrum of PVT consists of four lines. The peaks near 150 and 158 ppm are the characteristic C

peaks of the triazole ring, and the peaks near 45 and 58 ppm correspond to the A and B peaks of the polymer backbone.[33-35] The FT-IR spectrum of PVT contains the characteristic peaks of N=N, C=N, and C−N stretching frequencies at 1277, 1434, and 1659 cm^{-1}, respectively. The peak at 3438 cm^{-1} is due to absorbed moisture.

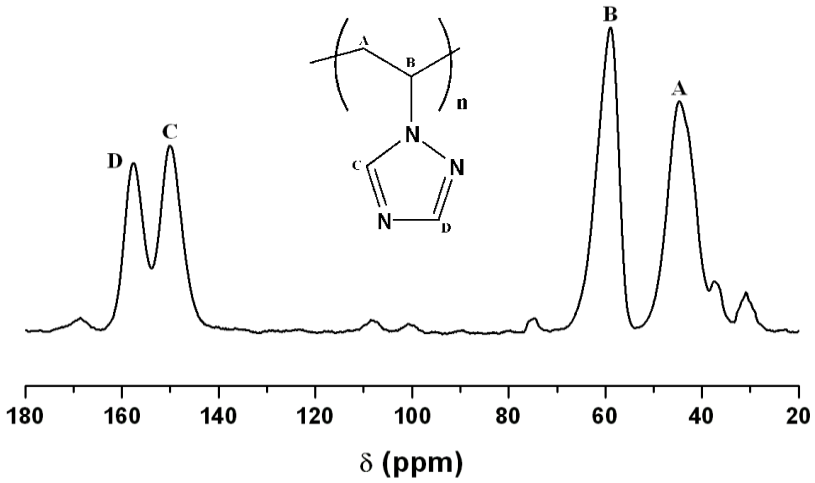

Figure 5.1: Solid state ^{13}C CPMAS NMR spectrum of PVT.

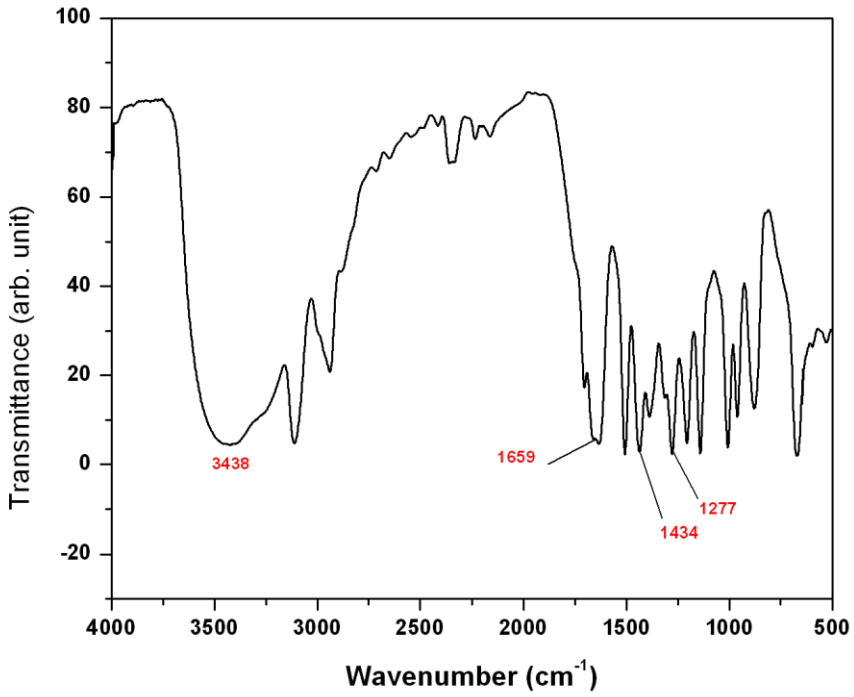

Figure 5.2: FT-IR spectrum of PVT.

5.2.3. Blend preparation

Blends were prepared by mixing two polymers (PBI and PVT) in DMAc. The concentration of the polymer solution in DMAc was kept 1% (w/v). The required amount of the two polymers was taken in the measured quantity of DMAc and mixing was continued for 2 days by stirring with the help of a magnetic stirrer in a closed glass vessel at room temperature. The homogeneous blend solutions were filtered through a 0.2-μm polytetrafluoroethylene (PTFE) membrane and then poured into a clean glass Petri dish at 70°C to cast the blend films. Transparent homogeneous thin films (Figure 5.3) were obtained and dried in a vacuum oven at 70°C for 3 days to evaporate the trace amount of solvent completely. The films were stored in a closed desiccator for further characterization.

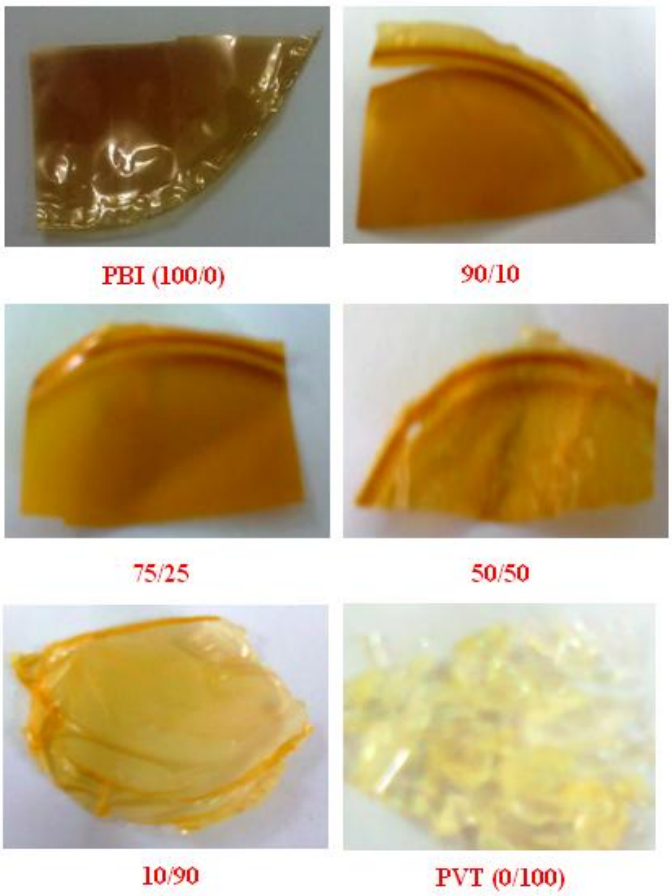

Figure 5.3: Photographs of PBI/PVT blend membranes.

5.3. Characterization techniques

5.3.1. FT-IR and SS-NMR spectroscopy

Fourier transform infrared (FT-IR) spectra of the thin blend films (~70 μm) were recorded on Nicolet 5700 FT-IR spectrometer at a resolution of 0.5 cm^{-1} with an average of 64 scans. ^{13}C CPMAS measurements were performed using a Bruker 400 MHz NMR spectrometer.

5.3.2. Absorption and fluorescence spectroscopy

Electronic absorption spectra were recorded on a Shimadzu model UV-3100 UV-visible spectrometer. Steady-state fluorescence emission spectra were recorded on a Jobin-Yvon Horiba spectrofluorimeter (Model Fluoromax-3). The 1% PBI and blend solutions in DMAc were spin-coated onto an optically transparent quartz plate and then the spectra were recorded from the spin-coated plate.

5.3.3. Thermal study

Thermogravimetric and differential thermal analysis (TG-DTA) were carried out on a Netzsch STA 409PC TG-DTA instrument, from 50°C to 800°C, with a scanning rate of 10°C/min in the presence of a nitrogen flow. A differential scanning calorimetry (DSC) device (Pyris Diamond DSC, Perkin-Elmer) was used to study the glass-transition temperatures (T_g) of the blend samples. Samples were kept at 50°C for 30 min under isothermal conditions. Samples then were scanned from 50°C to 450°C at a heating rate of 10°C/min. The PVT and blend samples with high PVT content (10/90) were scanned up to temperatures of 200°C. The reproducibility of DSC results was checked by repeating the experiment at least thrice. The DSC equipment was calibrated using In and Zn as calibration materials prior to scanning the blend samples.

5.3.4. Morphological investigations

The morphology of the blend samples were studied using field-emission scanning electron microscopy (FESEM). The samples were prepared by depositing one drop of 1% solution of the neat polymers and the blend samples on a glass slide. The glass slides then were dried in an oven at 60°C. They then were coated with gold, and their micrographs were obtained using a FESEM apparatus (Model Ultra 55, Carl Zeiss)

5.3.5. Doping level, swelling ratio and thickness increase after doping with phosphoric acid

The phosphoric acid doping level was calculated as the number of moles of PA present per PBI repeat unit. Doping level, swelling ratio, and thickness increase measurements were carried out by immersing the dry membranes in phosphoric acid (PA) for 3 days. The weight (W_d), length (L_d), and thickness (T_d) of the membrane were measured before dipping in PA. The weight (W_w), length (L_w) and thickness (T_w) of the wet membranes were measured after 3 days of dipping in PA. Surface-absorbed PA was wiped before the measurements. Swelling ratio and thickness increase values of the membranes were calculated as

$$\text{Swelling Ratio} = \frac{L_w - L_d}{L_d} \times 100\% \qquad (5.1)$$

$$\text{Thickness increase} = \frac{T_w - T_d}{T_d} \times 100\% \qquad (5.2)$$

The doping level calculation was determined by finding the weight of the acid absorbed by the membranes and for that the doped membranes that were dried in a vacuum oven at 100°C for 24 h and then weighed (W_{acid}). Equation 3 was used to calculate the number of moles of PA per PBI repeat unit.

$$\text{Doping level (PA mols/PBI repeat unit)} = \frac{W_{acid} - W_d}{W_d \times F_{PBI}} \times \frac{MW_{PBI}}{MW_{PA}} \qquad (5.3)$$

where MW_{PA} and MW_{PBI} are the molecular weights of PA and PBI, respectively. F_{PBI} is the weight fraction of PBI in the blend compositions. All of the measurements were

carried out with three different pieces of similarly sized samples. The results represented here are the averages of three sets of data.

5.3.6. Conductivity study

A four-point-probe technique is used to measure the proton conductivities of the blend samples. The impedance of the membranes was measured with an impedance analyzer, using a Zahner impedance spectrometer (ZENNIUM PP211) over a frequency range from 1 Hz to 100 Hz. The acid loaded membrane was cut into a rectangular shape and mounted onto the in-house-built conductivity cell. First, the conductivity of the membranes was measured from 30°C to 160°C. After the first heating scan, the cell is cooled while maintaining the dry conditions inside the vacuum and, again, the conductivity was measured from 30°C to 160°C. The data presented here are the second heating scans data. The conductivities of the samples were obtained from the direct-current potential difference between the two inner electrodes. The conductivity was calculated with the following equation:

$$\sigma = \frac{D}{RBL} \qquad (5.4)$$

where, σ is the proton conductivity (S/cm), D is the distance between the electrodes, and B and L are the thickness and width of the blend samples, respectively. In all cases R was obtained from Nyquist plots.

5. 4. Results and Discussion

5.4.1. FT-IR study

The FT-IR spectra of PBI, PVT and blend samples (collected from thin films) in the 3600-3000 cm^{-1} region are shown in Figure 5.4. Spectra of PBI consists several N–H stretching bands in the 3600-3000 cm^{-1} region. The peak at 3408 and 3144 cm^{-1} are because of free non-hydrogen bonded N–H stretching and self associated N–H stretching, respectively.[37-40] The peak at 3063 cm^{-1} is due to the stretching frequency of

aromatic C–H groups. It is observed that the peak at 3408 cm^{-1} is shifting to lower frequency and becomes broad with increasing PVT concentration (Figure 5.4).

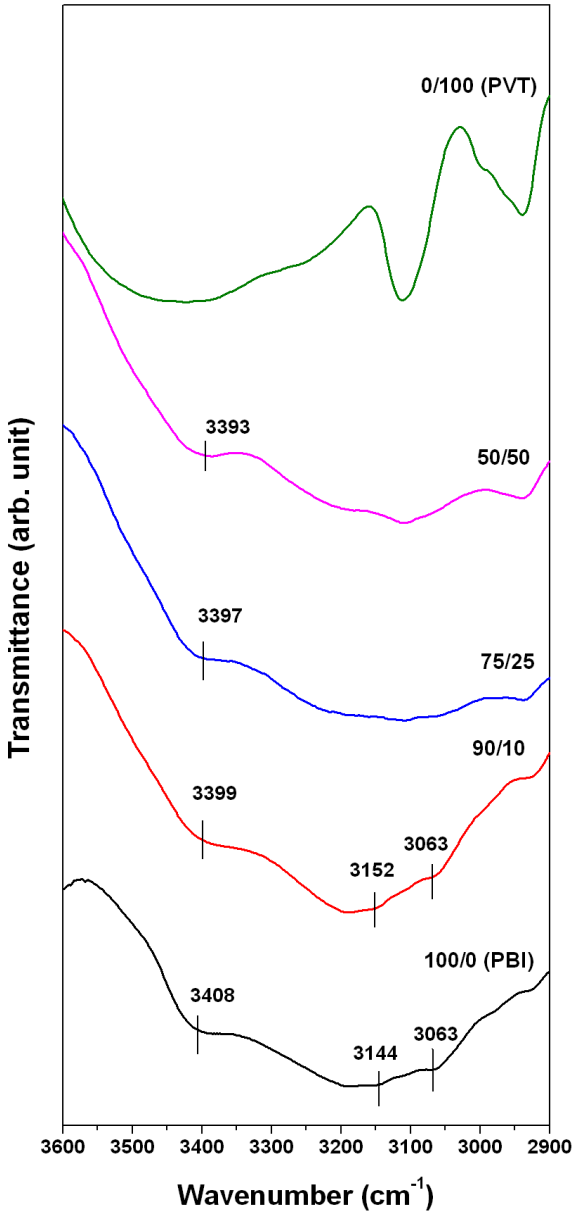

Figure 5.4: FT-IR spectra (3600-2900 cm^{-1}) of the PBI/PVT blend film samples at their indicated compositions.

In case of the 50/50 blend, the peak shifted to 3393 cm^{-1}. This peak is not visible in 25/75 and 10/90 (PBI/PVT) blends, because of overlapping of the PVT peaks with these

peaks. However, the aromatic stretching peak at 3063 cm^{-1} does not change its position. The red-shift of the free N–H band upon blending indicates the formation of specific interactions between N–H groups of PBI with functionalities of PVT. From Figure 5.4, it is also observed that the self-associate N–H peak at 3144 cm^{-1} is shifting toward higher frequency and increases its intensity. In the case of the 90/10 blend, the peak shifted to 3152 cm^{-1}. This shifting and intensity enhancement can be attributed to the weakening of self-associated N–H–N hydrogen bonding of the PBI chains. Hence, from the IR studies, it is clearly evident that the N–H functionalities of PBI take part in the interaction with PVT upon blending.

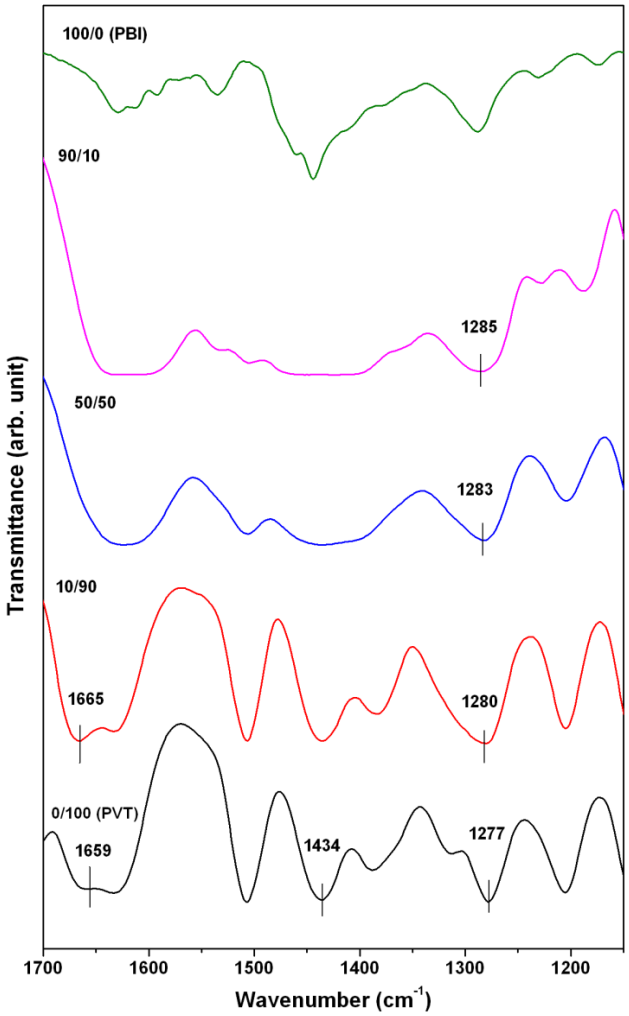

Figure 5.5: FT-IR spectra (1700-1100 cm^{-1}) of the PBI/PVT blend film samples at their indicated compositions.

It is expected that the interaction between the two polymers will also induce changes in the PVT stretching frequencies. To understand this, we carefully analyze the FT-IR spectra of PVT, PBI, and blend films in the region of 1700-1150 cm^{-1} (Figure 5.5). The peak at 1277 cm^{-1} in pure PVT represents the characteristic peak of the ring N–N bond. The peak at 1434 and 1659 cm^{-1} are the characteristic peaks of C–N and C═N bonds, respectively.[33-35] Among three N atoms of the PVT ring, one is connected to the vinyl chain; hence, it cannot be involved in any interaction. The other two N atoms can form hydrogen bonding with N–H group of PBI. From Figure 5.5, it is visible that the N–N stretching frequency at 1277 cm^{-1} is broadened and shifts to higher frequency as the PBI content in the blend is increased. When the PBI content is 90%, the 1277 cm^{-1} peak is shifted to 1285 cm^{-1}. The peak at 1434 cm^{-1} does not change its position but becomes broad with increasing PBI content in the blend. As the PBI content in the blend is increased, the peak at 1659 cm^{-1} is shifted to lower frequency and shows substantial broadening. These changes indicated that an N–H···N type of interaction is present between the two polymers. Thus, IR data confirmed the presence of hydrogen bond interactions between the two polymers in the blend.

5.4.2. Solid State ^{13}C CPMAS study

The interactions of the blend components can induce changes in line shape and/or shifts in the ^{13}C resonance frequencies in the NMR spectra of the blend components, in comparison with the spectra of the neat polymers. Solid-state NMR has been used to study the interactions in the blends, because of the fact that this type of interaction strongly influences the electron density around the carbons bearing the interacting functionalities and induce changes in carbon chemical shifts, as well as changes in line shape. The solid-state NMR spectra of the PBI, PVT, and blend samples are shown in Figure 5.6. The spectrum of PBI consists of several lines. The peak at 155 ppm is due to the carbons of the imidazole rings attached to phenylene rings, the peak at 146 ppm is due to the carbons that connect the benzimidazole rings in the benzimidazole system, and the peak at 133 ppm is due to the aromatic carbons bound to the N atoms. The remaining peaks at 124 and 115 ppm are due to the protonated carbons

of PBI with a contribution from the nonprotonated carbon of the phenylene ring to the line centered at 124 ppm.[44]

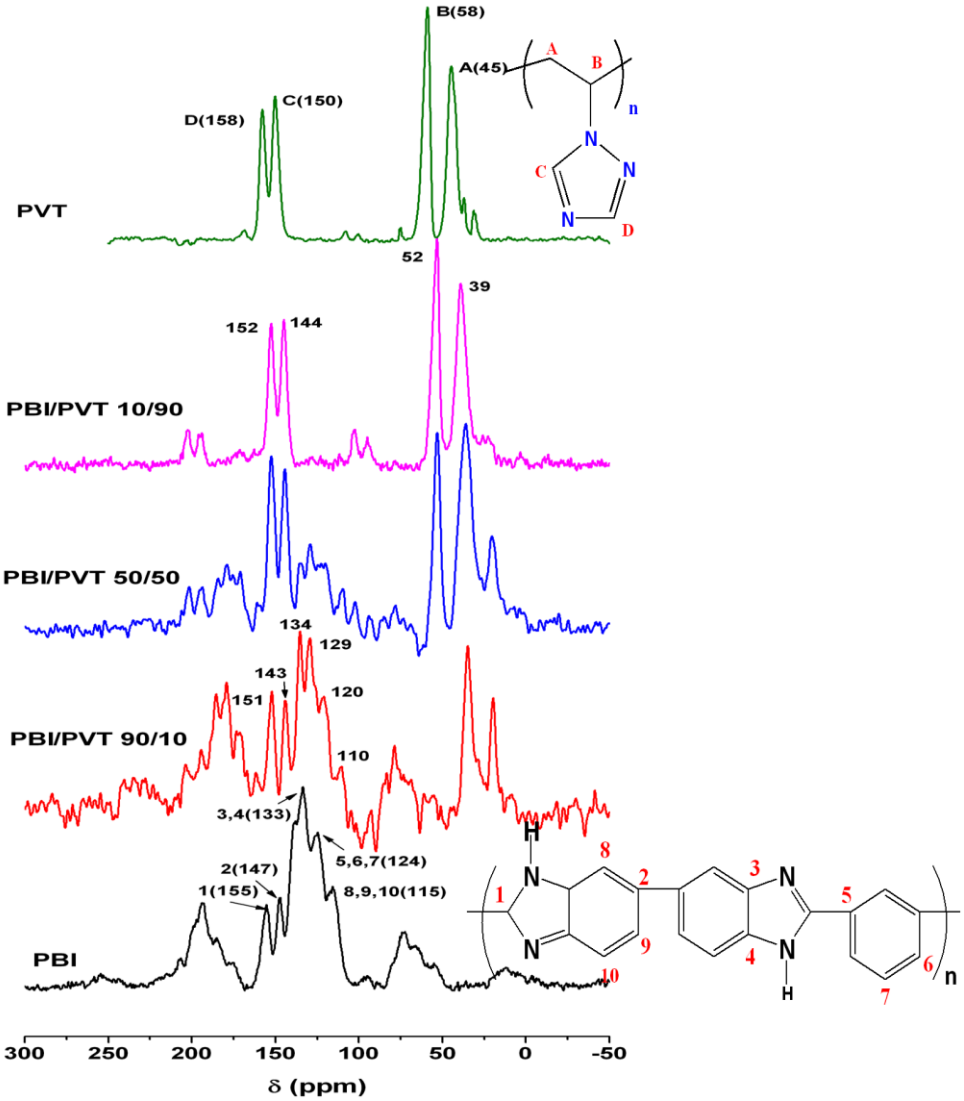

Figure 5.6: ^{13}C CPMAS NMR spectra of PBI, PVT and blend samples.

The PVT spectra consist of four lines. The peaks near 150 and 158 ppm are the characteristic C and D peaks of the triazole ring, and the peak near 45 and 58 ppm corresponds to structures A and B of the polymer backbone. From Figure 5.6, it is observed that the PBI peaks 155, 147, 133, 124, and 115 ppm have been shifted to the higher field in the case of the PBI/PVT blends, and it is more pronounced in the case of

the 90/10 sample. After the 90/10 samples, the peaks are not shifting for other blend samples; however, it is observed that, in the blend samples, the intensity of PBI peaks are gradually decreasing and PVT peaks are gradually appearing with increasing PVT concentration. Figure 5.6 also shows that the PVT peaks are also shifting to the higher field. So this shifting in chemical-shift values indicates the presence of interactions between the two polymers. Thus, FT-IR and solid-state NMR studies agree well and prove the presence of an interaction between PBI and PVT.

5.4.3. Absorption and emission spectroscopy

The absorption and fluorescence emission spectra of PBI, PVT, and blend samples are studied in solid state. The absorption spectrum of PBI (Figure 5.7) in solid state shows two distinct peaks: a lower wavelength peak at ~255 nm and higher wavelength absorption at ~343 nm.[45] The higher wavelength peak at 343 nm corresponds to the $\pi \rightarrow \pi^*$ transition. PVT does not display any absorption maxima. All the blend samples exhibit two distinct peaks. The intensity of these peaks is lower than that of PBI. This may because of a lower percentage of PBI in the blend. However, in the blends, the $\pi \rightarrow \pi^*$ peak is red-shifted significantly. This indicates more delocalized electron density in the imidazole moieties. The N–H groups of imidazole take part in the interaction with PVT in the case of blends, hence allowing more delocalization of electrons in the imidazole ring, resulting in a red-shift of the $\pi \rightarrow \pi^*$ peak.

The emission spectra of the PBI and blend samples recorded from solid state are shown in Figure 5.8. The emission spectrum of PBI shows one fluorescence band at 517 nm. Usually, PBI shows two emission bands, which are assigned to the 0–0 and 0–1 transitions from the excited ^1L_b state in the benzimidazole ring of PBI.[41,42,45] In this case, only one peak is observed, which is due to the 0–1 transition. The lower wavenumber is not observed in PBI because in the solid state PBI is in the aggregated state.[41] The emission bands for blend samples are observed at lower wavelengths, relative to PBI. This blue shifting of the emission bands in the blend samples can be attributed to the interactions between the polymers. The emission intensity of the blend

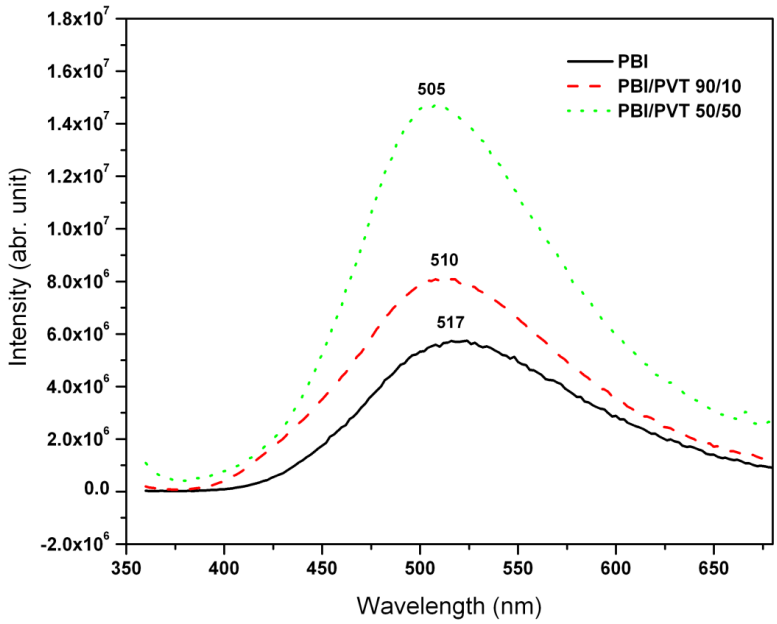

Figure 5.7: Absorption spectra of PBI and blend samples at the indicated composition. All the spectra were recorded in the solid state.

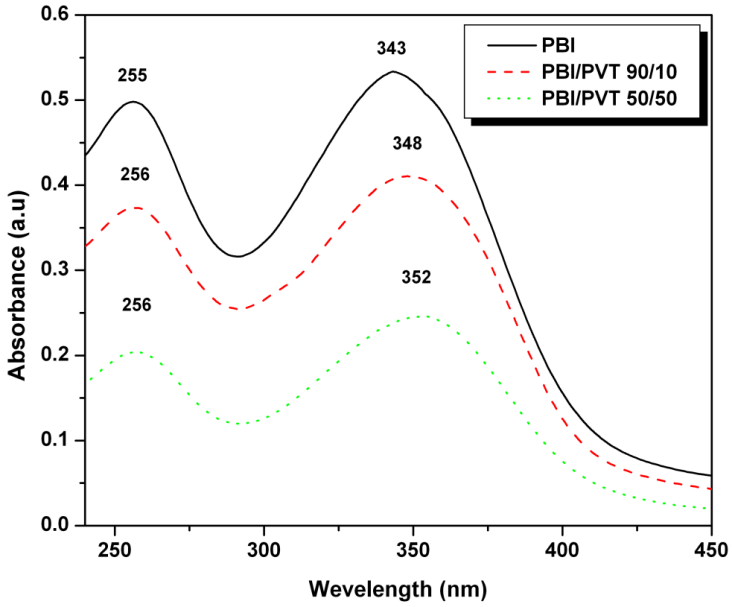

Figure 5.8: Fluorescence emission spectra of PBI and blend samples. Excitation wavelength (λ_{exc}) is 350 nm. All the spectra were recorded in the solid state.

samples increases as the PVT content in the blend increases (Figure 5.8). This increase in intensity is quite unexpected, given the fact that, in the blend, the concentration of PBI is lower, compared to that of neat PBI. This unexpected intensity increase, in the case of the blend, may be due to increased electron delocalization that can be attributed to the strong interactions between the two polymers.

5.4.4. Thermal study

The thermal stabilities of PBI, PVT, and blend membranes before and after doping with PA are performed under a nitrogen atmosphere at a heating rate of 10°C/min. The representative TGA curves are shown in Figure 5.9. Two different weight losses are observed for PBI before doping (Figure 5.9A). The first weight loss, which occurs at ~100-120°C, is due to loosely bound absorbed water molecules, and the second weight loss at 570-600°C is because of the degradation of the polymer backbone. PVT shows an exponential weight decay up to 20% (by weight) until 300°C, which can be attributed to absorbed water (Figure 5.9A). Above 350°C, a remarkable weight loss is observed, which is due to the thermal decomposition of the side groups and the polymer chain. From Figure 5.9A, it is observed that all the blend samples in their undoped state are thermally stable up to 300°C, except the initial weight loss, which varies, depending on the composition of the blend; this observation indicates that these are stable materials and can be used for high-temperature applications.

All the samples are doped with 85% PA for 3 days, and their TGA results show their first major weight loss between 50°C and 150°C, which corresponds to the water content of PA (Figure 5.9B) and loosely bound PA. After the initial weight loss, a gradual weight loss is observed up to 600°C, which is due to the successive dehydration of PA. The initial weight loss increases very nominally with increasing PVT content in the blend, because of the lower thermal stability of PVT.

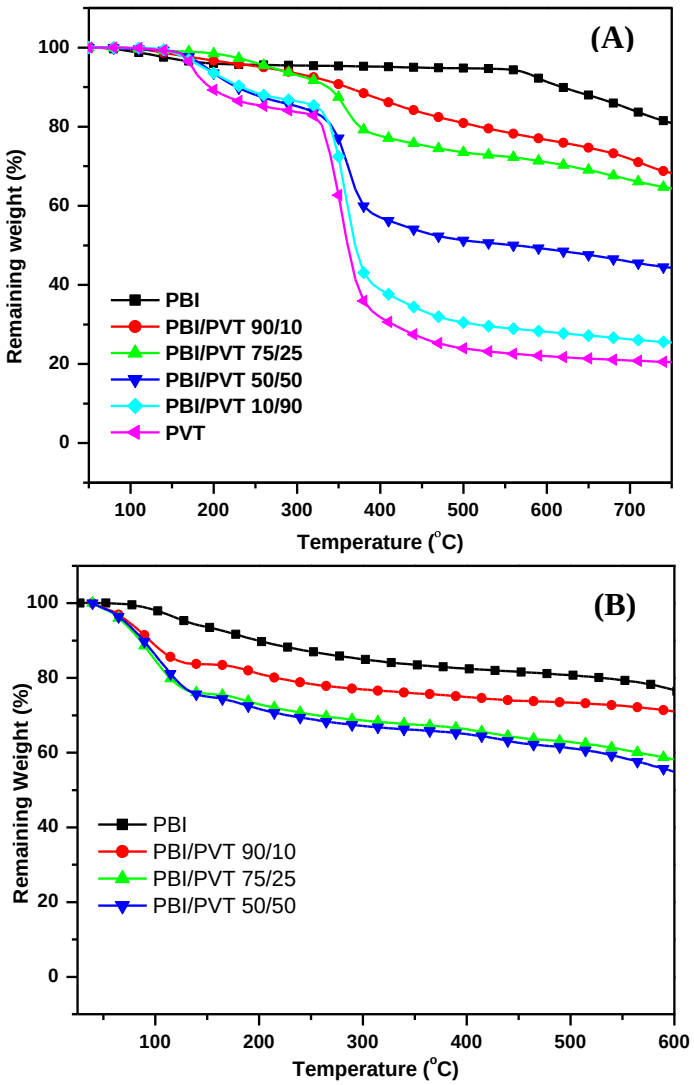

Figure 5.9: TGA curves of PBI, PVT and blend samples (A) before doping and (B) after doping with PA at their indicated compositions.

5.4.5. Miscibility studies of blends

The films obtained after blending samples are homogeneous and transparent (Figure 5.3), indicating the miscibility of the two polymer components. The detailed FT-IR study and solid-state NMR study of these blend films evidenced the presence of specific interactions between the two polymers, which resulted in miscible blends. The miscibility of polymers blends can be easily determined by measuring the T_g value of

the blends. A miscible polymer blend exhibits only one T_g value and when two polymers are partially miscible or completely immiscible, they exhibit more than one T_g value, because they possess more than one phase and each phase undergoes its glass transition at a unique temperature corresponding to its composition.[46]

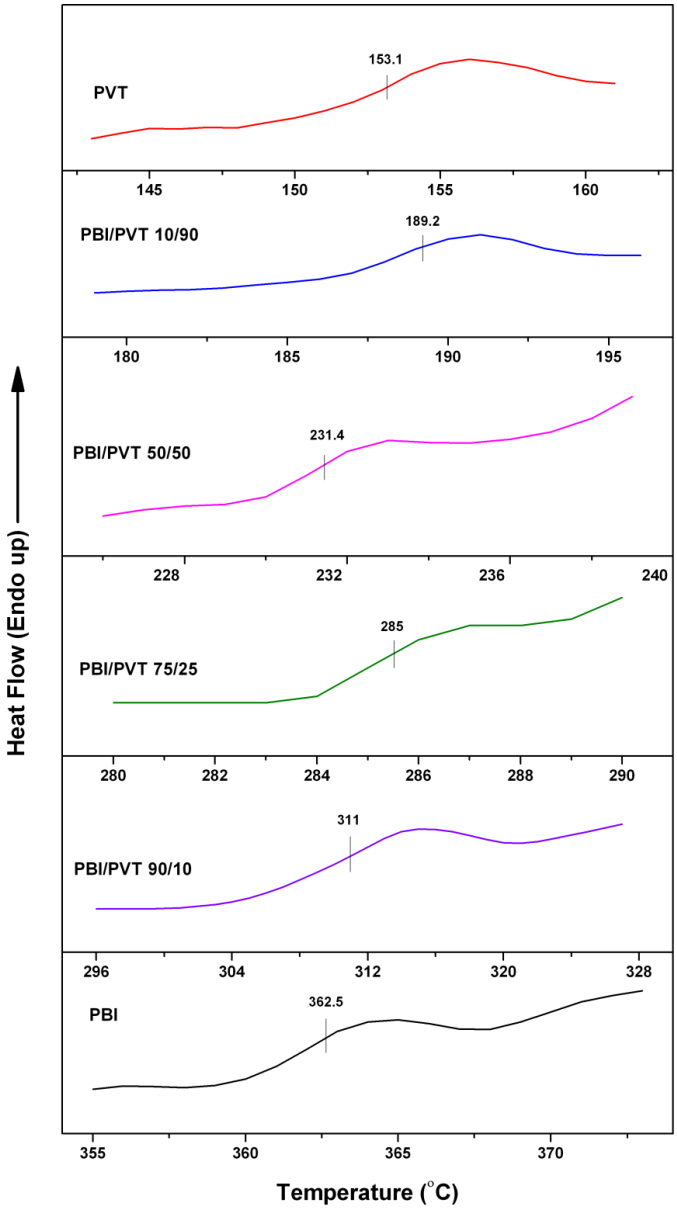

Figure 5.10: DSC thermograms of neat PBI, PVT and blends. The horizontal lines and the corresponding values in the thermograms are the T_g of the samples.

The glass-transition temperature (T_g) of the PBI, PVT, and blend samples are measured by using differential scanning calorimeter (DSC). The DSC measurement shows that the glass-transition temperatures of PBI and PVT are 362 and 153°C, respectively. These T_g values match well with the earlier reported values.[33-35,42] The DSC thermograms of PBI and blend samples are shown in Figure 5.10. It is observed that all the blends exhibit a single T_g value, which decreases as the PVT content in the blend increases. This observation indicates the complete miscibility of the blends. The T_g values of the blends are between the T_g values of neat polymer, which also can be attributed to complete miscibility of the two polymers. The Gordon-Taylor formula (equation 5.5) can be used to evaluate the dependency of T_g on the blend composition.

$$T_g = \frac{W_1 T_{g1} + kW_2 T_{g2}}{W_1 + kW_2} \qquad (5.5)$$

where W is the weight fraction, T_g is the glass-transition temperature of the blends, T_{g1} and T_{g2} are those of the pure components (PBI and PVT, respectively), and *k* is an adjustable fitting parameter (the Gordon-Taylor constant) that describes the strength of the intermolecular interaction between the components in miscible polymer blends; the lower the value of k, the poorer the interaction.[47] The T_g versus composition plot is shown in Figure 5.11. The dotted lines in Figure 5.11 are drawn using the Gordon-Taylor equation with k values of 1 and 1.5. The T_g-composition curve of the PBI/PVT system forms a sigmoidal curve, as a function of composition, and it exhibits negative deviation from the Gordon-Taylor equation. The T_g value fits well for k = 1.5. It has been demonstrated in the literature that the resulting value of k for thermodynamically miscible blends is close to unity, which is indicative of intimately mixed amorphous phases. Hence our value of k, which is close to unity, proves that the present blend is a thermodynamically miscible blend. When the PVT concentration is low, the T_g value of the blend is lower than the Gordon-Taylor T_g value. However, at high PVT concentration (90%), the T_g value is higher than the Gordon-Taylor T_g value. Hence, the above fitting clearly indicates a strong intermolecular interaction between the polymers, which was also proved from spectroscopic studies, resulting in miscible blends.

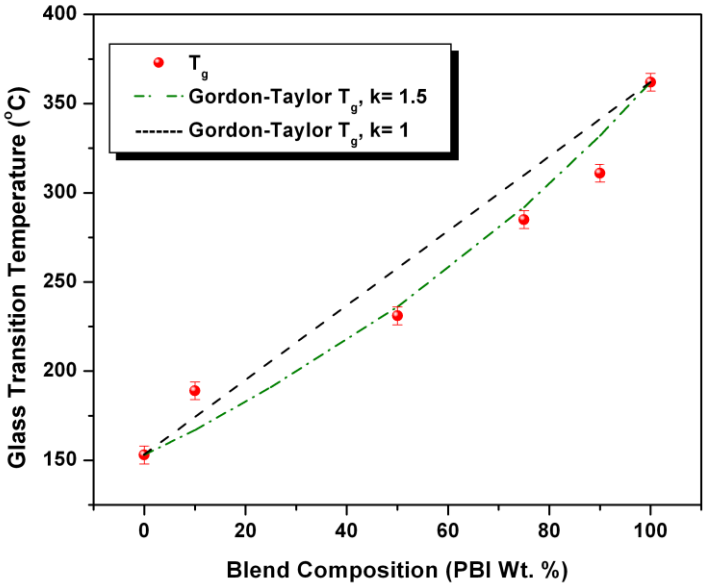

Figure 5.11: Variation of the glass transition temperature (T_g) of the blend samples as a function of blend composition. The solid points (●) are the experimentally obtained T_g from the DSC study, and the dotted lines are the calculated T_g curve according to the Gordon-Taylor equation with k= 1 and 1.5.

5.4.6. Morphological study

The blend membranes appear very homogeneous, which is attributed to miscibility (Figure 5.3). No phase separation is visible. This result is consistent with the FT-IR, SS-NMR, and DSC results. The homogeneity of the blend membranes are also studied by FE-SEM. The FE-SEM images of PBI, PVT, and a few representative blend images are shown in Figure 5.12. The morphology of PBI and PVT is featureless, which is consistent with earlier reports.[33-35,48] However, the morphology of the blend membranes is completely different from the neat polymers. It is interesting to note that blend samples exhibit a porous morphology and the pore size and nature are highly dependent on the blend composition. The porous morphology transforms to particle morphology at high PVT contents of the blend. Figure 5.12 clearly demonstrates that the pore size increases with increasing PVT content in the blend; the bigger pores are seen in the case of the 75/25 blends; after that, pore size become smaller with increasing

PVT content. Beyond 50/50 blends, the pores transform to particles, as seen in the case of the 10/90 samples. This morphology characteristic is seen throughout the membrane. We do not know the exact reason for this type of morphology; however, it can be said that, since the current blend is a miscible system, a new phase has been formed, which displays this type of morphology. Earlier, it was shown that the miscibility arises from the specific interactions, such as hydrogen bonding, or weak charge-transfer complexing can influence conformational changes of the individual polymer chains of the blends which result in local ordering and microstructure in the miscible polymer blends.[49,50]

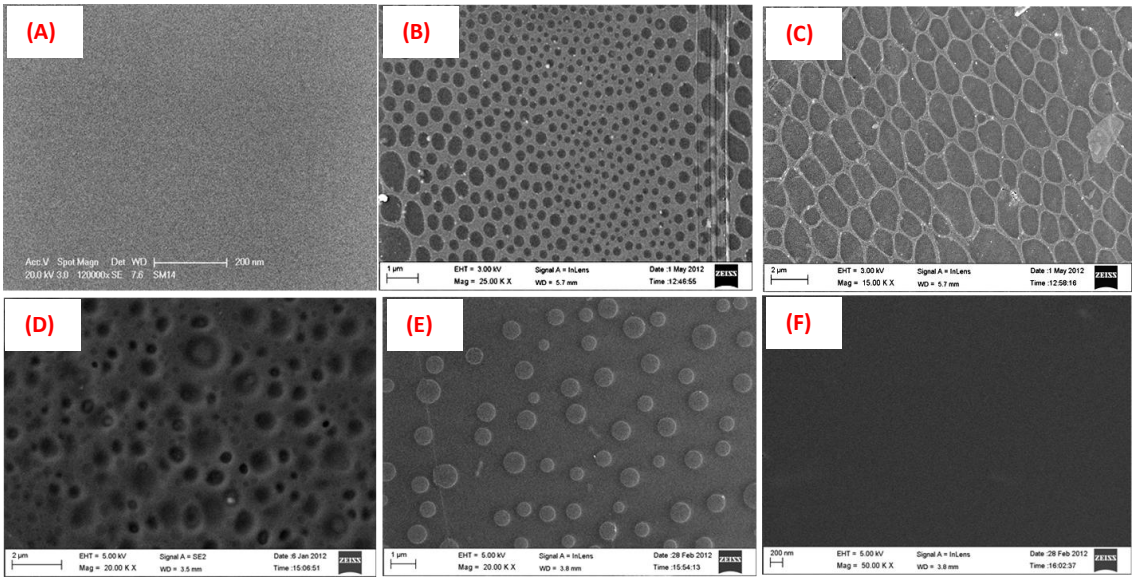

Figure 5.12: FE-SEM images of (A) PBI and PBI/PVT blends (B) 90/10, (C) 75/25, (D) 50/50, (E) 10/90, and (F) PVT.

We expect to see better properties of the blends compared to neat a polymer which is the manifestation of this porous morphology. We have discussed the properties of the blends in the next few sections and it is indeed true that the blend properties are better than the neat polymers. The phosphoric acid doped PEMs are prepared by dipping these porous membranes in the PA bath, and it is reasonable to expect that the pores will be filled with PA and most likely with higher amount of PA. Recently, significant number of reports in the literature also demonstrated that the microporous morphology

can indeed be very useful to absorb the larger amount of PA.[51,52] Further work is in progress to study the suitability and durability of these membranes in a working PEMFC.

5.4.7. Swelling ratio and thickness increase in phosphoric acid

The swelling ratio and thickness increase for the acid doped membrane are important criteria of polyelectrolyte membrane for real fuel cell applications, because very thick membranes are not suitable for the membrane electrode assembly (MEA) fabrication. The PBI membrane increases in thickness quite significantly after PA doping. The swelling ratio, thickness increase, and PA loading of acid-doped PBI and blend membranes are shown in Table 5.1.

Table 5.1. Swelling and acid loading data of blend membranes after dipping in PA for three days. The standard deviations are shown in the parenthesis.

Sample (PBI/PVT)	Swelling ratio (%)	Thickness increased (%)	PA loading (mols/PBI repeat unit)
100/0 (PBI)	43.13 (1.5)	150 (23.54)	10.21 (1.92)
90/10	32.99 (0.16)	41.66 (11.79)	11.40 (0.46)
75/25	39.03 (1.37)	37.5 (0)	15.85 (0.18)
50/50	42.79 (1.2)	49.93 (10)	18.82 (2.31)

From the table, it is observed that the swelling ratio and thickness increase of the blend membranes are significantly lower than those for PBI. Hence, these membranes are suitable for MEA fabrication. This significant decrease of swelling ratio and thickness in the case of blend membranes may be the result of their porous morphology. Because of these morphological features, when the blend membranes are dipped into PA, the porous structure of membrane accommodate the acid molecule in the pores, as a result of that, the thickness does not increase much, compared to that for neat PBI, and swelling of the membrane becomes less. The PA loading of the membrane increases with increasing PVT content in the blend (Table 5.1), since the N atoms of PVT can

also interact and form acid-base complexes with the PA molecules. Also, the porous morphology of the blend membranes allows impregnation of a higher amount of PA.

5.4.8. Proton conductivity

Proton conductivity of polyelectrolyte membrane is the most crucial property for a material to become a suitable PEM for use in fuel cells. The proton conductivities of all of the blend membranes are measured in the temperature range of 30-160°C. All the membranes are immersed in PA solution for 3 days for acid doping before the measurement. The PA-loaded membranes are fixed in the homemade four-probe conductivity cell, and impedance is measured by varying the temperature from 30°C to 160°C. These first heating data are not reliable, because water is present in the membrane. Hence, after the first heating scan, we cooled the cell and again measured the impedance by varying the temperature. The conductivity data presented here represent the second heating data, and the conductivity is measured without any humidification. The proton conductivities of a few representative membranes obtained from the Nyquist plots (Figure 5.13) are plotted against temperature and shown in Figure 5.14. As expected in all the cases the proton conductivity increases with increasing temperature.

The proton conductivities of the blend samples are higher than that of the neat PBI. There are three reasons for the higher conductivity of blends: (i) because of the presence of both imidazole and triazole rings, the blend membranes are holding more PA, which increases the conductivity (ii) because of the porous morphology and (iii) because of the fact that triazole and imidazole rings are present in the same membrane and, hence, the proton conduction becomes more easy and feasible, compared to neat polymer. The proton conductivity of PBI at 160°C is 3.9×10^{-2} S/cm. For the 50/50 blend, the proton conductivity at 160°C is 1.1×10^{-1} S/cm, which is one order of magnitude higher, compared to neat PBI. Aslan et al. reported a maximum conductivity of PVT/(poly-(styrenesulfonic acid)$_2$ and PVT/(styrenesulfonic acid)$_4$ blend membrane is 1.5×10^{-2} S/cm at 150°C and under anhydrous conditions.[53] In another report, Gün̈day et al. used 1H-1,2,4-triazole (Tri) as a proton solvent in different polymer host

matrices, such as poly(vinylphosphonic acid) (PVPA), and poly(2-acrylamido-2-methyl-1-propane sulfonic acid) (PAMPS) to form PVPATri$_x$ and PAMPSTri$_x$, where x is the molar ratio of Tri to the corresponding polymer repeat unit.[31] The maximum proton conductivity they could get is 2.3×10^{-3} S/cm at 120°C for PVPATri$_{1.5}$ and 9.3×10^{-4} S/cm at 140°C for PAMPSTri$_2$. In the literature, the reported conductivity of PVT at 150°C is 5×10^{-3} S/cm. However, when we tried to measure the conductivity of PA-doped PVT, it could not be measured after 60°C. At high temperature (>60°C), the dissolution of polymer in PA is observed, which is flowing out of the conductivity cell. We did not face any problem with our blend samples and could measure up to 160°C.Therefore the conductivity values for PBI/PVT blends are much higher than the reported values.

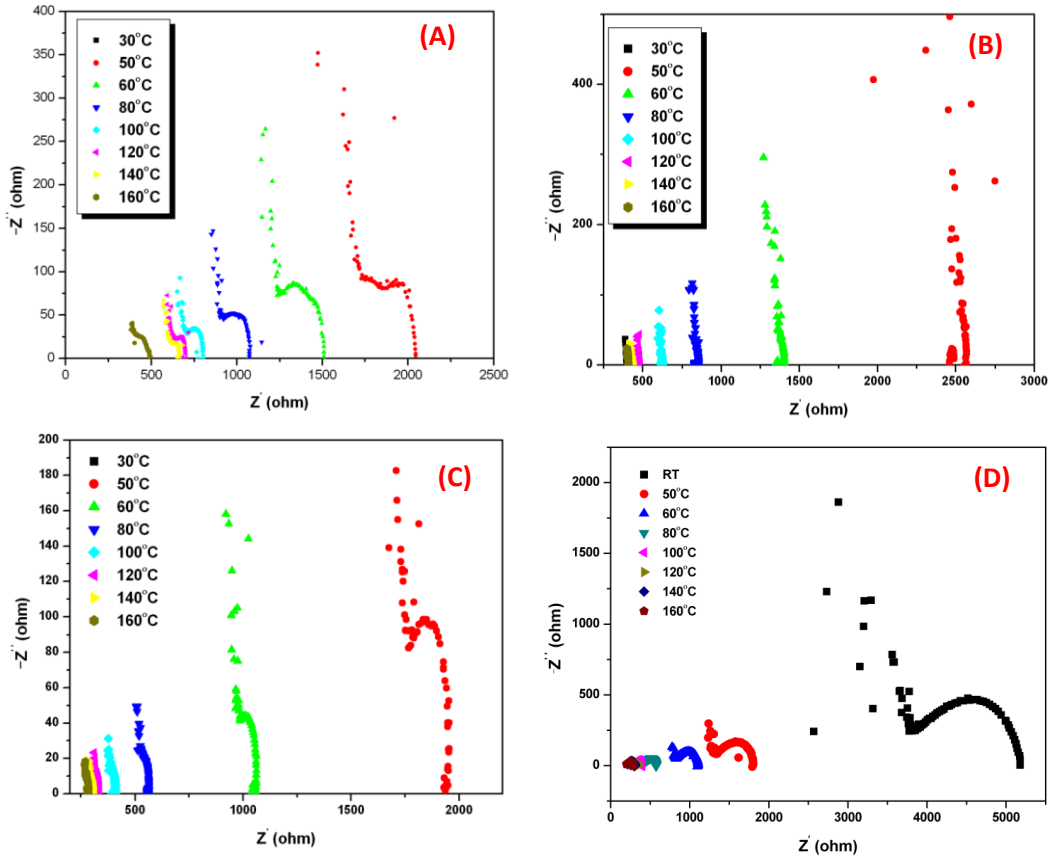

Figure 5.13: Nyquist plots of (A) PBI and blends (PBI/PVT) (B) 90/10, (C) 75/25 and (D) 50/50.

Another reason of the high proton conductivity of the blend membranes is their morphology. The blend membranes have porous morphology (Figure 5.12). Because of the presence of pores the blends membranes can hold more PA than PBI. This increases the proton conductivity since conductivity is directly proportional to the amount of PA in the membrane. Also the porous nature of the membrane facilitates better proton conduction resulting high proton conductivity. A careful comparison of morphology (Figure 5.12) and conductivity (Figure 5.14) data brings an important correlation between the morphology and conductivity of the membrane. The porous nature increases as we increase the PVT content (up to 75/25 composition); the conductivity also increases up to 75/25 and then slowly drops since the porous nature decreases after 75/25 composition. For 10/90 sample does not have porous structure, hence its conductivity is much lower compare to other blends. Therefore the morphology (microstructure) of the membrane influences the conductivity.

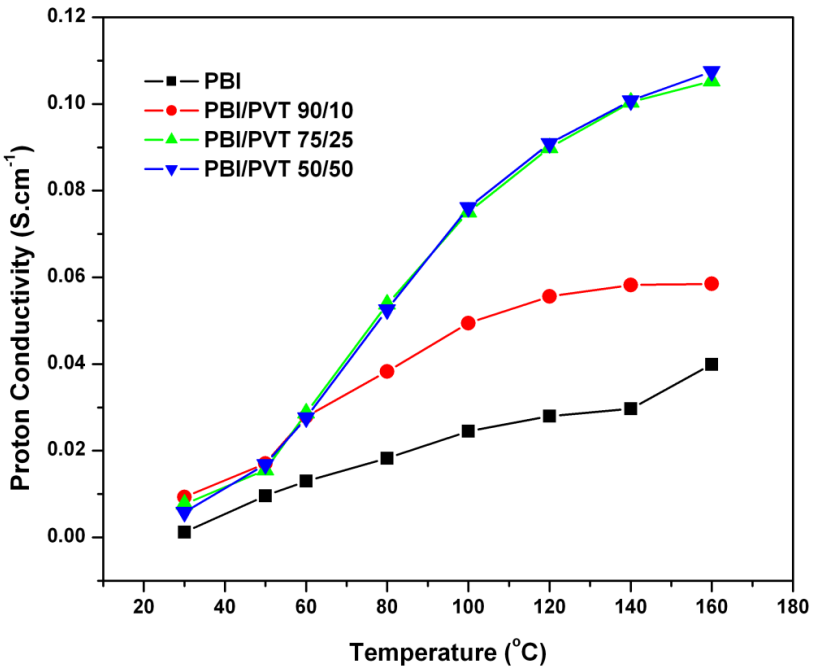

Figure 5.14: Proton conductivity against temperature for PBI/PVT blend membranes.

Two mechanisms contribute the proton transfer in PA doped heterocyclic polymer electrolyte membranes. One is based on rapid proton exchange between

phosphate and hetero cyclic moieties via hydrogen bonds (Grotthuss mechanism) and the second is on self diffusion of phosphate moieties (Vehicle mechanism).[54] For PA doped membranes Grotthuss mechanism is the predominant mechanism for proton conduction.[55] To understand the conduction mechanism the conductivity data against temperature plotted using the Arrhenius equation as follows

$$\ln(\sigma T) = \ln \sigma_{\circ} - \frac{E_a}{RT} \qquad (5.6)$$

Where σ is the protonic conductivity of the membrane (Scm^{-1}), σ◦ is the pre-exponential factor ($S\ K^{-1}\ cm^{-1}$), Ea is the proton conducting activation energy ($kJ\ mol^{-1}$), R is the ideal gas constant ($J\ mol^{-1}\ K^{-1}$) and T is the temperature (K). Arrhenius plots of temperature dependent conductivity are shown in Figure 5.15. The activation energy (E_a) is obtained from the slope of the linear fit of equation (5.6) and is shown in Figure 5.15.

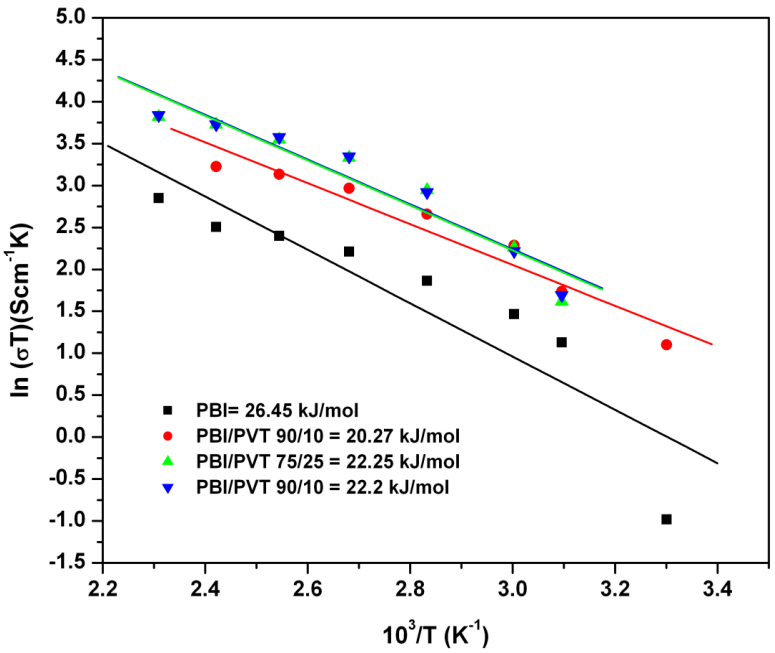

Figure 5.15: Arrhenius plots for the proton conduction of the blend samples at their indicated compositions.

The data fits well with the equation, suggesting that the proton conduction is mainly governed by the Grotthuss mechanism. The E_a of the blend membranes are less compared to PBI. This is because triazole and triazole derivatives act as a proton transport facilitators for polymer electrolyte membranes.[33-35] That is why the proton conductivity of the blend membranes are higher than neat PBI. Also porous morphology facilitates faster proton conduction resulting lower E_a than neat PBI.

5. 5. Conclusion

Novel blends of PVT and PBI of various compositions have been prepared using a solution blending technique. FT-IR and solid-state NMR, as well as photophysical studies, indicate the presence of a specific interaction between the two polymers, allowing them to form a miscible blend. The blend samples show a single composition-dependent T_g value, which decreases as the PVT concentration in the blend increases. These observations suggest that PBI and PVT form a miscible blend. The N−H···N interaction between the two polymers is the driving force for this miscibility. The swelling ratio and thickness increase of the blend samples are smaller than those of PBI. The proton conductivity of the blend membranes is higher than that of the neat PBI and increases as the PVT concentration increases, up to the 75/25 (PBI/PVT) composition. The morphology of the blends governs the conduction behavior of the blends. These thermomechanically stable, highly conducting blends may be suitable for use as proton exchange membranes (PEMs) in high-temperature fuel cells.

5. 6. References

1. Blomen, L. J. M. J.; Mugerwa, M. N. In *Fuel Cell Systems*; Plenum Press, New York, **1993**.
2. Peighambardoust, S. J.; Rowshanzamir, S.; Amjadi, M. *Int. J. Hydrogen Energy* **2010**, *35*, 9349.
3. Trogadas, P.; Ramani, V. In *Encyclopedia of Electrochemical Power Sources*; **2009**, pp 716.
4. Rikukawa, M.; Sanui, K. *Prog. Polym. Sci.* **2000,** *25*, 1463.
5. Kerres, J. A. *J. Membr Sci.* **2001**, *185*, 3.
6. Asensio, J. A.; Sánchez, E. M.; Gómez-Romero, P. *Chem. Soc. Rev.* **2010**, *39*, 3210.
7. Zhang, H.; Shen, P. K. *Chem. Rev.* **2012**, *112*, 2780.
8. Li, Q.; He, R.; Jensen, J. Q.; Bjerrum, N. J. *Chem. Mater.* **2003**, *15*, 4896.
9. Seel, D. C.; Benicewicz, B. C. *J. Membr. Sci*. **2012**, 405, 57.
10. Mader, J. A.; Benicewicz, B. C. *Macromolecules* **2010**, *43*, 6706.
11. Bose, S.; Kuila, T.; Nguyen, T. X. H.; Kim, N. H. Lau, K.-t.; Lee, J. H. *Prog. Polym. Sci.* **2011**, *36*, 813.
12. Parka, C. H.; Leeb, C. H.; Guivera, M. D.; Lee, Y. M. *Prog. Polym. Sci.* **2011**, *36*, 1443.
13. Li, Q.; Jensena, J. O.; Savinell, R. F.; Bjerrum, N. J. *Prog. Polym. Sci.* **2009**, *34*, 449.
14. Shao, V.; Yin, G.; Wang, Z.; Gao, Y. *J. Power Sources* **2007**, *167*, 235.
15. Scharfenberger, G.; Meyer, W. H.; Wegner, G.; Schuster, M.; Kreuer, K. D.; Maier. J. *Fuel Cells* **2006**, *6(3–4)*, 237.
16. Granados-Focil, S.; Woudenberg, R. C.; Yavuzcetin, O.; Tuominen, M. T.; Coughlin, E. B. *Macromolecules* **2007**, *40*, 8708.
17. Nagamani, C.; Versek, C.; Thorn, M.; Tuominen, M. T.; Thayumanavan S. *J. Polym. Sci. Polym. Chem.* **2010**, *48*¸1851.
18. Michael, A. H.; Hossein, G.; Yu, S. K.; Brian, R. E.; James, E. M. *Chem. Rev.* **2004**, *104*, 4587.

19. Zhou, Z.; Li, S.; Zhang, Y.; Liu, M.; Li, W. *J. Am. Chem. Soc.* **2005**, *127*, 10824.
20. Kreuer, K. D.; Fuchs, A.; Ise, M.; Spaeth, M.; Maier, J. *Electrochim. Act* **1998**, *43*, 1281.
21. Schuster, M. F. H.; Meyer, W. H.; Schuster, M.; Kreuer, K. D. *Chem. Mater.* **2004**, *16***,** 329.
22. Li, S.; Zhou, Z.; Zhang, Y.; Liu, M.; Li, W. *Chem. Mater.* **2005**, *17***,** 5884.
23. Martwiset, S.; Woudenberg, R. C.; Granados-Focil, S.; Yavuzcetin, O.; Tuominen, M. T.; Coughlin, E. B. *Solid State Ionics* **2009**, *178*, 1398.
24. Sanghi, S.; Tuominen, M.; Coughlin, E. B. *Solid State Ionics* **2010**, *181*, 1183.
25. Subbaraman, R.; Ghassemi, H.; Zawodzinski Jr., T. A. *J. Am. Chem. Soc.* **2007**, *129*, 2238.
26. Subbaraman, R.; Ghassemi, H.; Zawodzinski Jr. T. *Solid State Ionics* **2009**, *180*, 1143.
27. Maalouf, M.; Ghassemi, H.; Zawodzinski, T.A. *ECS Trans.* **2010**, *25*, 19.
28. Saito, J.; Miyatake, K.; Watanabe, M. *Macromolecules* **2008**, *41*, 2415.
29. Aslan, A.; Bozkurt, A. *J. Power Sources* **2009,** *191*, 442.
30. Çelik, S. Ü.; Akbey, Ü.; Bozkurt, A. *Macromol. Chem. Phys*. **2008**, *209*, 593.
31. Günday, S. T.; Bozkurt, A.; Meyer, W. H.; Wegner, G. *J. Polym. Sci. Part B: Polym. Phys.* **2006**, *44*, 3315.
32. Ozden, S.; Celik, S. U.; Bozkurt, A. *J. Polym. Sci. Polym. Chem.* **2010**, *48*, 4974.
33. Çelik, S. Ü.; Aslan, A.; Bozkurt, A. *Solid State Ionics* **2008**, *179*, 683.
34. Aslan, A.; Celik, S. U.; Sen, U.; Haser, R.; Bozkurt, A. *Electrochim. Acta* **2009,** *54***,** 2957.
35. Celik, S. U.; Sen, U.; Haser, R.; Bozkurt, A. *J. Polym. Sci. Polym. Phys.* **2010,** *48***,** 1016.
36. Sen, U.; Bozkurt, A.; Ataa, A. *J. Power Sources* **2010**, *195*, 7720.
37. Musto, P.; Karasz,F. E.; MacKnight, W. J. *Macromolecules* **1991,** *24*, 4762.

38. Deimede, V.; Voyiatzis, G. A.; Kallitsis, J. K.; Qingfeng, L. N.; Bjerrum, J. *Macromolecules* **2000**, *33*, 7609.
39. Arunbabu, D.; Sannigrahi, A.; Jana, T. *J. Phys. Chem. B* **2008,** *112*, 5305.
40. Hazarika, M.; Arunbabu, D.; Jana, T. *J. Colloid Interface Sci.* **2010**, *351*, 374.
41. Sannigrahi, A.; Arunbabu, D.; Sankar, R. M.; Jana, T. *Macromolecules* **2007**, *40*, 2844.
42. Sannigrahi, A.; Arunbabu, D.; Sankar, R. M.; Jana, T. *J. Phys. Chem. B* **2007**, *111*, 12124.
43. Xue, H.; Gao, H.; Shreeve, J. M.; *J. Polym. Sci., Part A: Polym. Chem.* **2008**, *46*, 2414.
44. Grobelny, J.; Rice, D. M.; Karasz, F. E.; MacKnight, W. J. *Macromolecules* **1990**, *23*, 2132.
45. Sannigrahi, A.; Ghosh, S.; Lalnuntluanga, J.; Jana, T. *J. Appl. Polym. Sci*. **2009**, *111*, 2194.
46. Cakar, F.; Sakar, D.; Cankurtaran, O.; Karaman, F. *Eur. Polym. J.* **2007**, *43*, 507.
47. Ahn, T-K.; Kim, M.; Choe, S. *Macromolecules* **1997**, *30*, 3369.
48. Sannigrahi, A.; Ghosh, S., Maity, S.; Jana, T. *Polymer* **2011**, *11*, 4319.
49. Utracki, L. A. In *Polymer Blends Handbook*; Kluwer Academic Publishers: Dordrecht, **2002**.
50. Saito, H.; Takahashi, M.; Inoue, T. *Macromolecules* **1991**, *24*, 6356.
51. Mecerreyes, D.; Grande, H.; Miguel, O.; Ochoteco, E.; Marcilla, R.; Cantero, I. *Chem. Mater.* **2004,** *16*, 604.
52. Shen, C-H.; Jheng, L-C; Hsu, S. L-C.; Wang, J. T-W. *J. Mater. Chem.* **2011**, *21*, 15660.
53. Aslan, A.; Sen, U.; Bozkurt, A. *J. Electrochem. Soc.* **2009** *156*, B1112.
54. Pu, H.; Meyer, W. H.; Wegmer, G. *J. Polym. Sci., Part B: Polym. Phys*. **2002**, *40*, 663.
55. Yu, S.; Benicewicz, B. C. *Macromolecules* **2009**, *42*, 8640.

Chapter 6

Sulfonated polystyrene/graphene nanocomposite: A facile route for generation of graphene nanosheets

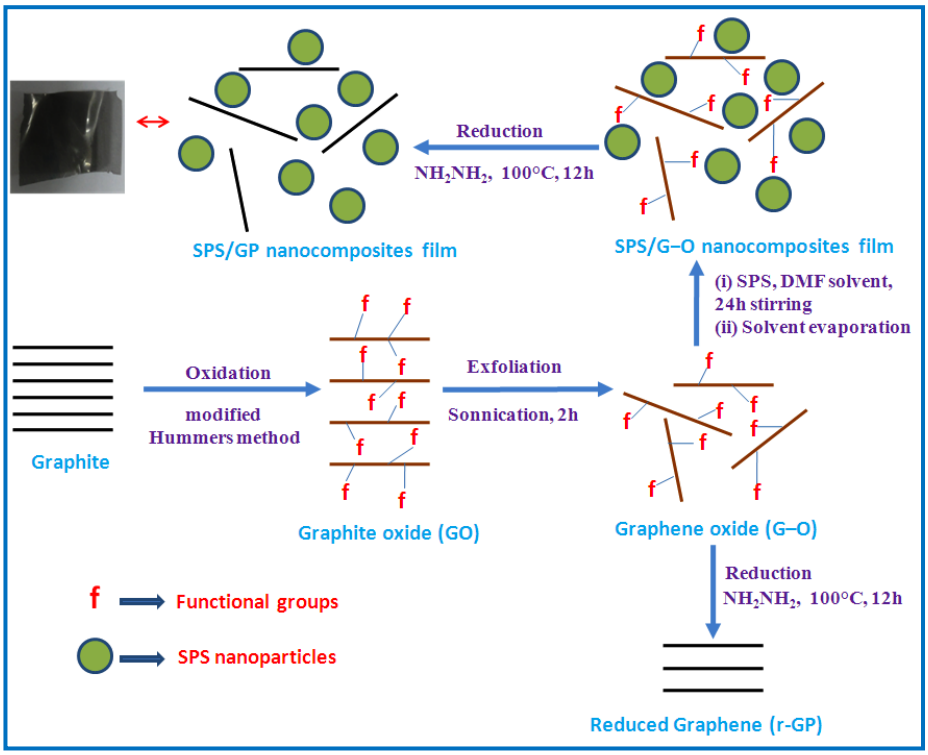

Single layer ~1 nm thick graphene (GP) nanosheets have been generated and stabilized in the presence of sulfonated polystyrene (SPS) nanoparticle. The nanocomposite display better thermal, mechanical and ionic conduction compared to pristine SPS.

Hazarika, M.; Jana, T. communicated to *J. Phys. Chem. C.*

6.1. Introduction

Ever increasing demand of polymer nanocomposites, owing to their unique properties and myriad applications, has been the primary focus of many material scientists. The dispersion of filler in nanometer length scale in the polymer matrix is the driving force for the improved properties (increased strength, decreased gas permeability, increased solvent and heat resistance etc.) compared to the pristine polymers.[1,2] Graphene (GP), a two-dimensional sp^2 bonded carbon sheet with one-atom thickness, is found to be the most prominent nanofillers to develop polymer nanocomposite in recent years among various others which include carbon nanotubes, clays, silica particles etc.[3-10]

GP has attracted significant attention in recent years due to its fascinating properties such as large surface area; high mobility of charge carriers, excellent mechanical properties, high thermal conductivity and thermal stability.[11-17] Among the various synthetic methods, chemical reduction of graphene oxide (G–O) is an easy method for low cost, large scale production of graphene. In this method first graphite is converted into graphite oxide (GO) which contains several functional groups such as hydroxyl, carboxyl, epoxy etc. and then GO layers are exfoliated into two dimensional graphene oxide (G–O) nanosheets by applying ultrasonic vibration or thermal shock.[18-20] Then G–O sheets are reduced to GP using reducing agents. However, this method has severe limitations like 100% conversion (incomplete reduction) of G–O to GP, tendency of GP sheets to reform into graphite layer due to instability of single layer GP. There are many efforts to overcome the above mentioned limitations. Among those, formation of nanocomposite with varieties of polymer is very much beneficial since it can stabilize the GP sheet as well as improves the polymer physical properties significantly.[3-5,11] Hu et al prepared nanocomposites of polystyrene (PS) particles with graphene via in situ emulsion polymerization of styrene and reduction of G–O to GP using hydrazine hydrate.[21] They have shown that the nanocomposites have high thermal stability and high glass transition temperature than PS. The electrical conductivity of PS increases from 1.0×10^{-10} Scm^{-1} to 2.9×10^{-2} Scm^{-1} for nanocomposites containing 2 wt% graphene.

In another study Zhou et al prepared poly(vinyl alcohol) (PVA)/graphene nanocomposites by reducing PVA/graphite oxide nanocomposite films in aqueous medium.[22] They observed a 40% increase in tensile strength and 70% improvement in elongation at break with 0.7 wt% of reduced GO. A bulk of reports on nanocomposites of varieties of polymers with graphene based materials are available in the literature.[3-5,23-27]

Spherical sulfonated polystyrene (SPS; Figure 1.12) nanoparticles have many applications in numerous areas among which its use as polymer template for nanoparticle synthesis and proton conducting membrane are the latest in the lot.[28-31] But the use of SPS is limited because of their poor mechanical property. SPS nanoparticles can be either prepared by emulsion copolymerization of styrene and styrene sulfonated or sulfonating pre-formed polystyrene particles.[32,33] Although nanocomposites of polystyrene (PS) with graphitic fillers are widely known in the literature[34-38] but relatively lesser numbers of reports have used SPS and graphitic fillers to prepare new materials.[39-42] The stable aqueous dispersion of graphitic nanoplatelets coated with anionic polymer, poly(sodium 4-styrenesulfonate) (PSS), pioneered by Ruoff[39] has emerged as an ideal candidate for the development novel polymer nanocomposites.[39-42] Recently, core-shell PS microspheres coated with GP sheets *via* π-π accumulation have been prepared to study their electrocatalytical and electrorehological properties.[36-38] However, the lack of reports on stabilization of GP sheets using SPS nanospheres motivated us to prepare the SPS/GP nanocomposite. Since SPS nanospheres have well defined core-shell structure with shell decorated with $–SO_3H$ functionalities,[32] we can expect greater degree of stabilization of G–O with SPS compared to the only PS spheres owing to the strong interactions between the functional groups of SPS and G–O. After the formation of stable SPS/G–O nanocomposite, one can readily reduce the G–O to GP to form SPS/GP nanocomposite. The composite of SPS in its particle form with GP would be interesting because the SPS particle might stop the reformation of GP sheet into layer graphitic structure by absorbing themselves into the GP sheets which will interfere the closeness between the sheets and also incorporation of GP will significantly improves the properties of SPS.

In this report, we have prepared nanocomposite of SPS nanospheres and graphene by chemically reduce G–O in the SPS polymer matrix. The properties of polymer graphene nanocomposites depend on the exfoliation and good dispersion of graphene in the polymer matrix. The effect of graphene on the properties of SPS is studied. The thermal and mechanical properties of the SPS/GP are investigated. The water uptake and proton conductivity of the SPS/GP nanocomposites are also measured.

6.2. Experimental Section

6.2.1. Materials

Styrene (SISCO, India) was purified as per the reported procedure. Sodium dodecyl sulfate (SDS, Merck), sodium bicarbonate (SISCO, India), and ammonium per sulfate (APS, Merck) as the monomer, surfactant, buffer, and initiator, respectively, were used as received from the suppliers. Sulfuric acid (Merck), dimethylformamide (Merck), graphite powder (Sigma-Aldrich), sodium nitrate (SISCO, India), potassium permanganate (Merck), hydrogen peroxide (Merck), hydrazine hydrate (Merck), deuterated dimethyl sulfoxide (DMSO-d_6) were used as received. Milli Q water was used for all the experiments.

6.2.2. Sulfonation of polystyrene particles

Polystyrene (PS) of 50 nm size which were prepared using emulsion polymerization technique as per method described earlier was used for the preparation of sulfonated PS (SPS).[43] PS (1 g, 5.43 mmol) was taken in round bottom flask and 10 ml of H_2SO_4 was added to the flask. The reaction mixture was stirred at 40°C for 30 minutes. The precipitate was filtered and washed with large quantities of water till the filtrate was neutral. Finally the product was washed with ethanol. Then the product was taken in a Petri dish and dried in oven at room temperature under vacuum for 24 hrs. The shape and size of both PS and SPS were determined from TEM image (Figure 6.1). PS particles are monodisperse, spherical and 50 nm in size. SPS particle size is also 50 nm but with core-shell morphology. The degree of sulfonation of SPS is 27.7%

determined from the ^{1}H NMR spectrum (Figure 6.2) using method as described earlier.[32,33]

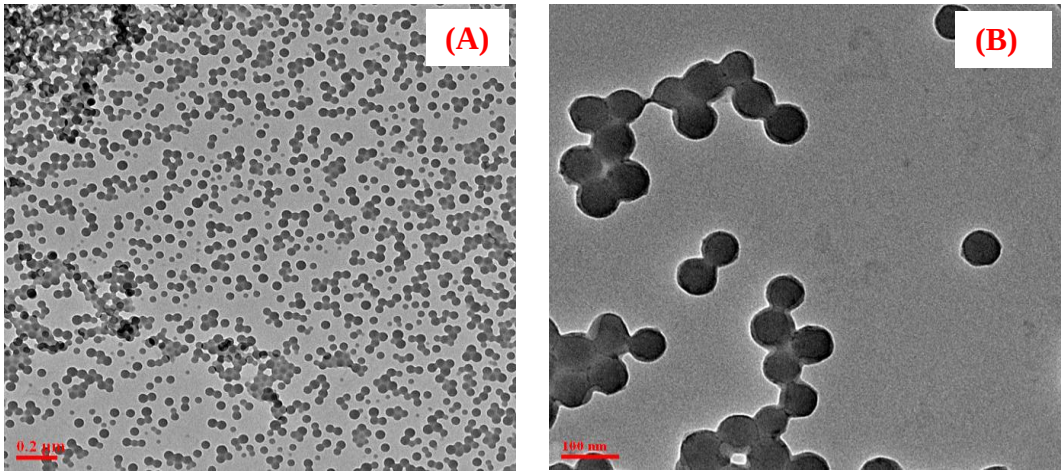

Figure 6.1: TEM image of (A) polystyrene particles (50 nm) (B) sulfonated polystyrene particles (50 nm).

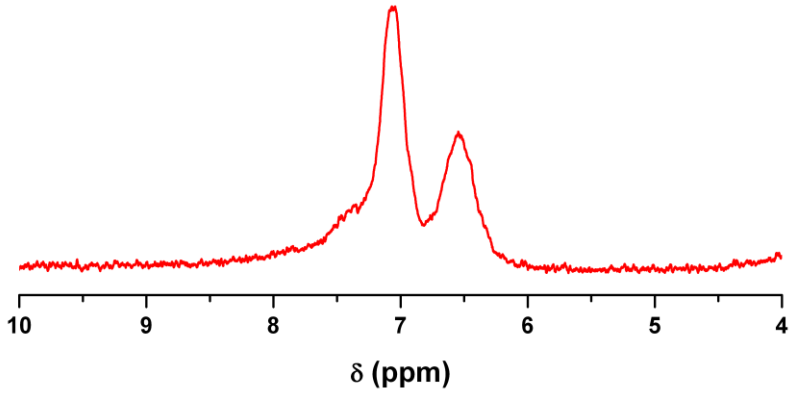

Figure 6.2: ^{1}H NMR spectrum of SPS.

6.2.3. Synthesis of graphene oxide (G–O) and reduced graphene (r-GP)

Natural graphite powder was oxidized to graphite oxide (GO) using a modified Hummers method.[44] About 1 g of graphite powder and 0.5 g of $NaNO_3$ were taken in 70 ml of concentrated H_2SO_4 which was kept in an ice bath. Then 3 g of $KMnO_4$ was gradually added. The mixture was stirred for 2 h and diluted with deionized water. After

that 5% of H_2O_2 was added into the solution until the color of the mixture changed into brilliant yellow, indicating fully oxidized graphite (graphite oxide). Then as obtained graphite oxide was re-dispersed in deionized water and then subjected to ultra-sonication for 2h to generate exfoliated graphene oxide (G–O) nanosheets. Then the mixture was filtered and washed with dilute HCl solution to remove metal ions. Finally the product was washed with deionized water to remove the acid.

Reduced graphene (r-GP) is obtained by chemical reduction of G–O. G–O was dispersed in water and to this hydrazine hydrate (1:1 in mass ratio) was added. The reduction was carried out at 100°C for 12h. The resulting r-GP obtained was centrifuged and washed with deionized water. The product was dried in vacuum oven at 65°C.

6.2.4. Synthesis of sulfonated polystyrene/graphene nanocomposites

In 10 ml of dimethyl formamide (DMF) required amount of GO is dispersed and sonicated for 2 hours. In another 10 ml DMF, sulfonated polystyrene (SPS) (1% by wt.) was dissolved. Both the solutions are mixed and the mixture was stirred for 24 hours. Then the mixture was poured in petri dish and the solvent was evaporated at 65°C. The resulting SPS/G–O nanocomposite film was dried in vacuum oven at 65°C for one day. To prepare SPS/graphene (SPS/GP) nanocomposite the SPS/G–O film was immersed in hydrazine hydrate solvent and refluxed at 100°C for 12 hours. After 12 hours the membrane was taken out and washed with water to remove excess hydrazine hydrate. Then the resulting SPS/GP films were dried in vacuum oven at 65°C for 2 days. The whole process for the formation of r-GP and SPS/GP is shown in Scheme 6.1.

The amount of GP in the SPS/GP composite is altered by taking required amount of GO in the reaction mixture. We have considered the amount of GO taken as the % of GP in nanocomposite. We have varied % of GP from 1% to 7%. The SPS/GP nanocomposites were obtained as free standing films (Figure 6.3) of thickness 80 μm. All the characterization as described in the next section were carried out from these films.

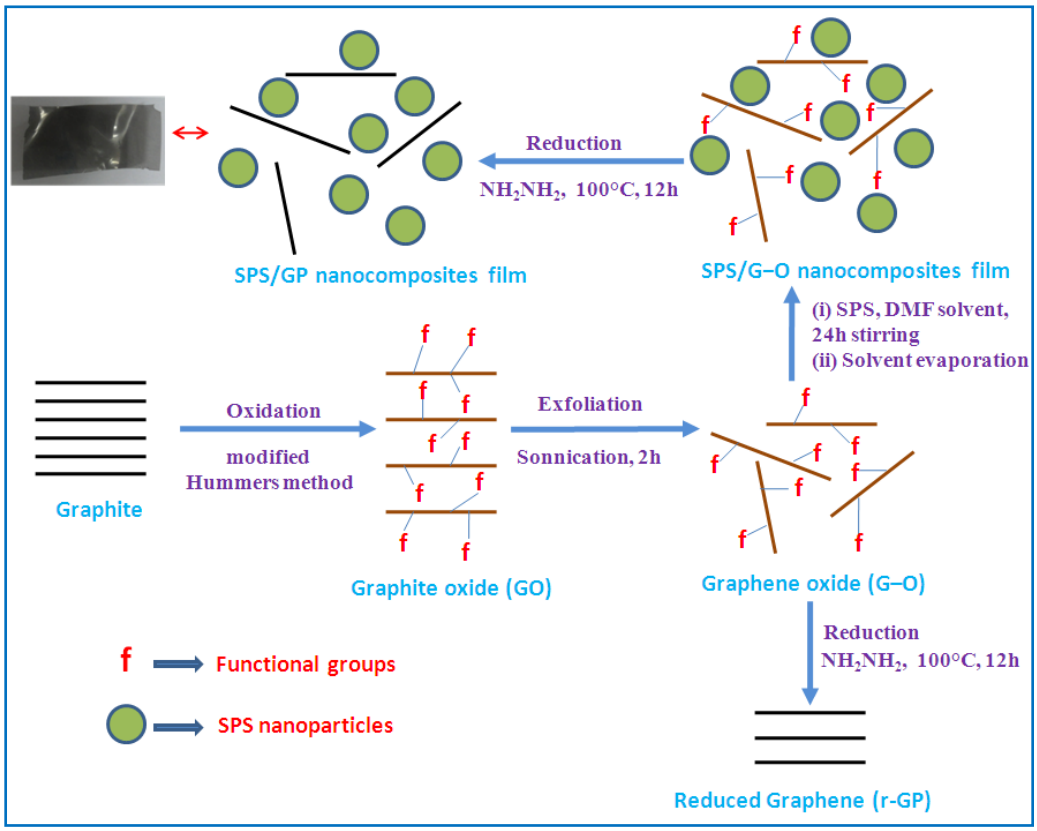

Scheme 6.1: Synthesis of reduced graphene (r-GP) and sulfonated polystyrene (SPS)/graphene (GP) nanocomposites.

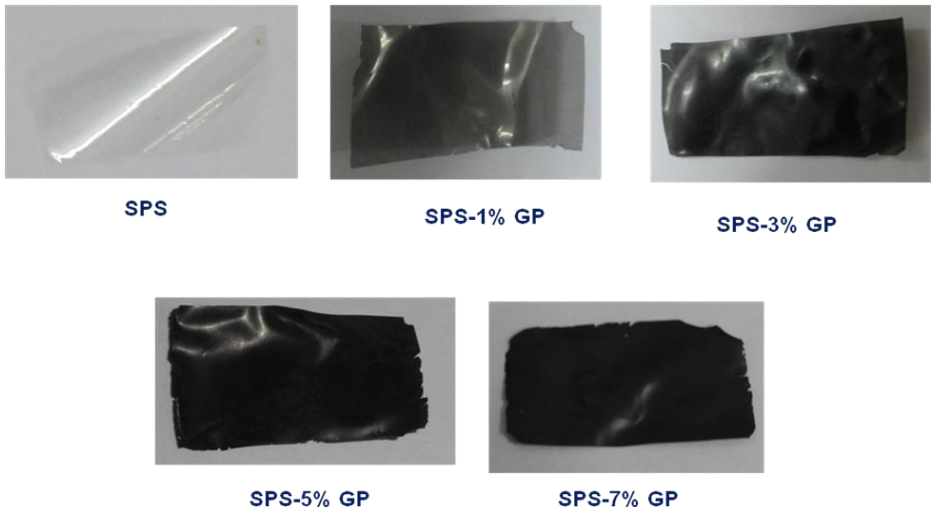

Figure 6.3: Photographs of SPS-GP nanocomposite films

6.3. Characterization techniques

6.3.1. FT-IR and Raman spectroscopy

Fourier transforms infrared (FT-IR) spectra of the thin nanocomposite films were recorded on a Nicolet 5700 FT-IR spectrometer at resolution of 0.5 cm^{-1} with an average of 32 scans. Raman spectra were recorded on a confocal Raman spectrometer (WITec Alpha 300R AFM) equipped with a Peltier-cooled CCD detector. Argon laser operating at 488 nm was used as an excitation source for the Raman scattering. All measurements were collected in air.

6.3.2. Wide angle X-ray diffraction (WAXD)

WAXD patterns of the samples were collected from an X-ray generator (Model PW 1729, Philips) with Cu Kα radiation (λ = 1.5418 Å) source at voltage 40 kV and 30 mA current in the 2θ range 5-45°.

5.3.3. Thermal study

Thermogravimetric and differential thermal analysis (TG-DTA) were carried out on a (Netzsch STA 409PC) TG-DTA instrument from 50-800°C with a scanning rate of 10°C/ min in presence of nitrogen flow. Dynamic mechanical analysis (DMA) of all the nanocomposite films was determined using TA Instrument Mechanical Analyzer (DMA) Q800. The storage modulus, loss modulus and tan δ were measured at a heating rate of 4°Cmin^{-1} under a preload force of 0.01N at a frequency of 1 Hz. The samples are kept at 50°C isothermally for 20 min inside the DMA machine and the scanned from 50 to 250°C at a heating rate 4°C min^{-1}.

5.3.4. Morphological investigations

A transmission electron microscope (TEM, FEI Tecnai Model No. 2083) operating at 120 kV was used to image and study the morphology of the samples. The sample was dissolved in little amount of DMF and the solution is diluted with water.

The TEM samples were prepared by drop casting samples on the carbon coated copper (200 mesh) grid. The atomic force microscope (AFM) images of the samples were captured in an AFM apparatus (model: Solver Pro M of NT-MDT) working in semi-contact mode. A microcantilever with a spring constant of 10 N/m was used to scan the samples.

5.3.5. Water uptake and conductivity study

Water uptakes of the nanocomposite membranes were obtained by immersing the dry membranes in water for 24 h. The weights of the membrane were measured before and after dipping in water. Water uptake values of the membranes were calculated as

$$\text{Water Uptake} = \frac{W_w - W_d}{W_d} \times 100\% \qquad (6.1)$$

where W_w and W_d are the weights of the wet and dry membranes, respectively.

Proton conductivities of the nanocomposite samples were measured with a four-point probe technique. The impedance of the membranes was measured with an impedance analyzer by using a Metrohm Autolab (PGSTAT302N) over a frequency range from 1 Hz to 100 Hz. The membranes were soaked in water for 24h. The soaked membranes were cut into rectangular shape and mounted onto the in-home built conductivity cell. The conductivities of the samples were obtained from the direct-current potential difference between the two inner electrodes. The conductivity was calculated with the following equation:

$$\sigma = \frac{D}{RBL} \qquad (6.2)$$

where, σ is the proton conductivity (S/cm), D is the distance between the electrodes, and B and L are the thickness and width of the blend samples, respectively. In all cases R was obtained from Nyquist plots. Conductivities were measured over a temperature range 30-50°C with 5°C interval.

6. 4. Results and Discussion

6.4.1. Synthesis and characterization of graphene oxide (G–O)

G–O is synthesized by following the procedures as shown in the scheme 1 and described in the experimental section. First graphite oxide is made by oxidation of graphite and then this oxide is exfoliated with help of sonnication to produce G–O. The oxidation of graphite to graphite oxide is confirmed by FT-IR (Figure 6.4).

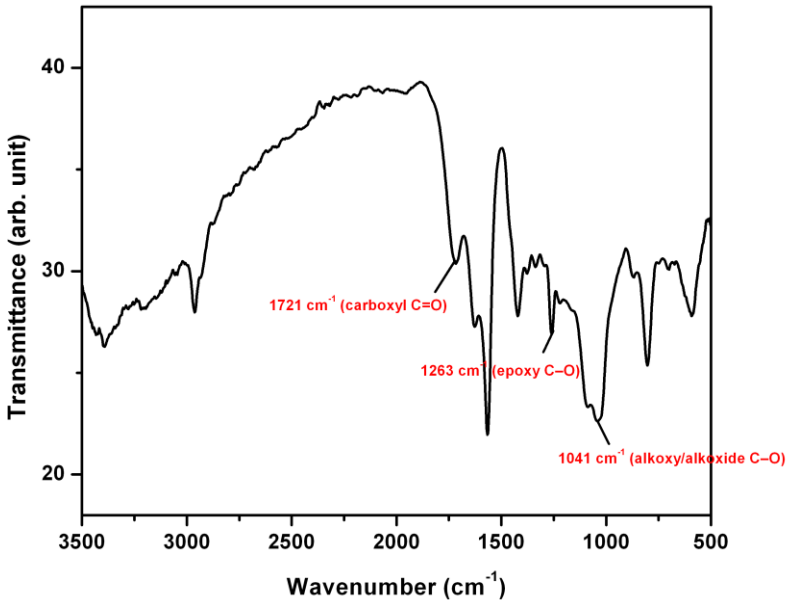

Figure 6.4: FT-IR spectra of graphite oxide

The spectrum consists of different characteristic peaks of oxygen functionalities in the region 900-2200 cm^{-1}. The peak at 1721 cm^{-1} corresponds to carboxyl C=O stretching frequency. The peaks at 1263 cm^{-1} and 1063 cm^{-1} indicate the presence of epoxy and alkoxy or alkoxide groups, respectively. These peaks confirmed the presence of functional groups in the graphite oxide. Modified Hummer method used to make graphite oxide introduces several functional groups such as carbonyl (-C=O), hydroxyl (–OH), carboxyl (–COOH) attached to the layers of graphite. The powder X-Ray patterns of graphite and graphite oxide (GO) are shown in Figure 6.5.

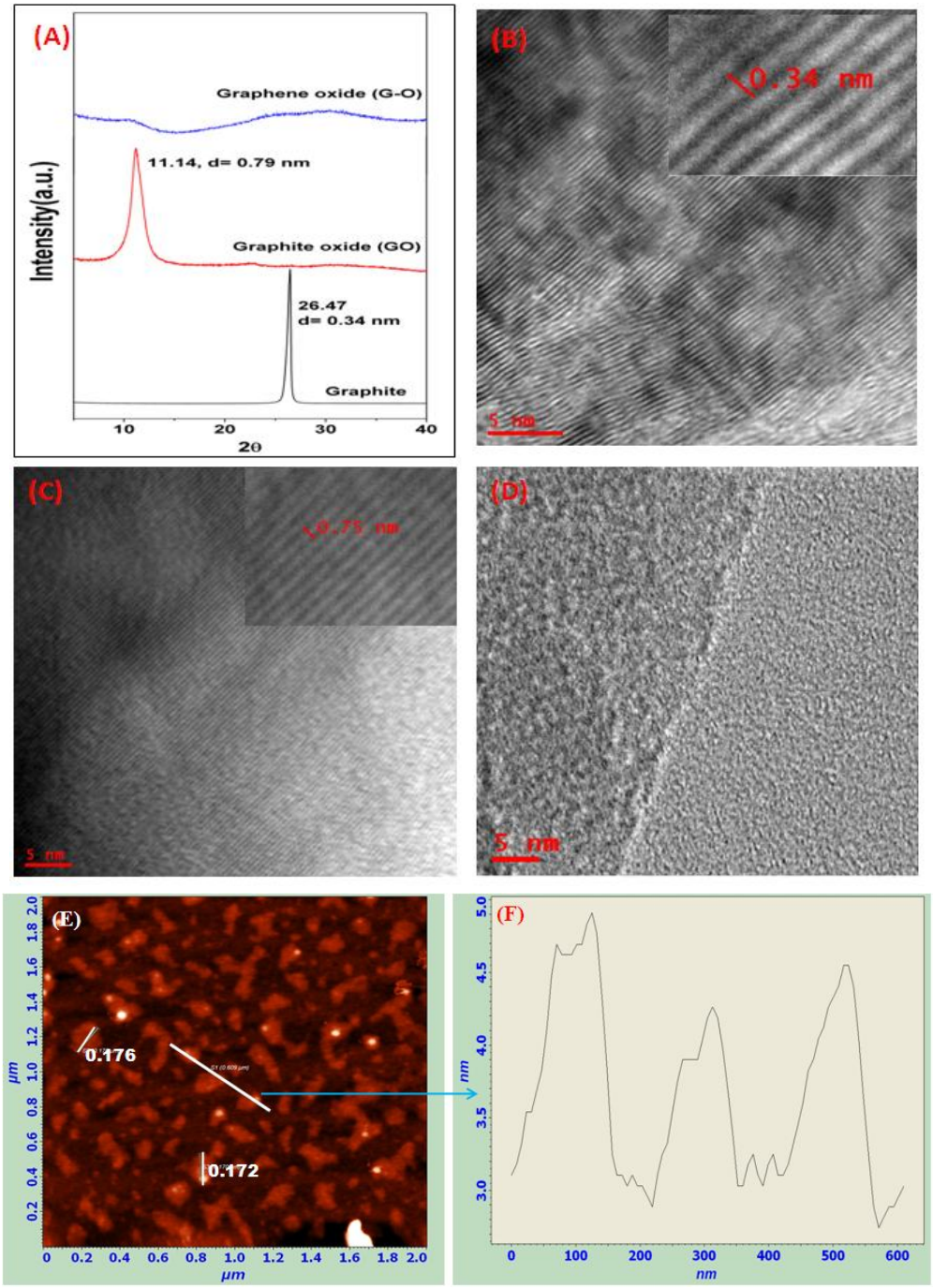

Figure 6.5: (A) XRD patterns of graphite, graphite oxide (GO) and graphene oxide (G–O) (B), (C) and (D) TEM images of pristine graphite, GO and G–O, respectively, (E) AFM image of G–O (F) AFM height profile of G–O. Inset: Interlayer distances of graphite and GO.

Graphite has a characteristic peak at $2\theta \approx 26^0$ which corresponds to an interlayer separation of 0.34 nm. After oxidation of graphite the peak at $2\theta \approx 26^0$ is completely suppressed and an additional characteristic peak appears at $2\theta \approx 11^0$ with interlayer spacing 0.79 nm. The complete absence of 0.34 nm interlayer spacing in case of graphite oxide (GO) indicating the complete oxidation of graphite and bigger interlayer spacing of GO than graphite. In case of exfoliated GO or G–O the d spacing at $2\theta = 11°$ (Figure 6.5) is disappeared completely indicating the complete exfoliation of GO to G–O as shown in the Scheme 6.1.

High resolution TEM image (Figure 6.5) of pristine graphite, GO and G–O clearly reveal the increase in interlayer thickness in the case of GO and complete exfoliation in the case of G–O. The TEM micrograph of G–O (Figure 6.5D) has no planes attributing the complete exfoliation happening in 2h sonication of GO. The interlayer distances measured from the TEM micrographs (Inset of Figure 6.5B, 6.5C) are matching with the distance obtained from XRD patterns (Figure 6.5A). AFM image and height profile (Figure 6.5E and 6.5F) of G–O confirms the formation of ~1 nm thick and ~170 nm long graphene oxide nanoplatelets, indicating that sonication of GO produces single layer G–O sheets. These above results confirm that the resulting G–O sheets consist of only single layer.

6.4.2. Preparation of sulfonated polystyrene (SPS)/graphene oxide (G–O) nanocomposite

The single layer ~1 nm thick and ~170 nm long G–O nanoplatelets, as discussed in the previous section, are mixed with SPS nanospheres in different weight % loading (1%, 3%, 5% and 7%) to prepare SPS/G–O nanocomposite as shown in the Scheme 6.1. After 24 h of stirring, the solvent (DMF) is evaporated and SPS/G–O nanocomposite films are obtained. Since both SPS and G–O have many functional groups available at their surfaces, it is reasonable to expect the presence of strong interactions between SPS and G–O which drives the formation of nanocomposite. Indeed this is found to be true as evident from the IR data as description follows. The important stretching frequencies of SPS, GO and SPS/G–O are marked in the Figure 6.6.

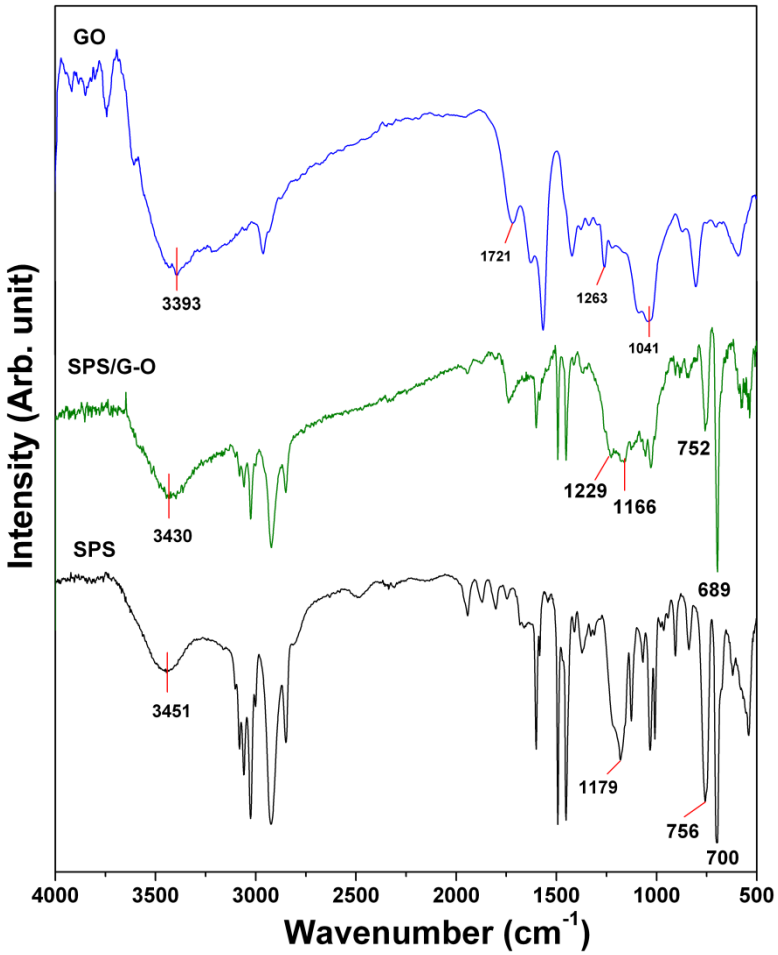

Figure 6.6: FT-IR spectra of SPS, GO and SPS/ GO nanocomposites.

The nanocomposite consists both SPS and GO peaks indicating the presence of both the constituents. The O–H stretching of $–SO_3H$ of SPS at 3451 cm^{-1} shifted to lower wavenumber (3430 cm^{-1}) and becomes broader in case of nanocomposite attributing that $–SO_3H$ of SPS is involved in the interaction with G–O nanoplatelets.[23] Similarly the asymmetric stretching of $–SO_3H$ of SPS shifted from 1179 cm^{-1} to 1166 cm^{-1} in nanocomposite. Also a substantial shift (700 cm^{-1} to 689 cm^{-1}) of out of plane blending vibration of PS ring is obtained in case of nanocomposite. These results clearly indicate the strong interaction between SPS and G–O and these interactions resulted in the stable nanocomposite formation. The 1263 cm^{-1} peak of GO is due to C–

OH stretching and this also is observed in substantial shift to lower wavenumber at 1229 cm^{-1}.[23]

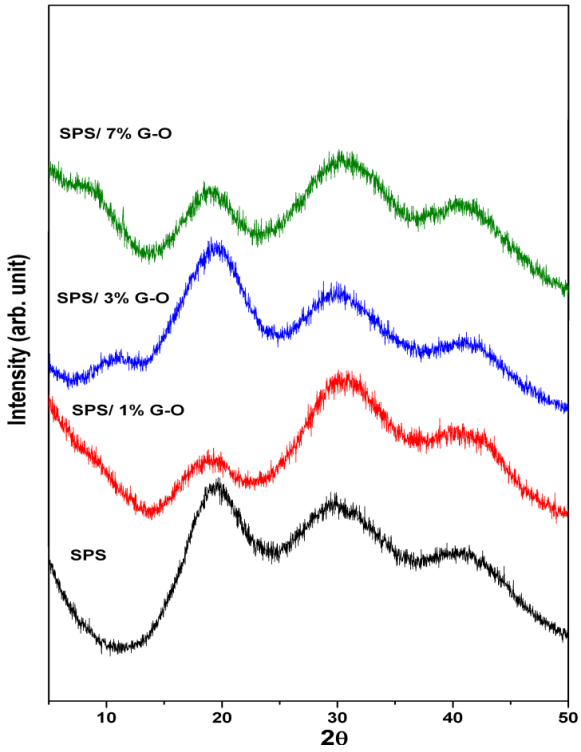

Figure 6.7: XRD patterns of SPS and SPS/G–O nanocomposites.

Figure 6.7 represents the XRD patterns of SPS/G–O nanocomposites along with pristine SPS. All the nanocomposites have similar diffraction patterns like native SPS attributing the formation of well dispersed nanocomposite. Most importantly, all nanocomposite do not display any peak at around 2θ ≈11° (d= 0.79 nm), which is present in GO (Figure 6.5A) indicating that in the nanocomposite graphene sheets are completely exfoliated as single layer graphene. As mentioned in the previous section G–O has been prepared from GO by sonicating and G–O has no layer structure as shown in Figure 6.5. Figure 6.7 clearly proves that SPS/G–O nanocomposite has no layer structure, in fact it is expected that the exfoliation of graphene sheets would be more in nanocomposite since SPS particles will be separating the nano sheet further as shown in Scheme 6.1.

6.4.3. Preparation of SPS/GP from SPS/G–O nanocomposite

The SPS/G–O nanocomposite films are reduced to SPS/GP nanocomposite films by refluxing the former in hydrazine hydrate at 100°C for 12h as shown in Scheme 6.1.

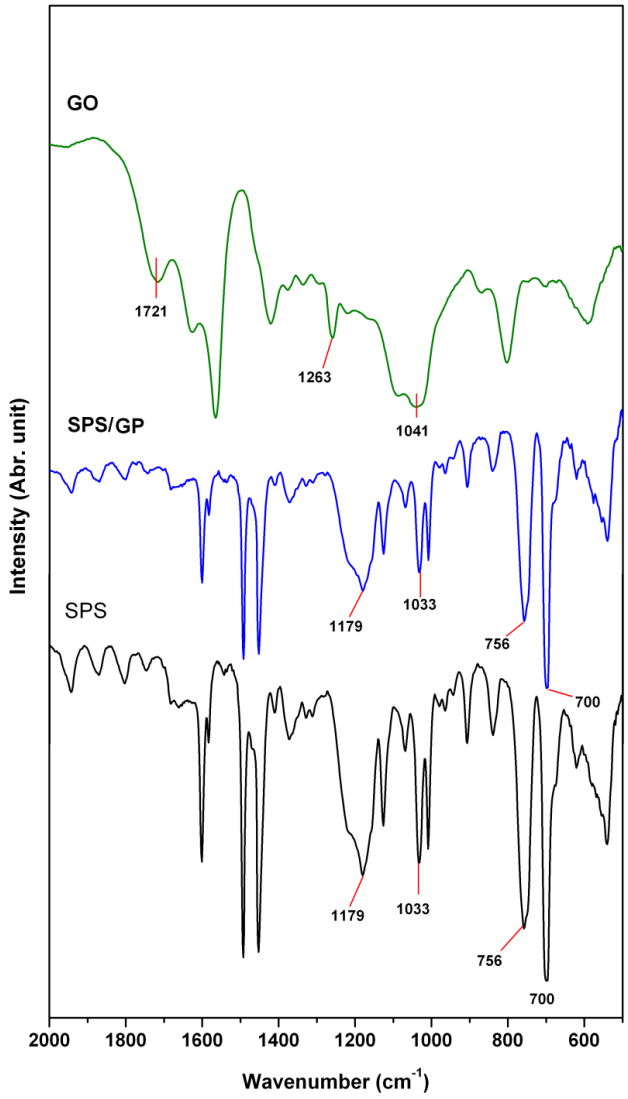

Figure 6.8: FT-IR spectra of SPS, GO and SPS/GP nanocomposites.

All the graphene sheets with functional group convert to only single layer graphene sheet. These films are characterized thoroughly to prove the presence of graphene sheet as well as SPS particle. We believe the SPS nanospheres do not allow the single layer graphene to reassemble in to the graphite layer structure. To validate our

hypothesis, we conducted a control experiment (Scheme 6.1), in which we reduced G–O to GP in absence of SPS nanospheres by maintaining similar reaction condition as in SPS/G–O to SPS/GP. The resultant material is named as reduced graphene (r-GP) as presented in Scheme 6.1. The FT-IR spectra of SPS/GP nanocomposite film are shown in Figure 6.8 along with SPS and GO. Peaks corresponding to the functional groups of GO is not observed in the nanocomposite and also there is complete absence of peak shifting and broadening of SPS peaks in nanocomposite. These results indicate that GO is reduced to graphene (GP), and GP is present along with the SPS in the nanocomposite without any functional group interactions.

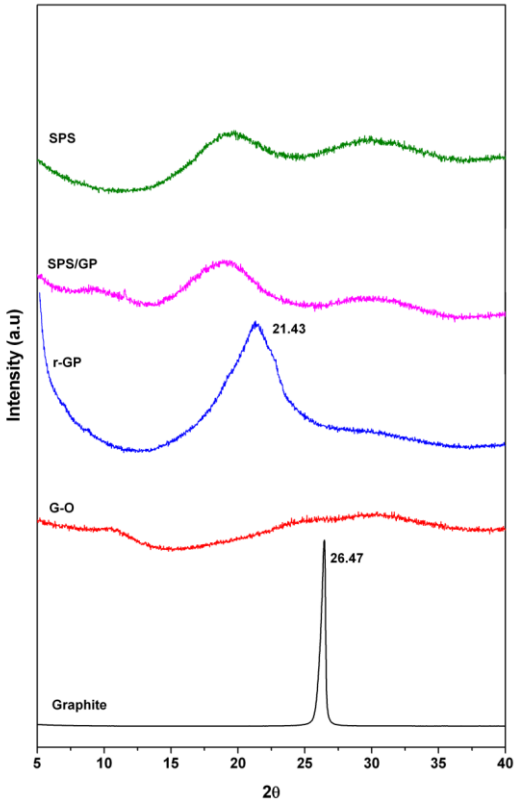

Figure 6.9: XRD patterns of graphite, G–O, SPS, SPS/GP nanocomposite film and reduced GP (r-GP).

When exfoliated GO is reduced, after reduction there is a probability that the reduced graphene layers may agglomerate and forms the layer structure again owing to the strong van der Waals force of attraction between single graphene layer. But in the

nanocomposite graphene layers are in the exfoliated state which can be seen from the XRD pattern of SPS/GP nanocomposite (Figure 6.9). The SPS/GP XRD pattern is similar to SPS and has no interlayer spacing indicating that GP sheets are completely in exfoliated state and present as single layer in nanocomposite. On the other hand when G–O is reduced in absence of SPS to produce r-GP, it shows strong graphite diffraction at 2θ= 21.4° corresponding to interlayer spacing 0.41 nm. This clearly indicates that in absence of SPS nanospheres the graphite sheets are agglomerated to produce graphite like structure. The presence of exfoliated GP sheets in SPS/GP nanocomposite is due to the fact that SPS nanospheres adsorb to the GP sheets surface and interfere in the process of recombination of GP sheets because of their particle nature and as a result the GP sheets stay away from each other yielding well exfoliated nanocomposite.

To prove further that GP is present as single layer thick sheet in SPS/GP nanocomposite, we looked into the AFM topography (Figure 6.10).

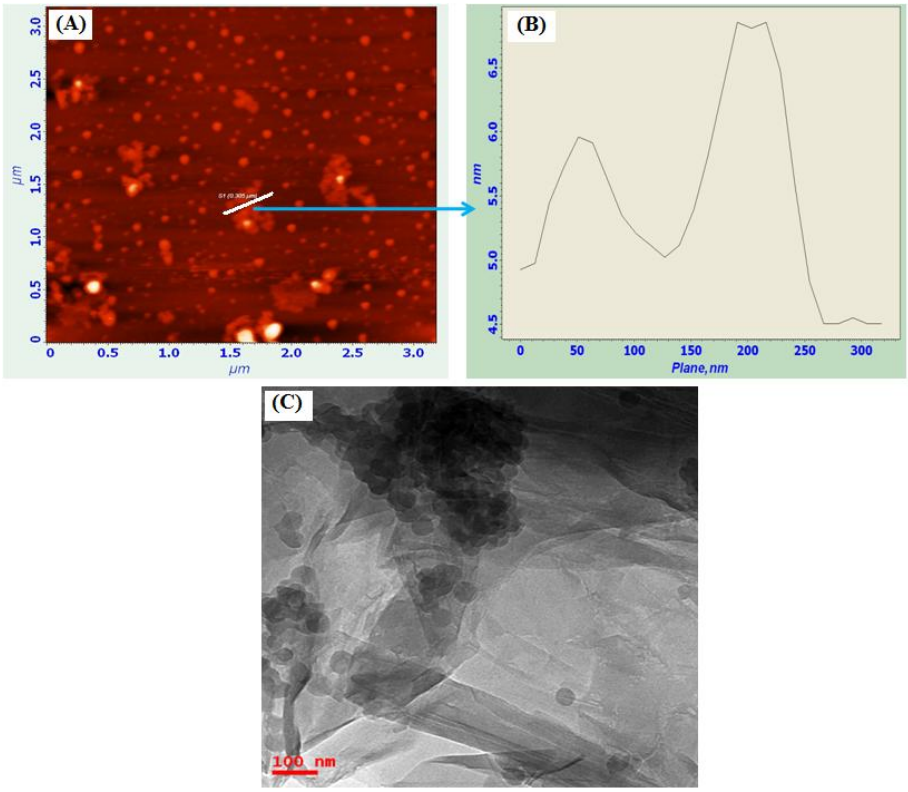

Figure 6.10: AFM image (A), height profile (B) and TEM image (C) of SPS/GP nanocomposite.

As seen from the image and height profile the particles are sitting on the GP sheet surface and the sheets are well dispersed in the SPS matrix. The thickness of the sheets is varying with ~1-2 nm indicating the presence of single layer graphene sheet. Once again TEM image (Figure 6.10) clearly display the particle nature of SPS in the composite, it also clearly indicate the presence of GP sheets along with SPS particle.

The Raman spectra of graphite, GO, SPS/GP nanocomposites and r-GP are shown in Figure 6.11. The Raman spectrum of graphite shows a prominent G band at 1553 cm^{-1} corresponding to the first-order scattering of the $E2_g$ mode[45] of the planar sp^2 hybridized carbon atoms. In GO, the G band broadened and shifted to 1603 cm^{-1} and in addition another peak at 1369 cm^{-1} corresponding to D-band is observed. The D-band indicates disorder sp^3 carbon atom and originates due to edge effects.[20,21,36] The D-band occurs due to extensive oxidation. The Raman spectrum of SPS/GP also contains both G and D bands (at 1606 and 1366 cm^{-1}, respectively) in which D-band further shifted toward higher frequency indicating exfoliation of graphene layer. I_D/I_G (the intensity of D and G) is 0.96 in case of GO whereas it is 0.48 in case of SPS/GP. The decrease of I_D/I_G ratio in case of SPS/GP attributing that proportion of sp^2 C atoms increased after reduction from GO to GP by restoring sp^3 to sp^2 C atoms.[36,45,46] This observation shows that the GO is converted to graphene in the SPS/GP nanocomposites.

It is interesting to note that the Raman spectrum (Figure 6.11) of reduced graphene (r-GP) which is prepared by reducing GO in absence of SPS nanospheres displays only the G band at 1552 cm^{-1} (similar to graphite) and the D-band disappears, and the Raman spectra is almost like graphite Raman spectra. This indicates that in absence of SPS nanospheres the graphene layer agglomerated and goes back to the layer structures. Hence, it can be confirmed that in SPS/GP nanocomposites, SPS nanospheres prevent the reduce graphene layers from agglomeration. As a result this drives the formation of nice dispersion of graphene layers in the SPS polymer matrix.

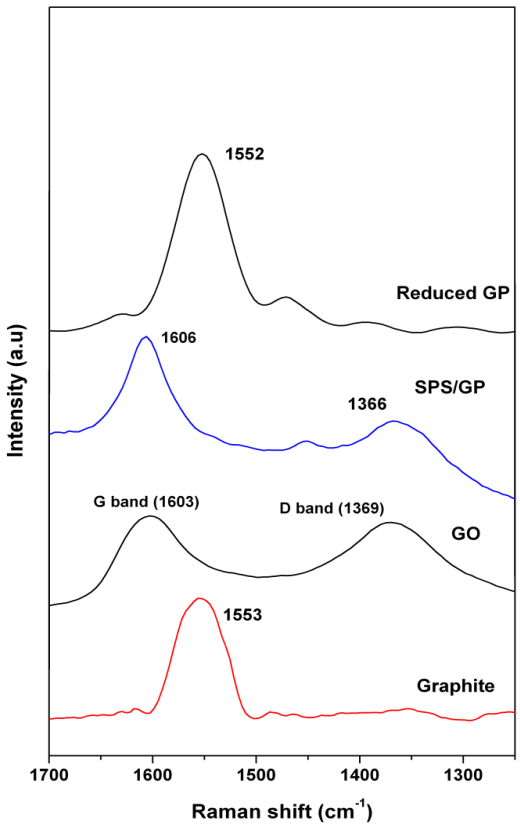

Figure 6.11: Raman spectra of graphite, GO, SPS/GP nanocomposite and r-GP.

6.4.4. Properties of SPS/GP nanocomposites

Several properties e.g. thermal, mechanical, conductivity etc. of nanocomposite are studied and compared with pristine SPS. The thermal stability of GO, SPS/GP nanocomposite films and SPS are shown in Figure 6.12. It is observed that GO is thermally stable up to 270°C. The first weight loss occurs at 100°C which is due to presence of water between the GO layers. The weight loss at 270°C is due to pyrolysis of labile oxygen containing functional groups such as carboxylate, epoxy hydroxyl etc.[47,48] But chemically reduced graphene is thermally stable because most of the functional groups are reduced. For reduced graphene also weight loss at 100°C is observed. This is due absorbed water by the graphene layers. The thermal stability graphite and reduced graphene are nearly same. In case of SPS/GP nanocomposites the

thermal stability increases compared to SPS with increasing loading percentage of graphene. This is more clearly visible from the DTG curve (Figure 6.12B).

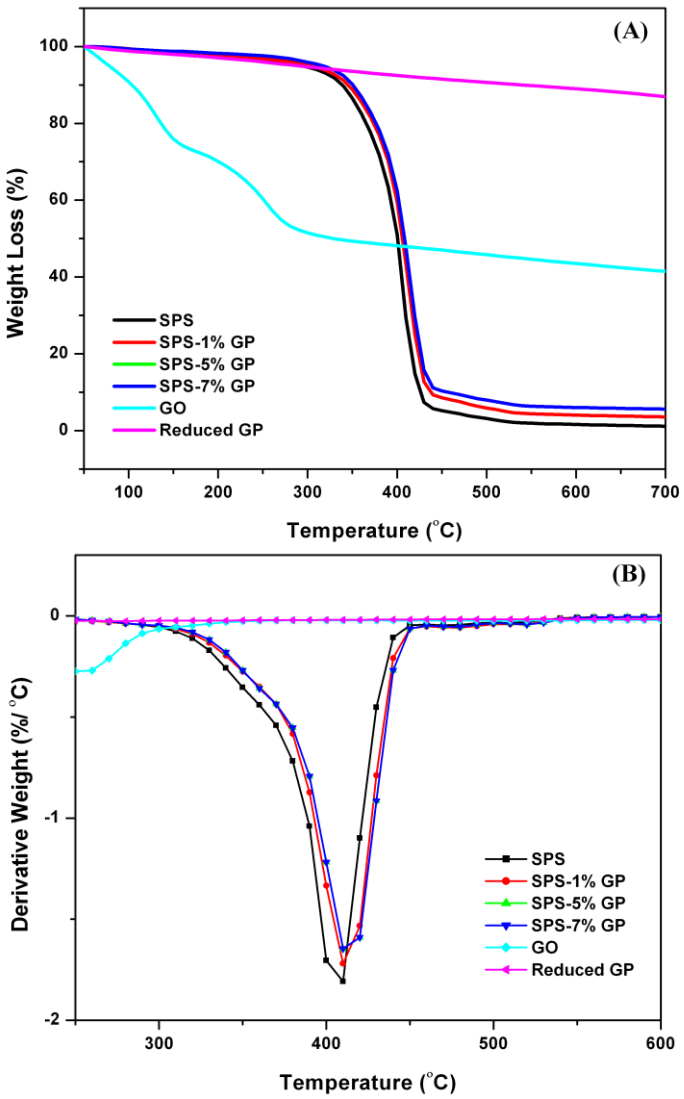

Figure 6.12: (A) TGA curves and (B) Derivative curves of TGA of SPS, GO, reduced graphene and SPS-GP nanocomposites.

Thus the thermal stability of SPS is little improved in the nanocomposites. Usually graphene layers just like other layered material such as clay act as thermal barrier and slows down the thermal decomposition of the polymer matrixes. But the thermal stability of SPS/GP is not increased much as expected and the reason for little

improvement is that although the layer structure of graphene is stable, it has high thermal conductivity. So this makes graphene layers difficult to slow down the heat transfer, thus the thermal stability of SPS/GP nanocomposites is improved only slightly.

The thermo-mechanical properties of SPS/GP nanocomposites measured using DMA are shown in Figure 6.13 and 6.14. The storage moduli (E′) of SPS and SPS/GP nanocomposites at different temperature are tabulated in Table 6.1. Figure 13 and Table 6.1 data clearly show that the storage modulus (E') of SPS/GP nanocomposites increases with increasing GP content in the nanocomposites. Almost ~90% increase in mechanical strength is observed for 7% GP loading. It is also to be noted that the % of increase of mechanical reinforcement is more near the glass transition (T_g) temperature. The T_g of all samples are close to 100°C (discussed later). We observed ~143% increase in mechanical strength at 90°C which is very close to T_g of the sample. This increase in storage modulus can be attributed to the higher stiffness and large surface area of the graphene sheets. GP is known to enhance the mechanical strength of the polymer nanocomposites for their above properties.

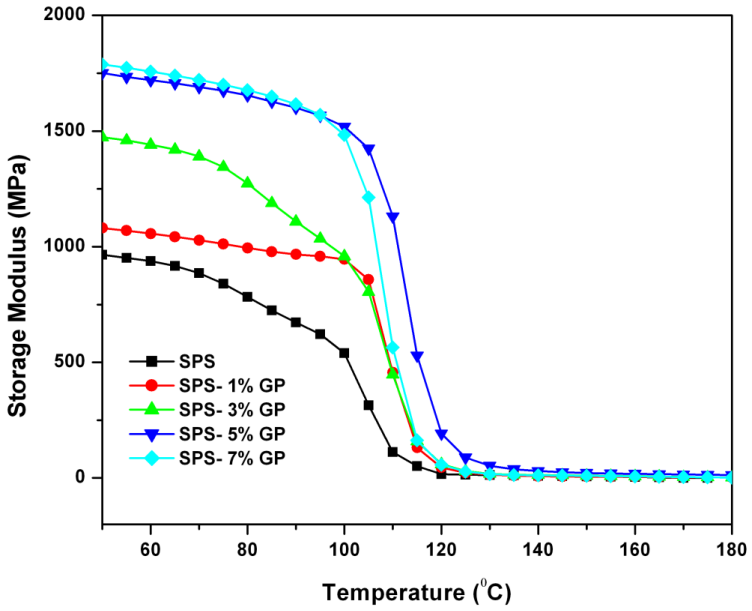

Figure 6.13: Temperature dependent storage modulus plots of SPS/GP nanocomposites obtained from DMA studies.

Table 6.1: Various thermo mechanical data of SPS/GP nanocomposites obtained from the DMA study

Sample	E′ (MPa) at 60°C	% increase	E′ (MPa) at 90°C	% increase
SPS	943		666	
SPS-1% GP	1056	11.98	973	46.09
SPS-3% GP	1442	52.92	1110	66.67
SPS-5% GP	1716	81.97	1593	139.19
SPS-7% GP	1765	87.17	1617	142.79

The loss modulus and tan δ plots as a function of temperature are shown in Figure 6.14. The peak temperature in these plots corresponds to the glass transition temperature (T_g) of the polymer and listed in Table 6.2. The results clearly indicate that the T_g of SPS increases with increasing graphene content in the nanocomposites. It could be observed that the T_g of SPS increases from 10 to 15°C in nanocomposites and this is due to the of the presence of graphene layer in the polymer matrix which perturb the mobility of the polymer chains resulting increase in the T_g of the polymer.

Table 6.2: Glass transition temperature obtained from DMA experiments

Sample	Loss modulus (MPa) T_g (°C)	Tan δ T_g (°C)
SPS	104	114
SPS-1% GP	109	116
SPS-3% GP	109	120
SPS-5% GP	112	127
SPS-7% GP	114	129

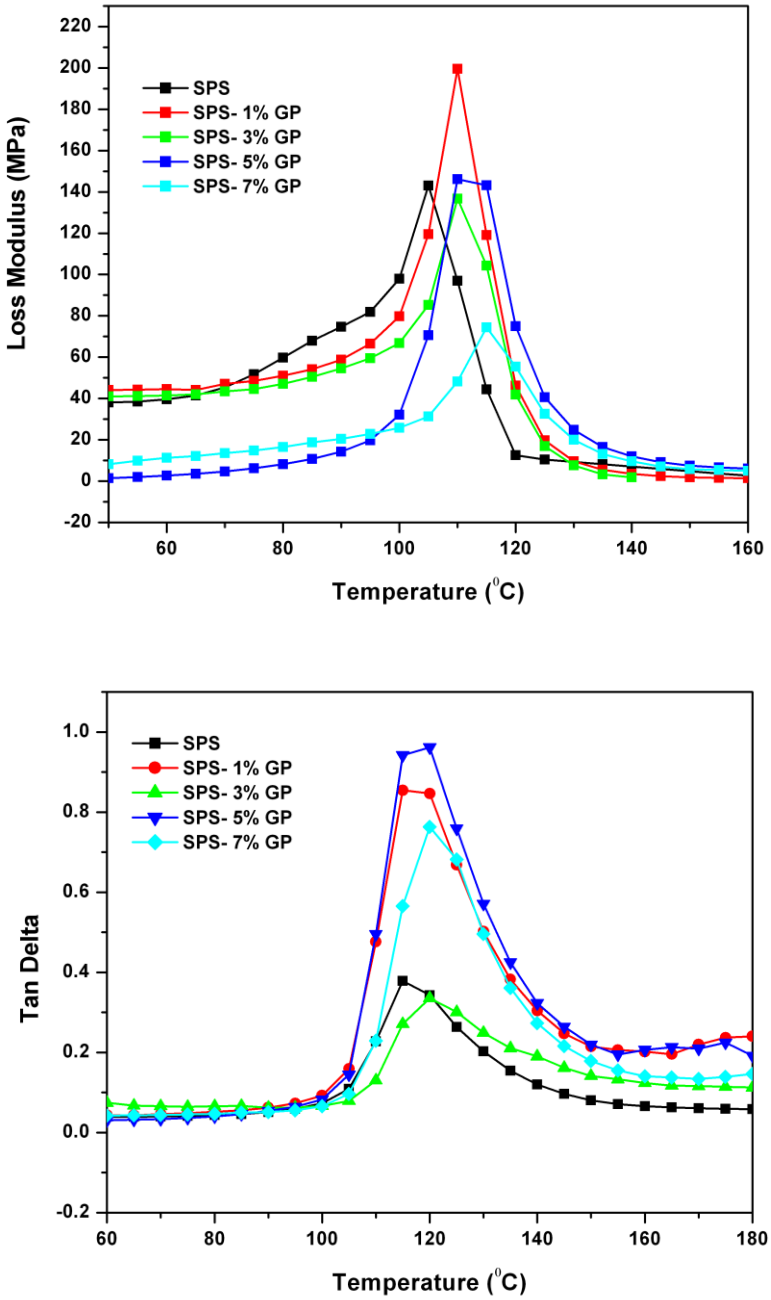

Figure 6.14: Temperature dependent (A) loss modulus (B) tan δ plot of SPS and SPS/GP nanocomposites.

Water uptake measurements were carried out to investigate the swelling properties of SPS and nanocomposite membranes. The water uptake values of SPS and SPS/GP nanocomposite samples are shown in Figure 6.15. The water uptake of SPS increases with increasing graphene content in the nanocomposite membranes. The water uptake of SPS is 4.7% and it increases to 19.38% for 7% graphene content. The larger surface area of nanocomposites is responsible for the increase in water uptake of nanocomposites compared to pristine SPS.

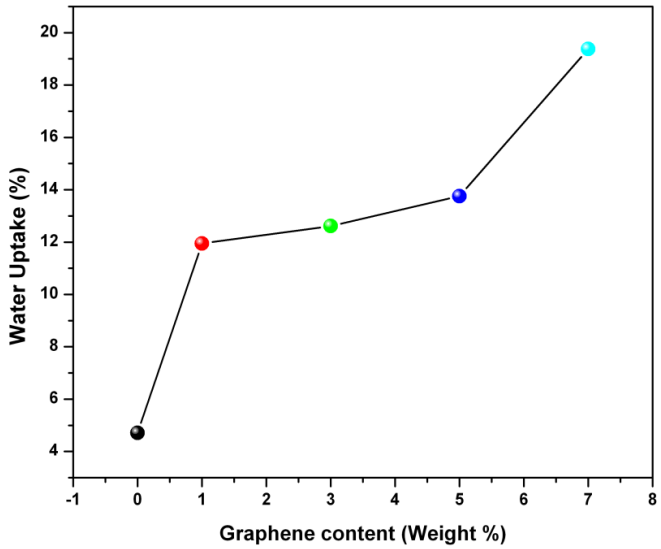

Figure 6.15: Water uptake of SPS and SPS/GP nanocomposites as a function of graphene content in the nanocomposites.

The proton conductivity of SPS and nanocomposite membranes were measured from 30°C to 50°C. All the membranes were soaked in water for 24h for water uptake before the measurement. The hydrated membrane fixed in the home made four probe conductivity cell and impedance was measured. The proton conductivities of the representative membranes obtained from the Nyquist plots (Figure 6.16).

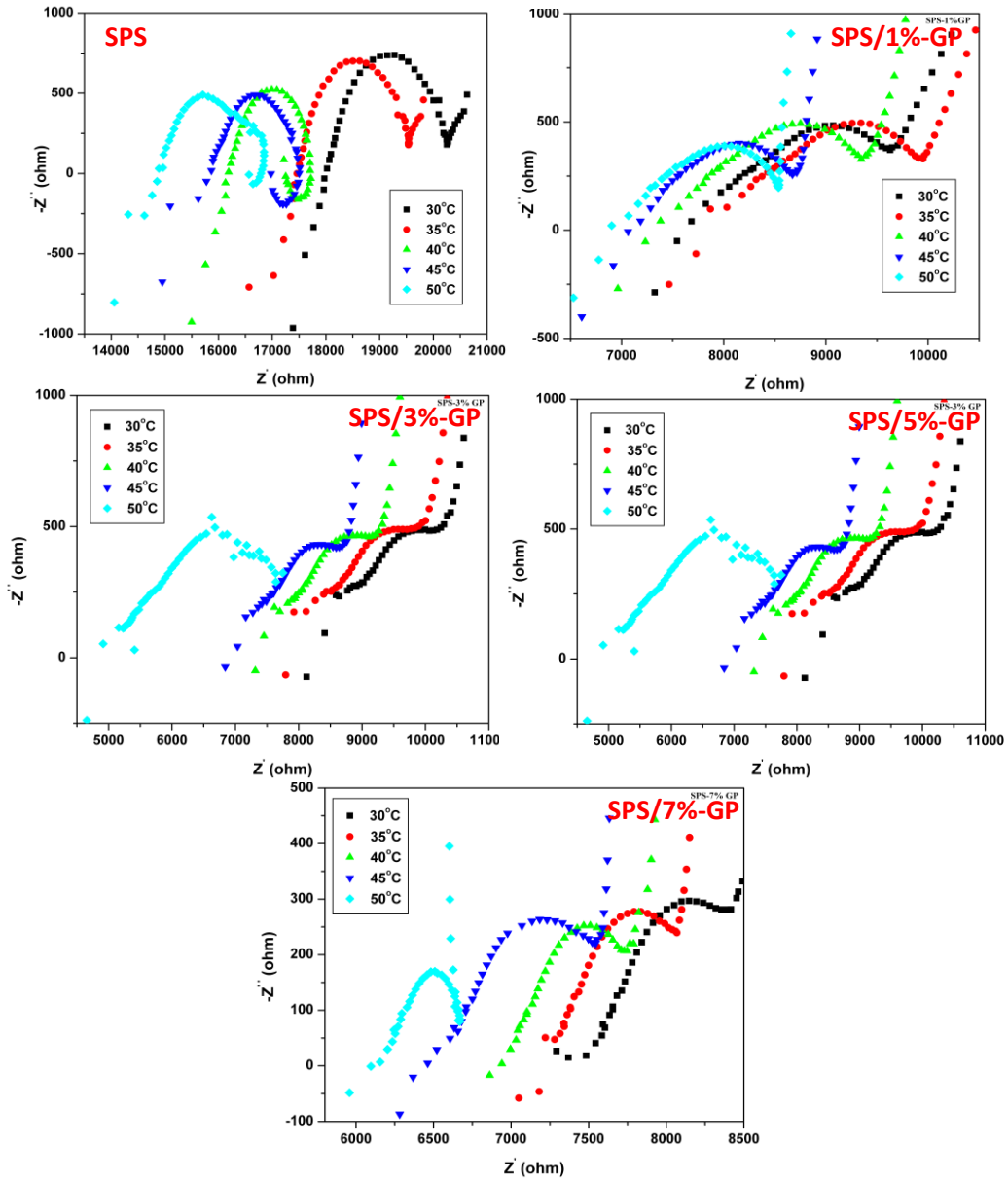

Figure 6.16: Nyquist plots of SPS and SPS/GP nanocomposite films.

Figure 6.17 compares the proton conductivity values of various membranes measured from 30 to 50°C. The proton conductivity of SPS increases with increasing graphene content in the membrane, however the temperature dependence of conductivity is not very prominent. The proton conductivity of SPS increases from 2×10^{-3} to 4.9×10^{-3} when the graphene content is 7% at 30°C and from 2.5×10^{-3} to

6.3×10^{-3} at 50°C. The proton conductivity of SPS depends on the percentage of water uptake and microstructure of the membranes. The water uptake increases with graphene content and because of this more water uptake the SPS/7%GP shows more proton conductivity compared to SPS. Another reason for improvement in conductivity may be attributed to combinations of highly conductive graphene in the polymer matrix.

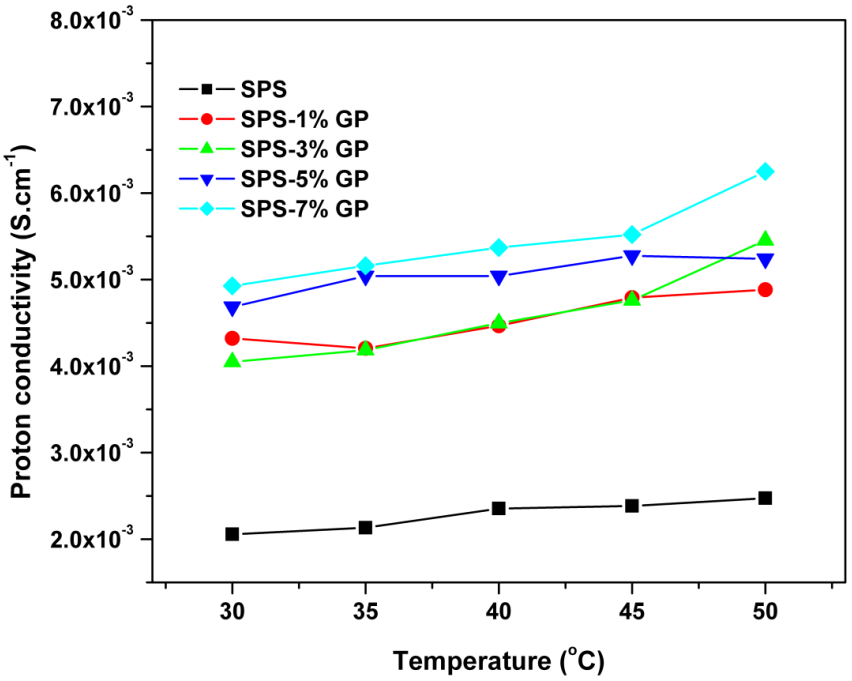

Figure 6.17: Temperature dependent proton conductivity of SPS/GP nanocomposite membranes

6. 5. Conclusion

Single layer ~1 nm thick and ~ 170 nm long graphene (GP) nanosheets have been generated and stabilized in the presence of sulfonated polystyrene (SPS) nanospheres. Exfoliated graphene oxide (G–O) nanosheets are solution blended with SPS nanospheres to produce SPS/G–O nanocomposites which then reduced to SPS/GP nanocomposites upon treatment with hydrazine hydrate. In-depth characterization of the nanocomposites with the help of X-Ray diffraction, Raman spectroscopy and atomic force microscopy clearly prove the formation of single layer GP in the SPS/GP

nanocomposite. Due to the strong interaction between $–SO_3H$ functionality of SPS and functional group of G–O; the spherical SPS particles are adsorbed on the graphene sheets which in turn perturb the recombination process of graphene sheet when G–O is reduced to GP. This results in stable SPS/GP nanocomposite. The nanocomposite display better thermal, mechanical and ionic conduction compared to pristine polymer. Hence in summary, SPS particles help to produce and stabilize single layer graphene sheets; in turn these GP nanosheets help to produce mechanically strong ion conducting SPS membrane.

6. 6. References

1. Giannelis, E. P. *Appl. Organomet. Chem*. **1998**, *12*, 675.
2. Novak, B. M. *Adv. Mater*. **1993,** *5*, 422.
3. Potts, J. R.; Dreyer, D.R.; Bielawski, C. W.; Ruoff, R. S. *Polymer* **2011**, *52*, 5.
4. Sengupta, R.; Bhattacharya, M.; Bandyopadhyay, S.; Bhowmick, A. K. *Prog. Polym. Sci*. **2011**, *36*, 638.
5. Kuilla, T.; Bhadra, S.; Yao, D.; Kim, N. H.; Bose, S.; Lee, J. H. *Prog. Polym. Sci*. **2010,** *35*, 1350.
6. Ajayan, P. M.; Schadler, L. S.; Giannaris, C.; Rubio, A. *Adv. Mater*. **2000**, *12*, 750.
7. Ghosh, S.; Sannigrahi, A.; Maity, S.; Jana, T. *J. Phys. Chem. C* **2011**, *115*, 11474.
8. Akcora, P.; Liu, H.; Kumar, S. K.; Moll, J.; Li, Y.; Benicewicz, B. C.; Schadler, L. S.; Acehan, D.; Panagiotopoulos, A. Z.; Pryamitsyn, V.; Ganesan, V.; Ilavsky, J.; Thiyagarajan, P.; Colby, R. H.; Douglas, J. F. *Nat. Mater*. **2009**, *8*, 354.
9. Ghosh, S.; Maity, S.; Jana, T. *J. Mater. Chem*. **2011**, *21*, 14897.
10. Verdejo, R.; Bernal, M. M.; Romasanta, L. J.; Lopez-Manchado, M. A. *J. Mater. Chem*. **2011**, *21*, 3301.
11. Stankovich, S.; Dikin, D. A.; Dommett, G. H. B.; Kohlhaas, K. M.; Zimney, E. J.; Stach, E. A.; Piner, R. D.; Nguyen, S. T.; Ruoff, R. S. *Nature* **2006**, *442*, 282.
12. Lee, C.; Wei, X.; Kysar, J. W.; Hone, J. *Science* **2008**, *321*, 385.
13. Yu, A.; Ramesh, P.; Itkis, M. E.; Bekyarova, E.; Haddon, R. C. *J. Phys. Chem. C* **2007**, *111*, 7565.
14. Balandin, A. A.; Ghosh, S.; Bao, W.; Calizo, I.; Teweldebrhan, D.; Miao, F.; Lau, C. N. *Nano Lett*. **2008,** *8*, 902.
15. Wu, Z.-S.; Ren, W.; Gao, L.; Zhao, J.; Chen, Z.; Liu, B.; Tang, D.; Yu, B.; Jiang, C.; Cheng, H.-M. *ACS Nano* **2009**, *3*, 411.
16. Routh, P; Layek, R. K.; Nandi, A. K. *Carbon* **2012**, *50*, 3422.

17. Loh, K. P.; Bao, Q.; Ang, P. K.; Yang, J. *J. Mater. Chem.* **2010**, *20*, 2277.
18. Nethravathi, C.; Rajamathi, J. T.; Ravishankar, N.; Shivakumara, C.; Rajamathi, M. *Langmuir* **2008,** *24*, 8240.
19. Szabó, T.; Szeri, A.; Dékány, I. *Carbon* **2005**, *43*, 87.
20. Stankovich, S.; Dikin, D. A.; Piner, R. D.; Kohlhaas, K. A.; Kleinhammes, A.; Jia, Y.; Wu, Y.; Nguyen, S. T.; Ruoff, R. S. *Carbon* **2007**, *45*, 1558.
21. Hu, H.; Wang, X.; Wang, J.; Wan, L.; Liu, F.; Zheng, H.; Chen, R.; Xu, C. *Chem. Phys. Lett.* **2010**, *484*, 247.
22. Zhou, T.; Chen, F.; Tang, C.; Bai, H.; Zhang, Q.; Deng, H.; Fu, Q. *Compos. Sci. Technol.* **2011**, *71*, 1266.
23. Bao, C.; Guo, Y.; Song, L; Hu, Y. *J. Mater. Chem.* **2011**, *21*, 13942.
24. Xu, C.; Cao, Y.; Kumar, R.; Wu, X.; Wang, X.; Scott, K. *J. Mater. Chem.* **2011**, *21*, 11359.
25. Kim, H.; Miura, Y.; Macosko, C. W. *Chem. Mater.* **2010**, *22*, 3441.
26. Higginbotham, A. L.; Lomeda, J. R.; Morgan, A. B.; Tour, J. M. *ACS Appl. Mater. Interface* **2009**, *1*, 2256.
27. Das, B.; Prasad, K. E.; Ramamurty, U.; Rao, C. N. R. *Nanotechnology* **2009**, *20*, 125705.
28. Yang, Z.; Niu, Z.; Lu, Y.; Hu, Z.; Han, C. C. *Angew. Chem. Int. Ed.* **2003**, *43*, 1943.
29. Lee, J. M.; Lee, D. G.; Lee, S. J.; Kim, J. H.; Cheong, I. W. *Macromolecules* **2009**, *42*, 4511.
30. Serpico, J. M.; Ehrenberg, S. G.; Fontanella, J. J.; Jiao, X.; Perahia, D.; McGrady, K. A. Sanders, E. H.; Kellogg, G. E.; Wnek, G. E. *Macromolecules* **2002**, *35*, 5916.
31. Hickner, M. A.; Ghassemi, H.; Kim, Y. S.; Einsla, B. R.; McGrath, J. E.; *Chem. Rev.* **2004**, *104*, 4587.
32. Hazarika, M.; Malkappa, K.; Jana, T. *Polym. Int.* **2012**, *61*, 1425.
33. Arunbabu, D.; Sanga, Z; Seenimeera, K. M.; Jana, T. *Polym. Int.* **2009**, *58*, 88.

34. Kim, H.; Hahn, H. T.; Viculis, L. M.; Gilje, S.; kaner, R. B. *Carbon* **2007**, *45*, 1578.
35. Wu, N.; She, X.; Yang, D.; Wu, X.; Su, F.; Chen. Y. *J. Mater. Chem.* **2012**, *22*, 17254.
36. Li, S.; Qian, T.; Wu, S.; Shen, J. *Chem. Commun.* **2012**, *48*, 7997.
37. Fan, D. Q.; Liu, Y.; He, J. P.; Zhou, Y. W.; Yang, Y. L. *J. Mater. Chem.* **2012**, *22*, 1396.
38. Zhang, W. L.; Liu, Y. D.; Choi, H. J. *J. Mater. Chem.* **2011**, *21*, 6916.
39. Stankovich, S.; Piner, R. D.; Chen, X.; Wu, N.; Nguyen, S. T.; Ruoff, R. S. *J. Mater. Chem.* **2006**, *16*, 155.
40. Vickery, J. L.; Patil, A. J.; Mann, S. *Adv. Mater.* **2009**, *21*, 2180.
41. Du, F-P.; Wang, J-J.; Tang, C-Y.; Tsui, C-P; Zhou, X-P; Xie, X-L.; liao, Y-G. *Nanotechnology* **2012**, *23*, 475704.
42. Luo, J.; Jiang, S.; Wu, Y.; Chen, M.; Liu, X. *J. Polym. Sci. Part A: Polym. Chem.* **2012**, *50*, 4888.
43. Arunbabu, D.; Sannigrahi, A.; Jana, T. *J. Appl. Polym. Sci.* **2008**, *108*, 2718.
44. Hummers, W. S.; Offeman, R. E. *J. Am. Chem. Soc.* **1958**, *80*, 1339.
45. Tuinstra, F.; Koenig, J. L. *J. Chem. Phys.***1970,** *53*, 1126.
46. Ansari, S.; Giannelis, E. P. *J. Polym. Sci., Part B: Polym. Phys.* **2009**, *47*, 888.
47. Tang, X-.Z.; Li, W. J.; Yu, Z. Z.; Rafiee, M. A.; Rafiee, J.; Yavari, F.; Koratkar, N. *Carbon* **2011**, *49*, 1258.
48. Yang, H. F.; Li, F. H.; Shan, C. S.; Han, D. X.; Zhang, Q. X.; Niu, L.; Ivaska, A. *J. Mater. Chem.* **2009**, *19*, 4632.

Chapter 7

Summary & conclusions

7.1. Summary

The thesis entitled "***Blends and Nanocomposites of Sulfonated Polystyrene and Polybenzimidazole***" describes the studies of blends and nanocomposites of different polymer systems. The thesis contains seven chapters which includes five working chapters, an introductory and a concluding chapter. The summary of the contents of each chapter is as follows.

Chapter 1

Chapter 1 deals with a brief introduction on polymer blending, highlighting the types, classification, methods of preparation and thermodynamic requirement for blending. The characterization techniques and importance of blending has also been discussed. This chapter also focuses a brief introduction on polymer nanocomposites, types and property enhancement of polymer nanocomposites. A brief picture of graphene, its synthesis and polymer-graphene nanocomposites have given. Finally this chapter discussed aims of this thesis.

Chapter 2

In this chapter the influence of sulfonation reaction time, temperature and the parent polystyrene (PS) particle size on the degree of sulfonation (DS), ion exchange capacity (IEC), morphology and glass transition temperature (T_g) of sulfonated polystyrene (SPS) particles was investigated. A longer reaction time (~2 h) at 40°C and a smaller particle size resulted in SPS particles with a high DS. It was found that a larger PS particle size did not readily yield SPS particles with a high DS even with a longer reaction time. Contrary to the popular belief in the literature that a higher DS ensures a high IEC, we observed that the proportionality of IEC to DS is primarily controlled by the SPS particle size. Larger IEC values were obtained for larger particles rather than smaller ones despite their similar DS, owing to the presence of strong interactions between $-SO_3H$ groups within the particles in the latter case which restricts the availability of free H^+ for ion exchange. The SPS particles displayed a core-shell

morphology in which the outer shell appeared because of sulfonation on the PS. The DS value and the SPS particle size significantly influenced the shell thickness and thereby the morphology of the SPS particles.

Chapter 3

This chapter described the formation of core (polystyrene)–shell (polybenzimidazole) nanoparticles from a new blend system consisting of an amorphous polymer polybenzimidazole (PBI) and an ionomer sodium salt of sulfonated polystyrene (SPS-Na). The ionomer used for the blending was spherical in shape with sulfonated groups on the surface of the particles. An in depth investigation of the blends at various sulfonation degrees and compositions using Fourier transform infrared (FT-IR) spectroscopy provided direct evidence of specific hydrogen bonding interactions between the N–H groups of PBI and the sulfonate groups of SPS-Na. The disruption of PBI chains self association owing to the interaction between the functional groups of these polymer pairs was found to be the driving force for the blending. Thermodynamical studies carried out by using differential scanning calorimeter (DSC) established partially miscible phase separated blending of these polymers in a wider composition range. The two distinguishable glass transition temperatures (T_g) which are different from the neat components and unaltered with the blends composition attributed that the domain size of heterogeneity (d_d) of the blends was >20 nm since one of the blend component (SPS-Na particle) diameter was ~70 nm. The diminish of PBI chains self association upon blending with SPS-Na particles and the presence of invariant T_g's of the blends suggested the wrapping of PBI chains over the SPS-Na spherical particle surface and hence resulting a core-shell morphology. Transmission electron microscopy (TEM) study provided direct evidence of core-shell nanoparticle formation; where core is the polystyrene and shell is the PBI. The sulfonation degree affected the blends phase separations. The higher degree of sulfonation favored the disruption of PBI self association and thus helped to form partially miscible two phases blends with core-shell morphology.

Chapter 4

In this chapter partially miscible polymer blends of polybenzimidazole (PBI) with poly(vinylidene fluoride-co-hexafluoro propylene) (PVDF-HFP) have been prepared for their use as polymer electrolyte membrane (PEM) in high temperature PEM fuel cell after being doped with phosphoric acid (PA). The miscibility of the blend membranes was confirmed by characterizing the samples using varieties of spectroscopic and thermodynamical techniques. Infrared (IR) and ^{13}C solid state NMR (SS-NMR) studies revealed the presence specific interactions between the two polymers. The composition dependent two glass transition temperatures (T_g) of the blend membranes attributed the partial miscibility of the two components. The significant decrease of crystallinity of PVDF-HFP, as observed from differential scanning calorimetry and X-ray diffraction studies, upon blending also attributed the interactions between the two polymers components which yielded the partially miscibility. The hydrophobicity of PVDF-HFP helped to control the PA loading and was found to be the responsible for decreased water uptake of the blend membrane compared to pristine PBI. The blending significantly reduced the increase in thickness and swelling ratio of the membranes upon doping with PA. The presence of fluorine atoms of PVDF-HFP in the blend membranes helped to obtain significantly higher proton conductivity than the native PBI and enhance the oxidative stability substantially. PA doped blend membranes displayed superior mechanical stability compared to neat PA doped PBI.

Chapter 5

In this chapter a novel polymer blend membranes of PBI and poly(1-vinyl-1,2,4-triazole) (PVT) were prepared using solution blending method. The aim of the work was to look into the effect of the blend composition on the properties e.g. thermo-mechanical stability, swelling and proton conductivity of the blend membranes. The presence of specific interactions between the two polymers in the blends was observed by studying the samples using varieties of spectroscopic techniques. Blends prepared in all possible

compositions were studied using a differential scanning calorimetry (DSC) and exhibited single T_g which lies between the T_g of the neat polymers. The presence of single composition dependent T_g attributed that the blend is a miscible blend. The N–H---N interactions between the two polymers were found to be the driving force for the miscibility. Thermal stability upto 300°C of the blend membranes, obtained from thermogravimetric analysis, ensured their suitability as PEM for high temperature fuel cell. The proton conductivity of the blend membranes have improved significantly compared to neat PBI because of the presence of triazole moiety which acts as a proton facilitator in the conduction process. The blend membranes showed considerably lower increase in thickness and swelling ratio than that of PBI after doping with phosphoric acid (PA). We found that the porous morphology of the blend membranes caused the loading of larger amount of PA and consequently higher proton conduction with lower activation energy compared to neat PBI.

Chapter 6

Recombination of graphene (GP) nanosheets to graphitic layer structure limits the large scale production of single layer GP and hence its applications. In this article, sulfonated polystyrene (SPS)/GP nanocomposite was prepared to address this issue. Exfoliated graphene oxide (G−O) was solution blended with spherical SPS nanoparticles to produce SPS/G−O nanocomposite and then converted to SPS/GP nanocomposite by treating with the reducing agent. X-ray diffraction, IR and Raman spectroscopy and Atomic force microscopy studies clearly proved the presence of single layer ~ 1nm thick graphene nanosheets in the SPS/GP nanocomposite. The presence of strong interactions between the functionalities of SPS and G−O facilitated the formation of nanocomposite. During the reduction of G−O to GP in the nanocomposite, GP sheets could not recombine into graphitic layer structure owing to the obstruction imposed by the SPS nanoparticles which were adsorbed on the GP sheets. The nanocomposite displayed superior thermal, mechanical and ionic conductivities compared to pristine SPS. Significant mechanical reinforcement, for example 90% increase in storage modulus in case of 7% GP loading, by GP nanosheets enabled us to prepare

mechanically strong SPS membrane which is otherwise brittle in nature. Nanocomposite exhibited higher proton conductivity compared to pristine SPS. In conclusion, a give-and-take approach was developed where SPS nanoparticles facilitated the formation of single layer GP nanosheets by blocking the recombination of these nanosheets into layer structure and in return GP nanosheets enabled the fabrication of mechanically stable ion conducting SPS membrane.

7.2. Conclusion

The following conclusions are drawn from the studies of "***Blends and Nanocomposites of Sulfonated Polystyrene and Polybenzimidazole"***

Chapter 2

1. A series of SPS particles with various degree of sulfonation (DS) are synthesized and characterized.
2. The DS, ion exchange capacity (IEC), morphology and glass transition temperature (T_g) of SPS particles depends not only on reaction time and temperature but also on the size of the parent polystyrene particles.
3. Smaller PS particles, a longer reaction time (*ca* 2 h) and 40°C temperature are found to be the best reaction conditions to achieve the higher DS.
4. It was found that the proportionality of IEC to DS is substantially influenced by the PS particle size: a higher IEC value is obtained for larger particles compared with smaller particles even though their DSs are similar; this is due to the strong interaction between the $-SO_3H$ groups within the particle for smaller particles.

Chapter 3

1. Sodium salt of SPS are prepared and used as template to prepare core (polystyrene)-shell (polybenzimidazole) nanoparticles by solution blending method.

2. The successful disruption of N–H self association of PBI and the presence of specific hydrogen bonding interaction between free N–H of PBI and the sulfonate groups of SPS-Na are the driving forces for the formation of partially miscible two phases blends of PBI and SPS-Na particles with core-shell morphology.
3. Because of the presence of interaction between the two polymers, PBI chains wrap on the SPS-Na spheres forming of core–shell type morphology.

Chapter 4

1. Partially miscible blends of PBI with PVDF-HFP at various compositions have been prepared by blending method.
2. The presence of hydrogen bonding interactions between the functional groups of two polymers is found to be the driving force for their partial miscibility.
4. Though the PA doping level of PBI in the blend membranes are not significantly increases because of the high hydrophobic nature of PVDF-HFP but the proton conductivity of the blend membranes are significantly increased in the blend membranes.
5. Also the oxidative and mechanical stabilities of blend membranes are improved compare to neat PBI.

Chapter 5

1. Novel miscible blend of PVT and PBI of various compositions have been prepared using a solution blending technique.
2. The N−H···N interaction between the two polymers is the driving force for this miscibility.
3. The proton conductivity of the blend membranes is governed by its morphology and it increases with increasing PVT concentration.
4. The morphology of the blends governs the conduction behavior of the blends. These thermo-mechanically stable, highly conducting blends may be

suitable for use as proton exchange membranes (PEMs) in high-temperature fuel cells.

Chapter 6

1. Exfoliated graphene oxide (G–O) nanosheets are solution blended with SPS particles to produce SPS/G–O nanocomposites which then reduced to prepare SPS/GP nanocomposites.
2. Adsorbed SPS particles on the graphene sheets perturb the recombination process of graphene sheet when G–O is reduced to GP resulting a stable SPS/GP nanocomposite.
3. The nanocomposite display better thermal, mechanical and ionic conduction compared to pristine polymer.

7.3. Scope of Future Work

The present thesis has addressed the importance of blending and nanocomposite in the improvement of polymer properties. It also addresses the importance of various polymers specially PBI as PEM membrane in PEMFC. We believe the findings of this thesis will have great impact on the future development of polybenzimidazole (PBI) for its use in PEMFC application. The studies carried out in this thesis could direct researchers to conceive the potentiality of new issues. Few of such important scope for future work are listed below:

1. Chapter 3 deals with the formation of core (polystyrene)-shell (polybenzimidazole) blend membrane. Effort should be made to study the application of these membranes as PEM in PEMFC.

2. Effort should be made to prepare porous PBI membranes for the application in PEMFC by removing the core PS from core (polystyrene)-shell (polybenzimidazole) blend membrane.

3. Different water insoluble derivatives of 1, 2, 4-triazole can be prepared and blended with PBI. The proton conductivity of these blend membranes can be explored.

4. Attempts must be made to prepare the PBI/ Poly(1-vinyl-1,2,4-triazole) blend by *in-situ* blending method.

5. The SPS/GP nanocomposite can be prepared in water medium and the property improvement of the polymer can be compared when the nanocomposite was prepared in DMF medium.

6. Finally the fuel cell testing of the PA doped PBI and PBI blend membrane can be studied.

Publications and Presentations

PUBLICATIONS

1. Synthesis of crosslinked nanoparticles poly(styrene-co-divinylbenzene-co-sulfopropyl methacrylate) by emulsion polymerization: Tuning the particle size and surface charge density, Dhamodaran Arunbabu, **Mousumi Hazarika**, Tushar Jana, *Bull. Mater. Sci.*, **2009**, *32*, 633-641.
2. Formation of core (polystyrene)-shell (polybenzimidazole) nanoparticles using sulfonated polystyrene as template, **Mousumi Hazarika**, Dhamodaran Arunbabu, Tushar Jana, *J. Colloid Interface Sci.* **2010**, *351*, 374-383.
3. Particle size dependent properties of sulfonated polystyrene nanoparticles, **Mousumi Hazarika,** , Kuruma Malkappa, Tushar Jana, *Polym. Int.* **2012**, *61*, 1425-1432.
4. Proton exchange membrane developed from novel blends of polybenzimidazole and poly(vinyl-1,2,4-triazole), **Mousumi Hazarika**, Tushar Jana, *ACS Appl. Mater. Interfaces*, **2012**, *4 (10)*, 5256-5265.
5. Novel proton exchange membrane for fuel cell developed from Blends of polybenzimidazole with fluorinated polymer, **Mousumi Hazarika**, Tushar Jana, Communicated to *Eur. Polym. J.*
6. Sulfonated polystyrene/graphene nanocomposite: A facile route for generation of graphene nanosheets, **Mousumi Hazarika**, Tushar Jana, Communicated to *J. Phys. Chem. C.*

Note: Publications 2-6 are included in this thesis.

CONFERENCE PRESENTATIONS

1. Poster Presented on **"Core-shell polymeric nanostructure formation by blending polybenzimidazole and sulfonated polystyrene**" *7 th Annual in-house symposium CHEMFEST* **2010** of the School of Chemistry, University of Hyderabad, Hyderabad, India.
2. Poster Presented on **"Formation of core (polystyrene)–shell (polybenzimidazole) nanoparticles using sulfonated polystyrene as template**" *8 th Annual in-house symposium CHEMFEST* **2011** of the School of Chemistry, University of Hyderabad, Hyderabad, India.
3. Poster Presented on **"Formation of core (polystyrene)–shell (polybenzimidazole) nanoparticles using sulfonated polystyrene as template**" MACRO 2010-Frontiers of Polymers & Advanced Materials; December 15-17, Indian Institute of Technology, New Delhi, India.
4. Oral presentation on "**Miscible blends of poly(vinyl-1,2,4-triazole) and polybenzimidazole"** *9 th Annual in-house symposium CHEMFEST* **2011** of the School of Chemistry, University of Hyderabad, Hyderabad, India.